

**STRUCTURE-FUNCTION STUDIES OF THE METABOTROPIC GLUTAMATE
RECEPTOR TYPE 6 (mGluR6) AND COMPARISON WITH RHODOPSIN**

by

Kalyan Chakravarthy Tirupula

Bachelor of Science, Acharya N G Ranga Agriculture University, 2001

Master of Science, Drexel University, 2004

Submitted to the Graduate Faculty of
School of Medicine in partial fulfillment
of the requirements for the degree of
Doctor of Philosophy

University of Pittsburgh

2011

UNIVERSITY OF PITTSBURGH

SCHOOL OF MEDICINE

This dissertation was presented

by

Kalyan Chakravarthy Tirupula

It was defended on

April 4th, 2011

and approved by

Dr. Alexander Dömling, Associate Professor, Department of Pharmaceutical Sciences

Dr. William R. Millington, Professor and Chair, Department of Pharmaceutical Sciences,

Albany College of Pharmacy and Health Sciences

Dr. Sunil Saxena, Associate Professor, Department of Chemistry

Dissertation Advisor: Dr. Judith Klein-Seetharaman, Associate Professor, Department of

Structural Biology

Copyright © by Kalyan Chakravarthy Tirupula

2011

**STRUCTURE-FUNCTION STUDIES OF THE METABOTROPIC GLUTAMATE
RECEPTOR TYPE 6 (mGluR6) AND COMPARISON WITH RHODOPSIN**

Kalyan Chakravarthy Tirupula, M.S.

University of Pittsburgh, 2011

Metabotropic glutamate receptor subtype 6 (mGluR6), a class C G protein coupled receptor (GPCR), plays a key role in visual signal transduction and is also implicated in addiction. Certain mutations in mGluR6 have been reported to cause congenital stationary night blindness. In spite of the importance of mGluR6, knowledge of the molecular basis of its function is lacking. It is imperative to improve the current understanding of its structure-function relationships, so that selective ligands that modulate its activity can be discovered. Furthermore, functional characterization of mGluR6 is also expected to lead to a better understanding of the general principles underlying the activation mechanism of GPCR family. Rhodopsin is the prototypical class A GPCR and serves as a good comparative model to establish general mechanistic patterns of activation of GPCRs. This thesis describes experimental and computational approaches to characterize the structure-function relationship of mGluR6 and its comparison with rhodopsin.

Firstly, inducible stable cell lines with high levels of mGluR6 expression were established. Proper trafficking and folding of mGluR6 in these cell lines were verified. To determine mGluR6 function, existing cell-based and novel membrane-based functional assays were optimized and developed, respectively. These efforts led to the establishment of a robust system that expresses properly folded and functional mGluR6 and enabled structure-function studies to be carried out. Several transmembrane cysteine mutants were created and analyzed

with the goal to study the role of the transmembrane domain of mGluR6 in activation mechanism. TM6 of mGluR6 like rhodopsin was found to play a key role in its activation supporting the hypothesis that these two GPCRs may share a general mechanism of activation despite the large sequence divergence. Additional support for this hypothesis was obtained from computational sequence analysis which showed that the highly ranking residues involved in long-range interaction in rhodopsin overlap with the allosteric binding pocket of mGluR6. Finally, with the aim to identify selective ligands for mGluR6, an integrated computational-experimental approach was undertaken. Novel allosteric ligands and possibly selective orthosteric ligands for mGluR6 were identified. Further characterization of these ligands may lead to design of selective ligands for mGluR6.

ACKNOWLEDGEMENTS

I express my deep gratitude to Judith for giving me an opportunity to pursue my PhD endeavors in her lab. Judith's interdisciplinary training in computational and experimental work aligned with my interests. It helped me immensely in learning these two different approaches to understand receptor-ligand interactions and structure-function studies. This thesis is a testimony of the integration of several different projects involving interdisciplinary approaches that advance our understanding of structure-function relation for G protein coupled receptors. Judith is an excellent mentor. She guided me through my research efforts and encouraged me to think independently. I learned from her that every experiment and every data point counts. Judith's knack of making sense of complex data and her attention to details always amazed me. I also learned from Judith how to organize and present data in an effective way. Judith goes to great lengths to help her students. Judith made it possible for me to switch from the Computational Biology program to Molecular Biophysics and Structural Biology program after the first year of graduate school when I realized that I wanted to be primarily an experimental scientist with knowledge of computational biology. Judith is a great leader and an example to follow. Walking in her footsteps is tough but that is one thing I would really like to do.

I am thankful to my committee members Dr. Alex Dömling, Dr. William Millington and Dr. Sunil Saxena for their insights during committee meetings. I would also like to thank Dr. Dömling for his collaboration in small molecule screening studies. I am also thankful to Dr.

Millington for exposing me to the exciting world of dipeptides and its effects on modulating drug addiction. I also thank Dr. Alessandro Bisello and Dr. Chris Langmead for collaborations on cAMP assays and computational sequence analysis studies, respectively. I thank Dr. Guillermo Calero for helping me with detergent screens.

I would like to thank all members, both past and present, of Judith's lab for being helpful and cooperative. Special thanks to my colleagues in the lab - Harpreet Dhiman, Subhdeep Moitra, Dr. Leelavati Murthy and Dr. Naveena Yanamala for their help with stable cell line establishment, sequence analysis, GTP-Eu functional assays and allosteric ligand screening, respectively.

I thank all the administration staff and faculty of Department of Structural Biology for providing a friendly and pleasant environment in the department. I also thank my fellow graduate students and friends who made my life at Pittsburgh a fun-filled experience.

I am greatly indebted to my parents and sisters for their love and support in all my pursuits. Finally, I was fortunate to meet my girlfriend and colleague, Arpana, in Judith's lab. I thank Arpana for her love and all the wonderful memories we shared during our PhD journey.

Dedicated with love to

Arpana

TABLE OF CONTENTS

ACKNOWLEDGEMENTS	IX
LIST OF TABLES	XXV
LIST OF FIGURES	XXVII
ABBREVIATIONS	XXXI
1.0 INTRODUCTION.....	1
1.1 CLASSIFICATION AND STRUCTURES OF G-PROTEIN COUPLED RECEPTORS.....	1
1.1.1 Overview.....	1
1.1.2 Classification and description of the major classes of GPCRs.....	4
1.1.2.1 Class A GPCRs.....	5
1.1.2.2 Class B GPCRs.....	5
1.1.2.3 Class C GPCRs.....	6
1.1.3 Structures of GPCRs.....	6
1.1.3.1 Difficulties obtaining membrane protein structures.....	6
1.1.3.2 Available structures of GPCRs.....	9
1.2 RHODOPSIN: A PROTOTYPIC GPCR.....	11
1.2.1 Function of rhodopsin	11
1.2.2 Rhodopsin misfolding in Retinitis Pigmentosa	12
1.2.3 Dark-state structure of rhodopsin.....	14
1.2.4 Structural changes during activation of rhodopsin.....	16

1.2.5	Comparison of other GPCR structures with rhodopsin structures.....	17
1.3	METABOTROPIC GLUTAMATE RECEPTORS (MGLURS)	21
1.3.1	Subtypes and classification	22
1.3.2	General function of mGluRs.....	23
1.3.3	mGluRs in addiction.....	23
1.3.4	Structural organization of mGluRs	24
1.3.5	Available structures of mGluRs	25
1.3.6	Activation mechanism of mGluRs.....	27
1.3.7	Pharmacology of mGluRs: the therapeutic potential of allosteric ligands	28
1.4	METABOTROPIC GLUTAMATE RECEPTOR SUBTYPE 6	31
1.4.1	mGluR6 function in vision	31
1.4.2	Putative function of mGluR6 in addiction	32
1.4.3	mGluR6 ligands	32
1.4.4	mGluR6 signal transduction cascade.....	32
1.5	OPEN QUESTIONS, AIMS, ACCOMPLISHMENTS AND CONTRIBUTIONS	35
1.5.1	Open questions.....	35
1.5.2	Specific aims.....	36
1.5.3	Outline of approaches	37
1.5.4	Summary of research accomplishments and contributions.....	39
2.0	EXPERIMENTAL PROCEDURES	42
2.1	CLONING OF MGLURS	42
2.1.1	Wild-type (WT) human mGluR6.....	42

2.1.1.1	Introduction of Kozak sequence into pMT3-GRM6.....	42
2.1.1.2	Cloning of mGluR6 into pACMV-tetO.....	43
2.1.2	Transmembrane cysteine mutants of mGluR6.....	45
2.1.3	Rhodopsin like mGluR6 mutants.....	46
2.1.3.1	7TMC	46
2.1.3.2	7TM	47
2.1.3.3	CRD-7TMC	47
2.1.3.4	XR-7TMC	48
2.1.3.5	XR-7TMC double cysteine mutants	49
2.1.4	mGluR6:Rhodopsin chimeras	49
2.1.5	mGluR5.....	54
2.1.6	mGluR2 and mGluR3	56
2.2	PROTEIN EXPRESSION.....	57
2.2.1	COS-1 and HEK293S cell maintenance.....	57
2.2.2	DEAE-dextran transient transfection of COS-1 cells	58
2.2.3	Establishment of mGluR stable cell lines in HEK293S cells	59
2.2.4	Optimizing spinner flask growth conditions for mGluR6 stable cells.....	63
2.2.4.1	Standard spinner flask growth conditions.....	63
2.2.4.2	Optimized growth conditions for mGluR6 expression	63
2.2.5	Expression of Gαβγ heterotrimer complex in insect cells	65
2.2.5.1	Sf9 cell maintenance, growth conditions and cryopreservation	65
2.2.5.2	Plaque assay.....	66
2.2.5.3	Viral amplification	68

2.2.5.4	Expression of $G\alpha_0\beta_3\gamma_{13}$ heterotrimer	69
2.3	PROTEIN PREPARATIONS.....	70
2.3.1	Purification of rhodopsin	70
2.3.1.1	Preparation of 1D4 sepharose.....	70
2.3.1.2	Binding of solubilized rhodopsin to 1D4 sepharose	74
2.3.1.3	Elution of rhodopsin from 1D4 sepharose	74
2.3.2	Membrane preparations of mGluRs by sucrose flotation	75
2.3.3	Detergent extraction and purification of mGluR6	76
2.3.3.1	Optimization of purification protocol	77
2.3.4	Purification of $G\alpha_0\beta_3\gamma_{13}$ complex from insect cells.....	78
2.3.5	Purification of transducin	82
2.4	IMMUNOFLUORESCENCE	84
2.4.1	Collagen coating of coverslips	84
2.4.2	Growing and preparing cells on coverslips for imaging	84
2.4.3	Immunostaining	84
2.5	FUNCTIONAL ASSAYS	86
2.5.1	[³⁵ S]GTP γ S filter binding assay.....	86
2.5.1.1	Transducin activation by rhodopsin	86
2.5.1.2	Transducin activation by mGluR6	87
2.5.1.3	Testing $G\alpha_0\beta_3\gamma_{13}$ complex activation by mGluR6	87
2.5.2	Cell based cAMP functional assay	88
2.5.3	Membrane based GTP-Eu fluorescence assay	89
2.6	DEGLYCOSYLATION WITH PNGASE F	93

2.7	ANALYTICAL PROCEDURES.....	93
2.7.1	Absorption spectra	93
2.7.1.1	Rhodopsin	93
2.7.1.2	mGluR6.....	94
2.7.1.3	Anthocyanins	95
2.7.2	Meta II decay assay for rhodopsin.....	96
2.7.3	SDS-PAGE	97
2.7.4	Western blot.....	98
2.7.5	Dot blot	99
2.7.6	Cysteine quantification with 4,4'-dithiodipyridine.....	99
2.8	COMPUTATIONAL METHODS	100
2.8.1	mGluR sequence analysis.....	100
2.8.2	GPCR structures from the Protein Data Bank.....	101
2.8.2.1	mGluR structures.....	101
2.8.2.2	Class A GPCR structures	102
2.8.3	Manipulation of GPCR structure files.....	103
2.8.3.1	Extraction of ligand binding pockets	103
2.8.3.2	Extracting inter-residue contacts	103
2.8.4	Homology modeling.....	103
2.8.4.1	Homology models of the EC domain of mGluR6.....	104
2.8.4.2	Homology models of the TM domain of mGluR6	105
2.8.5	Docking studies	106
2.8.5.1	Preparation of mGluR receptor files.....	106

2.8.5.2	Preparation of ligand files	107
2.8.5.3	Docking parameters and protocol	108
2.8.5.4	Analysis of docked structures	109
2.8.6	Generative REgularized ModeLs of proteins (GREMLIN) analysis.....	109
2.8.6.1	Method description	109
2.8.6.2	Model selection	111
2.8.6.3	GPCR ligand binding pockets.....	112
3.0	ESTABLISHMENT OF MGLUR6 EXPRESSION SYSTEMS: LOCALIZATION AND FOLDING OF MGLUR6 AND COMPARISON TO RHODOPSIN	118
3.1	SUMMARY	118
3.2	INTRACELLULAR LOCALIZATION OF WILD-TYPE RHODOPSIN AND ITS MUTANTS P23H AND N15S.....	119
3.2.1	Rationale.....	119
3.2.2	Localization results.....	119
3.2.3	Consequences of rhodopsin results for mGluR6 studies.....	120
3.3	LOCALIZATION OF WILD-TYPE MGLUR6 AND TRUNCATION MUTANTS	122
3.3.1	Rationale.....	122
3.3.2	Immunofluorescence studies of mGluR6 wild-type and 7TMC	123
3.3.3	Localization results obtained with CRD-7TMC	125
3.3.4	Localization of XR-7MC	127

4.0	DETERGENT SCREEN FOR SOLUBILIZATION AND PURIFICATION OF MGLUR6	128
4.1	SUMMARY	128
4.2	DETERGENT SOLUBILIZATION OF MGLUR6	129
4.2.1	Preliminary solubilization experiments.....	129
4.2.2	Detergent screen	131
4.3	IMMUNOAFFINITY PURIFICATION.....	135
4.4	CHARACTERIZATION OF GLYCOSYLATION	137
4.4.1	Glycosylation sites in rhodopsin and mGluR6.....	137
4.4.2	Deglycosylation studies of rhodopsin and mGluR6.....	138
4.5	STUDIES ON OLIGOMERIZATION IN PURIFIED MGLUR6.....	139
4.5.1	Rationale.....	139
4.5.2	Results.....	140
4.5.3	Involvement of TM domain cysteines in oligomerization	141
5.0	OPTIMIZATION OF FUNCTIONAL ASSAYS FOR MGLUR6	144
5.1	SUMMARY	144
5.2	CELL BASED CAMP FUNCTIONAL ASSAY	145
5.2.1	Optimization of cell culture and assay conditions	145
5.2.2	Agonist response	148
5.2.3	Antagonist response.....	150
5.2.4	Effect of DMSO on cAMP assay	152
5.3	ACTIVATION ASSAY FOR MGLUR6 IN MEMBRANES.....	154
5.3.1	[³⁵ S]GTPγS assay with mGluR6 in membranes and purified Gαβγ.....	154

5.3.2	Development of GTP-Eu fluorescence assay.....	155
5.3.2.1	Rationale	155
5.3.2.2	Optimization of conditions.....	156
5.3.2.3	L-glutamate dose response	159
5.4	<i>IN VITRO</i> FUNCTIONAL ASSAYS WITH PURIFIED RECEPTOR.....	161
5.4.1	[³⁵ S]GTPγS assays in detergent micelles.....	161
5.4.1.1	Transducin (G _t) activation assay for rhodopsin and mGluR6.....	161
5.4.1.2	Activation of transducin (G _t) at low pH in the presence of high concentrations of glutamate.....	163
6.0	EXTRACELLULAR ORTHOSTERIC LIGANDS	166
6.1	SUMMARY	166
6.2	HOMOLOGY MODELS OF EXTRACELLULAR AMINO TERMINAL LIGAND BINDING DOMAIN OF MGLUR6.....	167
6.3	VALIDATION OF THE DOCKING APPROACH.....	168
6.3.1	Primary validation.....	168
6.3.1.1	Validation of the docking approach for closed mGluR structures and optimization of the mGluR6 ligand binding pocket.....	168
6.3.1.2	Validation of the docking approach for open mGluR structures.	170
6.3.2	Secondary validation	172
6.4	VIRTUAL LIGAND SCREENING OF SELECTIVE AGONISTS FOR MGLUR6.....	174
6.4.1	Library creation.....	174
6.4.1.1	Non-tetrazole containing molecules.....	174

6.4.1.2	Tetrazole containing molecules.....	175
6.5	DOCKING OF DIPEPTIDES TO MGLURS.....	177
6.6	EXPERIMENTAL TESTING OF POTENTIAL LIGANDS.....	179
7.0	TRANSMEMBRANE ALLOSTERIC LIGANDS	182
7.1	SUMMARY	182
7.2	ALLOSTERIC LIGANDS FOR MGLURS.....	183
7.3	HOMOLOGY MODELS OF TRANSMEMBRANE REGIONS	184
7.4	VALIDATION OF DOCKING	185
7.4.1	Preferential binding of allosteric ligands to active and inactive TM structures of mGluRs.....	185
7.4.2	Prediction of allosteric ligands for mGluR6.....	187
7.5	EXPERIMENTAL TESTING OF POTENTIAL ALLOSTERIC LIGANDS ON MGLUR6 FUNCTION	189
7.5.1	Demonstration of direct inverse agonism of PHCCC	191
7.5.2	Effect of PHCCC on activity of XR-7TMC.....	193
8.0	CYTOPLASMIC ALLOSTERIC LIGANDS	195
8.1	SUMMARY	195
8.2	EFFECT OF ANTHOCYANINS AND PORPHYRINS IN VISION	196
8.3	EFFECT OF ANTHOCYANINS AND PORPHYRINS ON RHODOPSIN FUNCTION.....	197
8.3.1	Binding studies of C3G and Ce6 to rhodopsin by docking.....	197
8.3.2	Binding studies of C3G and Ce6 to rhodopsin by NMR.....	199
8.3.3	Effect of C3G and Ce6 on function of rhodopsin	200

8.3.3.1	C3G enhances regeneration rate of rhodopsin.....	200
8.3.3.2	C3G has no effect on Meta II decay	201
8.3.3.3	C3G slightly inhibits G protein activation.....	202
8.3.3.4	Ce6 inhibits G protein activation.....	203
8.4	EFFECT OF ANTHOCYANINS AND PORPHYRINS ON MGLUR6 FUNCTION.....	204
8.4.1	Effect of anthocyanins on function of mGluR6.....	204
8.4.2	Effect of Ce6 on function of mGluR6.....	205
9.0	ROLE OF TM CYSTEINES IN MGLUR6 ACTIVATION	207
9.1	SUMMARY	207
9.2	RATIONALE	208
9.3	IMPORTANCE OF TM CYSTEINES.....	208
9.3.1	Identification of conserved cysteines in TM of mGluRs	208
9.3.2	Structural modeling of the cluster of cysteines in TM 5 and 6.....	211
9.3.3	Comparison of mGluR6 with rhodopsin and other mGluRs	213
9.4	COMPARISON OF EXPRESSION LEVELS OF WILD-TYPE AND CYSTEINE MUTANTS.....	215
9.5	ACTIVATION STUDIES	217
9.5.1	Agonist response	217
9.5.1.1	Forskolin stimulated cAMP formation in cells.....	217
9.5.1.2	GTP-Eu binding in membranes.....	219
9.5.1.3	Comparison of cAMP and GTP-Eu results	220
9.5.2	Antagonist response (cAMP formation in cells)	221

9.5.3	Allosteric ligands.....	223
9.6	CONCLUSIONS: CONTRIBUTION OF CYSTEINES IN ACTIVATION OF MGLUR6	224
10.0	RHODOPSIN-MGLUR6 CHIMERAS.....	227
10.1	SUMMARY	227
10.2	RATIONALE AND CONSTRUCTS	228
10.3	RETINAL BINDING.....	230
11.0	IDENTIFICATION OF ALLOSTERIC COUPLING SITES IN GPCRS.....	232
11.1	SUMMARY	232
11.2	IMPORTANCE OF ALLOSTERIC COMMUNICATION.....	233
11.3	PRIOR WORK IN GPCR RESIDUE COUPLING ANALYSIS	235
11.3.1	Statistical Coupling Analysis (SCA)	235
11.3.2	Graphical Models for Residue Coupling (GMRC)	238
11.4	GREMLIN RESULTS.....	239
11.4.1	General observation	239
11.4.2	Enumeration of domain edges.....	241
11.4.3	Long-range couplings involving the ligand binding pockets	242
11.4.4	A minimal ligand binding pocket.....	246
11.4.5	Identification of top ranked long-range interactions in rhodopsin	248
11.4.6	Involvement of long-range interactions in activation of rhodopsin.....	252
11.4.6.1	Edges involving EC and TM domain	252
11.4.6.2	Edges involving IC domain	255
11.5	EXTENDING FINDINGS TO CLASS C GPCRS	256

12.0	SUMMARY	258
13.0	FUTURE RESEARCH DIRECTIONS.....	262
13.1	IMMEDIATE GOALS.....	262
13.1.1	Test the effect of PHCCC on the activity of C754A, C765A and C793A double cysteine mutants.....	262
13.1.2	Optimization of functional assays for mGluR2, mGluR3 and mGluR5 to evaluate selectivity and specificity of binding of dipeptides and other ligands..	263
13.1.3	Evaluate effect of DMSO on GTP-Eu binding assay	264
13.1.4	Imaging mGluR6 trafficking in cells under optimized cell culture conditions that prevent its constitutive activation	265
13.1.5	Development of an <i>in vitro</i> functional assay for purified mGluR6 in detergent micelles	266
13.1.6	Docking validation of antagonists to open mGluR structures	266
13.2	LONG TERM GOALS.....	268
13.2.1	Large scale virtual and experimental screens to identify ligands for mGluR6.....	268
13.2.2	Functional characterization of chimeras.....	269
13.2.3	Cysteine accessibility and EPR studies of mGluR6.....	270
13.2.4	Comparison of GREMLIN analysis with other sequence analysis methods and extension of GREMLIN analysis to Class C GPCRs	271
	APPENDIX A . LIST OF ORTHOSTERIC LIGANDS FOR MGLUR1, 3 AND 6.....	273
	APPENDIX B . PUBLICATIONS.....	274
	BIBLIOGRAPHY.....	276

LIST OF TABLES

Table 1.1 Summary of structural information available on GPCRs	10
Table 1.2 Classification and properties of different subtypes of mGluRs	22
Table 1.3 Summary of amino terminal ligand binding domain structures of mGluRs	26
Table 1.4 Competitive and allosteric ligands for mGluRs	30
Table 2.1 PCR conditions for amplification of rhodopsin gene fragments (chimeras)	51
Table 2.2 PCR conditions for amplification of mGluR6 gene fragments (chimeras)	52
Table 2.3 PCR conditions for amplification of mGluR6:Rhodopsin chimeras	53
Table 2.4 List of PDB entries for extracellular ligand binding domains of mGluRs	101
Table 2.5 List of PDB entries of available GPCR structures	102
Table 2.6 Ligands co-crystallized with GPCR structures	113
Table 2.7 Common ligand binding pockets defined for GPCRs with structural information	114
Table 2.8 Defining a minimal GPCR pocket	115
Table 2.9 List of buffers and reagents	116
Table 2.10 List of constructs and stable cell lines created or used in this thesis.	117
Table 4.1 List of non ionic detergents that solubilize cells better than 4% OG.	133
Table 4.2 Synthetic lipids and ionic detergents that solubilize cells better than 4% OG.	134
Table 6.1 Summary of results from secondary validation	173

Table 6.2 Summary of dipeptide docking results	178
Table 7.1 Docking of allosteric ligands to active and inactive models of mGluR6	188
Table 7.2 Comparison of docking predictions and cAMP assay results for allosteric ligands...	190
Table 9.1 L-glutamate induced response for WT and cysteine mutants (cAMP formation)	219
Table 9.2 EC ₅₀ [μM] values for agonists at active cysteine mutants compared to WT	219
Table 9.3 L-glutamate induced response for WT and cysteine mutants (GTP-Eu binding).....	220
Table 9.4 L-AP4 and LY341495 induced response for WT and cysteine mutants (cAMP formation)	223
Table 9.5 Effect of PHCCC on WT and double cysteine mutants activity (cAMP assay).....	224
Table 11.1 Comparison of edge distribution from null set (control) and GREMLIN	241
Table 11.2 List of top ranked residues and the most persistent edges.....	249
Table 11.3 Persistent edges categorized based on the long-range contacts between different domains.	251

LIST OF FIGURES

Figure 1.1 Schematic of a GPCR depicting secondary structure and its orientation in the membrane.....	3
Figure 1.2 Structural organization and location of ligand binding sites in different classes of GPCRs.....	4
Figure 1.3 Fraction and composition of membrane proteins in the PDB	8
Figure 1.4 Retinitis Pigmentosa mutations in rhodopsin	13
Figure 1.5 Inactive and active structures of rhodopsin.....	15
Figure 1.6 Schematic of mGluR domain organization	25
Figure 1.7 Schematic representation of a rod and ON bipolar synapse and function of mGluR6	34
Figure 2.1 Domain organization of mGluR6:Rhodopsin chimeras	49
Figure 2.2 Activation of sepharose by CNBr and coupling of protein to the activated gel.....	71
Figure 2.3 Purification of $G\alpha_0\beta_3\gamma_{13}$ from insect cells using optimized protocol	81
Figure 2.4 Fluorescence of 5nM GTP-Eu reagent from different lots.....	91
Figure 2.5 Standardization of quantification of purified mGluR6.....	95
Figure 2.6 Cartoon of a multiple sequence alignment and its mapping to a Markov random field	110
Figure 3.1 Localization of wild-type (WT) and mutant rhodopsin.....	121

Figure 3.2 Schematic of different mGluR6 truncation mutants compared to wild-type	123
Figure 3.3 Localization of wild-type and 7TMC mGluR6 constructs in stable cell lines	124
Figure 3.4 Localization of truncated mGluR6 constructs in stable cell lines	126
Figure 4.1 Preliminary solubilization experiments to extract mGluR6 from COS-1 cells	130
Figure 4.2 Detergent screen for solubilization of mGluR6.....	132
Figure 4.3 Immunoaffinity purification of mGluR6 from HEK293 stable cells	136
Figure 4.4 Glycosylation of wild-type and truncated mutants of mGluR6.....	138
Figure 4.5 Dimerization and oligomerization of wild-type and XR-7TMC mGluR6	141
Figure 4.6 Dimerization and oligomerization of XR-7TMC cysteine mutants	142
Figure 5.1 cAMP assay to test function of mGluR6 and UBP1112 (antagonist)	147
Figure 5.2 cAMP agonist dose-response curves for mGluR6 in cAMP assay	149
Figure 5.3 Competition dose-response curves for LY341495.....	151
Figure 5.4 Effect of DMSO on the cAMP assay	153
Figure 5.5 G protein heterotrimer ($G\alpha\beta\gamma$) activation by mGluR6	155
Figure 5.6 Screening of $MgCl_2$ and GDP for optimizing GTP-Eu assay	157
Figure 5.7 Screening of NaCl, saponin and mGluR6 membranes for optimizing GTP-Eu assay	158
Figure 5.8 L-glutamate dose-response curves for mGluR6 (GTP-Eu binding).....	160
Figure 5.9 Transducin (G_t) activation by rhodopsin and mGluR6	162
Figure 5.10 Low pH activation of transducin	164
Figure 5.11 Transducin activation by mGluR6 in the presence of pH corrected L-glutamate...	165
Figure 6.1 Primary validation of docking approach for agonist bound close conformation of ATD	169

Figure 6.2 Comparison of L-glutamate binding pose in mGluR6 before and after optimization	170
Figure 6.3 Primary validation of the docking approach for agonist bound close conformation of the ATD	171
Figure 6.4 Top and interesting hits from of non-tetrazole library screening	175
Figure 6.5 Top-ranked and interesting hits from the tetrazole library screening.....	176
Figure 6.6 Comparison of ligand binding pockets of mGluR1, mGluR3 and mGluR6	177
Figure 6.7 cAMP assay to test the effect of dipeptides on the function of mGluR6	180
Figure 6.8 cAMP assay to test the effect of virtual screen hit Omega_352 on mGluR6 function	181
Figure 7.1 Differences in energy between allosteric ligands docked to active and inactive models of mGluRs.....	187
Figure 7.2 cAMP assay to test the effect of predicted allosteric ligands on the function of mGluR6.....	189
Figure 7.3 Competition dose-response curves for PHCCC	192
Figure 7.4 cAMP assay to test function of PHCCC on the XR-7MC construct of mGluR6.....	193
Figure 8.1 Absorption spectra of C3G alone at different pH conditions	198
Figure 8.2 Effect of C3G on function of rhodopsin.....	201
Figure 8.3 Transducin (G _t) activation assay in presence of Ce6	203
Figure 8.4 cAMP assay to test effect of C3G, C3R on the function of mGluR6.....	205
Figure 8.5 cAMP assay to test an effect of Ce6 on cAMP levels in induced and uninduced cells	206
Figure 9.1 Multiple sequence alignment of transmembrane region of mGluRs.....	210
Figure 9.2 Location of transmembrane (TM) domain cysteines.....	212

Figure 9.3 Comparison of TM helices V and VI of rhodopsin and mGluRs.....	214
Figure 9.4 Quantifying expression levels Wild-type and mutant mGluR6 membranes	216
Figure 9.5 Comparison of agonist induced activity in different cysteine mutants	218
Figure 9.6 Effect of LY341495 on the activity of WT and cysteine mutants of mGluR6.....	222
Figure 10.1 Design of mGluR6: Rhodopsin chimera	229
Figure 10.2 Retinal binding to rhodopsin and chimera.....	231
Figure 11.1 Multiple sequence alignment of class A GPCRs.....	237
Figure 11.2 Distribution of GREMLIN edges between different domains	240
Figure 11.3 Edge distributions in the common ligand binding pockets (GREMLIN vs. null set)	244
Figure 11.4 Peptide (CVX15) and different small molecule ligand-binding mapped onto rhodopsin.....	245
Figure 11.5 Edge distributions in the minimal ligand binding pockets (GREMLIN vs. null set)	247
Figure 11.6 Location of minimal ligand binding pocket residues in rhodopsin structure	248
Figure 11.7 Persistent long-range contacts mapped onto structure of rhodopsin.	253
Figure 11.8 Alignment of amino acid residues of TM involved in persistent edges	257

ABBREVIATIONS

1D4	: C-terminal tail of rhodopsin used as affinity tag
ADT	: AutoDockTools
AMP	: Adenosine monophosphate
APS	: Ammonium persulfate
ATD	: Amino terminal domain
C3G	: Cyanidin-3-glucoside
C3R	: Cyanidin-3-rutinoside
cAMP	: Cyclic AMP
Ce6	: Chlorin e6
CPCCOEt	: 7-(Hydroxyimino)cyclopropa[b]chromen-1a-carboxylate ethyl ester
CRD	: Cysteine rich domain
DFB	: Difluorobenzaldazine
DM	: n-Dodecyl- β -D-Maltopyranoside
DMSO	: Dimethyl sulfoxide
EC	: Extracellular
Eu	: Europium
FK	: Forskolin
GREMLIN	: Generative REGularized ModeLS of proteins

G_t	: Transducin (Cognate G protein heterotrimer for rhodopsin)
GTP	: Guanosine-5'-triphosphate
HA	: Hemagglutinin tag
IC	: Intracellular
LY341495	: (2S)-2-Amino-2-[(1S,2S)-2-carboxycycloprop-1-yl]-3-(xanth-9-yl) propanoic acid
mGluRs	: Metabotropic glutamate receptors
MOI	: Multiplicity of infection
MPEP	: 2-methyl-6-((3-methoxyphenyl)ethynyl)-pyridine
MRF	: Markov random field
MWCO	: Molecular weight cut off
NMR	: Nuclear magnetic resonance
OG	: n-Octyl-β-D-Glucoside
PAGE	: Polyacrylamide gel electrophoresis
PCR	: Polymerase chain reaction
PDB	: Protein data bank
pfu	: Plaque forming units
PHCCC	: N-phenyl-7-(hydroxylimino)cyclopropa[b]chromen-1a-carboxamide
PMSF	: Phenylmethylsulfonyl fluoride
rmsd	: root mean square deviation
SDS	: Sodium dodecyl sulfate
TM	: Transmembrane

1.0 INTRODUCTION

Understanding the molecular mechanism of action of proteins is critical to rationally design drugs that will selectively modulate their function. In many proteins like receptors, the sites of activation can be located distant from the sites of ligand binding. This is particularly true for receptor proteins, the object of this thesis. Thus, long-range mechanistic effects need to propagate through the structure to mediate communication between the ligand binding and activation sites. Such mechanistic understanding is critical for function but is poorly understood for many receptors. The work in this thesis is aimed at understanding the structure-function relationship of the pharmaceutically most important class of receptors – the G protein coupled receptors (GPCRs).

1.1 CLASSIFICATION AND STRUCTURES OF G-PROTEIN COUPLED RECEPTORS

1.1.1 Overview

GPCRs are membrane spanning signal transducers that sense extracellular stimuli and communicate them to the inside the cell. The human genome consists of approximately 1000 GPCR members making them the largest family of receptors and proteins in general in the

human genome (Takeda et al., 2002). GPCRs respond to a range of stimuli that are of external origin including light, odorants, taste molecules, pheromones and physiological ligands such as ions, nucleotides, neurotransmitters, lipids and peptides that regulate different activities (Vassilatis et al., 2003). The role GPCRs in signaling and their location on the cell membrane makes them attractive drug targets. It has been calculated that 26.8% of all Food and Drug Administration (FDA) approved drugs are aimed at GPCRs making them the largest group of drug targets (Overington et al., 2006).

GPCRs derive their name from their ability to recruit intracellular heterotrimeric G proteins ($G\alpha\beta\gamma$) and regulate G protein activity. Upon activation by external stimuli, GPCRs trigger the catalytic exchange of GDP to GTP in the $G\alpha$ subunit of the receptor associated G-protein heterotrimer (Bourne et al., 1991). The GTP-bound $G\alpha$ subunit dissociates from the receptor and the $G\beta\gamma$ subunits. Both $G\alpha$ and $G\beta\gamma$ modulate several intracellular signaling pathways including stimulation or inhibition of adenylate cyclases and activation of phospholipases, as well as regulation of certain ion channels (Hamm, 1998). It is now established that GPCRs can also signal independent of G-protein heterotrimers through GPCR kinases (GRKs), β -arrestins, SH2 domain-containing signaling proteins, small GTP-binding proteins, PDZ domain-containing proteins and polyproline-binding proteins, further increasing the complexity of their signaling (Hall et al., 1999; Rajagopal et al., 2005).

The activation of GPCRs is a result of several structural changes in the receptor (Ballesteros et al., 2001b). Structurally, all GPCRs share a unique transmembrane (TM) alpha helical bundle motif containing seven helices that is formed by a single polypeptide chain. The amino terminal region of the helical bundle along with the loop regions connecting the helices on the cell exterior constitute the extracellular (EC) domain while the carboxy terminal region along

with the loops located inside the cell constitute the intracellular (IC) domain (Figure 1.1). The activation mechanism of GPCRs primarily involves ligand binding in the TM and/or EC regions which ultimately result in structural changes in the TM and IC regions that recruit G protein heterotrimers, GRKs and β -arrestins (Figure 1.1) (Rosenbaum et al., 2009). In some GPCRs the carboxy terminus is quite long and contains specific domains that recruit intracellular effectors such as PDZ, Homer and SH2 proteins (Bockaert et al., 2003; Enz, 2007; Hall et al., 1999).

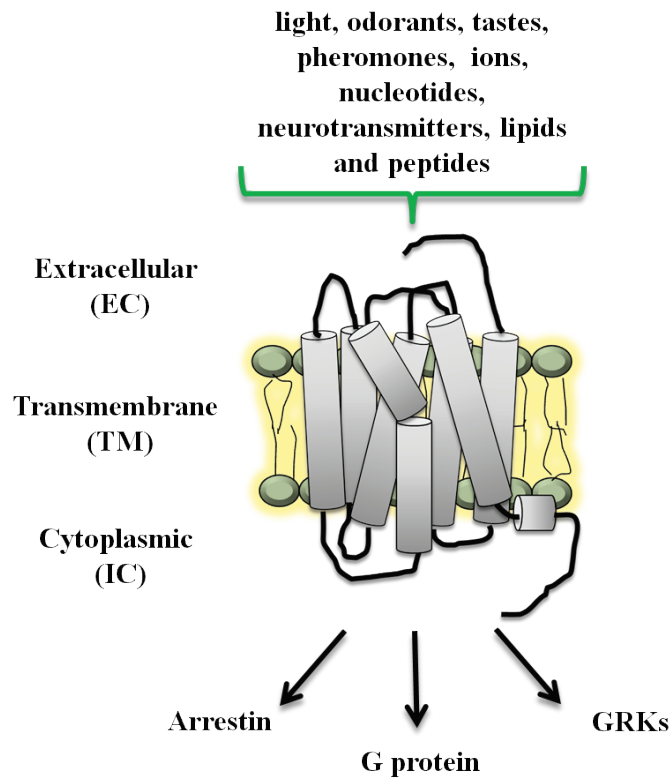


Figure 1.1 Schematic of a GPCR depicting secondary structure and its orientation in the membrane

Shown in the cartoon are the seven transmembrane helices with the extracellular and intracellular loops. To highlight the diversity in the GPCR family examples of ligands that bind GPCRs are also listed.

1.1.2 Classification and description of the major classes of GPCRs

Based on sequence and structure similarity, all GPCRs are divided into at least five distinct families (Fredriksson et al., 2003): rhodopsin (family A, also known as class A), secretin (family B, also known as class B), glutamate (family C, also known as class C), adhesion and frizzled/taste2. Structurally, all GPCRs share the common seven helical TM bundle and the TM helices are the most conserved regions in this family. For example, within a given family there is typically 25% sequence identity in the TM region along with a unique set of residues and conserved motifs (Pierce et al., 2002). Apart from the TM region there is very little similarity between the families.

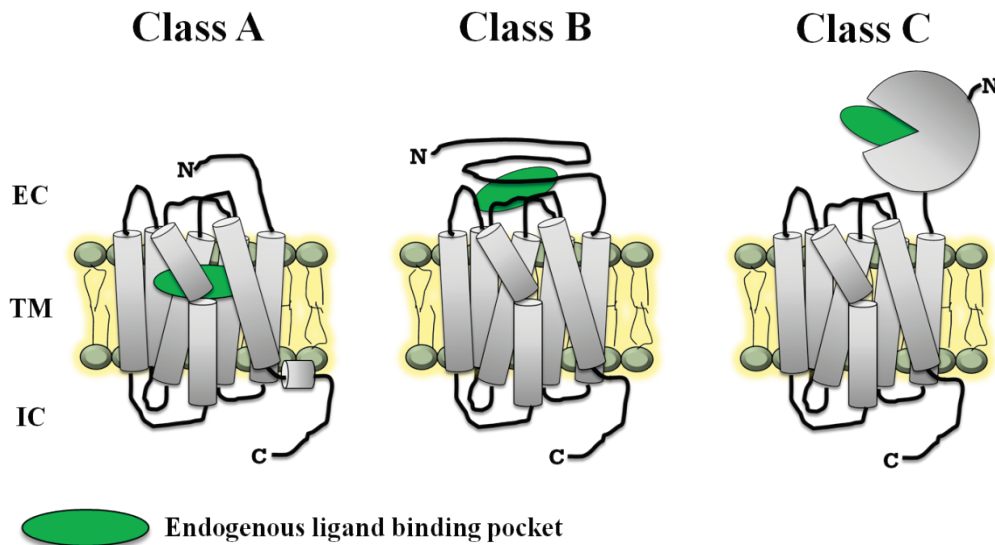


Figure 1.2 Structural organization and location of ligand binding sites in different classes of GPCRs

The figure represents the structural organization of class A, B and C GPCRs. In general, the size of the N-terminus varies in different classes with class C having the largest. The ligand binding pockets are shown in green.

1.1.2.1 Class A GPCRs

Among all the classes of GPCRs, Class A is the largest. These receptors bind an enormous diversity of ligands including odorants, peptides, biogenic amines or lipid-like substances. There are at least 284 human non-olfactory Class A GPCRs (Davies et al., 2007; Vassilatis et al., 2003). The endogenous ligands for the majority of receptors in this class bind inside the TM domain (Figure 1.2) (Bockaert and Pin, 1999). In certain sub-classes in this family like peptide binding receptors and glycoprotein hormone receptors, the ligand binding domain includes the regions from the N-terminus and the EC loops (Bockaert and Pin, 1999; Kristiansen, 2004). The prototypical member of this class and in general for the entire GPCR family is the photoreceptor protein rhodopsin. Rhodopsin is the dim light photoreceptor in the mammalian eye. The inverse agonist 11-*cis*-retinal is covalently bound in the TM region of rhodopsin and keeps it extremely stable against inadvertent activation. The thermal activation of a single rhodopsin molecule bound to 11-*cis*-retinal occurs on average every 420 years. Dark adapted rhodopsin is highly sensitive and can be activated by a single photon (Baylor, 1996). There is a wealth of structure-function data available for this receptor which recently includes crystal structures of both active and inactive structures (Ahuja and Smith, 2009; Choe et al., 2011a; Choe et al., 2011b; Fishkin et al., 2004; Okada et al., 2004; Palczewski et al., 2000; Scheerer et al., 2008; Standfuss et al., 2011).

1.1.2.2 Class B GPCRs

There are approximately 50 class B human receptors (Davies et al., 2007; Vassilatis et al., 2003). These receptors have been reported to bind large peptides such as secretin, parathyroid hormone, glucagon, calcitonin, vasoactive intestinal peptide, growth hormone releasing hormone and pituitary adenylyl cyclase activating protein (Davies et al., 2007; Vassilatis et al., 2003). The

N-terminus of class B GPCRs is generally 60-80 amino acids larger as compared to class A N-termini (Soudijn et al., 2004). The endogenous ligand binding site for this class of receptors consists mostly of a part of the extended N-terminus and the EC loops (Figure 1.2) (Bockaert and Pin, 1999; Kristiansen, 2004).

1.1.2.3 Class C GPCRs

There are 22 class C GPCRs expressed in humans (Rondard et al., 2011). The receptors in this class respond to excitatory neurotransmitters like glutamate and γ -aminobutyric acid (GABA), Ca^{2+} , taste molecules, amino acids, pheromones and odorants (Pin et al., 2003). All class C GPCRs in addition to the seven helical TM bundle have an extended amino terminus approximately 500 amino acids long that harbors the endogenous ligand binding pocket (Figure 1.2) similar to bacterial periplasmic binding proteins (O'Hara et al., 1993). Also unique to this class of receptors is the obligate receptor homo- or heterodimerization (Pin et al., 2003) via a disulfide bond in the amino terminal domain or by association of coiled coil regions in the carboxy terminus. The metabotropic glutamate receptors (mGluRs) and the GABA receptors are the most widely studied receptors of this class.

1.1.3 Structures of GPCRs

1.1.3.1 Difficulties obtaining membrane protein structures

Obtaining experimental structural data for membrane proteins like GPCRs is challenging for a number of reasons. First, structural techniques such as X-ray crystallography and NMR spectroscopy require large quantities of proteins purified to homogeneity. For membrane proteins, both the production and purification steps are difficult. Membrane proteins usually

display very low expression levels and tend to aggregate when removed from their native membrane environment. Secondly, the need for mimicking membranes requires addition of lipids or detergents that interfere with structural techniques, for example by creating large background signals in NMR and increasing the effective molecular weight of the membrane protein-detergent complex making it less favorable for NMR studies. Thus, determining membrane protein structures has been a challenge, a fact that is reflected by the limited number of membrane protein structures resolved and deposited to date in the Protein Data Bank (PDB) (Berman et al., 2000). As of the end of November 2010, 1331 membrane protein structures have been deposited in the PDB which corresponds to only 2% of all the structures reported (Figure 1.3). Moreover, only 262 out of these 1331 are unique membrane protein structures, as defined by a sequence cut-off of 95%. Thus, only a small number of unique membrane proteins are available as examples for different functional and structural categories that membrane proteins engage in (Figure 1.3). There is structural information available only for 7 GPCRs.

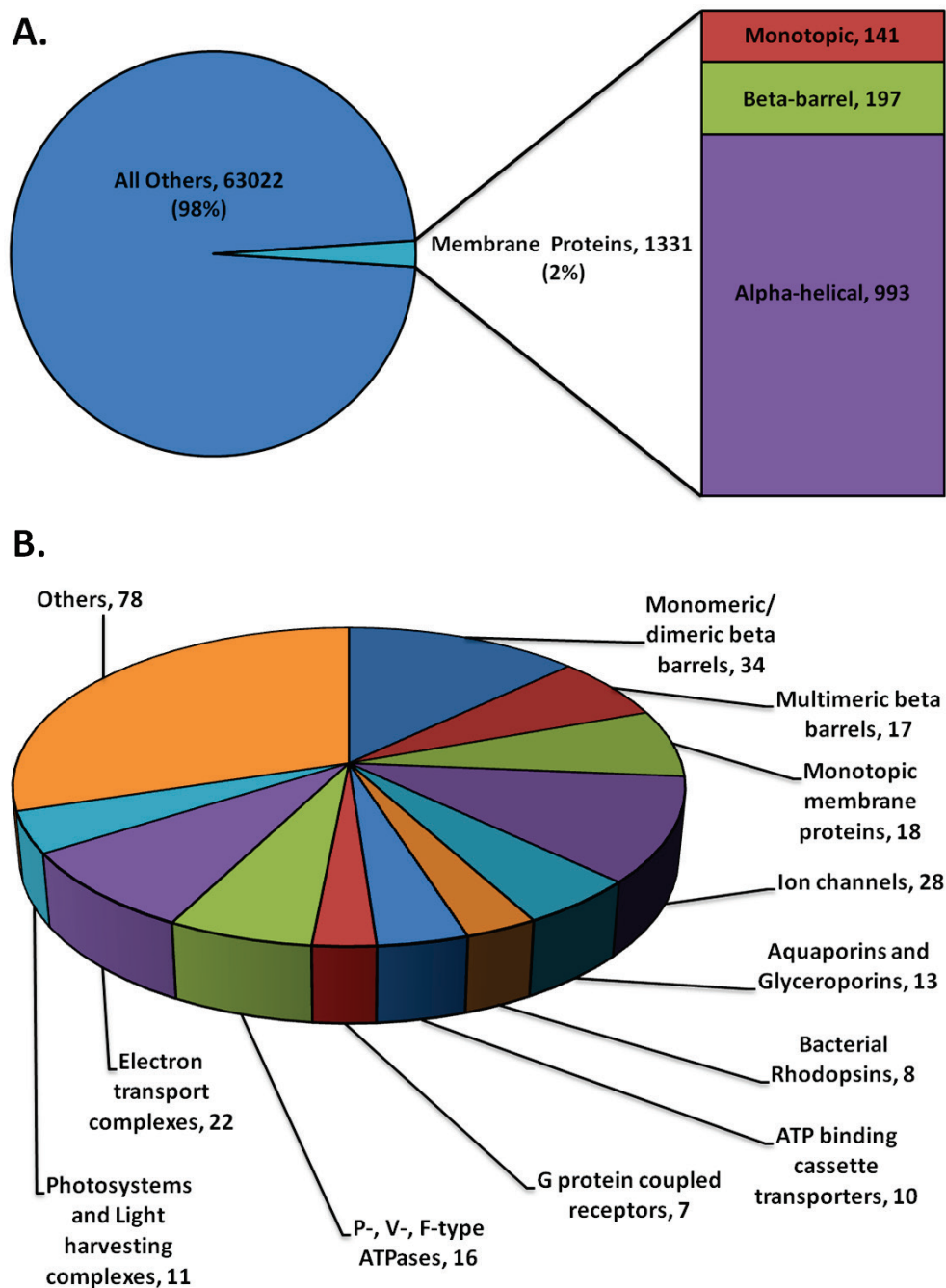


Figure 1.3 Fraction and composition of membrane proteins in the PDB

(A) The pie chart shows that of all structurally resolved proteins, 2% correspond to membrane proteins. The list on the right provides a breakdown of membrane proteins into different structural categories. (B) Structural and functional distribution of unique membrane protein structures. Data was retrieved on 11/26/2010 from the curated membrane protein database available at http://blanco.biomol.uci.edu/Membrane_Proteins_xtal.html.

1.1.3.2 Available structures of GPCRs

As of March 2011, there are a total of 45 structures representing seven different GPCRs deposited in the PDB (Table 1.1). Only class A GPCRs have been crystallized so far. The GPCRs for which structural information is available are bovine rhodopsin (BR; 20 structures including opsin), squid rhodopsin (SR; 2 structures) turkey β_1 adrenergic receptor (β_1 AR; 6 structures), human β_2 adrenergic receptor (β_2 AR; 10 structures), human A_{2A} adenosine receptor (A_{2A} ; 1 structure), human chemokine receptor CXCR4 (5 structures) and human dopamine D3 receptor (D3R; 1 structure). Rhodopsin was the first GPCR to be crystallized and the most detailed understanding of structure-function relationships of any GPCR has been gained for this protein (Palczewski, Kumasaka et al. 2000). Crystal structures of other GPCRs became available only during the last three years.

Table 1.1 Summary of structural information available on GPCRs

Receptor	PDB IDs [number of structures]	Ligands	Reference
Bovine Rhodopsin (BR)	1F88, 1GZM, 1HZX, 1JFP, 1L9H, 1LN6, 1U19, 2G87, 2HPY, 2I35, 2I36, 2I37, 2J4Y, 2PED, 3C9L, 3C9M, 3CAP, 3DQB, 3PQR, 3PXO [20]	Retinal, Ligand free	(Palczewski et al., 2000) (Li et al., 2004b) (Teller et al., 2001) (Yeagle et al., 2001) (Okada et al., 2002) (Choi et al., 2002) (Okada et al., 2004) (Nakamichi and Okada, 2006a) (Nakamichi and Okada, 2006b) (Salom et al., 2006) (Standfuss et al., 2007) (Nakamichi et al., 2007) (Stenkamp, 2008) (Park et al., 2008) (Scheerer et al., 2008) (Choe et al., 2011a) (Standfuss et al., 2011)
Squid Rhodopsin (SR)	2Z73, 2ZIY [2]	Retinal	(Murakami and Kouyama, 2008) (Shimamura et al., 2008)
Turkey β 1 adrenergic receptor (β1AR)	2VT4, 2Y00, 2Y01, 2Y02, 2Y03, 2Y04 [6]	Cyanopindilol, Dobutamine Carmoterol, Isoprenaline Salbutamol	(Warne et al., 2008) (Warne et al., 2011)
Human β 2 adrenergic receptor (β2AR)	2R4R, 2R4S, 2RH1, 3D4S, 3KJ6, 3NY8, 3NY9, 3NYA, 3P0G, 3PDS [10]	Carazalol, Timolol, ICI 118,551, (molecule from Kolb et al, 2009), Alprenolol, BI-167107, FAUC50	(Rasmussen et al., 2007) (Cherezov et al., 2007) (Hanson et al., 2008) (Bokoch et al., 2010) (Wacker et al., 2010) (Rasmussen et al., 2011) (Rosenbaum et al., 2011)
Human A2A adenosine receptor (A2A)	3EML [1]	ZM241385	(Jaakola et al., 2008)
Human chemokine receptor CXCR4	3ODU, 3OE0, 3OE6, 3OE8, 3OE9 [5]	IT1t, CVX15	(Wu et al., 2010)
Human dopamine D3 receptor (D3R)	3PBL [1]	Eticlopride	(Chien et al., 2010)

1.2 RHODOPSIN: A PROTOTYPIC GPCR

1.2.1 Function of rhodopsin

Rhodopsin is a dim light photoreceptor present in the discs of the outer segment of rod photoreceptor cells in the retina. It constitutes approximately 85% of the total protein in the rod outer segment. The endogenous ligand for rhodopsin is the vitamin A derivative 11-*cis*-retinal, which is covalently attached to K296 in TM helix 6 (also see section **Error! Reference source not found.**). The key event in vision is the isomerization of 11-*cis*-retinal to all-*trans* retinal on incidence of light. This photo-isomerization of 11-*cis*-retinal in rhodopsin is extremely sensitive and responds to a single photon of light (Baylor, 1996). This event is followed by several transient intermediates that form in femto to nano second time scale and finally results in the formation of an active rhodopsin (Meta II) state in the micro second time scale (Fishkin et al., 2004). The Meta II state of rhodopsin binds the G protein heterotrimer (transducin; G_t - composed of α , β and γ subunits) and activates the alpha subunit (G_α) by catalyzing the exchange of GDP to GTP. G_α -GTP in turn activates phosphodiesterase (PDE), which hydrolyzes cyclic GMP and hyperpolarizes the photoreceptors by closing the cGMP gated ion channels. In dim light conditions, cyclic GMP keeps the channels in the photoreceptor membrane constantly open which depolarizes cells and leads to the release of the neurotransmitter glutamate in the synaptic cleft where rod cells meet ON bipolar cells (Protti et al., 2005) that express metabotropic glutamate receptors including uniquely mGluR6. G_α -GTP has intrinsic GTPase activity that hydrolyzes GTP to GDP and results in G_α -GDP, this step is also catalyzed by the regulator of G protein signaling (RGS) proteins. The inactive G_α -GDP combines with the $G_{\beta\gamma}$ to restore the holo-complex of G_t that can be re-activated by active rhodopsin. Rhodopsin is deactivated by

rhodopsin kinase (RK) that phosphorylates the C-terminus of rhodopsin on multiple serine and threonine residues. Phosphorylated rhodopsin then binds to β -arrestin, the binding of which blocks the interaction of rhodopsin with G_t . The Meta II state of rhodopsin ultimately decays to opsin and all-*trans* retinal with a half life of minutes. Rhodopsin is regenerated from opsin with a new molecule of 11-*cis* retinal that can re-enter the phototransduction cycle. A detailed review of different pathways and their regulation in visual signal transduction is given in (Chen, 2005).

1.2.2 Rhodopsin misfolding in Retinitis Pigmentosa

Retinitis pigmentosa (RP) is a disorder that initially causes night blindness and leads to progressive loss of vision in later life due to a gradual loss of rod and cone photoreceptor cells ultimately making patient blind. About 1 in 4000 people in the world is affected by RP (Hartong et al., 2006). Mutations in rhodopsin that cause it to misfold have been implicated in this retinal degenerative disease, RP (RetNet: <http://www.sph.uth.tmc.edu/Retnet/disease.htm#03.202d>). In 50-60% of the cases reported so far, RP is inherited as autosomal recessive, 30-40% cases are autosomal dominant and 5-15% cases are due to X-linked inheritance. About 45 genes have been identified in which mutations cause the disorder. However, these genes account for only 60% of the cases, the rest remains unidentified. Mutations in rhodopsin, highlighted in purple in (Figure 1.4), are responsible for 25% of autosomal dominant cases (RetNet: <http://www.sph.uth.tmc.edu/Retnet/disease.htm#03.202d>).

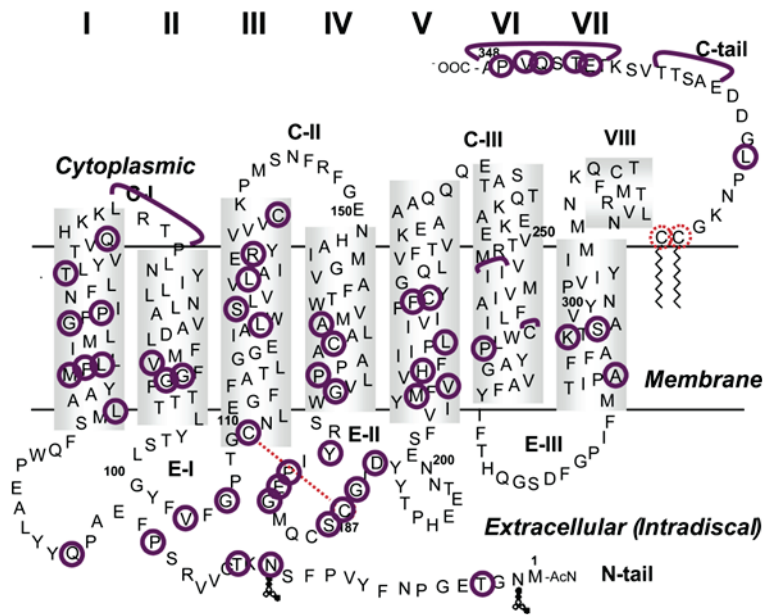


Figure 1.4 Retinitis Pigmentosa mutations in rhodopsin

This figure is a courtesy of Dr. Judith Klein-Seetharaman (source: Dr. Arpana Dutta's PhD thesis dissertation). Secondary structure representation of rhodopsin with residues responsible for RP is highlighted. Residues encircled in purple undergo point mutations and those marked with a purple line undergo deletions in RP. A disulfide bond between cysteines at positions 110 and 187 is shown in red dotted line and palmitoylation sites at Cys322 and Cys323 are encircled in red.

According to the human gene mutation database, more than 100 rhodopsin mutations are known to cause autosomal dominant RP (Krebs et al., 2010). Most of these mutations lead to misfolding and/or instability of rhodopsin as a result of which it is retained in the endoplasmic reticulum and is incapable of binding to its chromophore 11-*cis*-retinal (Kaushal and Khorana, 1994; Sung et al., 1991; Sung et al., 1993). Thus, aberrant folding of rhodopsin in the rod outer segments is believed to be one of the major causes of death of rod cells in autosomal dominant cases (Mendes et al., 2005).

Most of the mutations are present in the EC and TM regions, while a few mutations are present in the IC domain. Recent *in vitro* studies of RP mutations R135L, R135W (at the IC end

of TM3), P180A and G188R (second IC loop) demonstrated poor 11-*cis*-retinal retinal binding and variable levels of stability and folding compared to wild type rhodopsin (Iannaccone et al., 2006). This is similar to many other RP mutations that have been studied. However, this study in addition showed that the degree of misfolding is correlated with disease severity in patients. Studies to further provide a mechanistic understanding of the molecular basis for the severity in phenotype are needed. For example, RP mutants at the amino terminus of rhodopsin - P23H and N15S, are shown to misfold (Kaushal and Khorana, 1994; Tam and Moritz, 2009) in cells, but they differ drastically in disease severity (Innacone et al, unpublished results). In this thesis, I attempted to study trafficking and localization of the RP mutants P23H and N15S. There is considerable interest to use pharmacological chaperones to rescue these misfolded RP mutants (Krebs et al., 2010).

1.2.3 Dark-state structure of rhodopsin

The first crystal structure of a GPCR is that of rhodopsin and it is followed by several rhodopsin structures in different intermediate and active forms including opsin (Table 1.1). As described above rhodopsin is an integral membrane protein with seven TM helices with EC domain extending into the intradiscal space and the C-terminus facing the IC domain (Figure 1.5). The inverse agonist 11-*cis*-retinal is covalently bound to the side chain of K296 (Bownds, 1967; Wang et al., 1980) in the TM domain via a protonated Schiff base linkage which is stabilized by the counter-ion E113^{3.28} (Sakmar et al., 1989). The TM5 residues M207^{5.42}, F208^{5.43}, H211^{5.46}, F212^{5.47} and TM6 residues F261^{6.44}, W265^{6.48}, Y268^{6.51} and A269^{6.52} are most involved in retinal packing (Palczewski et al., 2000). The extracellular loop 2 (EC2) forms a stable beta sheet that is

closely packed against 11-*cis*-retinal forming a “plug” on the extracellular side of the ligand (Figure 1.5). There is a disulfide bond between C187 and C110 near the EC surface which is conserved in most of the GPCR family (Rader et al., 2004). The IC loops and the C-terminus are more flexible compared to the EC loops as evident from the lack of well ordered secondary structure and variable crystallographic B-factors in different crystal structures (Palczewski, 2006). In the IC domain there is a short amphipathic helix (helix 8) perpendicular to the TM helical bundle and it is anchored to the membrane via palmitoylation of C322 and C323. The TM and IC domains harbor conserved structural microdomains (Ballesteros et al., 2001b) in particular the ionic lock (E/DRY motif), CWxP motif (Shi et al., 2002) containing the rotamer toggle switch W265^{6.48} and the NPxxY motif (Fritze et al., 2003) all of which are shown to be important for activation of rhodopsin.

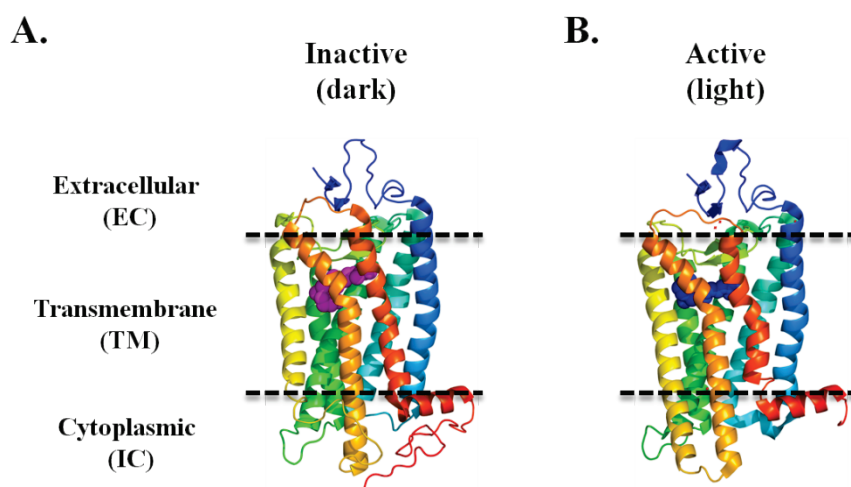


Figure 1.5 Inactive and active structures of rhodopsin

Cartoon representations of (A) inactive (dark; PDB id 1U19) and (B) active (light; PDB id: 3PXO) rhodopsin structures, colored from blue (N-terminus) to red (C-terminus). The bound 11-*cis*-retinal (magenta) and all-*trans*-retinal (blue) are shown as spheres in inactive and active structures respectively. The ordering on IC loop 2 (in blue) and the extension of TM5 (yellow) on the IC side are readily evident in the active structure compared to the inactive structure. The images were generated using PyMOL (Version 0.99rc6; <http://pymol.org/pymol>).

1.2.4 Structural changes during activation of rhodopsin

Recently, crystal structures of rhodopsin in its active Meta II and opsin states have been made available (Choe et al., 2011a; Park et al., 2008; Scheerer et al., 2008; Standfuss et al., 2011) (Table 1.1). Overall, compared to inactive structures, in the active structures there are relatively minor changes in TM1 - TM4 and helix 8 in the IC domain but there are major changes in TM5 - TM7 (Figure 1.5). A relative displacement of the IC ends of TM3 and TM6 was known previously to be the most prominent conformational change upon activation, while there are significant but smaller rearrangements in all parts of the IC domain (Altenbach et al., 2008; Hubbell et al., 2003; Park et al., 2008; Scheerer et al., 2008). Thus, the following picture for the events accompanying activation has emerged.

Photo-isomerization of 11-*cis*-retinal to all-*trans*-retinal results in movement of EC2 loop (Nakamichi and Okada, 2006a) that forms a “plug” on the extracellular side of the ligand. This EC2 movement is coupled to the outward rotation of TM5 owing to the rearrangement of hydrogen-bonding networks connecting EC2 and the extracellular ends of TM5. The shift in retinal β -ionone ring towards M207^{5.42} in TM5 triggers rearrangement of hydrogen network especially between TM3 and TM5. Several residues on TM3 like E113^{3.28}, G114^{3.29}, A117^{3.32}, G120^{3.35}, E122^{3.37} and W126^{3.41} are important in maintaining Meta II stability (Ou et al., 2011). H211^{5.46} interacts with E122^{3.37} and W126^{3.41} all of which are key for Meta II activation and point mutation studies of these residues all show effects on Meta II activation and stability (Lewis et al., 2006; Lin and Sakmar, 1996). Retinal isomerization also results in the rotation of W265^{6.48} (rotamer toggle switch) which results in reorientation of Y223^{5.58}, M257^{6.40} and Y268^{6.51} in TM6 (Ahuja and Smith, 2009; Patel et al., 2005).

The following reorganization of the IC domain is apparent from the active structures when compared to inactive structures (Park et al., 2008; Scheerer et al., 2008): (1) cytoplasmic loop 1 (IC1) makes a short helical turn, (2) TM5 is longer (1.5-2.5 turns) and is slightly shifted (2-3Å) towards TM6, (3) TM6 is displaced 6-7Å outward from the center and (4) there is a slight inward shift of TM7. This IC reorganization results in the breaking of the conserved ionic lock E/DRY and the rearrangement of the highly conserved NPxxY motif in TM7 (Ballesteros et al., 2001a; Fritze et al., 2003; Park et al., 2008; Scheerer et al., 2008). These rearrangements result in a more open IC domain that binds G_t (Scheerer et al., 2008).

In other GPCRs, during activation a change in distance between TM3 and TM6 upon ligand binding has also been experimentally observed similar to rhodopsin providing strong evidence that the mechanism of activation is fundamentally conserved (Gether, 2000; Hubbell et al., 2003; Schwartz et al., 2006; Shi et al., 2001). This is in line with the general view of the TM helices acting as rigid bodies in signal transduction by GPCRs (Altenbach et al., 2008; Farrens et al., 1996; Sakmar et al., 2002).

1.2.5 Comparison of other GPCR structures with rhodopsin structures

Other than bovine rhodopsin there are crystal structures available for six different GPCRs (Table 1.1). The recent advancement in obtaining crystal structures is partly due to the stabilization of GPCRs by replacing the IC3 loop with T4 lysozyme or a fragment of (Fab) monoclonal antibody domain (Rosenbaum et al., 2009). All GPCR structures share a similar overall structure in the TM regions. In contrast, even for rhodopsin from different species there are major changes in the IC domain. The IC domain of squid rhodopsin is markedly different from bovine rhodopsin. The IC ends of TM helices 5 and 6 (IC3 loop) along with helix 8 and an additional helix 9

(present only in squid rhodopsin) form a rigid protruding structure (Murakami and Kouyama, 2008). It is proposed that this IC domain feature is unique to G_q coupled GPCRs like squid rhodopsin. In bovine rhodopsin and other GPCRs the IC3 loop is thought to be flexible.

The first β 1AR structure to be crystallized was in complex with the antagonist cyanopindilol (Warne et al., 2008). Recently, additional structures bound with partial agonists dobutamine and salbutamol and full agonists carmoterol and isoprenaline became available (Warne et al., 2011). The overall structures are similar in all these wherein the receptor is thought to be present in an active, non signaling state formed on initial agonist binding. The EC2 loop forms a solvent exposed alpha helix towards the EC side in contrast to the buried beta sheet in rhodopsin. The ionic lock which is present in the dark (inactive) state of rhodopsin is broken in these structures even when bound to antagonists and partial inverse agonists. It has been suggested that even in the inactive state, β 1AR is never ‘fully off’ as seen in the dark state of rhodopsin (Congreve and Marshall, 2010). The cytoplasmic loop 2 (IC2) in β 1AR adopts an alpha helical structure which is different from the rhodopsin structure where it is in the extended conformation. Comparison of the ligand binding pockets suggests that all the ligands interact with S211^{5.42}. Additionally, full agonists also induce changes in the rotamer conformation of the side chains of both S212^{5.43} and S215^{5.46} that result in the weakening of TM4 and TM5 interactions and in the strengthening of TM5 and TM6 interactions which ultimately contracts the binding pocket by approximately 1Å. In the case of partial agonists, additional interaction with S215^{5.46} is absent (Warne et al., 2011).

The second GPCR to be crystallized after rhodopsin was β 2AR. The first structures were crystallized in the presence of the antagonist carazalol (Cherezov et al., 2007; Rasmussen et al., 2007). The structures of β 2AR are more similar to β 1AR than to rhodopsin. Like in β 1AR the

EC2 loop adopts an alpha helical structure, while the IC2 loop resembles an extended structure as present in rhodopsin. In contrast to rhodopsin, the TM domain is much more open and the kink observed in TM1 of rhodopsin is absent in β 2AR. The binding pocket of carazolol overlaps with that of retinal in rhodopsin with maximal overlap in the non-aromatic region of the ligands. The aromatic (β -ionone ring in retinal) portion is buried much deeper in the TM domain of rhodopsin than that in β 2AR. The ligand arrangement observed in β 1AR and β 2AR is similar. Also similar to β 1AR, the ionic lock which is present in the dark (inactive) state of rhodopsin is broken in the antagonist (carazolol) bound structures. Subsequently partial inverse agonist (timolol) (Hanson et al., 2008), inverse agonist(s) (ICI 118,551, compound from (Kolb et al., 2009)) and antagonist (alprenolol) bound structures (Wacker et al., 2010) were made available. These structures were similar to the carazolol bound structures with minor differences in the binding of ligands. Recently, two agonist bound structures, one stabilized with a nanobody and the other with covalently anchored agonist were crystallized (Rasmussen et al., 2011; Rosenbaum et al., 2011).

Like in β 1AR, all ligands binding to β 2AR interact with S203^{5.42}, while agonists make additional contacts with S207^{5.46}. In the nanobody-stabilized structure the nanobody is bound at the cytoplasmic domain in a manner similar to that of the G_t peptide binding in the active structure of opsin (Rasmussen et al., 2011; Scheerer et al., 2008). Also, in the IC domain, outward movements of TM6 and TM5 (approximately 11Å) and inward movements of TM7 and TM3 are observed. This is markedly different from the inactive carazolol bound structure but is similar to the active opsin structure. Interestingly, in the nanobody stabilized structure, the IC2 loop has an alpha helical structure similar to that of β 1AR. The transition between active and inactive structures of β 2AR is proposed to be triggered by the repacking of the residues P211^{5.50},

I121^{3.40}, F282^{6.44} and N318^{7.45} at the waist of the TM that induces small rotations in TM5 and TM6 (Sprang, 2011). The covalently bound agonist structure lacks the conformational changes observed at the IC domain of the nanobody-stabilized active structure. It was proposed that the agonist bound structures are intrinsically unstable and prefer inactive states unless stabilized by G protein or nanobody (Rasmussen et al., 2011).

In the A2A receptor structure, the EC2 loop lacks the secondary structure which is in contrast to rhodopsin, β 1AR and β 2AR (Jaakola et al., 2008). The antagonist (ZM241385) binding in the A2A structure is unique as it is oriented almost perpendicular to the plasma membrane and positioned more towards the EC side with maximal interactions with EC2 and EC3 loops. Like in β 1AR and β 2AR, the ionic lock is broken in the A2A structure.

In 2010, crystal structures of CXCR4 (Wu et al., 2010) and D3R (Chien et al., 2010) became available. The CXCR4 structures were crystallized with the antagonist, IT1t, and the cyclic peptide inhibitor, CVX15. The CXCR4 structures prominently lacked helix 8 that is present in rhodopsin, β 1AR, β 2AR and A2A. The IC half of the TM bundle of CXCR4 is more similar to other GPCR structures compared to the EC half. Unlike in other GPCRs, the ligand binding pocket is larger, more open and closer to the EC surface. Also, the small molecule antagonist only contacts residues in TM 1, 2, 3 and 7 compared to ligands in other GPCR structures that also contact helices 4, 5 and 6.

The D3R structure was crystallized with the antagonist eticlopride (Chien et al., 2010). The EC2 domain is shorter and lacks well defined secondary structure as present in other GPCR structures. Interestingly, the IC2 loop has an alpha helical structure only in one of the monomers in the asymmetrical crystal dimer suggesting an inherent conformational flexibility of this domain. The binding site of eticlopride overlaps with the carazalol binding site in β 1AR. Like in

dark-state rhodopsin, the D3R structure is the only other structure with the ionic lock present in the inactive state of the receptor.

Overall, structurally the TM domain conformations share more similarity on the IC half compared to EC half. This is not surprising considering that enormous diversity of ligands that bind on EC half of TM, compared IC half which only interacts with conserved G protein partners.

1.3 METABOTROPIC GLUTAMATE RECEPTORS (MGLURS)

Metabotropic glutamate receptors are class C GPCRs that modulate glutamate mediated neurotransmission. Glutamate is the most important excitatory neurotransmitter in the brain and plays an important role in many different functions of the central nervous system such as memory, learning, sensory processing like vision, synaptogenesis and pain transmission (Bleakman and Lodge, 1998; Collingridge and Singer, 1990; Conn and Pin, 1997; Hollmann and Heinemann, 1994; Monaghan et al., 1989). Dysfunction of glutamate signaling plays a role in the pathogenesis of brain damage associated with various neurological disorders and neurodegenerative diseases (Meldrum, 2000; Meldrum et al., 1999; Monaghan et al., 1989). Larger concentrations of glutamate in the extracellular space are toxic and complex systems have evolved to regulate and respond to glutamate concentrations both temporally and spatially. The actions of glutamate are regulated by ionotropic and metabotropic glutamate receptors (mGluR). mGluRs are both functionally and pharmacologically different from ionotropic receptors. Ionotropic glutamate receptors are ion channels that directly control the activation state of neurons, while mGluRs are GPCRs that modulate signaling via G proteins.

1.3.1 Subtypes and classification

There are eight different subtypes of mGluRs. There are also alternative splice forms of mGluRs that differ by length and composition of the C-terminal sequence following the last TM helix (Conn and Pin, 1997; Minakami et al., 1993; Pin et al., 1992; Tanabe et al., 1992). The different subtypes are further divided into three groups based on sequence homology, signal transduction and pharmacological properties (Table 1.2) (Nakanishi, 1994; Pin and Duvoisin, 1995). Group I mGluRs (mGluR1 and 5) are coupled to $G\alpha_q$ which increases phospholipase C activity, while group II (mGluR2 and 3) and group III (mGluR4, 6, 7 and 8) receptors are coupled to $G\alpha_{o/i}$ which decreases adenylyl cyclase (AC) activity on activation (Enz, 2007; Swanson et al., 2005).

Table 1.2 Classification and properties of different subtypes of mGluRs

Information on intracellular actions and tissue expression are obtained from (Niswender and Conn, 2010).

Group	subtype	G protein coupling	Intracellular actions	Tissue expression
I	mGluR1 mGluR5	Excitatory G_q coupled	Phospholipase C stimulation MAP kinase phosphorylation	Neurons (postsynaptic) mGluR5 is also present on astrocytes
II	mGluR2 mGluR3	Inhibitory G_o coupled	Decrease cAMP levels Activation of K^+ channels Inhibition of Ca^{++} channels	Neurons (pre and post synaptic)
III	mGluR4 mGluR6 mGluR7 mGluR8	Inhibitory G_o coupled	Decrease cAMP levels Activation of K^+ channels Inhibition of Ca^{++} channels	Neurons (presynaptic) mGluR6 is restricted to ON bipolar retinal cell (post synaptic)

1.3.2 General function of mGluRs

mGluRs are predominantly expressed in the central nervous system (CNS). Group I mGluRs are generally located postsynaptically and play an important role in regulating fast synaptic transmission mediated by glutamate. Therefore, they are involved in synaptic plasticity phenomena, including long-term potentiation and long-term depression (Pin et al., 2003). Group II mGluRs are present both pre- and post-synaptically and are thought to have a role in drug addiction, anxiety and schizophrenia (Pin et al., 2003). Group III mGluRs are mostly present pre-synaptically and function to inhibit glutamate release (Pin et al., 2003). Among group III mGluRs, mGluR6 is uniquely expressed on the ON bipolar cells of retina and its disruption results in loss of dim light (scotopic) vision (Masu et al., 1995; Nomura et al., 1994; Ueda et al., 1997; Zeitz et al., 2005). Like rhodopsin, mGluR6 has a key role in visual transduction, especially in scotopic vision (see section 1.4.1).

1.3.3 mGluRs in addiction

Most drugs of abuse have been shown to stimulate excitatory glutamatergic transmission through brain reward circuitries (Kalivas and Duffy, 1998; Kenny and Markou, 2004). Group II mGluRs in particular have been implicated in nicotine addiction in studies with animal models (Kenny et al., 2003a; Kenny et al., 2003b). However, the specific role of mGluRs in addiction has not been firmly established and a systematic analysis of the role of different subtypes has not been carried out. The dipeptide glycine-glutamine (Gly-Gln; derived from β -endorphin) is a modulator of addiction to a variety of drugs as established by the laboratory of W.R. Millington and coworkers (Cavun et al., 2005; Goktalay et al., 2006; Resch et al., 2005). Rats that were simultaneously

administered nicotine and Gly-Gln were found to be less susceptible to nicotine addiction than rats administered nicotine alone (Goktalay et al., 2006). Similar effects were observed independently in rats when Gly-Gln was administered prior to the intake of substances of abuse including morphine (Cavun et al., 2005) and alcohol (Resch et al., 2005). While glutamatergic signal transduction has been implicated as the underlying mechanism for this effect, the actual target(s) for Gly-Gln are not known. Recently mGluR6 and mGluR8 have been implicated in heroin addiction through genome-wide association studies (Nielsen et al., 2008).

1.3.4 Structural organization of mGluRs

All classes of GPCRs including mGluRs consist of a seven helix TM bundle, the G-protein interacting IC domain and EC domain (Figure 1.1). However, mGluRs as members of the class C GPCRs have very low sequence identity to other GPCRs especially class A and are additionally distinguished by their unique, large extracellular amino terminal domain (ATD) that serves as the endogenous ligand binding site (Figure 1.2). ATD also forms an inter-subunit disulfide bridge resulting in covalently bound mGluR homodimers (Romano et al., 1996). In mGluRs there is an additional cysteine rich domain (CRD) connecting ATD with the TM domain (Figure 1.6). Cysteine mutation studies that disrupt the inter subunit disulfide bond in the ATD indicate that these receptors can still associate and form functional dimers through non-covalent interactions (Romano et al., 2001; Tsuji et al., 2000). However, disruption of the intra-subunit disulfide bond between the ATD and CRD results in loss of activity in response to orthosteric ligands (Rondard et al., 2006). Finally, the TM regions of mGluRs are shown to harbor allosteric binding sites which modulate receptor function (Pin et al., 2004).

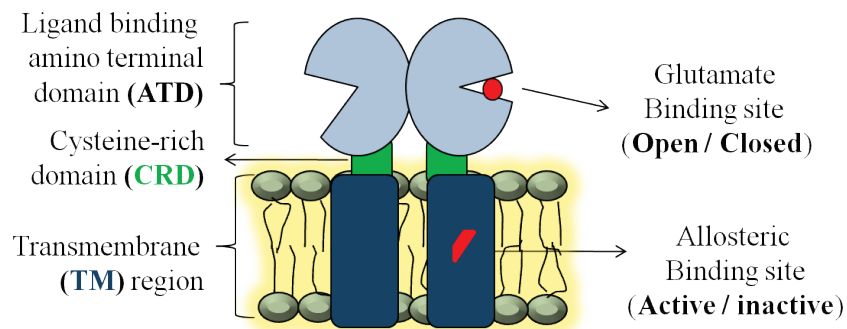


Figure 1.6 Schematic of mGluR domain organization

mGluRs have an extracellular amino terminal ligand binding domain (ATD), cysteine rich domain (CRD) and transmembrane (TM) regions. A disulfide bridge in the ATD is formed between individual subunits of the homodimer. The ATD is proposed to exist in equilibrium between open and closed conformations, with agonist binding shifting the equilibrium to the open conformation. The TM domains in mGluRs harbor an allosteric ligand binding pocket (shown in red).

1.3.5 Available structures of mGluRs

The soluble EC domain of mGluRs have been expressed as independent fragments lacking the TM regions and are shown to still bind glutamate and glutamate-derived agonists/antagonists equally well as the full length receptors (Okamoto et al., 1998). The EC domains share homology with the bacterial Leu/Ile/Val-binding protein (PDB id: 2LIV) (O'Hara et al., 1993; Sack et al., 1989). Direct structural information on mGluRs is also available for several EC domains. The soluble EC domains of mGluR1 (Kunishima et al., 2000; Tsuchiya et al., 2002), mGluR3 (Muto et al., 2007) and mGluR7 (Muto et al., 2007) have been published. Recently, crystal structures of mGluR5 were made available in the PDB (see Table 1.3 for details). The EC domain is proposed to exist in equilibrium between open and closed conformations (Kunishima et al., 2000), with

agonist and antagonist binding shifting the equilibrium to the closed and open conformations respectively (Table 1.3).

Table 1.3 Summary of amino terminal ligand binding domain structures of mGluRs

The ATD structures are crystallized without ligands and with agonists and antagonists. The details of individual chains are also given in the table. ^aAntagonists are highlighted in bold.

Receptor	Ligand	CHAIN A	CHAIN B	PDB (Å)	Ref.
Rat mGluR1	--	Open	Open	1EWT (3.7)	(Kunishima et al., 2000)
	--	Closed	Open	1EWV (4)	
	Glutamate	Closed	Open	1EWK (2.2)	
	Glutamate	Closed	--	1ISR (4.0)	(Tsuchiya et al., 2002)
	S-MCPG^a	Open	Open	1ISS (3.3)	
	LY341495	Open	Open	3KS9 (1.9)	(Dobrovetsky et al, 2009) To be published
Rat mGluR3	Glutamate	Closed	Closed	2E4U (2.35)	(Muto et al., 2007)
	DCG-IV	Closed	Closed	2E4V (2.40)	
	1S,3S-ACPD	Closed	Closed	2E4W (2.40)	
	1S,3R-ACPD	Closed	Closed	2E4X (2.75)	
	2R,4R-APDC	Closed	Closed	2E4Y (3.40)	
Rat mGluR7	--	Open	--	2E4Z (3.3)	(Dobrovetsky et al, 2009) (Dobrovetsky et al, 2010) To be published
	LY341495	Open	Open	3MQ4 (2.8)	
Rat mGluR5	Glutamate	Closed	Closed	3LMK (2.44)	

Very little is known about the structure of the TM domain of mGluRs. The only crystallized GPCR for a long time was rhodopsin (Palczewski et al., 2000). Only recently crystal structures for six other class A GPCRs became available (Table 1.1). The rhodopsin crystal structure has served as a reliable template for a large number of homology modeling studies of various members of the GPCR family (Archer et al., 2003; Filipek et al., 2003), including mGluRs (Malherbe et al., 2003a; Malherbe et al., 2003b). TM Models for mGluR1 and mGluR5

were shown to fit experimental evidence remarkably well (Malherbe et al., 2003a; Malherbe et al., 2003b). We demonstrated using computational studies that the TM domains exist in active or inactive forms and they preferentially bind positive or negative allosteric modulators (Figure 1.6) (Yanamala et al., 2008) (chapter 7.0).

1.3.6 Activation mechanism of mGluRs

In mGluRs, ATD serves as the endogenous ligand binding site, in contrast to rhodopsin which has the binding site in the TM domain (Figure 1.2). Based on the crystallographic data of the ATD of mGluRs (Kunishima et al., 2000; Tsuchiya et al., 2002) and FRET-based studies of mGluR1 (Tateyama et al., 2004) it was proposed that in the resting state, the TM domains of the two monomeric receptor subunits in a dimer are associated and activation is a result of inter-subunit rearrangements. On the other hand, from the recent ATD and CRD domain crystal structures (Muto et al., 2007) it has been hypothesized that the dimerization of the domains precedes activation. Thus, changes in inter-subunit interactions may play an important role in mGluRs and in general for class C GPCR activation.

In contrast to these inter-subunit activation models, conformational changes within receptors are known to be at the heart of the activation mechanism of class A GPCRs (Hubbell et al., 2003; Klein-Seetharaman, 2002). Support for such intra-molecular changes being important for mGluRs has come from the discovery of allosteric ligands. These allosteric ligands bind in a pocket analogous to the retinal binding pocket in rhodopsin (Noeske et al., 2006), in line with a general similarity between rhodopsin and mGluR activation. Allosteric ligands do not compete with glutamate for its binding pocket in the ATD and can positively or negatively modulate the response of mGluRs to glutamate. Allosteric ligands are shown to serve as direct agonists and

antagonists only in the absence of the ATD (Goudet et al., 2004). We have shown that the conformational changes observed in rhodopsin when translated to mGluRs can adequately explain whether a ligand is a positive or negative modulator in a large number of cases (Yanamala et al., 2008) (chapter 7.0). Thus, the TM domain may play a similar role in activation of all GPCRs which I will refer to here as the “generality hypothesis”, as proposed in numerous studies (Gether, 2000; Goudet et al., 2004; Rondard et al., 2011; Schwartz et al., 2006).

1.3.7 Pharmacology of mGluRs: the therapeutic potential of allosteric ligands

The preferred conformation of glutamate when bound to different mGluRs varies very little as evident from the crystal structures of different mGluRs (Table 1.3). There are several glutamate analogs that have been developed to act as agonists and antagonists of mGluRs but very few of them are specific to a given subtype (Table 1.4). However, the therapeutic potential of glutamate competitors has been limited. More recently non-competitive ligands have been discovered that are more specific for a given mGluR subtype. Typically, these ligands alter the effects of glutamate binding to a receptor, as positive or negative allosteric modulators. Modulatory drugs are promising because they only act when receptor activation has occurred and are generally more specific for receptor subtypes than competitive drugs. The difference between negative and positive modulation can be very subtle, as has been shown for the benzaldazine and MPEP analogs where the position of identical ring substitutions alters the effect of the drug on mGluR5 (O'Brien et al., 2003; Wood et al., 2011). Detailed experimental mutagenesis and chimera studies, in conjunction with modeling, have revealed that allosteric ligands bind to the TM domain of mGluRs (Fukuda et al., 2009; Hermans et al., 1998; Litschig et al., 1999; Malherbe et al., 2006; Pagano et al., 2000; Varney et al., 1999). The therapeutic potential of allosteric drugs

targeted at mGluRs has been demonstrated for treatment of a number of conditions, including pain, epilepsy, Parkinson's disease, cognitive disorders, drug abuse, anxiety and schizophrenia (Conn and Pin, 1997; Kew, 2004).

mGluR1 and mGluR5 (group I) are pharmacologically the best characterized mGluRs as evident from the variety of allosteric ligands that are available for these two subtypes (Table 1.4). In general group III mGluRs are pharmacologically poorly characterized.

Table 1.4 Competitive and allosteric ligands for mGluRs

The ligands are taken from IUPHAR database (Sharman et al., 2011) and from (Niswender and Conn, 2010). The second row in the table lists ligands that are known to bind all mGluRs. In each group the first row refers to ligands that bind to all subtypes in the particular group.

Group	Subtype	Agonist	Antagonist	Allosteric regulator
I/ II/ III	Non selective	L-glutamate (1S,3R)-ACPD	LY341495	
I	Group I preferred	(S)-3HPG (S)-3,5-DHPG Ibotenate L-CCG-I L-Quisqualate	(S)-MCPG (S)-4C3HPG (S)-4CPG DCG-IV	
	mGluR1		AIDA LY367385	BAY 367620, CPCCOEt, DM-PPP, EM-TBPC, JNJ16259685, FTIDC, NPS2390, R214127, Ro01-6128, Ro67-4853, Ro67-7476, VU71, YM298198
	mGluR5	CHPG		5-MPEP, ADX-47273, BOMA, CDDPB, CPPHA, DFB, Fenobam, MPEP, MTEB, MTEP, PTeB, SIB-1757, SIB-1893, VU29
II	Group II preferred	(1S,3R)-ACPD (2R,3R)-APDC DCG-IV L-CCG-I LY354740 LY379268	(S)-MCPG eGlu LY341495 MGS0039	
	mGluR2	(S)-4C3HPG MGS0028	MSOP	3-MPPTS, 4-MPPTS, PTBE, LY487379, BINA
	mGluR3	NAAG		
III	Group III preferred	(R,S)-4-PPG (S)-3,4-DCPG L-AP4 (1S,3R)-ACPD L-CCG-I L-SOP	LY341495 MAP4 MPPG CPPG	
	mGluR4	ACPT-I FP0429		PHCCC, SIB-1893, MPEP, VU0155041
	mGluR6	1-benzyl-APDC ACPT-I LY354740 LY379268	DCG-IV MSOP	
	mGluR7		(S)-MCPG DCG-IV MCCG MSOP MSOPPE	AMN082, MMPPI
	mGluR8	ACPT-I D-AP4 LY354740	DCG-IV MSOP	

1.4 METABOTROPIC GLUTAMATE RECEPTOR SUBTYPE 6

Rat mGluR6 was first isolated from a retinal cDNA library in 1993 and it was shown that it negatively regulates adenylyl cyclase and reduces forskolin-elevated cAMP levels in response to agonist (Nakajima et al., 1993). Human mGluR6 was cloned and its response to several agonists was characterized in 1997 (Laurie et al., 1997). mGluR6 is uniquely expressed in the ON bipolar cells and like rhodopsin plays a key role in scotopic (night) vision (Nomura et al., 1994; Ueda et al., 1997).

1.4.1 mGluR6 function in vision

Bipolar cells are the second order neurons that relay the signal from the photoreceptor cells to enable vision. There are two fundamentally different types of bipolar cells, ON and OFF. ON bipolar cells preserve the signaling information from the photoreceptor cells, and OFF-bipolar cells inverse it. Most mammals have nine cone bipolar cells (ON and OFF types) and only one rod bipolar cell (ON type) (Ghosh et al., 2004; Pignatelli and Strettoi, 2004). The OFF bipolar cells produce excitatory signals under photopic conditions (daylight). The ON bipolar cells produce excitatory signals under scotopic conditions (night). OFF bipolar cells are activated like most neurons by ionotropic glutamate receptors (iGluR), which are glutamate-gated cation channels. In contrast, ON bipolar cells uniquely express mGluR6 (Nomura et al., 1994; Ueda et al., 1997) which is involved indirectly in modulation of synaptic transmission and cell excitability.

1.4.2 Putative function of mGluR6 in addiction

In addition to its key role in night vision, mGluR6 has been implicated in heroin addiction and methadone maintenance treatment of chronic addiction through genome-wide association and pharmacogenetic studies (Fonseca et al., 2010; Nielsen et al., 2008). It is suggested that a pharmacogenetic epistatic effect between single nucleotide polymorphism variants in myocardin (which has also been previously associated with the risk of opioid dependence disorder) and mGluR6 genes appears to modulate inter-individual variations in methadone maintenance treatment response (Fonseca et al., 2010). In the same genome wide association study that identified mGluR6 another group III member, mGluR8 was also identified to have a role in addiction (Nielsen et al., 2008)

1.4.3 mGluR6 ligands

Several mGluR6 agonists (L-2-amino-4-phosphonobutyrate (L-AP4), L-serine-O-phosphate (L-SOP), L-glutamate (L-Glu), carboxycyclopropyl glycine (L-CCG-I), (R,S)-PPG, ACPT-I) and antagonists (MAP4, MSOP, DCG-IV, MPPG, CPPG, LY341495) have been identified (Lavreysen and Dautzenberg, 2008). However, there are no selective competitive or allosteric ligands developed for mGluR6 (Table 1.4).

1.4.4 mGluR6 signal transduction cascade

Our current understanding about GPCR mediated signal transduction is from studying the mechanisms of vertebrate photo-transduction. Earlier studies have suggested that the mGluR6

signal transduction cascade is analogous to photo-transduction in photoreceptors (de la Villa et al., 1995; Nawy and Jahr, 1990a, b; Shiells and Falk, 1990; Walters et al., 1998). Light-induced hyperpolarization of the photoreceptor cells reduces the glutamate release from the synaptic terminal (Protti et al., 2005). Like in the rest of the brain, glutamate is the most important excitatory neurotransmitter in the visual system. In dim-light conditions there is a tonic release of glutamate from photoreceptors which activates mGluR6 on the ON bipolar cells. In mGluR6 knockout mice, the b-wave in electroretinograms that is a characteristic of ON bipolar cell activity is absent (Masu et al., 1995; Tagawa et al., 1999). Furthermore, electroretinograms in human subjects with mutations in mGluR6 also lack b-waves and are found to be the cause for congenital stationary night blindness (CSNB) (Dryja et al., 2005; O'Connor et al., 2006; Zeitz et al., 2005).

Like in rhodopsin, mGluR6 triggers a G protein cascade which hyperpolarizes the cell by closing a non-selective cation channel (Figure 1.7). The specific channel associated with the mGluR6 signal cascade has been recently identified to be the transient receptor potential cation channel subfamily M member 1 (TRPM1) (Koike et al., 2010; Morgans et al., 2009; Shen et al., 2009). Recently, several mutations in TRPM1 have been associated with CSNB in humans (Nakamura et al., 2010). TRPM1 is predominantly expressed in the eye and skin (Koike et al., 2010). Remarkably, Appaloosa horses skin coloration has been linked to CSNB (Bellone et al., 2008), thus, linking eye and skin conditions. It has been proposed that TRPM1 takes a role in melanoma associated retinopathy, a rare disease condition of both skin and eye (Morgans et al., 2010).

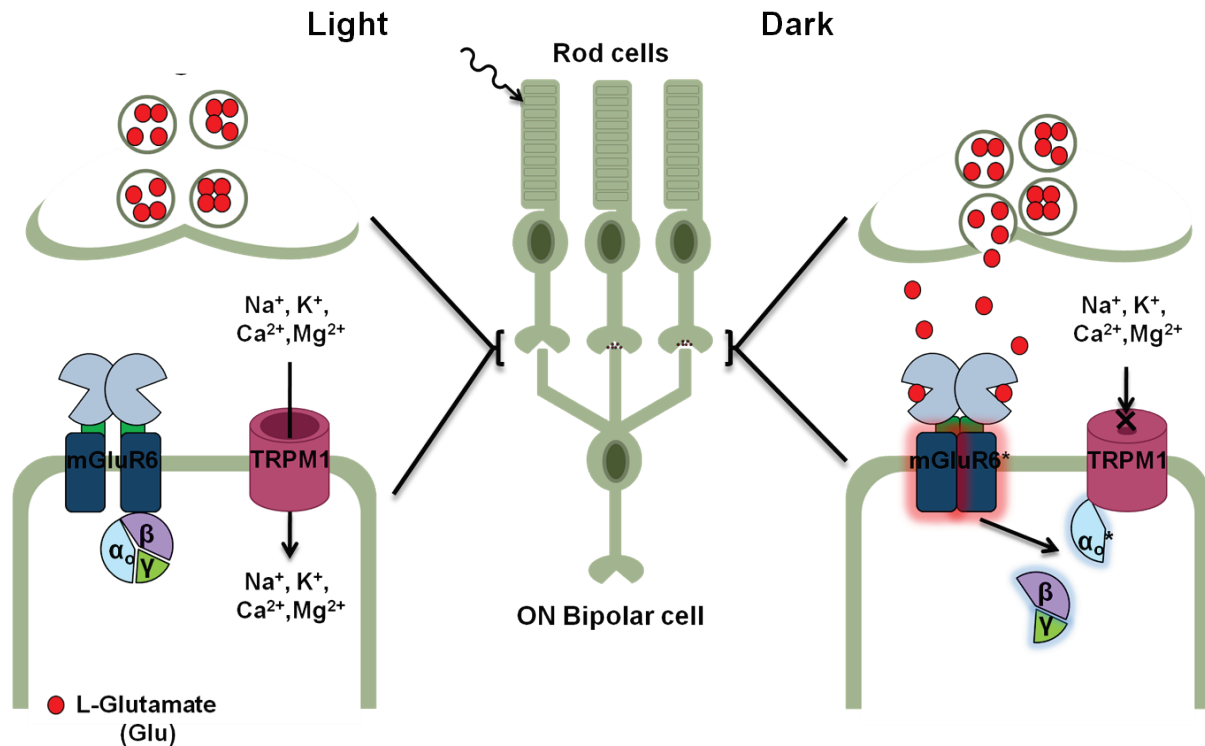


Figure 1.7 Schematic representation of a rod and ON bipolar synapse and function of mGluR6

Shown in the figure are rod cells forming a synapse with the ON bipolar cells. Under dim light conditions, the rod cells are depolarized and there is a tonic release of glutamate which results in activation of mGluR6 on concomitant closure of TRPM1 channel in ON bipolar cells. Shown in red circles is glutamate.

The $G\alpha$ subunit of the G protein heterotrimer activated by mGluR6 is $G\alpha_{o1}$ (Dhingra et al., 2002; Huang et al., 2003; Nawy, 1999; Vardi et al., 1993; Weng et al., 1997). Electroretinograms of mice lacking $G\alpha_o$ also lack the b-wave, much like the mGluR6 knockout mice (Dhingra et al., 2000). The involvement of a specific $G\beta$ subunit in the mGluR6 signaling cascade is still not clear. Evidence based on cDNA hybridization of single-cell polymerase chain reactions suggests the presence of $G\beta_{3/4}$ in ON bipolar cells (Huang et al., 2003). However, immunofluorescence and co-immunoprecipitation, studies suggest $G\beta_5$ as a possible candidate

(Morgans et al., 2007). The likely $G\gamma$ subunit partner is $G\gamma_{13}$ which is also shown to be present in ON bipolar cells (Huang et al., 2003) and forms dimers with all $G\beta$ subunits (Blake et al., 2001).

Other members of the mGluR6 signal cascade involve (but are not limited to) regulators of G-protein signaling (RGSs), cGK, L7/pcp2 and nyctalopin (Duvoisin et al., 2005). RGSs are known to enhance the GTP hydrolysis activity of $G\alpha$ subunits. The probable RGS candidates involved in mGluR6 signaling are RGS7 and RGS11 as they were shown to complex with $G\beta_5$ in ON-bipolar cells (Morgans et al., 2007). Deactivation of mGluR6 is proposed to involve phosphorylation of mGluR6 by cGMP-dependent kinase (Duvoisin et al., 2005; Morgans et al., 2010). The L7/pcp2 purkinje cell protein contains a 19 amino acid GoLoco or GPR motif (G protein regulatory) and may prolong mGluR6 activity by inhibiting re-association of $G\alpha_o$ and $G\beta\gamma$ (Duvoisin et al., 2005). Finally, it has been proposed that nyctalopin participates in mGluR6 signaling (Morgans et al., 2010), because like the $G\alpha_o$ and the mGluR6 knockout mice, the b-wave is absent in the nyctalopin knockout mice and in patients with CSNB (Demas et al., 2006). The actual function of nyctalopin and the second messenger signal between $G\alpha_o$ and TRPM1 are still unknown (Morgans et al., 2010).

1.5 OPEN QUESTIONS, AIMS, ACCOMPLISHMENTS AND CONTRIBUTIONS

1.5.1 Open questions

It is clear that, like rhodopsin, mGluR6 takes a key role in visual signal transduction, specifically in scotopic vision. However, rhodopsin is the prototypical GPCR, and its structure-function relationship is well characterized. In contrast for mGluR6, and class C GPCRs in general, the

mechanism of activation is poorly understood. In addition to its key role in night vision, mGluR6 has been implicated in heroin addiction and methadone treatment of chronic addiction through genome-wide association and pharmacogenetic studies (Fonseca et al., 2010; Nielsen et al., 2008). However, mGluR6 selective agonists and antagonists have not been reported yet thus preventing pharmacological characterization. In this thesis I have studied the following open questions.

(a) Is the GPCR activation mechanism conserved between class A and C GPCRs? Support for the notion that the TM domain changes its conformation and that this is an important event for mGluRs signaling has come from the discovery of allosteric ligands, an observation consistent with a general similarity between rhodopsin and mGluR activation. The TM domain may play a similar role in activation of all GPCRs, referred to in this thesis as the “generality hypothesis”.

(b) Are there allosteric ligands and selective orthosteric ligands for mGluR6? Unlike other members of the mGluR family, no allosteric ligands are known for mGluR6. Absence of such selective ligands makes pharmacological characterization of mGluR6 difficult, thus hindering development of modulators to enhance night vision and characterization of the hypothesized role of mGluR6 in addiction.

1.5.2 Specific aims

This thesis aims to investigate structure-function relationships of mGluR6 and identify ligands specific for mGluR6. The long-term goal of this thesis is to understand the role of mGluR6 in vision and addiction. I propose the following specific aims to address the open questions stated above:

Specific aim 1: To enable mGluR6 structure-function studies.

Specific aim 2: To identify ligands for mGluR6.

Specific aim 3: To investigate the conformational changes in the TM domain on activation.

1.5.3 Outline of approaches

Both, experimental and computational approaches have been integrated here to carry out structure-function studies and identify selective ligands for mGluR6. Firstly, due to the lack of a well-established expression system for mGluR6, mammalian stable cells lines with high levels of mGluR6 expression had to be created. Following this, robust functional assays in the cellular and membrane environment were optimized and developed to characterize the function and activation mechanism of mGluR6. Computational approaches followed by functional assays in cells and in membranes were adopted to screen potential selective ligands for mGluR6. Finally, a sequence based computational approach was carried out to identify allostery and long-range interactions in rhodopsin and these observations were extended to further characterize the activation mechanism of mGluR6. Specifically, the following experiments were carried out address the three specific aims.

Specific aim 1. To enable mGluR6 structure-function studies. To enable structure-function studies we need an expression system to produce medium-large quantities of mGluR6. GPCRs including mGluR6 are difficult to express in heterologous systems. Moreover it is a challenge to extract GPCRs from cell membranes and reconstitute them into detergent solutions while retaining the receptor function. There was a lack of (a) cell lines with high expression for

mGluR6, (b) robust functional assays and (c) purification protocols for mGluR6. Thus, we focused our efforts to develop these in order to address our open questions. Wild-type, truncated mutants lacking the ligand binding domain (for allosteric ligand binding studies) and TM domain cysteine mutants (for activation studies) of mGluR6 were cloned into expression vector pACMV-tetO containing a tetracycline inducible promoter (chapter 2.0). Stable HEK293S cell lines were created with high levels of receptor expression. Folding of mGluR6 was verified by confocal immunofluorescence, glycosylation and dimerization studies (chapters 3.0 and 4.0). A cAMP based functional assay was optimized and implemented to establish functionality of mGluR6 in cells (chapter 5.0). A high throughput Europium based fluorescence assay in membranes was developed to determine the function of mGluR6 in membranes and to test the activity of mGluR6 in presence of different ligands (chapter 5.0). In order to enable studies with purified mGluR6 it was imperative to check its functionality in presence of detergents. For this, large scale detergent screens were performed to identify suitable detergents for mGluR6 purification (chapter 4.0). The cloning of wild-type and mutant mGluR6, establishment of stable cell lines, receptor folding, detergent screens and development of functional assays are described in chapters 2.0 to 5.0.

Specific aim 2. To identify ligands for mGluR6. Potential ligands were computationally identified in a two-step process: i) three dimensional structural models were created for the mGluR6 ligand binding domain by building homology models and ii) a virtual library of molecules was screened using ligand docking methods (chapter 6.0). The computationally identified ligands were tested for their effect on activity of mGluR6 using functional assays. The

screening procedure and experimental testing of both competitive (chapter 6.0) and allosteric ligands (chapters 7.0 and 8.0) are described.

Specific aim 3. To investigate the conformational changes in the TM domain accompanying activation. In mGluRs ligand binding in the ATD activates the IC domain through TM regions. But the actual conformational changes in TM domain during activation are not yet identified. The role of the TM domain in the activation mechanism of mGluR6 was investigated by mutating conserved endogenous cysteines in TM5 and TM6 and probing the resulting functional changes in the receptor (chapter 9.0). In order to take advantage of the well-established detergent reconstituted functional assays for rhodopsin mGluR6 and rhodopsin, chimeras where the TM domain of mGluR6 was switched with that of rhodopsin were created (chapter 10.0). Additionally, computational sequence analysis tools were used first to identify long-range interactions involved in activation of rhodopsin and then the findings were extended to mGluR6 (chapter 11.0).

1.5.4 Summary of research accomplishments and contributions

With respect to the three specific aims pursued in this thesis, the following contributions were achieved.

Accomplishments and contributions to Aim 1: Several mammalian expression systems producing functional wild-type mGluR6 and its mutants were established thus providing general systems that can be used for functional and pharmacological characterization of mGluR6. The

optimal growth and induction conditions in cell culture plates and spinner flasks were optimized to express large amounts of receptor proteins. I have addressed the needs for optimization of the well known cell based cAMP functional assay and also developed a novel Europium fluorescence based high-throughput functional assay. I showed that mGluR6 expressed in HEK293S cells are active in cell and membrane environments. Efforts to obtain purified mGluR6 involving detergent screening for solubilization and reconstitution and optimization of antibody affinity purification of mGluR6 have also been initiated.

Accomplishments and contributions to Aim 2: I have identified novel orthosteric and allosteric ligands for mGluR6 both computationally and experimentally. Based on a virtual library screen a tetrazole containing molecule (Omega_352) was identified to be a selective agonist for mGluR6. Initial trials of experimental testing of this ligand so far lacked activity. The lack of activity could also be a result of the potential cyclization of the molecule during synthesis.

I also predicted the binding of dipeptides (Gly-Glu and Gly-Gln) to mGluR6. These dipeptides have been previously shown to modulate addiction in mice through glutamatergic systems. The docking studies predicted that all the dipeptides may act as agonists. The predictions were successfully validated in terms of binding (although not agonism versus antagonism) of Gly-Glu and Gly-Gln. Both molecules acted as inverse agonists. These findings for the first time provide direct evidence that dipeptides may act through mGluRs.

I tested the potential allosteric ligands 11-*cis* retinal, all-trans retinal, PHCCC, DFB, MPEP and CPCCOEt – all predicted to bind in the TM domain of mGluR6 for modulatory activity of mGluR6 function. Out of these I showed that PHCCC is a direct inverse agonist for mGluR6. This makes PHCCC first such ligand for mGluR6.

I have contributed to the finding that that anthocyanins and porphyrins (Ce6) modulate rhodopsin activity by directly interacting at the cytoplasmic domain. I tested if these compounds had any effect on mGluR6 activity and found that Ce6 inhibits mGluR6 activity.

Accomplishments and contributions to Aim 3: I identified that TM6 plays a key role in the activation of mGluR6 based on activation assays with conserved endogenous TM cysteines mutated to alanine. TM6 is the most conserved helix in mGluRs and our findings strongly support the generality hypothesis that this helix plays a major role in activation of Class A and Class C GPCRs alike.

I designed mGluR6:Rhodopsin chimeras wherein the TM domain of mGluR6 is replaced with that of rhodopsin. Preliminary characterization of these chimeras suggests that they can bind 11-*cis*-retinal (the ligand for rhodopsin) when it is added directly to the cells expressing these constructs, providing further support to our hypothesis that the function of TM domains is conserved between class A and C GPCRs.

Using computational sequence analysis I identified long-range interactions between the extracellular and intracellular domains. I showed that these are mediated via the retinal (ligand) binding domain supporting key role of the class A GPCR ligand binding site in activation. These findings when extended to mGluRs suggest that the allosteric communication sites in rhodopsin and in mGluRs are conserved, further providing evidence that the activation mechanism in these divergent GPCR classes is probably conserved.

2.0 EXPERIMENTAL PROCEDURES

2.1 CLONING OF MGLURS

For easy reference, all the constructs and stable cell lines created or used in this thesis and described in this chapter are listed in Table 2.10.

2.1.1 Wild-type (WT) human mGluR6

The plasmid containing human mGluR6 cDNA (pMT3-GRM6) with a C-terminal 1D4 tag was a kind gift from Dr. Phyllis R. Robinson, University of Maryland, Baltimore (Weng et al., 1997).

2.1.1.1 Introduction of Kozak sequence into pMT3-GRM6

Presence of Kozak sequence immediately upstream of start codon is shown to enhance translation and increase protein expression in mammalian cells (Kozak, 1987). To increase mGluR6 expression in transient transfections I introduced Kozak sequence in pMT3-GRM6 by PCR. A forward primer is designed to introduce Kozak sequence between start codon and EcoRI site. A reverse primer is designed to bind downstream of ApaI a unique restriction site in the mGluR6 gene. The primer sequences and details are given below:

- Forward primer: 5'-CTGCAAGAATTCACCATGGCGCGGC -3'; EcoRI site is in italics, Kozak sequence is underlined and start codon is in bold.

- Reverse primer (R1): 3'–CGGCTGCCTGGGCTACAGCCTCCTG–5'

The pMT3-GRM6 is used as a template in PCR reaction to amplify a 2.2kb fragment. This fragment is gel purified and restriction digested with EcoRI and ApaI and ligated back into the parent vector (PCR template) restriction digested with EcoRI and ApaI. The resulting construct pMT3-KOZ-GRM6 was verified by sequencing.

2.1.1.2 Cloning of mGluR6 into pACMV-tetO

The procedure for sub-cloning human mGluR6 gene into a tetracycline inducible expression vector pACMV-tetO which was previously engineered to successfully express membrane protein rhodopsin (Reeves et al., 1996) is described here. The sub-cloning procedure involved multiple steps and multiple parent constructs as there were no unique sites to move mGluR6 directly from pMT3 to pACMV-tetO. As a starting material I used a previously cloned truncated version of mGluR6 (pACMV-tetO-GRM6-516) prepared by Dr. Gulsum Anderson. This construct contained the nucleotide sequence coding for the transmembrane region of mGluR6 (S583 to F845; full length mGluR6 is 877 amino acids long) and also lacked the start codon. To this construct I added the missing 5' and 3' gene sequence to generate full length mGluR6 as described below:

- i. Introduction of the nucleotide sequence missing in the 5' region: The missing 5' sequence was obtained by performing a partial restriction digest of the clone pMT3-KOZ-GRM6 with KpnI. The 2.1kb fragment obtained from the partial digest of pMT3-KOZ-GRM6 with KpnI was ligated into the KpnI digested and linearized pACMV-GRM6-516. The resultant clones were restriction mapped and sequenced for correct orientation of the KpnI fragment. The clone was verified and named pACMV-tetO-

GRM6-(1-516). This clone had the sequence for mGluR6 from the beginning of N-terminus to the end of transmembrane region (M1 to F845).

ii. Introduction of the nucleotide sequence missing in the 3' region: Here, mGluR6 gene sequence from another parent vector pMT3-GRM6-partial is used. pMT3-GRM6-partial contains a truncated mGluR6 cDNA, received from Dr. Phyllis Robinson's laboratory by accident before we got the correct one. It is similar to pMT3-GRM6 described in section 2.1.1 but nucleotide sequence coding for amino acids 20 - 363 of mGluR6 is missing. In other words the clone results in first 19 amino acids at the N terminus followed by N364-K877 and the 1D4 tag. The partial mGluR6 cDNA along with the 1D4 tag is amplified by PCR using these primers:

- Forward (**GLU6FOR**): 5'-CTTGAGATCTGGCCATACAC-3';
- Reverse (**XNMGR6R**): 5'-AACCTCGAGAATTTGCGGCCGCT-3'; XhoI site is in italics, NotI site is underlined.

The amplified sequence is restriction digested with ApaI and XhoI and ligated into similarly treated pACMV-GRM6-(1-516) construct. The resultant clones were restriction mapped and sequenced to verify the full length mGluR6 with 1D4 tag (ETSQVAPA).

The clone is named pACMV-tetO-GRM6(1-877). The gene sequence in this clone is flanked by KpnI and XhoI restriction sites. The sequence results also identified a silent mutation A → G at nucleotide 2196 (numbering as in genbank file NM_000843 – CDS sequence of human mGluR6). This mutation does not alter the translation of corresponding amino acid, T732. This clone was used to establish stable cell lines.

2.1.2 Transmembrane cysteine mutants of mGluR6

There are a total of 22 cysteines in human mGluR6. All the cysteines are predicted to be involved in disulfide bonds except for three cysteines (C754, C765 and C793) which are present in the transmembrane (TM) region. I systematically mutated these three cysteines to alanine so that there are two (double cysteine mutants: C754A, C765A, C793A), one (single cysteine mutants: C754A/C765A, C765A/C793A, C754A/C793A) or no (cys-less mutant: C754A/C765A/C793A) free cysteines in the TM region. The mutants were created by using the QuikChange® Multi Site-Directed Mutagenesis Kit from Stratagene (catalog # 200514; now part of Agilent Technologies). I designed three primers with the help of primer designing tools available on Stratagene website. Each of these primers carries mutations to convert codons for cysteines to alanine. The primers (base pair mutations are in bold; codons with mutations are underlined) are:

- C754A-For: 5'–TGTCTCTCATCGGC**GCC**CTGGGCTACAGCC–3'
- C765A-For: 5'–CCTGCTCATGGTCACG**GCC**CACAGTGTACGCCATC–3'
- C793A-For: 5'–CACCATGTACACCACC**GCC**ATCATCTGGCTGGCA–3'

For mutagenesis, the protocol suggested by the supplier (Stratagene; Multi-site directed mutagenesis) was followed. The PCR reactions were set up with pACMV-tetO-GRM6(1-877) as a template and all possible combinations of primers to obtain single, double or cys-less mutants. All the cysteine mutants were verified for accuracy by DNA sequencing over entire mGluR6 gene sequence.

2.1.3 Rhodopsin like mGluR6 mutants

2.1.3.1 7TMC

This clone was designed to express transmembrane and the cytoplasmic regions (S583 to K877) of mGluR6, with an initial N-terminus methionine and the 1D4 tag at the C-terminus. I used a previously cloned truncated version of mGluR6 gene in pMT4-GRM6-585 prepared by Dr. Gulsum Anderson. This clone lacked the start codon, but contained the nucleotide sequence coding for S583 to K877 with C-terminus 1D4 tag. The 5' and 3' sequencing revealed a unique NotI site at the 3' end and no KpnI site at the 5' end. I designed a forward primer to introduce the KpnI site and the start codon. Following primers were used to fix and PCR amplify the 7TMC gene fragment from pMT4-GRM6-585:

- Forward (**583REPAIR**): 5'–AAGAATT*CGGTACCAT***GT**CCCCCTG–3'; EcoRI site is underlined, KpnI site is in italics and start codon is in bold.
- Reverse (**GLU6REV**): 5'–ATCATGGTTCGACCATTGAA–3'

The amplified sequence has a unique KpnI and NotI site at the 5' and 3' end respectively. The PCR product was treated with restriction enzymes KpnI and NotI and ligated into similarly treated pACMV-tetO-GRM6(1-877) which has flanking KpnI and NotI. The resultant clones were restriction mapped and sequenced to verify the transmembrane and cytoplasmic regions of mGluR6 with 1D4 tag with flanking by KpnI and XhoI restriction sites. The resulting construct pACMV-tetO-GRM6-(583-877)-7TMC was verified by sequencing. The sequence results identified a silent mutation C → T at nucleotide 2445 (numbering as in genbank file NM_000843 – CDS sequence of human mGluR6). This mutation does not alter the translation of corresponding amino acid, G815.

2.1.3.2 7TM

This clone was designed to express only the transmembrane region (S583 to F845) of mGluR6, with an initial N-terminus methionine and the 1D4 tag at the C-terminus. I used a previously cloned truncated version of mGluR6 in pMT4-GRM6-516 prepared by Dr. Gulsum Anderson. This clone lacked the start codon but contained the sequence coding for the transmembrane region of mGluR6. I used the same exact procedure as described for the cloning of pACMV-tetO-GRM6-(583-877)-7TMC with the exception of using pMT4-GRM6-516 instead of pMT4-GRM6-585. The resulting construct pACMV-tetO-GRM6-(583-F845)-7TM was verified by sequencing. The sequence results identified a mutation AGC → GGC at the sixth amino acid of the 1D4 tag resulting in a glycine instead of serine. I verified that the antibody against 1D4 fails to recognize the construct because of the mutation in the tag.

2.1.3.3 CRD-7TMC

This clone was designed to express the cysteine rich domain (CRD) along with transmembrane and the cytoplasmic regions (S516 to K877) of mGluR6. I designed primers to introduce an NheI site and a start codon immediately upstream of S516 in pACMV-tetO-GRM6(1-877) using site directed mutagenesis kit from Stratagene. The primers used are:

- Forward (**CRD7-FS**):
5 –ACGAGGTGCCCTCGGCTAGCAT**GTCTCTGTGCAGCCT**–3’; NheI site is underlined, start codon is in bold and S516 codon is in italics.
- Reverse (**CRD7-RS**): reverse complement of forward primer
5’–AGGCTGCACAGAGACATGCTAGCCGAGGGCACCTCGT–3’

After site directed mutagenesis the pACMV-tetO-GRM6(1-877) with inserted NheI site was restriction digested with NheI and XhoI. This restriction fragment was ligated into similarly cut (NheI and XhoI digest) and CIP treated pACMV-tetO-gp160(Co-89.6) vector. The resulting construct pACMV-tetO-GRM6-CRD-7TMC(516-877) was verified by sequencing.

2.1.3.4 XR-7TMC

This clone was designed include 8 extra amino acids immediately upstream of S583 as compared to 7TM (section 2.1.3.2) construct of mGluR6 gene. The construct has the mGluR6 gene from P575 to K877 (as compared to S583 to K877 in 7TMC construct). I designed primers to introduce 24 nucleotides (8 codons) immediately upstream of S516 in pACMV-tetO-GRM6-(583-877)-7TMC using site directed mutagenesis kit from Stratagene. The primers used are:

- Forward (**XR7TMCF**):

5'–GCTGGGATACCAT**GCCTGTGGT***GCGCCTGAGCTGGTCCTCCCCCTGGGCAG*–3'; KpnI site is underlined, start codon is in bold and the 8 codons are in italics.

- Reverse (**CRD7-RS**): reverse complement of forward primer

5'– CTGCCCAGGGGGAGGACCAGCTCAGGCGCACCACAGGCATGGTACCCAGC–3'

After site directed mutagenesis, the pACMV-tetO-GRM6-(583-877)-7TMC with 8 codons inserted was restriction digested with KpnI and XhoI. This restriction fragment was ligated into similarly cut (KpnI and XhoI digest) and CIP treated pACMV-tetO-GRM6 (1-877) vector. The resulting construct pACMV-tetO-GRM6-XR-7TMC (575-877) was verified by sequencing.

2.1.3.5 XR-7TMC double cysteine mutants

These mutants are created similar to double cysteine mutants using same primers and site-directed mutagenesis methods as described in section 2.1.2. In this case the template used was pACMV-tetO-GRM6-XR-7TMC (575-877) (see section 2.1.3.4).

2.1.4 mGluR6:Rhodopsin chimeras

These constructs were chimeric proteins wherein TM domain of mGluR6 is switched with that of rhodopsin. I designed three different chimeric proteins (#1, #2 and #3) with variable N-terminus lengths of rhodopsin as shown in Figure 2.1.

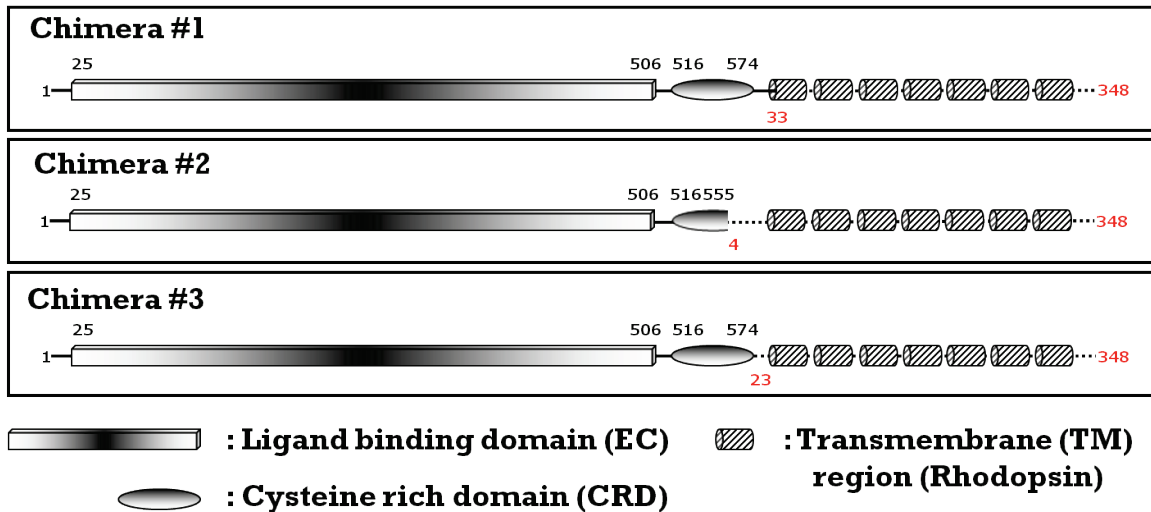


Figure 2.1 Domain organization of mGluR6:Rhodopsin chimeras

Residue numbering for mGluR6 and rhodopsin is in black and red font respectively. The chimeras have variable lengths of rhodopsin N-terminus and corresponding changes at the C-terminus of mGluR6 CRD.

In chimera #1 there was severe truncation of N-terminus (loss of initial 33 amino acids) of rhodopsin which was shown to result in unfolding (Doi et al., 1990). I created chimera #2 and

chimera #3 instead to verify the expression and possible retinal binding of these constructs. Chimera #2 has mGluR6 fragment from 1 – 555 amino acids followed by 4 – 348 amino acids of rhodopsin, while Chimera #3 has mGluR6 fragment from 1 – 574 amino acids followed by 23 – 348 amino acids of rhodopsin. These are cloned into pMT3 vector. The chimeras were generated using overlap PCR. Below is the list of primers and templates.

Universal primers

pMT4_new_F (**MF**): 5' – GGC TTG AGA TCT GGC CAT ACA C – 3'

pMT4_new_R (**MR**): 5' – GGT CGA ACC ATG ATG GCA GC – 3'

Overlap fusion primers for Chimera #2

mG6Rh_2_F (**C2F**): 5' – GTT CAC ATG C ACC GAA GGC CCA AAC TTC TAC – 3'

RhmG6_2_R (**C2R**): 5' – GCC TTC GGT GCA TGT GAA CTC GTC CAC CTG – 3'

Overlap fusion primers for Chimera #3

mG6Rh_3_F (**C3F**): 5' – GC CCC ACA CCG TTC GAG GCT CCG C – 3'

RhmG6_3_R (**C3R**): 5' – CTC GAA CGG TGT GGG GCG GCA GC – 3'

Internal primers: These primers are also used in section 2.1.1.2.

Forward (**GLU6FOR**): 5' – CTTGAGATCTGGCCATACAC – 3';

Reverse (**XNMGR6R**): 5' – AACCTCGAGAATTTGCGGCCGCT – 3'; XhoI site is in italics, NotI site is underlined.

Template DNA:

pMT4: pMT3 vector with opsin gene

pMT3-KOZ-GRM6: pMT3 with mGluR6 described in section 2.1.1.2.

The chimeras were generated in three PCR steps which are described here. The naming conventions followed to describe the cloning of the chimeras are:

- **2.1** : mGluR6 fragment of chimera #2
- **2.2** : Rho fragment of chimera #2
- **2** : 2.1 and 2.2 fusion fragment for chimera #2
- **3.1** : mGluR6 fragment of chimera #3
- **3.2** : Rho fragment of chimera #3
- **3** : 3.1 and 3.2 fusion fragment for chimera #3

- i. Generation of 2.2 and 3.2 (Rhodopsin) fragments: These fragments were generated using pMT4 as template. The concentrations of buffer components and PCR cycle conditions are provide in Table 2.1.

Table 2.1 PCR conditions for amplification of rhodopsin gene fragments (chimeras)

PCR rxn mix	μl	[Final]		
pMT4 DNA	1	~10 ng	PCR cycle	
2mM dNTP (1mM total)	5	0.2mM each	Segment 1	95C for 2'
10x reaction buffer	5	1x	Segment 2	95C for 20''
25mM MgSO4	3	1.5mM	(35 cycles)	57C for 10''
Forward (C2F or C3F)	1.5	0.3uM		70C for 40''
Reverse (MR)	1.5	0.3uM	Segment 3	4C hold
DMSO	1.5	3% v/v		
KOD hot start polymerase	1	2.5u		
Water to make up the volume	50			

- ii. Generation of 2.1 and 3.1 (mGluR6) fragments: Initial attempts to obtain mGluR6 fragments failed even after varying different PCR conditions like annealing temperature, template concentration, primer concentration and DMSO. I indentified that there was contamination in pMT3-KOZ-GRM6 template DNA. Therefore I generated new pMT3-KOZ-GRM6 as described below:

Step 1: pMT3-KOZ-GRM6 was digested with EcoRI/NotI yielding three fragments, from this the smallest EcoRI /NotI I fragment was gel purified.

Step 2: pACMV-tetO-mGluR6 (1-877) was digested with NotI yielding two fragments which NotI /NotI fragment was gel purified.

Step 3: pMT4 was digested with EcoRI/NotI and de-phosphorylated with CIP. The linearized plasmid template was gel purified.

Step 4: All three fragments from step 1 to step 3 were ligated in one step using DNA ligase.

Step 5: several clones were screened by restriction digestion and the final clone was verified by DNA sequencing. This clone was named pMT3-KOZ-GRM6 (new) and was used to generate mGluR6 fragments for the chimeras.

Generating mGluR6 fragments for the chimera required several iterations of PCR optimizing different components of the buffer each time. The critical condition for this reaction was to increase the DMSO concentration to 6% instead of 3%. Other parameters PCR buffer concentrations and cycle conditions are provide in Table 2.2.

Table 2.2 PCR conditions for amplification of mGluR6 gene fragments (chimeras)

Note: The optimal DMSO concentration was 6% as compared to 3% v/v.

PCR rxn mix	μl	[Final]		
pMT3-KOZ-mGluR6 (new) #26	1	~10 ng	PCR cycle	
2mM dNTP (1mM total)	5	0.2mM each	Segment 1	95C for 2'
10x reaction buffer	5	1x	Segment 2	95C for 20''
25mM MgSO4	3	1.5mM	(35 cycles)	57C for 10''
Forward (MF)	1.5	0.3uM		70C for 1'10''
Reverse (C2R or C3R)	1.5	0.3uM	Segment 3	4C hold
DMSO	3.0	6% v/v		
KOD hot start polymerase	1	2.5u		
Water to make up the volume	50			

iii. PCR fusion step to generate chimera #2 and #3: mGluR6:Rhodopsin fusions were first attempted to be generated by adding individual fragments (2.1, 2.2, 3.1 and 3.2) and the universal primers MF and MR (also used to generate individual fragments). Different conditions of annealing temperature, template concentration, primer concentration and DMSO concentrations were tested. However, a 1.5kb non-specific band was always observed on the agarose gel. There was non-specific amplification with universal primers as they were already used to generate individual fragments. Fresh primers had to be used to generate fusion fragment. The reaction worked when I replaced universal primers with internal primers. I used 400ng of each fragment in the reaction as opposed to 10ng template for a standard PCR. The concentrations of buffer components and PCR cycle conditions are provide in Table 2.3.

Table 2.3 PCR conditions for amplification of mGluR6:Rhodopsin chimeras

PCR reaction components	μl	[Final]		
(2.1 and 2.2) or (3.1 and 3.2)	x	~400 ng each	PCR cycle	
2mM dNTP (1mM total)	5	0.2mM each	Segment 1	95C for 2'
10x reaction buffer	5	1x	Segment 2	95C for 20''
25mM MgSO4	3	1.5mM	(35 cycles)	57C for 10''
Forward (GLU6F)	1.5	0.3uM		70C for 1'10''
Reverse (XNMGR6)	1.5	0.3uM	Segment 3	4C hold
DMSO	3.0	6% v/v		
KOD hot start polymerase	1	2.5u		
Water to make up the volume	50			

The PCR fragments (#2 and #3) were digested with EcoRI and MluI and gel purified and ligated into similarly treated pMT4 (also de-phosphorylated by using CIP) treated and gel purified. The colonies were screened and clone #2.24 and #3.28 verified by DNA sequencing.

These clones were named pMT3-mGluR6:Rho (1-555:4-348) or chimera #2 and pMT3-mGluR6:Rho (1-574:23-348) or chimera #3.

2.1.5 mGluR5

The cDNA for this construct for human mGluR5 isoform 1 was obtained in pIRESpuro2 vector from Dr. Marlene Jacobson at Merck Research Laboratories (770 Sumneytown Pike, West Point, PA 19486). mGluR5 was cloned into pACMV-tetO with a C-terminal 1D4 tag in three different steps as described below:

Step 1: mGluR5 gene I obtained does not have KpnI or Sall sites in the gene. I designed PCR primers to insert KpnI and Sall sites immediately upstream of start codon and stop codon respectively of mGluR5 gene.

- Forward (**GRM5F**): 5'–CCTTTCCTAAAGGTACCAT**TGGTCCTTCTGT**–3';
KpnI site is underlined and start codon is in bold.
- Reverse (**GRM5R**): 5'–GACATTCAGTCGACAACGACGAGGAGCTCT– 3';
Sall site is underlined, KpnI site is in italics and anti-codon for stop is in bold.

The mGluR5 gene fragment with KpnI and Sall restriction sites was PCR amplified with standard PCR protocols, except that the reaction needed 5% DMSO.

Step 2: There is a Sall site between K877 and the 1D4 tag in pACMV-tetO-mGluR6 (1-877). Additionally, in this construct there another Sall site 43 nucleotide base pairs upstream of the start codon. I performed site directed mutagenesis (Stratagene) to disrupt the Sall site 43 nucleotide base pairs upstream of the start codon. The primers used are:

- Forward (**GRM6-Sall-FS**):

5'-TCAGTGATAGAGATCGT**GG**ACGAGCTCGTTTAGTG-3'; The C to G nucleotide mutation that disrupts the SalI site is highlighted in bold.

- Reverse (**GRM6-SalI-RS**): reverse complement of forward primer; 5'-CACTAAACGAGCTCGTCCACGATCTCTATCACTGA-3'

The resulting construct after site directed mutagenesis pACMV-tetO-SalI*-GRM6(1-877) was verified by DNA sequencing to lack the SalI site 43 nucleotide base pairs upstream of the start codon.

Step 3: The PCR fragment from step 1 and the template pACMV-tetO-SalI*-GRM6(1-877) were treated with KpnI and SalI. mGluR5 gene was then ligated back into the linearized vector. After DNA sequencing of the resulting clone, I found that there was an extra 200bp fragment between KpnI and the start codon (probably carried over from PCR) in the resulting mGluR5 clone in pACMV-tetO-SalI*. In the next step I removed this extra sequence.

Step 4: I designed fresh primers to insert KpnI immediately upstream of the start codon of mGluR5.

- Forward (**GRM5-KpnI-FS**):
5' – GCTTGA**ACTCCTTT**CCTAAAG**GGTACCAT**GGTCCTTCT – 3'; KpnI site is underlined and the start codon is in bold.
- Reverse (**GRM5-KpnI-RS**): reverse complement of forward primer; 5' – AGAAGGACCATGGTACCTTTAGGAAAGGAGTTCAAGC – 3'

The resulting construct after site directed mutagenesis was treated with KpnI to drop the extra 200bp fragment. The linearized vector was then ligated back. The resulting construct pACMV-tetO-SalI*-GRM5 was verified by sequencing to contain the mGluR5 gene between KpnI and SalI sites, with a 1D4 tag between SalI site and stop codon.

2.1.6 mGluR2 and mGluR3

The cDNAs for human mGluR2 and mGluR3 were purchased from Open Biosystems (IMAGE CLONE - 8322671 and 4792430 respectively for mGluR2 and mGluR3). These were verified by sequencing and named pCR4-TOPO-mGluR2 and pBluescript-mGluR3. The genes for mGluR2 and mGluR3 were cloned into pACMV-tetO with a C-terminal 1D4 tag in two different steps as described below.

Step1: mGluR2 and mGluR3 were PCR amplified with forward and reverse primer engineered to insert KpnI and SalI sites immediately upstream of start codon and stop codon respectively. Below is list of forward and reverse primers used for mGluR2 and mGluR3 respectively:

- Forward (**GRM2_F**): 5'–GCCGGTACCAT**G**GGATCGCTGCTTGC – 3'; KpnI site is underlined and the start codon is in bold.
- Reverse (**GRM2_R**): 5'–CAAGGTCGACAGCGATGACGTTGTCGAGTCC –3'; SalI site is underlined.
- Forward (**GRM3_F**):
5'–GCCGGTACCAT**G**AAGATGTTGACAAGACTGCAAGTTCTTACC –3';
KpnI site is underlined and the start codon is in bold.
- Reverse (**GRM3_R**): 5'–CAAGGTCGACAGAGATGAGGTGGTGGAGTCC –3'; SalI site is underlined.

The mGluR2 and mGluR3 genes with KpnI and SalI restriction sites were PCR amplified with standard PCR protocols, except that the reaction needed 5% DMSO.

Step 2: The PCR fragments and pACMV-tetO-Sall*-GRM6(1-877) were treated with KpnI and Sall. The digested PCR fragments were ligated back into the linearized vector separately for mGluR2 and mGluR3. The clones for mGluR2 and mGluR3 were verified by sequencing to contain the gene between KpnI and Sall sites, with a 1D4 tag between Sall site and stop codon. The clones were named pACMV-tetO-Sall*-mGluR2 and pACMV-tetO-Sall*-mGluR3.

2.2 PROTEIN EXPRESSION

2.2.1 COS-1 and HEK293S cell maintenance

Cells stored in liquid nitrogen were thawed as quickly as possible by placing vials in a 37°C water bath after removal from liquid nitrogen. The cells were transferred to a 15 ml Falcon tube and slowly (over 2 min) 10 ml of media A was added to allow slow diffusion of the cryo-preservative DMSO from the cell. Cells were pelleted at 1000 rpm for 10 min in a Sorvall Legend RT bench top centrifuge, the supernatant was aspirated and 10 ml of fresh media A was added. The cells were resuspended in 10ml of media A and transferred to a 15 cm tissue culture dish containing 10 – 15ml of media A and incubated at 37°C, 5% CO₂ (Nuair DH Autoflow). Cells were fed every three to four days, until approximately 80-90% confluence was reached.

Cells were usually split 1:5 upon reaching approximately 80-90% confluence. Each 15cm plate was washed twice with 20 ml of buffer B. Two ml of 0.05% trypsin-EDTA was added to each plate and was incubated at 37°C for 1-2 min, the plates were gently tapped until the cells detached from the surface. To this 8ml of media A was added to inactivate trypsin. Gently collect

the cells by pipetting up and down 3-10 times. Transfer 2ml of this cell suspension into new dishes with 20ml of media A.

For long-term storage of cells, 70-90% confluent plates (15 cm) were trypsinized as described above. After centrifugation at 1000 rpm for 10 min, the supernatant was discarded and the pellet was resuspended in 10 ml of 10% DMSO in media A. One ml aliquots were prepared in cryogenic storage vials (Nunc) and placed in cryo freezing container (cooling rate of 1°C/min; Nalgene). The boxes were kept at -20°C for one hour and then moved to -70°C in freezer overnight. The following day, the vials were transferred to liquid nitrogen.

2.2.2 DEAE-dextran transient transfection of COS-1 cells

COS-1 cells were transiently transfected with pMT3 constructs as described in (Oprian et al., 1987) with minor modifications as described below. Confluent cells on 15 cm dishes were transiently transfected with plasmid-DNA. All solutions were equilibrated at 37°C. 15µg plasmid-DNA per plate was added to 10 ml of a solution of 0.25mg/ml DEAE-dextran, 0.1M Tris-HCl pH 8 in media C. The cells were aspirated, washed with 25 ml DMEM and incubated with the DNA-mixture for 6h at 37°C. After 6 h of incubation, the DNA mix was removed and without washing 2 ml of shock buffer containing 10% DMSO and 6mM Dextrose in buffer B was added and incubated for 2 min. Shock buffer was removed and 15ml 0.1mM chloroquine in media A was added to the cells. The cells were then incubated for 2h. After aspirating the chloroquine solution, and washing with 25 ml DMEM, the cells were incubated overnight with 30 ml media A. The cells were usually harvested 55h – 72h after the addition of DNA. After aspirating the medium, cells were washed with 20 ml buffer B. They were then lifted off the

plates in 2 ml buffer B with a rubber policeman. Subsequent manipulations were performed on ice.

2.2.3 Establishment of mGluR stable cell lines in HEK293S cells

pACMV-tetO vectors containing wild-type and mutant mGluR6 were used to stably transfect HEK293S cells. Ric16-tetR9 (originally from Phil Reeves: Ric15-tetR9) cells which grow under blasticidin (5 μ g/ml) selection were available as cryostocks in our lab. These are HEK293S stable cell lines which were transfected with pCDNA6-TR (Invitrogen) which has the gene for operon repressor (TetR protein) and a selectable marker gene blasticidin (Reeves et al., 2002). These cells have the necessary background to transfect wild-type and mutant mGluR6 in pACMV-tetO and establish stable cell lines. The Ric16-tetR9 cells were debanked and maintained in media D with blasticidin (5 μ g/ml). Routine growth, splitting and trypsinization, long-term storage and reviving from frozen stocks were as described in section 2.2.1. HEK293S cells were transfected by the method of Chen and Okayama (Chen and Okayama, 1987) as modified by O'Mahoney and Adams (O'Mahoney and Adams, 1994).

A day before transfection the cells from 10cm cell culture dish were split 1:8 or 1:10 (approximately 1-2 million cells per plate) in media A and blasticidin (5 μ g/ml) media (**NOTE:** media switched from DMEM-F12 to DMEM). It is recommended to count and put 2 million cells per plate for better control. On the day of transfection the cells are 30-40% confluent. For transfection the following cocktail was prepared. The volumes reported are for transfecting one 10cm plate. In a falcon tube add 30 μ g DNA, 440 μ l sterile dH₂O, 50 μ l of 2.5M CaCl₂ and 500 μ l BES (2X BES: 50mM N,N-bis(20hydroxy ethyl)-2-amino ethane sulfonic acid+250mM NaCl+1.5mM Na₂HPO₄, pH 7.2) in that order, respectively. After the addition of BES, the

mixture was incubated for exactly 1 min and then gently added to the cells. After gentle distribution of the solution on the cells, plates were incubated at 35°C, 3% CO₂ for 19 h. After one hour the efficiency of the transfection was checked by light microscopy. If the transfection was successful, the DNA precipitate looked like fine sand between the cells and sometimes red crystals formed after longer incubation. However, large colorless crystals formed in between the cells during the overnight incubation were indicative of a failed or inefficient transfection. After 19 h incubation, the medium was removed and the plate was washed twice with 10 ml of buffer B. The cells were then fed with media A and blasticidin (5µg/ml) and the cells were returned to 37°C, 5% CO₂. At this stage and for all further operations, the pipettes were changed for each mutant and plate so as to prevent any contamination of different transfected mutants with each other. After 23 h, the plate was washed with buffer B, trypsinized and split 1:10 (0.5 - 1 million cells/plate; I prefer 0.5 million or less). The number of plates depends on the screening, usually 6 - 9 plates for each transfection (2 – 3 plates for selection with 1mg/ml, 2mg/ml and 3mg/ml with G418). To each plate 1 ml of 1x trypsin (0.05%) was added and the plates were incubated at 37°C for one min. This was followed by addition of 9 ml of media A and blasticidin. The cells were thoroughly pipetted up and down such that the cells did not clump. This was important for avoidance of mixed clones. 1 ml of this was diluted with 9 ml of buffer B. Of this diluted cell suspension, 40µl was mixed with 40µl of Trypan Blue. 10 µl was pipetted under a glass coverslip on a hemacytometer and the cells were counted. 2-5 single cells should be counted under the microscope, corresponding to 0.5 – 1 x 10⁶ cells per plate. After further 20h, the plates were fed with media A and blasticidin containing 1 or 2 or 3mg/ml geneticin (G418). Media was replaced every 2-3 days with fresh media (with selection) until colonies formed and reached workable size (in about 2 weeks). The medium was aspirated from a plate where the colonies that were being

picked had been circled. 8 colonies could be picked per plate. Cloning rings and vacuum grease was autoclaved beforehand. Using sterile forceps, the cloning rings were dipped in vacuum grease until the ring was completely covered from the bottom and were then placed on the colony. 40 μ l of 1X trypsin (0.05%) was added to each of the 8 colonies in cloning rings. 1 min after the addition of trypsin to the first cloning ring, 40 μ l of media A was added to each cloning ring in the same sequence as the trypsin had been added. Using a 200 μ l eppendorf pipette, the solutions were pipetted up and down 5 times before being transferred to a 24 well plate containing 1 ml of media A with the appropriate amount of geneticin (1 or 2 or 3mg/ml, see above; **Note:** At this point I removed blasticidin selection from plates). Media was replaced every 2-3 days until cells were confluent. As soon as confluency was reached, the cells were trypsinized and transferred into two chambers in a 6-well dish with a difference in cell number of 1:4.

Transfer of cells to 6 well plates: Prepare 6 well plates with 3ml of complete media for each well. Aspirate the media on the cells (24 well plate) and add 300 μ l of trypsin to each well and leave for 1 min. Add 1200 μ l (use 1ml pipette and add 600+600 μ l) of media A with geneticin (G418) and gently pipette up down. Remove 300 μ l and add it to one 1 well and the remaining (1200 μ l) in another well. Change media on cells every 2-3 days. The well with higher cell density was induced for screening of the clones, while the one with lower densities was maintained and used for making glycerol stocks. As soon as the cells in the higher density well reached confluency they were induced by adding induction media (media E). The cells were harvested 48h post induction and were further analyzed by Western blot to evaluate protein expression.

Harvesting of cells after induction: Aspirate the media and gently dislodge and collect cells in 1.5ml ice cold buffer B (with protease inhibitors). Unlike COS-1 cell harvesting, HEK293 cell harvesting does not require scraping of the cells the plates. Rather, cells were detached by pipetting. Transfer the cells into an eppendorf tube. Centrifuge the cells for 5 min at 5000rpm and 4C. Carefully aspirate the PBS and add 500µl of solubilization buffer (buffer B with protease inhibitors and 4%OG). The cells were solubilized for 1.5h. This was followed by collecting the supernatant by centrifuging at 35,000rpm for 30min in TLA 100.2 or MLA-130. The collected supernatant was snap-frozen in liquid nitrogen and stored at -20°C. The supernatant was collected for all the clones.

Picking of clones with high protein expression: The supernatant from the clones was processed using a dot blot to identify clones with high levels of receptor expression. Dot blot is carried out as described in section 2.7.5. Since all the clones are tagged with 1D4 epitope, I used rhodopsin as positive control. Best clones for experimental studies are picked based on high levels of protein expression relative to other clones and in comparison to positive control (rhodopsin). See Table 2.10 for information on clones and constructs.

Making cryostocks of the clones: When the cells from the low density well reached confluency they were split 1:1 or 1:2 into one or two 10cm cell culture dishes. After the cell reached confluency on the 10cm plate, DMSO stocks were made from one of the plate. Three 1ml DMSO stocks were made from one 10cm plate. 70-90% confluent plates were washed twice with buffer B and trypsinized with 1ml trypsin for 1min. 10ml of media A (no selection) was added and cells were collected in a 15ml falcon tube. Cells were centrifuged at 1000rpm (approximately 600g) for 10min. After aspirating the media cells were gently resuspended in 3ml of cryo-media (media A with 10% DMSO) and transferred into cryo vials in 1ml aliquots and

frozen as described for COS-1 cells in section 2.2.1. The other plate was maintained as a backup until the glycerol stocks were safely made and transferred to liquid nitrogen storage containers.

2.2.4 Optimizing spinner flask growth conditions for mGluR6 stable cells

2.2.4.1 Standard spinner flask growth conditions

The stable cell lines were split every 3-4 days and were maintained in media A with Geneticin (1-3mg/ml of G418). For growing suspension cultures 2-3 days old confluent stable cell lines were trypsinized and transferred to a spinner flask with pre-warmed (37°C) 500ml media F. **Note:** No Geneticin was added for suspension cultures. The spinner flasks were incubated at 37°C, 5% CO₂ at 45-50rpm stirring rate. On 5th day the cells are induced in the spinner flasks. For induction, 6ml of 20% glucose, 8% NaHCO₃ and 5ml each of tetracycline and sodium butyrate from 100X stocks were added. The cells were harvested 55h post induction.

2.2.4.2 Optimized growth conditions for mGluR6 expression

Described here are the optimal growth conditions, time of induction and harvest for maximal mGluR6 expression from stably expressing HEK293S cells. The basic DMEM media for suspension culture (media F) was further supplemented with components A, B and C (media G) as described by Reeves et al (Reeves et al., 2002) to increase the cell density. Five 15 cm cell plates were grown for one 500ml spinner flask culture. The cells were transferred to spinner flasks when they reached 80 - 90% confluency.

Starting spinner flask culture (Day 0): 500ml of pre-warmed (37°C) media G was added to each spinner flask. Each plate was washed 2 times with 20ml of buffer B and 2ml of trypsin was added. The plates were kept at 37°C for one minute and then 8ml of media G from spinner

flask was added to each plate. Cells were resuspended gently but carefully to disperse them thoroughly (avoid clumping). Five plates of cells (50ml) were added to each 500ml culture in one spinner flask. Usually the density in the spinner flask at this point was 0.4 – 0.5 million cells per ml. One can even count the cells and add them to spinner flask to control for cell density.

Maintenance of spinner flask culture (Day 4): The cell density on this day was usually 1.4 – 1.6 million cells / ml. Cells were counted to verify that they are in this range. To each of the spinner flask with 500ml culture, these supplements were added: 6ml of 20% glucose, 15ml of bovine serum and approximately 2-4ml of 8% NaHCO₃ to increase the pH of media to neutral using visual cue (usually the media becomes bit yellowish if cells are growing fine; At neutral pH the media is bright pink).

Induction of cells in spinner flask (Day 6): The cell density on this was day usually 1.8 – 2.0 million cells / ml. Cells were counted to verify that they are in this range. To each of the spinner flask with 500ml culture, these supplements were added: 6ml of 20% glucose, 4ml of 8% NaHCO₃, and 5ml each of tetracycline and sodium butyrate from 100X stocks. **Note:** For convenience cells were induced in the morning around 9am on day 6; this way cells can be harvested end of the day, around 4am, on Day 8 (approximately 55 hours after induction).

Harvesting cells from spinner flasks (Day 8): Cells were harvested 55h after induction (**Note:** Our observations from cAMP and GTP-Eu functional assays suggested that to obtain active mGluR6, cells before harvesting need to be incubated in buffer H for 2h.) This additional step will be needed to obtain active mGluR6 from spinner flasks. For harvesting, cell culture from each spinner flask was divided into two 250ml conical bottom centrifuge tubes and centrifuged in SLA-1500 rotor (sorrall machine) at 2000 rpm for 10 minutes. **Note:** The conical bottom tubes are not shaped to fit in the SLA-1500 rotor but the tubes can withstand 2000 rpm

without any deformation. The media was aspirated and cells were washed in each tube (contains pellet from 250ml cell culture) with 20ml of ice cold buffer B. The cells were transferred to a 50ml falcon tube. Finally, the 250ml tube was rinsed with 5ml ice cold buffer B and transferred to the 20ml suspension in 50ml tube. The 50ml tubes were then centrifuged at 1000g for 10 minutes. The buffer was carefully aspirated. The wet weight of the pellet was usually ~3g. This pellet can be used directly for purification of the protein. For long term storage the 50ml tubes were snap frozen in liquid nitrogen and stored at -80°C .

2.2.5 Expression of $G\alpha\beta\gamma$ heterotrimer complex in insect cells

To set up *in vitro* functional assays for purified mGluR6 a cognate G-protein complex is needed. The likely $G\alpha\beta\gamma$ partners for human mGluR6 are $G\alpha_o$ (Dhingra et al., 2002; Dhingra et al., 2000; Huang et al., 2003; Nawy, 1999; Vardi et al., 1993; Weng et al., 1997), $G\beta_{3/4}$ (Huang et al., 2003) and $G\gamma_{13}$ (Blake et al., 2001; Huang et al., 2003). Also, recent immunofluorescence and co-immunoprecipitation, studies suggest $G\beta_5$ -RGS complex enhances the GTPase activity of $G\alpha_o$ (Morgans et al., 2007). I obtained baculovirus stocks of the G protein heterotrimer ($G\alpha_o$: M21-31A, $G\beta_3$: SF93-22B and HA tagged $G\gamma_{13}$: SF93-114A) from Dr. James Garrison (University of Virginia, Charlottesville, VA). Described in this section are the protocols for growing, amplifying viral stocks and expression of $G\alpha_o\beta_3\gamma_{13}$ heterotrimer from insect cells.

2.2.5.1 Sf9 cell maintenance, growth conditions and cryopreservation

Sf9 insect cells of 8th passage were obtained from Dr. Jinwoo Ahn's laboratory (University of Pittsburgh). These cells double every 24h and maintain viability of >98%. The cells were maintained in the range of 1 to 4 million/ml in a suspension growth media I. Typically

the cells are diluted to give 1 million/ml and incubated in shaking incubator at 27°C – 28°C and 135rpm (**Note:** The cells are diluted by adding fresh media to cells in old media. There is a mixture of spent and fresh media which is desirable for insect cell growth). After two days (i.e., on third day) when the cells reach a density of approximately 4 million cells/ml the cells were diluted back to 1 million/ml and passaged similarly. A cell density of 8 million/ml was usually considered high so cells were passaged every two days (**Note:** Optionally, the cells are diluted to 0.5 million/ml on Fridays so that the cell density would be approximately 4 million/ml by Monday. There was no decrease in cell viability or growth at 0.5 million/ml dilution.). Every two weeks the cell culture was gently centrifuged at 600g for 7-10min without brake at room temperature to remove the spent media completely and resuspended in fresh media. This is a standard practice done to prevent build up of toxic substances in the cell culture.

The cells are grown in suitable quantities to make cryo stocks. For example a 50ml culture at 3 million/ml cell density can be used to make ten 1ml cryostocks at 15 million/ml cell density. Cryostocks were prepared in 46.5% of conditioned medium (medium after spinning the cells down) with 46.5% of fresh media I and 7% DMSO. Cells were transferred into cryo vials in 1ml aliquots and frozen as described for COS-1 and HEK293S cells in section 2.2.1. Cryostocks (15 million cells/ml) of the cells from the 9th passage were made and stored in our lab for future use.

2.2.5.2 Plaque assay

Plaque assay was done to estimate the viral titer in pfu/ml units (pfu: plaque forming units). For each viral titer to be estimated 6 dilutions were made in duplicates. The plaque assay was done in 6 well plates. Log phase growing cells were taken, centrifuged and collected. The cells were resuspended to a density of 0.5 million/ml. 2 ml of these cells were added per well in a

6 well plate and incubated in a 27°C incubator (without CO₂) for 1h to let the cells settle down and anchor to the surface. Usually there will be 50% confluency. While the cells are settling down 10-log dilutions of viral supernatant were prepared by sequentially diluting 0.5ml of previous dilution in 4.5ml of Grace's insect medium, un-supplemented (without any antibiotics or serum) in sterile 12ml disposable tube. There should be 10 dilutions ranging from 10⁻¹ to 10⁻¹⁰. Also, sterile 4% agarose was melted in a microwave and kept at 42°C until use. The Sf-900 insect plaque medium (1.3X) was kept at 42°C. After 1h of incubation the plate was taken out. The plates were labeled in columns of two with desired dilutions of viral inoculums to be added (use 10⁻³ to 10⁻⁷ or 10⁻⁵ to 10⁻⁹ dilutions; depending on viral titer) and one set as control (No virus). Media from the plates was aspirated and immediately replaced with 1ml of the corresponding viral dilution. The cells were incubated for 1h at 27°C. Plaque overlay was prepared in the meantime by mixing Sf-900 insect plaque medium (30ml) and 4% agarose (10ml) in an empty sterile bottle. The plaque medium was then kept at 40-42°C in a water bath. 2ml of plaque media was used per well.

After the second 1h incubation, the viral inoculums on the cells was removed and replaced with 2ml of plaque media with liquefied agarose. It was made sure that the monolayer of cells does not get desiccated during removal of inoculums and overlaying with agarose. The gel was allowed to solidify (10-20min) in the hood before moving. After the gel hardens six well plates were placed in a zip lock bag with a moist paper towel. The bag was sealed and incubated in 27°C incubator. The plates were checked for plaques, usually visible by 6th day. The number of plaques was monitored every day until they do not change in number (approximately 9 days). A dilution giving 3-20 plaques is ideal to estimate the titer. The titer was estimated with the following formula:

$$\text{Viral titer pfu/ml} = (1/\text{dilution}) \times (\text{number of plaques}) \times (1/\text{ml of inoculums per plate})$$

2.2.5.3 Viral amplification

The number of cells required for amplification which depends on the volume of virus to be harvested was calculated. Usually the cells were infected at approximately 2 million/ml in a total volume of 250ml. Cells were harvested around log-phase when the cell density is around 4 million/ml for optimal viral amplification. The viral titer was estimated (see section 2.2.5.2) and the volume of viral inoculums needed for infecting the cells (MOI: Multiplicity of infection) was calculated. For amplification purposes, the MOI of infection was low (0.01 – 0.1).

$$\text{Viral inoculums (ml)} = (\text{desired MOI in pfu/ml} \times \text{total number of cells}) / (\text{viral titer pfu/ml}).$$

Cells were infected at an MOI = 0.05. Cells were centrifuged in sterile conical bottom flasks at 600g at room temperature for 7-10min without brake so that there are enough cells for a final 250ml cell culture (500 million cells = 2 million/ml * 250ml). The media was removed and cells resuspended in Grace's Insect media, unsupplemented and viruses in 1/20th the final volume of cells to be grown (example: for 250ml of final cell culture volume, the cells were resuspended in 12.5 ml) and transferred to conical bottom tubes (same tubes were used for centrifuging) or conical flasks. This gives a cell density of 40 million/ml for infection. The tubes/flasks were placed for 1h in a shaking incubator at 27°C and at 200 or 300 rpm shaking respectively for conical bottom tubes and conical flasks. After 1h media I was added to the final volume and transferred to conical flasks and the cells were grown normally. For amplification purposes, viruses were harvested when the viability reaches to 20-30% (5-6 days). For harvesting the viral supernatant, cells were centrifuged at 2500g for 15-20min and the viral supernatant was collected into a sterile bottle. The supernatant was removed carefully avoiding any particulate matter, if

needed the supernatant was sterile filtered (0.45 μ m) before storage at 4°C protected from light. Additionally, 1ml aliquots were stored in -80°C freezer.

2.2.5.4 Expression of G α_0 β_3 γ_{13} heterotrimer

Sf9 cells were co-infected with the M21.31A (G α_0), SF93-22B (G β_3) and SF93-114A (HA-G γ_{13}) viral stocks at an MOI of 3 for each individual viral stock. For details on viral stock and infection see section 2.2.5 and 2.2.5.3 respectively. The only difference in infecting cells for protein expression and viral amplification is to increase the MOI (up to 10) and harvest the cells early (approximately 48h post infection) before the viability decreases to 75-80%. For harvesting, the cells were centrifuged at 800g at 4°C for 5min with centrifuge brake off. Each 1 liter of culture was divided into two 500ml or three 333ml fractions for spinning. The media supernatant was carefully poured off and the cells were gently resuspended in 500ml of ice cold buffer J for every 1000ml of culture. The cells were centrifuged 800g at 4°C for 5min with centrifuge brake off. The cells were washed two more times with 250ml of ice cold buffer J. Finally, the cells were resuspended in a final volume of 100ml ice cold buffer K and divided into two 50ml falcon tubes to yield a 500ml cell pellet per tube. The tubes were centrifuged as before and the supernatant discarded. The cell pellet was snap frozen and stored at -70°C. Approximately, 5mg cell pellet was obtained from 500ml cell culture.

2.3 PROTEIN PREPARATIONS

2.3.1 Purification of rhodopsin

Rhodopsin was always handled under dim-red light illumination. Bovine retinæ were purchased from J. A. Lawson Co. (Lincoln, NE) and stored frozen at -80°C. The usual yields of rhodopsin from retina are about 1-1.5 mg. The number of retina needed for purification was thawed and then suspended in equal volume of buffer B. Retinæ were mixed using a spatula and then transferred in small quantities to a dounce homogenizer of appropriate dimensions depending on the volume in use. The retinæ were then homogenized until no clumps were visible. After homogenization of the entire volume of retinæ, dodecyl maltoside (DM) was added from a 10% stock to obtain a final concentration of 1%. This mixture was then end-over-end mixed at 4°C for 1.5-2 h. This was followed by centrifugation of 35,000 rpm in a 70Ti rotor (Beckman) separate out the remove unsolubilized components. Rhodopsin in the solubilized component is purified by antibody affinity chromatography (see section 2.3.1.2) of rhodopsin using 1D4 column. Preparation of 1D4 column is described in section 2.3.1.1.

2.3.1.1 Preparation of 1D4 sepharose

CNBr-activated sepharose 4B was prepared from CNBr and sepharose 4B (Kumel et al., 1979), based on the rapid reaction of cyanogen halides with the hydroxyl groups of carbohydrates at high pH to form cyanate esters (Figure 2.2). The monoclonal anti-rhodopsin antibody 1D4 (Oprian et al., 1987) was coupled to CNBr-activated sepharose 4B via its amino groups (Oprian et al., 1987) with minor modifications.

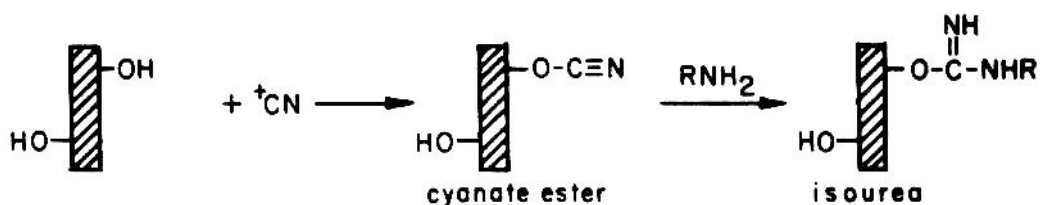


Figure 2.2 Activation of sepharose by CNBr and coupling of protein to the activated gel

This figure is taken from ref. (Kohn and Wilchek, 1978).

Activation of sepharose by CNBr and coupling of protein to the activated gel: Prior to coupling, 1D4 was purified from a myeloma cell line provided by R.S. Molday (University of British Columbia) as follows. 1500 mg 1D4 antibody (stored at -20°C) was thawed. 300 ml of Protein A-sepharose 4B were packed and equilibrated with 5 times the bed volume of buffer (1.5M glycine, 3M NaCl). All flow rates were between 0.5-1.5 ml/min, unless otherwise stated. The sample was diluted with 5 times its original volume of buffer (1.5M glycine, 3M NaCl). The sample was loaded, followed by washing with buffer (1.5M glycine, 3M NaCl) until a straight baseline at A_{280} was reached. The sample was eluted with approximately 300 ml of buffer (0.1M citric acid, 0.15M NaCl (pH 3)). Fractions of 4ml each were collected while monitoring A_{280} . In order to store the column for future use, it was regenerated with 300ml buffer (6M guanidinium-HCl) at a flow rate of 0.5ml/min. The column was stored at 4°C after washing with 2-10 times the bed-volume of buffer (50mM $\text{Na}_2\text{HPO}_4/\text{NaH}_2\text{PO}_4$ (pH 7), 0.01% thimerosal). Due to the poor stability of 1D4 at pH 3, the pH of the fractions was adjusted to pH 8.3 immediately after elution using 0.5M NaHCO_3 pH 10. Fractions containing 1D4 sepharose were combined and used directly for coupling, as long as the concentration of 1D4 was above 3 mg/ml. If the concentration was lower, the solution was first concentrated to up to 10 mg/ml before coupling. The concentration of antibody was determined using A_{280} ($A_{280} = 1.383$ is equal to a

concentration of 1mg/ml). Dialysis tubes (Spectrapor, 14 kD cut-off, but could be higher) were washed thoroughly with *aqua dest* and filled with the 1D4 solutions. Dialysis was against 5-10 l of 0.25M NaHCO₃, 0.5M NaCl (pH 8.3) buffer for four hours to overnight. Dialysis buffer was subsequently changed at least 3 times. After dialysis, the concentration was determined using A₂₈₀ as above.

The purified 1D4 antibody was coupled to CNBr-sepharose as described below. First, 20 ml CNBr-Sepharose was prepared. 100-200 mg of 1D4 antibody can be bound to this amount of CNBr-Sepharose. If 100 mg of 1D4 was coupled the capacity of the final product was typically 1mg rhodopsin/ml of 1D4 sepharose. 500 µl acetonitrile was added per 1 g of BrCN (Sigma). The volume increased after dissolving the BrCN, so that the final concentration was 1g/ml. This stock solution could be stored at -20°C. 20 g of sepharose 4B slurry (Sigma) was washed three times with water in a filter funnel. 20 g of sepharose corresponds to 30 ml of slurry. Water was removed by vacuum and the sepharose was added to 30 ml of buffer (3.3 M K₃PO₄ (pH of 11.9 at 10-fold dilution)). While stirring vigorously with a regular stirring bar under the hood, 1 ml of BrCN-solution was added and stirred for exactly 2 min. The suspension was transferred quickly to the filter funnel that contained ice-cold water and was vacuum-filtered immediately. The beads were washed with 300 ml of ice-cold buffer (0.25 M NaH₂PO₄/Na₂HPO₄ (pH 6)) followed by 500 ml 1mM HCl. All the washes were carried out extremely rapidly, such that vacuum-filtering of 100 ml took less than 30 seconds. Thus prepared CNBr-sepharose could not be stored. Coupling to 1D4 had to follow immediately after preparation, ideally within 2 min. If CNBr-sepharose was purchased from Pharmacia, 1g of the dry powder CNBr-sepharose was equivalent to approximately 3.5ml gel slurry. The dry CNBr sepharose was washed on a sintered

glass filter with 500 ml of 1mM HCl. All subsequent steps were the same for commercially available or self-made CNBr-sepharose.

The coupling of 1D4 to CNBr-sepharose was carried out at 3-10mg 1D4 per 1ml CNBr-sepharose 4B. 20 ml slurry was added to the concentrated sample of 1D4 containing 100 mg 1D4 in buffer (0.25M NaHCO₃, 0.5M NaCl (pH 8.3)). Coupling was allowed to proceed by end-over-end mixing until the supernatant after spinning down the beads for 5min contained less than 5% of the total protein (after 4-5 hours at RT). The supernatant was discarded. A volume equal to that of the original supernatant of blocking agent (1M ethanolamine pH8) was added. Blocking was allowed to proceed for 2 h at RT or overnight at 4°C. The beads were washed on a sintered glass filter 4 times with alternating solutions of buffer (0.25M NaHCO₃, 0.5M NaCl (pH 8.3)) and buffer (0.1M NaOAc, 0.5M NaCl (pH 4)). Buffer B containing 0.05% NaN₃ was added in equal volume as the beads. The coupled 1D4-sepharose was stored at 4°C.

The capacity of 1D4-Sepharose was determined as follows. 500µg ROS membranes were solubilized using (137mM NaCl, 2.7mM KCl, 1.8mM KH₂PO₄, 10mM Na₂HPO₄ (pH 7.2)) containing 1% DM by end-over-end mixing for 1 hour. ROS membranes were solubilized at a final rhodopsin concentration of 1 mg/ml. Unsolubilized material was removed by centrifugation for 30min at 4°C and 35000rpm (rotor 60Ti or 45Ti, Beckmann Ultra Centrifuge), or for volumes <1ml, 10min at 35000rpm (rotor TLA100.3) and the exact concentration was determined spectroscopically (as described in section 2.7.1.1). 200µl of 1D4-sepharose were added to the supernatant and rhodopsin was purified as described in Section 2.3.5.2. The capacity was calculated using the ratio between the rhodopsin purified and the amount of rhodopsin originally solubilized. Typically the capacity was 1 mg rhodopsin per 1 mg 1D4-sepharose if 100 mg of

1D4 was coupled to 20 ml of CNBr-sepharose. A capacity of up to 1.7 mg/ml could be obtained if correspondingly larger amounts of 1D4 were used.

2.3.1.2 Binding of solubilized rhodopsin to 1D4 sepharose

DM solubilized supernatant from retinae (see section 2.3.1) was used for purifying rhodopsin. The amount of rhodopsin in the supernatant was estimated by absorbance spectroscopy (see section 2.7.1.1). The amount of beads necessary to bind quantitatively the rhodopsin present in the supernatant was calculated from the 1D4 sepharose binding capacity, usually 1 mg of rhodopsin per ml settled beads. About 10% excess of 1D4-Sepharose over rhodopsin content was used. After end-over-end mixing for at least 6 hours at 4°C, the suspension was packed into a column. For 10-15mg of rhodopsin to be purified the dimensions of the column were 2.7 cm diameter x (2 to 3) cm. If smaller amounts were purified, i.e. 100-500 µg, Bio-Rad disposable chromatographic columns were used. The packed beads were washed at room temperature with at least 50 column volumes of buffer B containing 0.05% DM. This was followed by further washes with 10 bed volumes of 2mM sodium phosphate pH 6 with 0.05% DM. The flow rate was 0.5-1 ml/min.

2.3.1.3 Elution of rhodopsin from 1D4 sepharose

Rhodopsin was eluted from 1D4-Sepharose in 2mM sodium phosphate pH 6 with 0.05% DM and 70µM nonapeptide epitope. The elution flow rate from the column was set at 0.3-0.35 ml/min. All the elutions were monitored by absorbance spectroscopy 2.7.1.1. Usually rhodopsin completely eluted in approximately 5 column volumes of elution buffer.

2.3.2 Membrane preparations of mGluRs by sucrose flotation

Membranes from stable cells were prepared using a modified protocol which was originally communicated by Dr. Takahiro Yamashita (Department of Biophysics, Graduate School of Science, Kyoto University) (Yamashita et al., 2004; Yamashita et al., 2008). The sucrose floatation method of preparing plasma membranes from HEK293S is also described in more detail in (Li et al., 2004a). Membranes were always prepared from five 150mm plates. A confluent plate was split into five plates and the cells were grown for 3 days in media A until they reached approximately 90-95% confluency. The cells were then washed once with 25ml of buffer H and induced with media E. The plates were returned to the incubator for 48h. Cells were gently washed twice with buffer H and incubated for 2h with buffer H. The buffer was then carefully aspirated and the cells were gently washed once with 10 ml buffer B (**Note:** Wash only if cells are not coming off the plate). The cells were then dislodged by tapping the plate and gently pipetting up and down in 8 ml of buffer B per plate. All subsequent steps after the cells were harvested, were carried out on ice. The cells from all the plates were collected by centrifugation at 1000g for 5min to 10min. The cell pellet weight from 5 x 150mm plates was 1 – 1.2g. The cell pellet was homogenized in 5ml of buffer L with 50 % sucrose (**Note:** 50% sucrose is made in buffer E) with a dounce homogenizer (30-40 strokes). The homogenized sample was centrifuged at 20,000g for 15 min preferably in a swinging bucket rotor (SW32 Ti; 13000rpm). The cell membranes float on the aqueous surface or attach on the walls of the inner side of the tube. Carefully collect all the cell membranes in the supernatant. Use 1ml pipette with tip cutoff, to aid in collecting membranes. The supernatant was preserved in a new tube. The pellet was re-homogenized on ice in 5ml of buffer L with 50 % sucrose and centrifuged at 20,000g for 15 min. The membranes were collected along with supernatant and added to the supernatant collected

from the earlier step. Additionally at the end, use 1ml of buffer L with 50% sucrose to wash and collect residual membranes without disturbing the pellet and to the collected membrane supernatant. The pellet can be discarded at this point. There should be a total of 8-10ml supernatant. The supernatant was diluted with at least two volumes of buffer L (16 – 20ml). It was thoroughly mixed to disperse and sucrose was diluted from 50% to approximately 16.6%. The diluted supernatant was then centrifuged at 20,000 g for 15 min. (70 Ti; 13000rpm). If using fixed angle rotor (70 Ti) the supernatants were distributed into two tubes. Upon centrifugation, membranes get pelleted. The membrane pellets were resuspended with 25ml of buffer L and collected into one tube (if using centrifuge tubes for 70Ti rotor). The membrane pellet was collected by centrifugation at 20,000 g for 15 min. The final pellet volume is $1/10^{\text{th}}$ – $1/20^{\text{th}}$ of the cell pellet collected at harvest. The pellet was re-suspended in buffer M. If the wet weight of the initial cell pellet was 1g re-suspend membranes in 1000 μ l of buffer M. Similarly if the pellet weight was 0.8mg it was resuspended in 800 μ l of buffer M. The membranes were divided into 25 μ l aliquots, snap frozen in liquid nitrogen and stored at -80°C freezer. The protein concentration was between 4 – 7 mg/ml as estimated with Bradford assay (Bio-Rad; catalog #500-006).

2.3.3 Detergent extraction and purification of mGluR6

For harvesting, the cells from each 150mm plate were washed twice with 20ml of ice cold buffer B and were scraped using a rubber police man into 2ml of ice cold buffer B with 0.7mM PMSF and 0.005% benzamidine. In case of stable cell lines (HEK293S) the cells were dislodged by pipetting alone. For protein purification purposes harvested cells were immediately used without freezing.

For solubilization, n-Octyl- β -D-Glucoside (OG) detergent was added to a final concentration of 4% to the harvested cells. The detergent added cells were incubated with nutation at 4°C for 1-1.5 hours. The cells were then ultra-centrifuged at 50,000g for 30 min. The supernatant and pellet were separated for further analysis. To the detergent solubilized (in 4% OG) cell supernatant approximately 100 μ l of 1D4 sepharose beads (50% bead solution in buffer B) with a binding capacity of 1mg/ml were added for three 150mm tissue culture plates and incubate with nutation overnight at 4° C. The bead-supernatant mixture was then collected in a plastic (purification) protein purification column. The protein purification was carried out at room temperature with two minute wait between the washes and a five minute wait between elutions. The beads in the column were washed with 10 column volumes of wash buffer (buffer B with 0.88% OG). This was followed by high salt wash with 10 column volumes of buffer N with 500mM NaCl instead of 150mM NaCl (**Note:** The high salt wash was included to prevent the broad UV/vis absorbance peak at 280nm with a shift towards 260nm for the purified protein. By including high salt wash in the purification protocol I obtained a sharp 280nm absorbance peak for purified protein.). Next the column was washed with 20 column volumes of buffer N. The proteins were then eluted in buffer N with 70 μ M nonapeptide. All the fractions were collected and analyzed on Western blot for presence of 1D4 tagged mGluR6. Fractions containing the protein were pooled and snap frozen in liquid nitrogen and stored at -80°C for later use.

2.3.3.1 Optimization of purification protocol

There was a need to optimize the purification protocol for mGluR6 because (1) there was significant loss of protein in the pellet after solubilization and (2) the purified protein peak had a broad UV/vis absorbance peak at 280nm with a shift towards 260nm when high salt wash was

not followed in the purification procedure. I speculated that these problems could be because of the direct solubilization of cells with 4% OG which was inefficient and resulted in solubilized supernatant contaminated with nuclear components. I adopted Dr. Guillermo Calero's lab protocol where the cells are first disrupted with osmotic shock before detergent solubilization.

Membrane preparations by osmotic shock and subsequent solubilization: Use cell pellet prepared from five 145mm plates (see section 2.3.3) or 2g (wet weight) of cell pellet from spinner flask suspension culture (see section 2.2.4) for this membrane preparation. Cell pellet was resuspended in 5.5ml of buffer O and homogenized with 100 strokes in a dounce homogenizer and then centrifuged at 1000g for 15min at 4°C. The supernatant was transferred to a fresh tube and the pellet resuspended in 5.5ml of buffer O. The pellet was homogenized with 100 strokes in dounce homogenizer and additionally passed through 27 ½ gauge needle. The supernatant was collected by centrifuging at 1000g for 15min at 4°C and added to the supernatant from earlier step. Based on the volume of supernatant suitable amounts of 1M Tris-HCl pH 7.4 and 1M NaCl was added to bring their concentration to 50mM and 150mM respectively. Protease inhibitors were also added at this time. The supernatant was centrifuged at 100,000g for 45min at 4°C. The pellet was collected and detergent solubilization and purification was performed as described in section 2.3.3.

2.3.4 Purification of $G\alpha_0\beta_3\gamma_{13}$ complex from insect cells

For details of protein expression from insect cells see section 2.2.5. This protocol is an attempt to purify the $G\alpha_0\beta_3\gamma_{13}$ complex by anti-HA antibody affinity purification taking advantage of the N-terminus HA tag on $G\gamma_{13}$ (see section 2.2.5 for details). Generally the $G\alpha$ and $G\beta\gamma$ were purified separately and reconstituted later. In our case $G\alpha$ has no tag so I attempted to purify the entire

complex. The following references were used as guidance for developing our protocol: (Graber et al., 1992a, 1994; Graber et al., 1992b; Sternweis and Robishaw, 1984). Described here is the optimized protocol.

All the buffers were kept cold and the purification was carried out in a cold room. On the day of purification each 500ml cell pellet (prepared and snap frozen as described section 2.2.5) was thawed on ice in 7.5 times wet weight of buffer K. The cells were homogenized using dounce homogenizer (25 strokes). To the homogenized sample 7.5 times buffer K with 4% Brij® 58 was added to yield a final concentration of 2% Brij® 58. The detergent added samples were gently nutated at 4°C for 1-1.5h. The detergent extract was centrifuged for 30min at 100,000g. The supernatant was carefully removed avoiding any particulate matter. Aliquots from different steps were collected and analyzed on protein gels and Western blots to monitor purification of $G\alpha\beta_3\gamma_{13}$ (Figure 2.3).

The anti-HA antibody conjugated resin was obtained from Sigma (catalog # A2095). 1ml (1:1 suspension) of this resin was thoroughly resuspended and added to the detergent extract and incubated with nutation in cold for 3 - 4h. This mixture was then loaded onto a disposable plastic protein purification column (Bio-Rad). The flow through was collected in 15ml fractions. The beads on the column were washed with 20 column volumes of buffer P. After this, the column was washed with 30 column volumes of buffer Q, to exchange 2% Brij®58 to 0.001%. The $G\alpha\beta\gamma$ complex was then eluted in buffer Q with 10 μ M HA peptide (Anaspec; catalog #21158) Elutions were collected in 6 x 1 column volume aliquots with at least 15min incubation of column between each elution. This was followed by 5 x 1 column volumes low pH elutions with buffer R and buffer S, low pH buffers were previously used to elute $G\alpha$ without loss of activity (Graber et al., 1992a, 1994). The elutions were immediately neutralized by adding 50-75 μ l of

buffer T for 1ml of elution. It was made sure that the low pH elutions do not take longer than 10-15min as low pH might denature the antibody on the column. As soon as the elutions were complete the antibody columns were washed with 10 column volumes of buffer B. The HA-peptide and low pH elutions were pooled separately and were placed in dialysis bags/cassettes with 50,000 MWCO. The samples were dialyzed against 4l of buffer U with two buffer changes every 6h. The dialyzed samples were further concentrated by using Amicon Ultra-15 centrifugal filter devices with 50,000 MWCO (Millipore; catalog # UFC905008). As shown in Figure 2.3 relatively pure $G\alpha_o\beta_3\gamma_{13}$ complex is obtained by elutions with HA peptide and pH 2.5 elutions, while there is no elution of the complex at pH 4.0.

Regeneration of antibody column: The column was washed with 3 column volumes of 0.1M Glycine, pH 2.0, followed by 15 column volumes of buffer B. The pH of the column after 15 column volumes wash should return to neutral. The column was washed with 3 column volumes of buffer B 0.1% (15.3mM) sodium azide and stored at 4°C. The regenerated antibody column can be re-used for purification purposes.

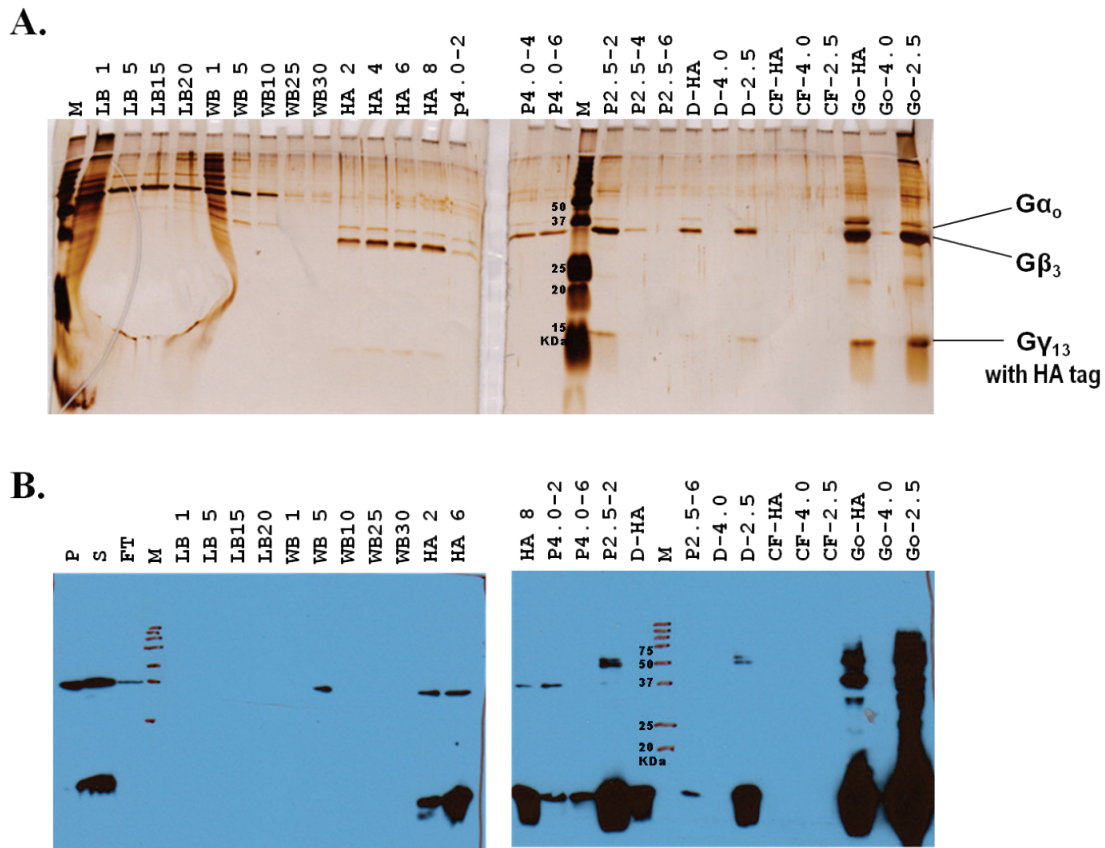


Figure 2.3 Purification of $G\alpha_0\beta_3\gamma_{13}$ from insect cells using optimized protocol

Samples collected at various steps of purification protocol are analyzed on (A) silver stained protein gel and (B) western blot. The samples are supernatant (S) and pellet (P) after detergent solubilization, flow through of supernatant from the column (FT), washes with buffer P (LB), washes with buffer Q (WB), HA peptide elutions (HA), pH 4.0 elutions (p4.0), pH 2.5 elutions (p2.5), HA peptide elutions after dialysis (D-HA), pH 4.0 elutions after dialysis (D-4.0), pH 2.5 elutions after dialysis (D-2.5), flow through from concentrator for dialyzed HA peptide (CF-HA), pH 4.0 (CF-4.0) and pH 2.5 (CF-2.5) elutions, concentrated elutions of HA peptide (Go-HA), pH 4.0 (Go-4.0) and pH 2.5 (Go-2.5). Samples were separated on a 15% SDS-PAGE gel. Western blot was probed with monoclonal mouse primary antibodies anti-Go (Chemicon; catalog # MAB3073) and anti-HA (from Covance; catalog # MMS-101P) (at 1 to 3,000 dilution each) and goat anti-mouse secondary antibody (at 1 to 10,000 dilution).

2.3.5 Purification of transducin

Transducin (G_t) was purified from bovine ROS as described (Baehr et al., 1982). All steps were carried out on ice and in light. Each vial of 50 retinae was divided into 2 x 50 ml Falcon tubes. Each fraction was homogenized in 15 ml of buffer (70mM K_2HPO_4/KH_2PO_4 (pH 6.8), 1mM MgOAc, 5mM β -mercaptoethanol, 0.1mM PMSF) containing 30% sucrose by vortexing for 1 min. After spinning at 4500 rpm for 6 min using an SA600 rotor, the supernatant was kept separately and the pellet resuspended by vortexing in 15 ml of buffer (70mM K_2HPO_4/KH_2PO_4 (pH 6.8), 1mM MgOAc, 5mM β -mercaptoethanol, 0.1mM PMSF) containing 30% sucrose. After spinning as above, all supernatants were combined and slowly mixed with one volume of buffer (70mM K_2HPO_4/KH_2PO_4 (pH 6.8), 1mM MgOAc, 5mM β -mercaptoethanol, 0.1mM PMSF). The crude ROS were pelleted (10000 rpm, 10 min, SA600 rotor). The pellet was homogenized using a manual homogenizer in a total volume of 40 ml of buffer (70mM K_2HPO_4/KH_2PO_4 (pH 6.8), 1mM MgOAc, 5mM β -mercaptoethanol, 0.1mM PMSF) containing 15% sucrose. Two 20 ml fractions of the homogenate were underlayered with 10 ml of 0.64 M sucrose in buffer (70mM K_2HPO_4/KH_2PO_4 (pH 6.8), 1mM MgOAc, 5mM β -mercaptoethanol, 0.1mM PMSF) utilizing a long needle. After spinning the samples (10 min, 10000 rpm, SA600 rotor), the pellet was resuspended in a total volume of 20 ml of buffer (70mM K_2HPO_4/KH_2PO_4 (pH 6.8), 1mM MgOAc, 5mM β -mercaptoethanol, 0.1mM PMSF) containing 0.64 sucrose solution by manual homogenization with a pestle and by passage through a No. 23 gauge needle. 4 sucrose gradient tubes were prepared in Beckman ultra-clear centrifuge tubes in the cold room as follows: 9 ml of 0.78 M sucrose in buffer (70mM K_2HPO_4/KH_2PO_4 (pH 6.8), 1mM MgOAc, 5mM β -mercaptoethanol, 0.1mM PMSF) was under-laid with 1 M sucrose in buffer (70mM

$\text{K}_2\text{HPO}_4/\text{KH}_2\text{PO}_4$ (pH 6.8), 1mM MgOAc, 5mM β -mercaptoethanol, 0.1mM PMSF), then with 1.2 M sucrose. About 5 ml of crude ROS were carefully overlaid on the top of each gradient. The balanced tubes were centrifuged (25000 rpm, 45 min, 4°C, SW28 rotor). The 0.78M/1M interface was recovered by aspirating and diluted to 50 ml with buffer (70mM $\text{K}_2\text{HPO}_4/\text{KH}_2\text{PO}_4$ (pH 6.8), 1mM MgOAc, 5mM β -mercaptoethanol, 0.1mM PMSF). The ROS solution was centrifuged (20000 rpm, 30 min, rotor Ti45) and washed 4 times with buffer (5mM Tris (pH 7.5), 5mM MgOAc, 5mM β -mercaptoethanol, 0.1mM PMSF), each resuspension followed by passage through a No. 23 needle. G_t was then extracted by three further washes with buffer (5mM Tris (pH 7.5), 5mM MgOAc, 5mM β -mercaptoethanol, 0.1mM PMSF) containing 100 μ M GTP. This extract was applied to either a hexylagarose or a DE52 column.

A 6ml (6 cm x 1.5 cm) hexyl agarose column (ICN) was equilibrated with buffer (5mM Tris (pH 7.5), 5mM MgOAc, 5mM β -mercaptoethanol, 0.1mM PMSF). The GTP extractions were applied to this column at a flow rate of 0.3 ml/min. The column was then washed with buffer (5mM Tris (pH 7.5), 5mM MgOAc, 5mM β -mercaptoethanol, 0.1mM PMSF) containing 100mM NaCl until reaching the pre-wash base-line of the equilibration (removal of GTP). At this point buffer (5mM Tris (pH 7.5), 5mM MgOAc, 5mM β -mercaptoethanol, 0.1mM PMSF) was supplemented with 300mM NaCl and 1ml-fractions were collected. Fractions containing the 280 nm peak were pooled and dialyzed over night against 1l of buffer (50% glycerol, 100M NaCl, 20M Tris (pH 7.5), 10mM β -mercaptoethanol, 5mM MgOAc). The protein was stored in 200 μ l aliquots at -20°C.

2.4 IMMUNOFLUORESCENCE

2.4.1 Collagen coating of coverslips

Coverslips were immersed individually in 90% Ethanol and then air dried in a culture dish for a few minutes. Enough (200ul/coverslip) collagen (0.3 mg/ml dissolve in water; BD Biosciences, 354259) was added to cover the surface of coverslips and left for one hour. After one hour, the collagen was aspirated and kept to dry overnight under ultra-violet light.

2.4.2 Growing and preparing cells on coverslips for imaging

A confluent 150mm cell culture plate of COS-1 or HEK293S stable cells was split 1:10 and the cells were added to a 150mm cell culture dish with collagen coated coverslips in it. The cells are usually 50-60% confluent 32-48 hours after plating. At this time, transfection was carried out in the case COS-1 cells (see section 2.2.2) while the HEK293S stable cells were induced. See section 2.2.1 for COS-1 and HEK293S cell culture procedures. Immunostaining of these coverslips were carried out 48-55h post-transfection.

2.4.3 Immunostaining

The immunostaining protocol, Hoescht stain and gelvatol reagents were obtained from the Centre of Biological Imaging at University of Pittsburgh (<http://www.cbi.pitt.edu/>). Leica TCS and Zeiss Meta 510 confocal fluorescence microscopes at this facility were used for imaging the cells. The adapted protocol is described here.

If cells were grown on coverslips in a 15cm dish, then coverslips with cells were carefully transferred to a 24 well plate. The non-cell coated side of the coverslips was placed facing the bottom of the well with media A or buffer B . The media in the wells was aspirated and the wells were washed 3 times with 1ml buffer B. To each well 500 μ l of 2% paraformaldehyde was added and cells were fixed by incubating for 15min. The cells were then permeabilized with 0.1% Triton X in buffer B (500 μ l/well) for 15min and rehydrated with 3 x 1ml washes with buffer B. Cells were then re-washed 5 times with 0.5% BSA in buffer B (1ml/well) and then blocked with 2% BSA in buffer B (500 μ l/well) for 45 min. Following this, cells were washed 5 times with 0.5% BSA in buffer B (1ml/well). Cells were then incubated with primary antibody (500 μ l/well; 1:1000 dilution for 2mg/ml 1D4 antibody) in 0.5% BSA in buffer B for 60 min (**Note:** The antibody solution was vortexed and centrifuged in a table top centrifuge at 13,000rpm for 5min to pellet BSA aggregates. This is required to obtain clean images.). Primary antibody was not added to controls. After the incubation, cells were washed 5 times with 0.5% BSA in buffer B (1ml/well). Add 500 μ l/well of 0.5% BSA in buffer B containing 1:500 dilution of 2mg/ml Alexafluor 488 goat anti-mouse secondary antibody (Invitrogen, A11029), 1:250 dilution of 6.6 μ M Rhodamine-Phalloidin (Invitrogen, R415) and 1:1000 dilution of 5mM DRAQ-5 (Biostatus, DR50201) and incubated for 60min (**Note:** The antibody solution was vortexed and centrifuged in a table top centrifuge at 13,000rpm for 5min to pellet BSA aggregates. This is required to obtain clean images.) After the incubation, cells were washed 5 times with 0.5% BSA in buffer B (1ml/well), followed by another 5 washes with buffer B. If nuclear stain DRAQ-5 is not available it can be substituted Hoechst stain which was added at this step. Hoechst stain was dissolved in water at 1 mg/100ml and stored in dark 4°C (**Note:** Hoechst is a carcinogen.). 500 μ l/well of Hoechst stain was added for 30 sec and replaced immediately

with buffer B. After this, cells were washed 3 times with buffer B 1ml/well). The coverslips were then mounted on to clear glass slides. A small drop of gelvatol or anti-fade was applied on a clean slide and the coverslips were placed with cells facing down on the gelvatol drop. Excess gelvatol was cleaned on the sides with a tissue paper. Cover slips were dried overnight at 4°C in the dark. They were kept stored at 4°C in the dark.

2.5 FUNCTIONAL ASSAYS

2.5.1 [³⁵S]GTP γ S filter binding assay

2.5.1.1 Transducin activation by rhodopsin

Rhodopsin activity was tested *in vitro* by quantifying transducin (G_t) activation using the filter binding assay (Wessling-Resnick and Johnson, 1987) with the following modifications. 5nM of rhodopsin was incubated with or without ligands (for example C3G or Ce6) in reaction buffer (10mM Tris, 100mM NaCl, 5mM MgCl₂, 0.1mM EDTA, 2mM DTT, 0.05% DM, pH 7.4) along with 1 μ M of G_t, 0.1 μ M [³⁵S]GTP γ S and 1 μ M GDP for 5 min with shaking at room temperature. C3G or Ce6 was added from DMSO stock solutions (100mM). Control samples without the ligand contained the equivalent amount of DMSO as a control.

After 5min and after an additional 30min, aliquots (10 μ l) were taken from the reaction mixture and filtered through nitrocellulose filters. Part of the reaction mixture after 5min was illuminated by exposure to yellow (>495nm) light for 30s and incubated at room temperature for 30min with shaking and then filtered through nitrocellulose filters. Immediately after applying the samples, the filters were washed with reaction buffer (10mM Tris, 100mM NaCl, 5mM

MgCl₂, and 0.1mM EDTA, 2mM DTT, 0.05% DM, pH 7.4). The nitrocellulose filters were measured for increase in radioactivity of trapped [³⁵S]GTPγS that is bound to activated G_t.

2.5.1.2 Transducin activation by mGluR6

mGluR6 activity is tested *in vitro* by quantifying G_t activation as described previously (Weng et al., 1997) with modifications. Instead of reconstituting the protein in lipid vesicles, purified mGluR6 (see section 2.3.3) was studied in DM detergent micelles. 50nM of mGluR6 was incubated with different concentrations L-glutamate (from 100mM stock) in reaction buffer (10mM Tris-HCl pH 7.0, 100mM NaCl, 5mM MgCl₂, 2mM DTT, 0.01%DM pH 7.4.) for 30 min at 4°C. Following this 1μM of G_t and 2μM [³⁵S]GTPγS was added to the reaction and left at room temperature. Aliquots were taken from the reaction mix at specific time points and the reactions were terminated by filtering through nitrocellulose filters. Immediately after applying the samples, the filters were washed with reaction buffer (10mM Tris-HCl pH 7.0, 100mM NaCl, 5mM MgCl₂, 2mM DTT, 0.01%DM pH 7.4.). The activation of mGluR6 was concluded from the increase in radioactivity of nitrocellulose filters in the presence of ligand compared to unactivated rhodopsin with the ligand. As a positive control rhodopsin activation was performed similarly with a 30s exposure to yellow light after the initial 30min incubation.

2.5.1.3 Testing Gα_oβ₃γ₁₃ complex activation by mGluR6

The purified Gα_oβ₃γ₁₃ complex from insect cells (see section 2.3.4) was tested for activity at mGluR6. For this mGluR6 was prepared in membranes (see 2.3.2; except that before harvesting cells they were not incubated for 2h with buffer H.) and its activity tested *in vitro* by quantifying G protein activation using the radioactive filter binding assay as reported for mGluR8 (Yamashita et al., 2004). 2nM of mGluR6 in membranes was incubated with 200nM of

G $\alpha_{\beta_3\gamma_{13}}$ in presence or absence of different ligands in the reaction buffer (50mM Hepes, 140mM NaCl, 5mM MgCl₂, 0.015% DM, 0.8 mg/ml L- α -phosphatidyl choline, pH 7.2) for 30min at 10°C. The activation reaction was triggered (time = 0min) by adding 0.1 μ M [³⁵S]GTP γ S and 3 μ M GDP to the reaction mix. Aliquots were taken from the reaction mix at specific time points and the reaction was terminated by adding stop solution (20mM Tris-HCl, 100mM NaCl, 25mM MgCl₂, 0.1 μ M [³⁵S]GTP γ S, 3 μ M GDP pH 7.4) and immediately followed by filtering through nitrocellulose filters. The filters were washed with wash buffer (20mM Tris-HCl, 100mM NaCl, 25mM MgCl₂, pH 7.4). The activation of mGluR6 is concluded from the increase in radioactivity of nitrocellulose filters over time as compared to the initial time point (0.5min).

2.5.2 Cell based cAMP functional assay

For cAMP assays the cells were grown in 24 well plates that were coated with collagen. For collagen coating, 100 μ l of collagen (0.3 mg/ml in sterile water) was added per well and air dried for one hour in a sterile hood. After one hour collagen was aspirated and the wells were left open to dry overnight under UV light in a sterile hood. A confluent 100mm plate with cells was washed with 10ml buffer B and incubated with 1ml of trypsin for 1min. The cells were then resuspended in 4ml of media A and the cells were counted. Depending on the cell density an aliquot of cells was removed and diluted with 25ml of media A to obtain a final cell density of 0.1 million cells/ml. One ml of this suspension was added to each well in a 24 well plate. The cells were then grown in cell culture incubator at 37°C and 5% CO₂. After 72h, each well in the 24 well plate was washed with 1ml of buffer H and then 1ml media E was added to each well. The cells were returned to cell culture incubator. After 48h, the cells were washed twice with buffer H (1 ml per well) to completely remove the growth media and 500 μ l of buffer H with

[³H]adenine (2 μCi/ml) was added/ well and the cells were returned to cell culture incubator for another 2h. This was followed by one more wash with buffer H (1 ml per well) and then the cells were incubated at 37°C with phosphodiesterase inhibitor 3-isobutyl-1-methylxanthine (1mM) prepared in buffer H (225μl/well). The cells were incubated at 37°C for 15 min and then 25μl antagonists (or buffer H) was added from 10x stocks and incubated for another 15min. Forskolin (10μM) was then added with or without ligands, from 10x stocks and the plates were returned to the incubator for another 15 min. The reaction was then stopped by addition of 25μl of 1.2 M trichloroacetic acid and incubated for additional 20min to 30min at room temperature. Later, 25μl of carrier solution (5mM each of adenine, adenosine, ATP, ADP, AMP, cAMP in water) was added and the plates were frozen overnight at -20°C followed by cAMP isolation by two-column chromatographic method with Dowex AG 50W-X4 and alumina columns (Salomon et al., 1974) set up in Dr. Alessandro Bisello's lab, University of Pittsburgh.

2.5.3 Membrane based GTP-Eu fluorescence assay

Initially to set up the assay in our lab I used Neurotensin membrane preparation (RBNXNT1M400UA; lot # 498-374-A) and neurotensin peptide (H-4435; lot# 1013131 Bachem) as controls and followed instructions provided by PerkinElmer:

http://las.perkinelmer.com/Content/relatedmaterials/posters/psh_automationoftrfbasedgtpbindin_g.pdf.

We optimized the conditions for GTP-Eu binding assay for mGluR6 membrane preparations using DELFIA® GTP binding buffers and GTP-Eu reagent (catalog #AD0261 and AD0260) from PerkinElmer. I describe here the optimized protocol. The reactions were performed in 96 well AcroWell™ plates (catalog #28148-575 from VWR scientific). The final

reaction mixture of 100 μ l/well contains 6 μ g membrane in 50mM HEPES, 20mM NaCl, 3mM MgCl₂, 3 μ M GDP and 100 μ g/ml saponin pH 7.4 along with desired concentration of L-glutamate. Each data point is set up as a triplicate. For measuring non-specific binding 5 μ M of GTP γ S was added to the reaction buffer. **Note:** Set up reactions in a 96 tube PCR plate (Fisherbrand, catalog # 14230232) in 125 μ l volume per well and then transfer 100 μ l of final reaction mixture to 96 well AcroWell™ plates using multichannel plate. The plates with the reaction mixture were incubated at room temperature for 30min on a plate shaker with slow shaking. After this pre-incubation step 10 μ l GTP-Eu reagent was added per well (100 μ l of reaction mixture) to obtain a final concentration of 5nM. The plate was incubated with shaking for another 30min and the reaction was terminated by vacuum filtration. The wells are washed two times with 300 μ l wash buffer (50mM Tris-HCl, 10mM MgCl₂ pH 7.5). The trapped GTP-Eu on the wells is measured immediately on VICTOR³™ Multilable Plate Reader (PerkinElmer Life Sciences) using default settings for measuring europium fluorescence (340nm excitation/615nm emission, 0.4ms delay and 0.4ms window) as recommended by the supplier. For mGluR2, 3 and 5 this assay, as optimized for mGluR6, is repeated except for replacing mGluR6 membranes with those of mGluR2, 3 and 5.

Provided below are important notes not mentioned by the supplier but important for the GTP-Eu assay:

- i. GTP-Eu reagent was made into 2 μ l aliquots under dim light conditions and stored in -20°C freezer. The aliquots are made to avoid repeated freeze thaw of samples.
- ii. It is highly recommended to measure the fluorescence of GTP-Eu reagent immediately after receiving from the supplier. I noticed that there is lot of variation among different lots (Figure 2.4). After receiving the reagent measure the fluorescence of GTP-Eu reagent

alone under the optimized experimental conditions. For this set up the reactions as described above but without the membranes and ligands. At the end of incubation measure the fluorescence before (panel A, Figure 2.4) and after the two washes (panel B, Figure 2.4) with 300 μ l wash buffer (50mM Tris-HCl, 10mM MgCl₂ pH 7.5). I noticed that the GTP-Eu reagent which had fluorescence counts > 140,000 (before washes) were reliable for my experiments. All my experiments are performed with GTP-Eu reagent from the lots # 470401 and # 594501. The GTP-Eu reagent from lot # 583762 with fluorescence counts < 50,000 (before washes) was not reliable for the experiments.

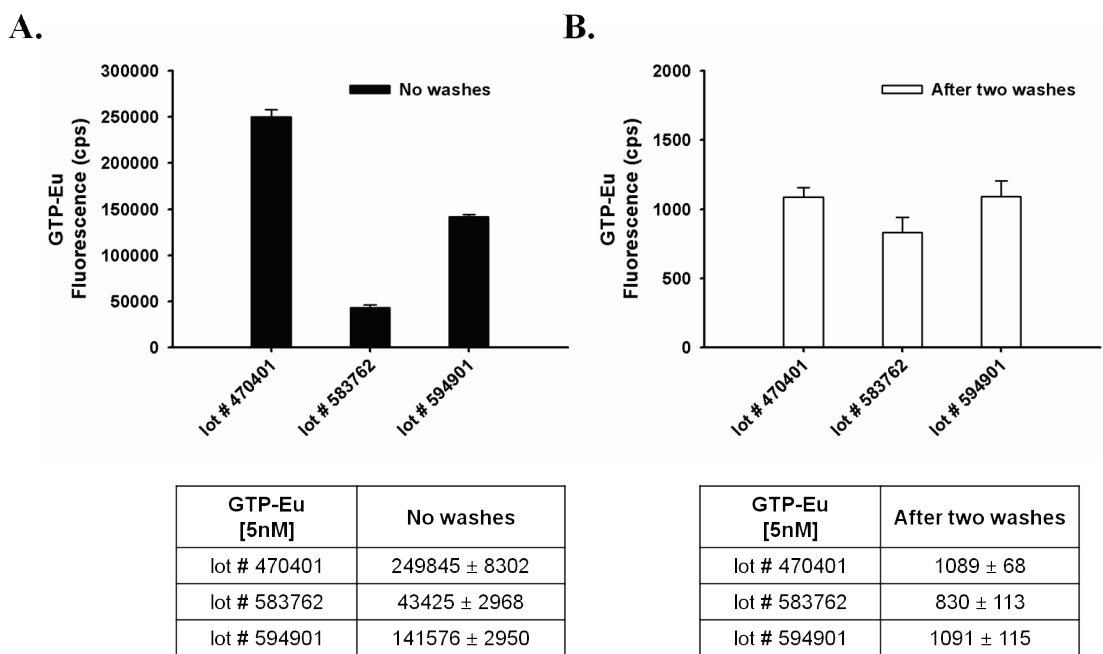


Figure 2.4 Fluorescence of 5nM GTP-Eu reagent from different lots

Shown in the figure are the fluorescence counts of 5nM GTP-Eu reagent (PerkinElmer; catalog #AD0261) from different lots. For measuring GTP-Eu alone fluorescence, reactions are set up in a 96 well plate without the membranes and ligands under optimized buffer conditions. Fluorescence counts are measured (A) before (no washes) and (B) after the two washes with 300 μ l wash buffer (50mM Tris-HCl, 10mM MgCl₂ pH 7.5). The tables below show the actual fluorescence counts.

- iii. The experiments were carried out under normal light conditions in the laboratory but the 96 well plate is always kept covered with aluminum foil to minimize the exposure of GTP-Eu reagent to light.
- iv. We used dot blot apparatus modified with a vacuum gauge connected to vacuum source instead of Vacuum manifold available from Millipore (catalog # MSVMHTS00).
- v. When using the dot blot apparatus for filtering care should be taken that the pressure is between 10 – 15 inches Hg. Membrane filter on the plate gets compromised beyond 15 inches Hg pressure. I noticed that 5 inches Hg is good enough to filter buffers from the wells.
- vi. Keeping the unused wells on the plate covered with tape (PerkinElmer TopSeal(R) catalog #6005185) improves filtering efficiency and to prevent accidental addition of reaction components to unintended wells.
- vii. After filtering the buffer from plates using the filter apparatus tap the plate gently on a set of paper towels laid flat on the table top to remove droplets of buffer that might be hanging under the wells of the plate.
- viii. The wells were presoaked with 300 μ l in the reaction buffer without membranes and ligands (50mM HEPES, 20mM NaCl, 3mM MgCl₂, 3 μ M GDP and 100 μ g/ml saponin pH 7.4) for at least 10min before adding reaction mixture from 96 well PCR tube plate.

2.6 DEGLYCOSYLATION WITH PNGASE F

The oligosaccharides on wild-type and mutant mGluR6 cleaved using PNGase F (New England Biolabs). Rhodopsin is used as a positive control for the deglycosylation experiments. The experiments were set up as described in this reference (Iannaccone et al., 2006) for rhodopsin. Reaction are set up in a 100 μ l volume containing 20mM Tris pH 8, 0.05% DM, 0.5% SDS, 5mM EDTA, 0.1mM PMSF, 1 - 5 μ g of receptor protein and with or without 500U PNGase F. Samples without PNGase F are used as negative controls. The samples were incubated for 3h at room temperature. After 3h 25 μ l sample was mixed with 25 μ l of Lammelli buffer and 20 μ l of this sample (25ng of protein sample) was loaded on a protein gel.

2.7 ANALYTICAL PROCEDURES

2.7.1 Absorption spectra

UV-visible absorption spectra were recorded with a Perkin–Elmer λ 25 spectrophotometer (PerkinElmer, Waltham, MA). All spectra were recorded with a bandwidth of 1nm, response time of 1sec and scan speed of 960nm/min. Measurements were taken at 25°C using a 10mm path length cell.

2.7.1.1 Rhodopsin

Absorbance spectra of purified rhodopsin in 2mM sodium phosphate and 0.05% DM at pH 6 was measured. Rhodopsin concentrations were calculated using the molar extinction co-

efficient of $40,600 \text{ M}^{-1}\text{cm}^{-1}$ (Wald and Brown, 1953) of the chromophore at 500nm (A_{500}). A_{500} was determined either directly from absorbance spectra of pure rhodopsin solutions or by absorbance difference spectroscopy. In a sample cuvette 500 μl of rhodopsin in 2mM sodium phosphate and 0.05% DM at pH6 was added, while the reference cuvette contained only the buffer. First, the dark spectrum was recorded. The rhodopsin solution was illuminated and the spectrum was again recorded. The difference between the two spectra allowed estimation of A_{500} and the concentration of rhodopsin was calculated as above. For the photobleaching, the samples in the cuvette were illuminated with a 150-W fiber optic light (Fiber Lite A-200; Dolan-Jenner, Woburn, MA) equipped with a $> 495 \text{ nm}$ long-pass filter (Oriel) for 30 sec. A final full bleached spectrum (250-650 nm) was recorded immediately after illumination.

2.7.1.2 mGluR6

An absorbance spectrum of purified mGluR6 was measured in buffer N. mGluR6 concentrations were calculated using the molar extinction co-efficient of $105480 \text{ M}^{-1}\text{cm}^{-1}$ at 280nm (A_{280}). The spectra were recorded in the 250 – 500nm range with 500 μl of mGluR6 in sample cuvette, while the reference cuvette contained only the buffer.

Verification of molar extinction coefficient for mGluR6 at 280nm (A_{280})

The molar extinction co-efficient for mGluR6 was theoretical estimated by VectorNTI® software (Invitrogen). I verified that the amount of purified mGluR6 as estimated from the Bradford protein estimation assay (Bio-Rad; catalog #500-006) using rhodopsin as a control (to generate standard curve) was comparable with the values calculated from the theoretical molar extinction co-efficient of $105480 \text{ M}^{-1}\text{cm}^{-1}$ at A_{280} (Figure 2.5).

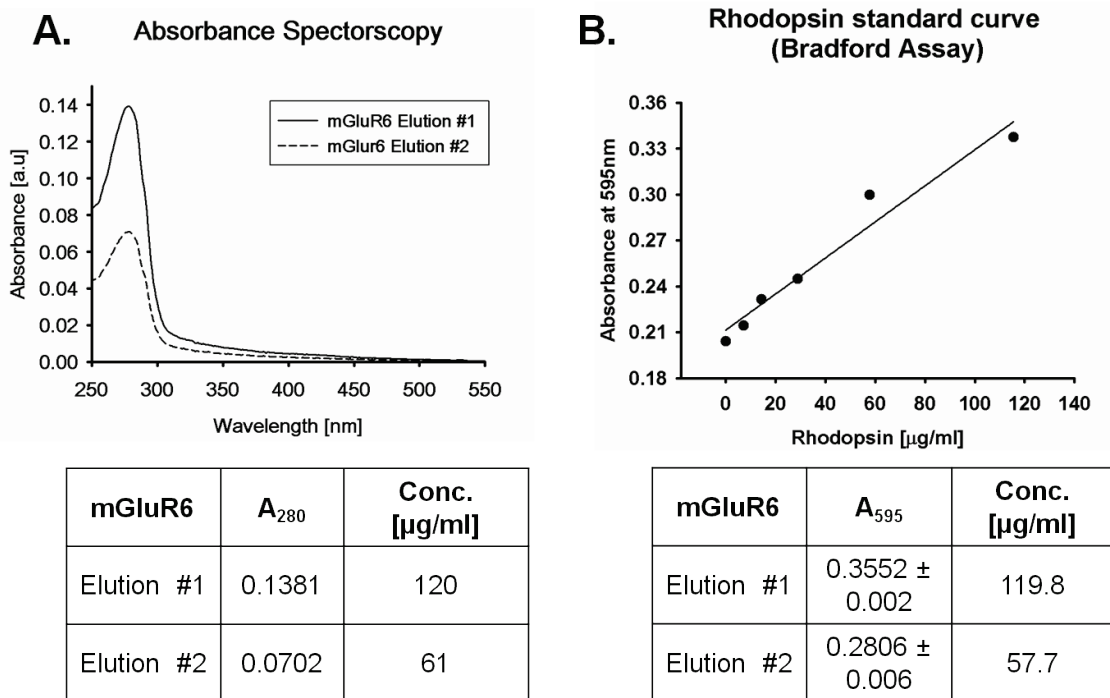


Figure 2.5 Standardization of quantification of purified mGluR6

(A) Absorbance spectrum of mGluR6 elutions. The concentrations as estimated from absorbance values at 280nm and theoretically estimated molar extinction coefficient ($105480 \text{ M}^{-1}\text{cm}^{-1}$) are given the table below. (B) Rhodopsin standard curve representing known concentrations plotted against their average ($n=2$) absorbance at 595nm in a Bradford assay. The linear regression equation with best fit for this data is: $y = 0.0012x + 2114$; $R^2 = 0.95$. Table below shows the concentration of mGluR6 (same samples used in A) as derived from the standard curve. The concentrations from both procedures are comparable

2.7.1.3 Anthocyanins

Anthocyanin stocks were prepared as a 25mM stock. Subsequent dilutions from this stock were made as a 1000-fold stock solution in DMSO (10mM, 5mM, 2.5mM, 1mM and 0.5mM), so that the final DMSO concentration was 0.1% (v/v) or less in the samples. At this concentration DMSO did not alter the pH of the solution. The spectra were recorded in the 250 – 650nm range by adding desired concentration of anthocyanins (from a 1000x stock) to the sample cuvette with 500 μl of buffer, while equal volume of DMSO was added to the reference

cuvette. For measuring absorption spectra of anthocyanins at different pH, the pH in the samples was adjusted by adding appropriate volumes from 1M stock solutions of glycine-HCl (pH 3), sodium acetate-acetic acid (pH 4 and 5), sodium phosphate (pH 6), HEPES-NaOH (pH 7.4) and Tris-HCl (pH 8) to give a final buffer concentration of 50mM.

2.7.2 Meta II decay assay for rhodopsin

Tryptophan fluorescence of rhodopsin was recorded using a Varian Cary Eclipse instrument. For Meta II decay studies, the data acquisition parameters were similar to those described previously (Farrens and Khorana, 1995): excitation and emission wavelengths were at 295nm and 330nm, with slit widths of 5nm and 10nm, respectively. Samples contained 0.25 μ M or 0.5 μ M (as indicated) of purified rhodopsin in 0.05% or 0.6% DM (as indicated) and sodium phosphate buffer at pH 6 was titrated with the working stock solutions of anthocyanins (C3G) and the fluorescence was measured in the dark and after illumination. The sample temperature was kept constant at 20°C during Meta II decay time course measurements. When C3G was present, the fluorescence data obtained was corrected for C3G absorbance at 295nm using the Parker equation (Birdsall et al., 1983; Parker, 1968), $F_{\text{(corrected)}} = F_{\text{(measured)}} * 2.303 * A / (1 - 10^{-A})$, where 'A' is the absorbance of the sample at 295nm, $F_{\text{(measured)}}$ and $F_{\text{(corrected)}}$ are the observed and corrected fluorescence values, respectively. The corrected fluorescence data obtained was analyzed using functions described in (Motulsky and Christopoulos, 2003). For Meta II experiments, the average of dark fluorescence was subtracted from the fluorescence counts after activation. The time $t=0$ was set to coincide with the illumination event. This data was fit using GraphPad Prism version 5.01, to one phase association kinetics using the equation, $Y = Y_0 + (\text{Plateau}-Y_0)*(1-\exp(-K*X))$ where Y_0 ($=0$) is the Y value (Light-Dark fluorescence) when X

(time) is zero, plateau is the Y value at saturation and K is the rate constant (min^{-1}). The half-life ($t_{1/2}$) was computed as $\ln(2)/K$. Graphs were generated using SigmaPlot 10.0 scientific graphing software or GraphPad Prism version 5.01 for Windows, GraphPad Software, San Diego California USA. The Meta II measurements were repeated at least three times.

2.7.3 SDS-PAGE

SDS-Polyacrylamide gel electrophoresis (PAGE) was carried out according to (Laemmli, 1970). Resolving gels (two 7.5% gels which are 1mm) were poured after mixing 3 ml of 30% acrylamide, 3 ml of 1.5M Tris-HCl pH 8.8, 5.8 ml of water, 120 μl SDS (10%), 80 μl APS (10%) and 6 μl TEMED. The gels were poured in glass panes and overlaid with ultra-pure water or 0.05 – 0.1% SDS to keep oxygen away and allow the top of the gel to polymerize well. The gels were allowed to set for 45 – 60min, which was evident by sharp line of refractive index change between the gel and the overlay. The overlay was replaced with stacking gel with the comb in place. Stacking gels (5% acrylamide) were poured after mixing 680 μl of 30% acrylamide, 1ml 0.5M Tris-HCl pH 6.8, 2.2 ml water, 40 μl SDS (10%), 80 μl APS (10%) and 4 μl TEMED. Laemmli protein loading dye (Sigma, S-3401) was used in 1:1 ratio to load proteins on the gel. Gels were run at 200V till the dye front reached the bottom of the gel.

Coomassie staining was done by heating the polyacrylamide gel with 45% methanol, 9% acetic acid, 0.2% Coomassie blue buffer for three times (10 minutes each) in a microwave. The gel was then de-stained with 25% methanol, 10% acetic acid. Silver staining was done following the instruction sheet in SilverSNAP Stain kit (Thermo Scientific, Waltham, MA).

2.7.4 Western blot

The protein samples were mixed with SDS-PAGE buffer and were separated by electrophoresis (200V for 1-1.5 hrs) on a 7.5% SDS-PAGE gel. Proteins were transferred from the gels to polyvinylidene difluoride (PVDF, Bio-Rad) membrane. PVDF membrane was activated by soaking in methanol. The cassette was assembled in a container with transfer buffer by making a sandwich with sponge/tissue paper/gel/membrane/tissue/sponge with the membrane facing the anode side of the cassette. This was then placed in the blotting container and the blot was run at 100V for 1h. The membranes were then processed immediately to detect proteins.

Processing membranes for detecting proteins: The procedure described here is common for detecting proteins on the membranes that are transferred from gels or for membranes from dot blots (2.7.5). The membranes were blocked in blocking buffer: buffer B with 0.05% Tween 20 and 5% dry milk powder at room temperature for 30-60min or at 4°C if left over night. The blots are then incubated for 1 hr at room temperature in 1D4 primary antibody diluted to 1:25000 in buffer B with 0.05% Tween 20. The blots were washed three times wherein each wash was for 15 minutes in wash buffer (buffer B with 0.05% Tween 20). Later, the blots were incubated in Horseradish peroxidase conjugated goat anti-mouse secondary antibodies (Bio-Rad) diluted 1:50000 in wash buffer for 30 minutes at room temperature. The blots were washed thrice for 15 minutes in wash buffer. The blot was then incubated with 6ml of West Pico Chemiluminescent Substrate from Pierce. The blots were then exposed to film in dark room and were developed.

2.7.5 Dot blot

This is a general description of dot blot to evaluate relative levels of protein expression in cells or membranes. Prepare dilutions in a 96 well plate as desired in buffer B. Pre-wet 0.2 μ m nitrocellulose membrane in buffer B (**Note:** PVDF membranes are not recommended). The dot blot apparatus was set up with the blot. Avoid using filter/blotting paper on the bottom of the nitrocellulose for support, though it avoids poking holes in the membranes it will cause concaving of the membrane. Also do not apply too much vacuum as it causes caving of the blot in the wells. Using multichannel pipette 200 μ l of buffer B was added and the blot was washed once. 10 - 20 μ l of sample was transferred on the blot using a multichannel pipette. The sample was left on the blot for at least 5min. After this, just enough vacuum was applied to drain the samples. The wells were washed two times with 200 μ l of buffer B. Again only enough vacuum to drain the buffer. The blot was then removed and the membrane was developed as a regular Western blot (see section 2.7.4).

2.7.6 Cysteine quantification with 4,4'-dithiodipyridine

4,4'-Dithiodipyridine (4-PDS) reacts with free sulfhydryl groups in cysteines to produce stoichiometric amounts of 4-thiopyridone that absorbs at 323 nm (Grassetti and Murray, Jr., 1967). The reaction rate and extent of labeling with 4-PDS can be used as a biophysical probe for evaluating the local environment of cysteines in a protein.

An absorbance spectrum of 500 μ l of 0.25 μ M mGluR6 buffer N in the sample cuvette was obtained. The reference cuvette contained only the buffer. 4-PDS was added to both the sample and reference cuvettes from a 10mM stock solution to yield a final concentration of 25 μ M and

mixed thoroughly. After this absorbance spectrum was recorded every 10 min until the absorbance peak at 323nm was saturated. The difference spectra were obtained by subtracting the absorbance spectrum of mGluR6 alone from those obtained in the presence of 4-PDS to obtain change in absorbance at 323 nm. The number of cysteines reacting with 4-PDS per molecule of mGluR6 is estimated by taking the ratio of the absorbance at 323nm and at 280nm and multiplying it with the ratio of the molar extinction coefficient of mGluR6 ($105480\text{M}^{-1}\text{cm}^{-1}$) and 4-thiopyridone ($19,000\text{M}^{-1}\text{cm}^{-1}$). Cysteines react with 4-PDS in a 1:1 stoichiometric ratio and hence the number of cysteines reacting with 4-PDS was calculated from the 323 nm peak.

2.8 COMPUTATIONAL METHODS

2.8.1 mGluR sequence analysis

Python scripts were written to automate searching, preparing and filtering of sequences of mGluRs before submitting for alignment. Sequences of mGluRs were obtained as genbank files from the NCBI protein database (on 4/21/09) by using search terms "metabotropic", "G-protein" and key word "glutamate receptor". From the full length sequences, the TM region for each entry was isolated by removing amino acids before and after the genbank annotations for TM region ('7tm_3'). In few cases N-terminus of TM region was shorter suggesting incorrect annotation. I observed that defining the beginning of TM as 70 amino acids downstream of the start of cysteine rich domain (genbank annotation - NCD3G), over came this problem, improving accuracy. All duplicate sequences and sequences with less than 240 amino acids (incomplete sequences) were removed. A final set of 92 sequences was subjected to a multiple sequence

alignment (MSA) using the web interface for ClustalW with default settings (Chenna et al., 2003). Gaps at the N-terminus of the MSA were removed. The logo of the alignment was generated using WebLogo (Crooks et al., 2004). The amino acids numbering was based on the positions of human mGluR6 (NCBI Reference Sequence: NP_000834).

2.8.2 GPCR structures from the Protein Data Bank

2.8.2.1 mGluR structures

There were 14 crystal structures deposited in the protein data bank (PDB) available for extracellular ligand binding domains of four different mGluRs as of January 2011 (Table 2.4): mGluR1 (6 structures), mGluR3 (5 structures), mGluR5 (1 structure) and mGluR7 (2 structures). There are no full length mGluR structures available in the protein data bank.

When I prepared homology models of mGluR6 (see section 2.8.4.1) in October 2009 there were only 11 mGluR structures deposited in the PDB for three different mGluRs: mGluR1 (5 structures), mGluR3 (5 structures) and mGluR7 (1 structure).

Table 2.4 List of PDB entries for extracellular ligand binding domains of mGluRs

Recently deposited structure files (PDB IDs in bold) were not included in our homology models. Bottom row in the table provides the total number of PDB structures deposited for each mGluR.

Rat mGluR1	Rat mGluR3	Rat mGluR7	Rat mGluR5
1EWT	2E4U	2E4Z	3LMK
1EWV	2E4V	3MQ4	
1EWK	2E4W		
1ISR	2E4X		
1ISS	2E4Y		
3KS9			
6	5	2	1

2.8.2.2 Class A GPCR structures

As of January 2011, there were a total of 43 structures representing seven different GPCRs deposited in the PDB (Table 2.5). Only class A GPCRs have been crystallized so far. The GPCRs for which structural information is available are bovine rhodopsin (BR; 18 structures including opsin), squid rhodopsin (SR; 2 structures) turkey β_1 adrenergic receptor (β_1 AR; 6 structures), human β_2 adrenergic receptor (β_2 AR; 10 structures), human A_{2A} adenosine receptor (A_{2A}; 1 structure), human chemokine receptor CXCR4 (5 structures) and human dopamine D₃ receptor (D₃R; 1 structure).

Table 2.5 List of PDB entries of available GPCR structures

Bottom row in the table provides the total number of PDB structures deposited for each on the seven receptors.

Bovine Rhodopsin (BR)	Squid Rhodopsin (SR)	Turkey β_1 adrenergic receptor (β_1 AR)	Human β_2 adrenergic receptor (β_2 AR)	Human A _{2A} adenosine receptor (A _{2A})	Human chemokine receptor CXCR4	Human dopamine D ₃ receptor (D ₃ R)
1F88	2Z73	2VT4	2R4R	3EML	3ODU	3PBL
1GZM	2Z1Y	2Y00	2R4S		3OE0	
1HZX		2Y01	2RH1		3OE6	
1JFP		2Y02	3D4S		3OE8	
1L9H		2Y03	3KJ6		3OE9	
1LN6		2Y04	3NY8			
1U19			3NY9			
2G87			3NYA			
2HPY			3P0G			
2I35			3PDS			
2I36						
2I37						
2J4Y						
2PED						
3C9L						
3C9M						
3CAP						
3DQB						
18	2	6	10	1	5	1

2.8.3 Manipulation of GPCR structure files

2.8.3.1 Extraction of ligand binding pockets

The residues in the ligand pocket are defined as those which have at least one atom within 5Å of the ligand. Python scripts were written to extract residues within a ligand binding pocket using this cut-off distance from crystal structures and from docking studies.

2.8.3.2 Extracting inter-residue contacts

Python scripts were created to extract inter-residue distances. An inter-residue contact is defined if the distance between C β -C β (C α -C α in case of glycines) atoms is $\leq 8\text{\AA}$ (a definition used in CASP, also see (Dekker et al., 2004)). A long-range interaction is defined as an inter-residue contact or a statistically significant contact between two amino acids that are separated by at least 8 amino acids in sequence (again as used in CASP and described by (Dekker et al., 2004)).

2.8.4 Homology modeling

The three-dimensional homology models of proteins were built using MODELLER 9v8 (Eswar et al., 2007; Sali and Blundell, 1993). Python scripts were written to automate the submission and analysis of modeling jobs. A total of 30 models were generated using MODELLER. The best model from the top 30 models with lowest Discrete Optimized Protein Energy (DOPE) (Shen and Sali, 2006) and molpdf (modeler objective function) scores was picked by comparing Ramachandran plots created by PROCHECK software (Laskowski et al., 1993).

There was no structural information available for mGluR6 and hence homology models of EC and TM domain of were developed. Available crystal structures of mGluR1 and mGluR3 were used to generate EC domain of mGluR6. The only TM structure available for a long time was for rhodopsin. Recently few other class A GPCRs have been crystallized. Class A GPCR structures will be used to model TM domain structures for mGluR6.

2.8.4.1 Homology models of the EC domain of mGluR6

Closed conformation of mGluR6 was used to identify selective agonists for mGluR6, while open conformation was developed to screen for antagonists. When I built these models in October 2009 the mGluR structures deposited in the PDB were for rat mGluR1 (5 structures), mGluR3 (5 structures) and mGluR7 (1 structure). I used closed conformations available for mGluR1 and mGluR3 as templates to model mGluR6.

From available mGluR structure files the individual chains with closed conformation are isolated and saved: 1EWV_A (chain A of 1EWV), 1EWK_A, 1ISR_A, 2E4U_A, 2E4U_B, 2E4V_A, 2E4V_B, 2E4W_A, 2E4W_B, 2E4X_A, 2E4X_B, 2E4Y_A and 2E4Y_B. Also the coordinates for the hetero atom fields like water, ligands, glycosylation and ions were trimmed from these structure files. These files are then opened in swisspdb viewer (Guex and Peitsch, 1997) to fix the minor loss structure integrity of files when the heteroatom files are removed. This avoids problems when using these files with MODELLER. Using Python scripts I obtained the sequence of PDB files in 'fasta' format and aligned them with default parameters using ClustalX 2.0.12 (Larkin et al., 2007) on the local computer. The alignment was trimmed on the N and C terminus residues to remove over hangs. Also the cysteine rich domains were removed from the alignment. Finally the structure templates of mGluR1 and mGluR3 contained 36 – 512 and 40 – 511 residues respectively. The sequence identity between mGluR1 and mGluR3 in

these domains was 44% and the structure rmsd between their closed conformations was $< 1.25\text{\AA}$ conserved 3D structures. The sequence alignment of the aligned structure files was saved in 'msf' format and opened into the AlignX module of VectorNTI® (Invitrogen). By selecting align to profile option in AlignX mGluR6 sequence was aligned to the existing mGluR1 and mGluR3 alignment without disturbing it. The EC domain of mGluR6 shares a high sequence identity of 40 – 50% with mGluR1 and mGluR3. The final alignment was exported in 'fasta' format. These alignments were used to generate mGluR6 model using multiple template methods. **Note:** If there were gaps in the alignment files ('pir' format), it was made sure that the gaps were represented by '-' and not '.' to prevent problems with MODELLER. Python scripts were written to submit the jobs to MODELLER to generate 30 different models and to compare the DOPE (Discrete Optimized Protein Energy) (Shen and Sali, 2006) and molpdf (modeler objective function) (Eswar et al., 2007; Sali and Blundell, 1993) scores. The best model from the top 30 models with lowest DOPE and scores was picked by comparing Ramachandran plots created by PROCHECK software (Laskowski et al., 1993).

Open conformation of mGluR6 EC domain was developed using the same procedure as described above for closed conformation model except that the templates used in this case were: 1EWV_B, 1EWK_B, 1EWT_A, 1EWT_B, 1ISS_A and 1ISS_B.

2.8.4.2 Homology models of the TM domain of mGluR6

A three-dimensional model of the TM region of human mGluR6 was obtained by homology modeling using the same tools, scripts and methods used for generating EC structure models (see section 2.8.4.1). Structures of bovine rhodopsin (PDB ID: 1U19, chain A), turkey β_1 -adrenergic receptor (PDB ID: 2VT4, chain B), human β_2 -adrenergic receptor (PDB ID: 2RH1, chain A) and human A_{2A} adenosine receptor (PDB ID: 3EML, chain A) were used as templates

to generate an average model of human mGluR6. Sequences from the PDB were extracted and aligned using salign module of MODELLER (Eswar et al., 2008). The AlignX module of VectorNTI® (Invitrogen) was used to align mGluR6 to the sequence alignment of templates by using the ‘align to profile’ option in AlignX. The alignment was manually edited to align the cysteines in the second extracellular loop. Python scripts were used to submit modeling jobs and to aid in analysis. The best model from the top 30 models with lowest DOPE (Shen and Sali, 2006) and molpdf modeler objective function scores was picked by comparing Ramachandran plots created by PROCHECK software (Laskowski et al., 1993).

2.8.5 Docking studies

AutoDock Vina (Trott and Olson, 2010) was used to perform small molecule docking to receptor files. AutoDock Vina and AutoDock (Goodsell et al., 1996; Morris et al., 1998) belong to the same family of software but AutoDock Vina was shown to be faster in execution and more accurate in ranking large molecule (more flexible) docking compared to AutoDock, making it our preferred choice for docking (Chang et al., 2010).

2.8.5.1 Preparation of mGluR receptor files

The receptor files for AutoDock Vina were prepared using AutoDockTools (ADT) from MGLTools 1.5.4 (Sanner, 1999). The receptors files were opened in ADT and using ‘edit → Hydrogens → Add’ option, only polar hydrogens were added to the receptor. If performing docking with flexible receptor residues then these steps were followed: (1) use ‘Flexible Residues → Choose Macromolecule’ option to select the receptor, (2) pick the residues on the molecule to make flexible, (3) choose ‘Flexible Residues → Choose Torsions in ...’ to choose

the bonds to be flexible and finally (4) save the rigid and flexible receptor ‘pdbqt’ files separately using ‘Flexible Residues → Output’ option. In the cases where flexible receptor docking was not performed, the receptor file was saved as a ‘pdbqt’ file immediately after adding hydrogens.

A cubic grid box of 30Å x 30Å x 30Å dimensions was built centered around the ligand binding pocket with the offset of 1.0 (spacing of 1Å), to encompass the ligand binding pocket on the receptor. The x, y, z co-ordinates of the center of the grid box were noted since they were required to generate configuration files for docking see section 2.8.5.3.

2.8.5.2 Preparation of ligand files

In our docking studies the ligands were always flexible to increase docking efficiency as each individual ligand can sample all possible conformational space it can take.

- i. Ligands for validating docking approach: For validating our docking approach I collected known agonist and antagonists from literature and docked them to mGluR1, mGluR3 and mGluR6. The ligands (64 of them) were prepared using PRODRG server (Schuttelkopf and van Aalten, 2004), where each individual molecules were drawn and their energies minimized with full charges option. The molecules were then saved as ‘pdbq’ for AutoDock 3.0. These molecules were then reopened using ADT tools and processed further. **Note**: Always process ligands in ADT with hydrogens already added. When ligands are opened in ADT tools using ‘Ligand → Open’ option, the molecules are opened and ADT automatically merges all non-polar hydrogen atoms, adds gasteiger charges and assigns ‘TORSDOF’ (for rotatable bonds). After this the files were saved as ‘pdbqt’ files to be used for docking.

- ii. Ligands for virtual screening: Ligands for virtual screening were obtained from Dr. Alexander Doemling (University of Pittsburgh) as 'sdf' files with all possible enantiomers for each individual ligand. I wrote Python scripts to automate preparing of these ligands. First hydrogens were added to these molecules using Python implementation of OpenBabel (O'Boyle et al., 2008) and saved as 'mol2' files. Then 'mol2' files were then processed using prepare_ligand4.py script from MGLTools 1.5.4 (Sanner, 1999) to assign 'TORSDOF' (for rotatable bonds) and to save the molecules in 'pdbqt' format.

2.8.5.3 Docking parameters and protocol

The configuration files for AutoDock Vina were prepared using Python scripts. The docking was performed with these parameters - size_x = 30, size_y = 30, size_z = 30 (grid box dimensions); center_x = x, center_y = y, center_z = z (for determining x, y, z values see section 2.8.5.1); num_modes = 5 or 9 (Maximum number of binding modes are set 9 for small scale docking and 5 for library screens); energy_range = 5 (Maximum energy difference between best and worst default is 3 kcal/mol); exhaustiveness = 48 (default is 8; It is usually set between 48 – 64) and seed = " (optional; if not mentioned the seed was selected randomly). **Note**: In our studies the optimal values for seed and exhaustiveness were determined by extensive iterative docking with the receptor and one of the known ligand (usually L-glutamate) until lowest energies were obtained. These optimal values for seed and exhaustiveness were used in virtual screening to maintain uniformity in parameters for docking of several ligands to the receptor.

2.8.5.4 Analysis of docked structures

The ligand binding residues from the docked structures were extracted as described in 2.8.3.1. The ligand binding residues were compared if they overlapped with that of the known agonist binding pockets. For library screening, Python scripts were written to generate an excel file to list the docking energies and ligand binding residues for each individual ligand. The entries in the excel file are sorted by energies and for an overlap with the known agonist binding pocket. This was followed by visual inspection of top 50 -100 hits to identify interesting ligands.

2.8.6 Generative REgularized ModeLs of proteins (GREMLIN) analysis

2.8.6.1 Method description

We employed the Generative REgularized ModeLs of proteins (GREMLIN) developed by (Balakrishnan et al., 2010), for learning a model of the GPCR protein family. This method uses L1-regularized structure learning for learning the structure of a Markov random field (MRF). A MRF belongs to a class of models known as graphical models. Graphical models are able to compactly represent a multivariate distribution of random variables. This model does not use any notions of mutual information but instead defines a convex optimization problem which is guaranteed to learn the optimal model on convergence. Figure 2.6 shows a cartoon example of how we learn a graph of couplings from a MSA. This figure shows a cartoon figure of a multiple sequence alignment (MSA) and its corresponding mapping to a MRF. Note that column 2 is completely conserved (Y) and so S_2 is learned independent variable in the MRF. Also note that column 1 and column 4 co-vary with each other, whenever there is an 'S' in column there is an 'H' in column 4, also whenever there is an 'F' in column 1 there is a 'W' in column 4. This coupling is mapped as an edge between S_1 and S_4 in the MRF.

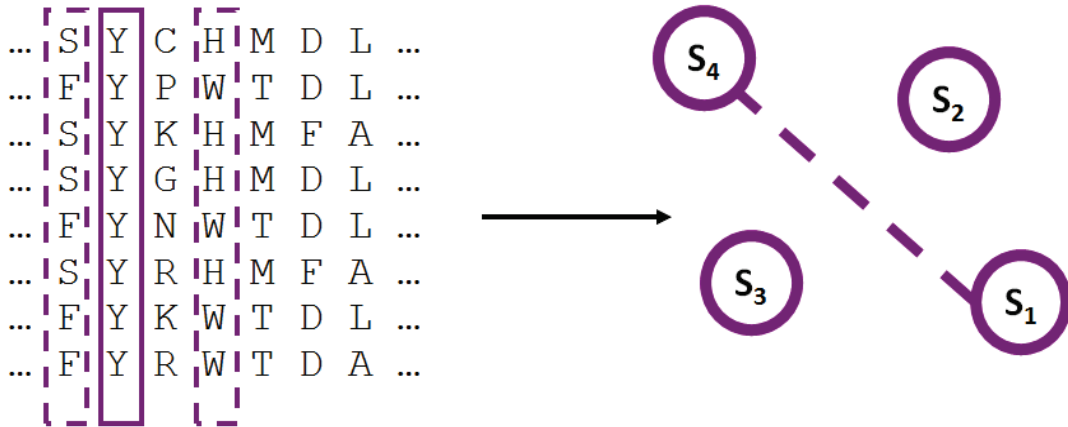


Figure 2.6 Cartoon of a multiple sequence alignment and its mapping to a Markov random field

This figure is adapted from (Balakrishnan et al., 2010). Shown in the figure is a cartoon figure of a multiple sequence alignment (MSA) and its corresponding mapping to a Markov random field (MRF). Note that column 2 is completely conserved ('Y') and so S_2 is an independent variable in the MRF. Also note that column 1 and column 4 co-vary with each other, this is mapped as an edge between S_1 and S_4 .

The probability of a particular sequence $x = (x_1, x_2, \dots, x_p)$ according to M is defined as:

$$P_M(x) = \frac{1}{Z} \prod_{s \in V} \phi_s(X_s) \prod_{(s,t) \in E} \psi_{st}(X_s, X_t)$$

where Z , the so-called partition function, is a normalizing constant defined as a sum over all possible assignments to X . ϕ and ψ are the node and the edge potentials of the MRF respectively.

Since the number of sequences in some classes of GPCRs are of less than 100 we want to insure against over fitting. For this purpose we employ L1-regularization for learning the structure of the MRF. L1-regularization learns a sparse set of edges in the graphical model. L1-regularization has useful properties such as statistical efficiency (Tropp, 2006) i.e. lesser number of samples are needed to learn an accurate model. The optimization problem essentially trades of

a likelihood term against a regularization term which accounts for the complexity of the model. This is a standard approach in most regularization settings. In particular we solve the following optimization problem by using block-regularized structure learning (Schmidt et al., 2008),

$$\begin{aligned} \max_{\{\Theta, \alpha\}} \text{pll}(\Theta) - \lambda_{\text{node}} \|v\|_2 - \lambda_{\text{edge}} \sum_{1 \leq s < t \leq p} \alpha_{st} \\ \text{subject to : } \forall (1 \leq s < t \leq p) : \alpha_{st} \geq \|w^{st}\|_q \end{aligned}$$

where, θ are the node and the edge potentials of the MRF which are the parameters of the model, $\text{pll}(\theta)$ corresponds to the pseudo likelihood function, λ_{node} is the edge penalty levied on the node potentials and λ_{edge} is the edge penalty on the edge potentials; v and w^{st} correspond to the node and edge potentials, respectively; p is the number of different types of values that a random variable in the MRF can take, which in this case is 21 (20 amino acids + 1 gap character).

The model is generative in that it can model $P_M(x)$ where x is any new sequence. This allows for both sampling and classification tasks. In this paper, we focus mainly on the results from the structure learning task. The topology of the graphical model will tell us about the network of interacting residues and will also be able to distinguish between direct and indirect couplings. By this approach we attempt to glean insight into the correlated mutations governing mechanisms of communication in GPCRs.

2.8.6.2 Model selection

The problem of model selection is choosing a model from among a number of candidate models. GREMLIN can return a range of models that vary in the level of complexity and predictive power. This is controlled by the user defined model complexity parameter (Edge Penalty). The user can dial up or dial down the model complexity parameter to get sparser or

denser models as desired. According to the principle of Occam's razor, a simpler model is preferred over a complex model. So model selection equates to choosing an appropriate edge penalty.

The typical approach is to do cross validation over the data set, however in our case, there is no ground truth. Instead we learn a null model from our data. We do this by doing a permutation test. We randomly permute the columns of our MSA in order to destroy all correlations between columns while retaining the column wise distribution of amino acids. We then run the structure learning code to learn a number of models. The lowest edge penalty at which the number of edges in the graphical model goes to zero is considered to be our null model. In our experiments we found that an edge penalty of 38 gave us our desired null model. We then learned all our models on the unpermuted dataset for an edge penalty of 38 or higher in order to get edges at a zero false positive rate. All the edges that are returned at this level of model complexity will be referred to as “**Sturdy**” edges. The subsequent analysis on GPCRs will be based on these sturdy edges unless otherwise stated.

2.8.6.3 GPCR ligand binding pockets

We mapped ligand binding pockets of different GPCRs onto bovine rhodopsin for comparative studies using GREMLIN. The amino acids numbering is based on the positions of bovine opsin (NCBI Reference Sequence: NP_001014890.1). Pair wise sequence/structure based alignments between rhodopsin (PDB ID: 1U19) and other GPCR structures was generated using the salign module from MODELLER (Eswar et al., 2008) for this purpose. All ligand binding pockets shown in this paper are mapped onto the structure of bovine rhodopsin.

In addition to comparing ligand binding pockets directly (i.e. extracting 5Å residues in PDB ID: 1F88 for rhodopsin to identify the retinal ligand binding pocket), we also generated

several combined sets of pocket residues. This was necessary because some GPCR structures have been crystallized with different ligands (Table 2.6).

Table 2.6 Ligands co-crystallized with GPCR structures

The peptide CVX15 binding CXCR4 is shown in bold. All other ligands are small molecules. The numbers in parenthesis denote the total number of available structures for individual receptors.

Receptor	PDB IDs [number of structures]	Ligands
Bovine Rhodopsin (BR)	1F88, 1GZM, 1HZX, 1JFP, 1L9H, 1LN6, 1U19, 2G87, 2HPY, 2I35, 2I36, 2I37, 2J4Y, 2PED, 3C9L, 3C9M, 3CAP, 3DQB [18]	Retinal, Ligand free
Squid Rhodopsin (SR)	2Z73, 2ZIY [2]	Retinal
Turkey β_1 adrenergic receptor (β_1 AR)	2VT4, 2Y00, 2Y01, 2Y02, 2Y03, 2Y04 [6]	Cyanopindilol, Dobutamine Carmoterol, Isoprenaline Salbutamol
Human β_2 adrenergic receptor (β_2 AR)	2R4R, 2R4S, 2RH1, 3D4S, 3KJ6, 3NY8, 3NY9, 3NYA, 3POG, 3PDS [10]	Carazolol, Timolol, ICI 118,551, (molecule from Kolb et al, 2009), Alprenolol, BI-167107, FAUC50
Human A2A adenosine receptor (A2A)	3EML [1]	ZM241385
Human chemokine receptor CXCR4	3ODU, 3OEO, 3OE6, 3OE8, 3OE9 [5]	IT1t, CVX15
Human dopamine D3 receptor (D3R)	3PBL [1]	Eticlopride

We defined a common ligand binding pocket for each individual receptor by combining ligand binding pockets from all available crystal structures (Table 2.7). Thus, for bovine rhodopsin, the common ligand pocket is the combination of the retinal binding pockets of 12 different structures (PDBs excluded are 1JFP and 1LN6 because these represent structure models from NMR structures of protein fragments ; 2I36, 2I37, 3CAP and 3DQB were excluded because these are opsin structures and have no retinal in them). Similarly, common pockets were created for squid rhodopsin (SR), turkey β_1 adrenergic receptor (β_1 AR), human β_2 adrenergic receptor

(β_2 AR), human A_{2A} adenosine receptor (A2A), human chemokine receptor CXCR4 and human dopamine D3 receptor (D3R). While most of the GPCR structures have small molecules as ligands, one CXCR4 structure has a peptide as a ligand (PDB ID: 3OE0) resulting in a large binding pocket. Therefore two additional binding pockets for human CXCR4 were defined – common ligand binding pocket excluding the peptide bound structure (CXCR4-c) and peptide binding pocket alone (CXCR4-pep).

Table 2.7 Common ligand binding pockets defined for GPCRs with structural information

The residues listed are analogous binding pockets mapped on to rhodopsin structure (1U19). The binding pockets are arranged in the order of decreasing size of the binding pocket (left to right). The numbers in the last row represent the number residues in the binding pocket. For CXCR4 two additional pockets without (CXCR4-c) and with peptide alone (CXCR4-pep) are defined.

CXCR4	CXCR4-pep	β_2 AR	β_1 AR	BR	SR	D3R	CXCR4-c	A2A
M1, G3, L31, Q36, F37, M44, T93, T94, T97, S98, F103, E113, G114, A117, T118, P171, L172, Y178, I179, P180, T193, A117, T118, P171, L172, Y178, I179, N200, F203, P180, T193, P194, H195, E196, E197, N200, F203, P180, T193, P194, H195, E196, E197, N200, F203, V204, M207, Y268, A272, I275, H278, Q279, S281, M207, Y268, A272, I275, H278, Q279, S281, P285, M288, T289, A292,	M1, G3, L31, T94, G114, A117, T118, P171, L172, Y178, I179, P180, T193, P194, H195, E196, E197, N200, F203, V204, M207, Y268, A272, I275, H278, Q279, S281, P285, M288, T289, A292,	M86, T94, T97, S98, F103, E113, G114, A117, T118, G121, E122, I179, P180, I189, Y191, F203, V204, M207, F208, H211, W265, Y268, A269, A272, P285, M288, T289, A292, F293, K296,	T94, T97, S98, E113, G114, A117, T118, G121, E122, I179, P180, I189, Y191, F203, V204, M207, F208, H211, W265, Y268, A269, A272, M288, T289, A292, F293, K296,	E113, G114, A117, T118, G121, E122, L125, Y178, E181, S186, C187, G188, I189, Y191, M207, F208, H211, F212, F261, W265, Y268, A269, A272, A292, K296,	M86, G90, E113, G114, A117, T118, G121, E122, L125, Y178, E181, S186, C187, G188, I189, M207, F208, H211, F212, F261, W265, Y268, A269, A292, K296,	T94, E113, G114, A117, T118, G121, E122, P180, G188, I189, V204, M207, F208, H211, W265, Y268, A269, A272, F273, M288, A292, K296,	L31, Q36, F37, M44, T93, T94, T97, S98, F103, E113, G114, A117, Y178, I179, P180, Y268, T289, A292,	T118, P180, E181, F203, M207, W265, Y268, A269, A272, F283, P285, M288, T289, A292,
39	31	30	27	27	25	22	18	14

Finally, to generalize across different GPCRs, we derived additional ligand pockets B1, B2, B3, B4, B5, B6 and B7 representing common sets of residues present in at least one, two, three, four, five, six and seven receptor ligand binding pockets, respectively. These combined ligand binding pockets are listed in Table 2.8.

Table 2.8 Defining a minimal GPCR pocket

The residues listed are analogous binding pockets mapped on to rhodopsin structure (1U19). The binding pockets are arranged in the order of decreasing size of the binding pocket (left to right). The numbers in the last row represent the number residues in the binding pocket. B1, B2, B3, B4, B5, B6 and B7 represent common sets of residues present in at least one, two, three, four, five, six and seven known receptor ligand binding pockets, respectively.

B1	B2	B3	B4	B5	B6	B7
M1, G3, L31, Q36, F37, M44, M86, G90, T93, T94, T97, S98, F103, E113, G114, A117, T118, G121, E122, L125, P171, L172, Y178, I179, P180, E181, S186, C187, G188, I189, Y191, T193, P194, H195, E196, E197, N200, F203, V204, M207, F208, H211, F212, F261, W265, Y268, A269, A272, F273, I275, H278, Q279, S281, F283, P285, M288, T289, A292, F293, A295, K296	M86, T94, T97, S98, F103, E113, G114, A117, T118, G121, E122, L125, Y178, I179, P180, E181, S186, C187, G188, I189, Y191, F203, V204, M207, F208, H211, F212, F261, W265, Y268, A269, A272, P285, M288, T289, A292, F293, K296	T94, T97, S98, E113, G114, A117, T118, G121, E122, Y178, I179, P180, E181, G188, I189, Y191, F203, V204, M207, F208, H211, W265, Y268, A269, A272, P285, M288, T289, A292, F293, K296	T94, E113, G114, A117, T118, G121, E122, P180, I189, F203, V204, M207, F208, H211, W265, Y268, A269, A272, M288, T289, A292, K296	E113, G114, A117, T118, G121, E122, P180, I189, F203, M207, F208, H211, W265, Y268, A269, A272, M288, A292, K296	E113, G114, A117, T118, G121, W265, Y268, A269, A272, A292	T118, M207, Y268, A292
61	38	31	22	18	10	4

Table 2.9 List of buffers and reagents

-
- ^A DMEM supplemented with 100units/ml Penicillin/Streptomycin (P/S), 10% bovine serum (BS)
- ^B Phosphate-buffered saline (PBS): 137mM NaCl, 2.7mM KCl, 1.8mM KH₂PO₄, 10mM Na₂HPO₄ (pH 7.2)
- ^C DMEM supplemented with 100units/ml P/S
- ^D DMEM-F12 supplemented with 100units/ml P/S, 10% fetal bovine serum (FBS)
- ^E DMEM supplemented with 10% BS, 100units/ml P/S, 2µg/ml tetracycline, 5mM Sodium butyrate; **Note:** When establishing stable cell lines FBS was used instead of BS.
- ^F DMEM (with no Ca²⁺) supplemented with 10% bovine serum, 100units/ml P/S, 0.1% (wt/vol) Pluronic Acid, 50µg/ml Heparin sulfate
- ^G DMEM (with no Ca²⁺) supplemented with 10% BS, 100units/ml P/S, 0.1% (wt/vol) Pluronic Acid, 50µg/ml Heparin sulfate and with 1ml each of component A, B and C (Mediatech; catalog # 99-182, 99-175 and 99-176) for 100ml of media
- ^H Hank's Buffered Saline Solution (HBSS): 0.44mM KH₂PO₄, 0.34mM Na₂HPO₄, 136.89mM NaCl, 5.37mM KCl, 1.26mM CaCl₂, 0.81mM MgSO₄, 4.17mM NaHCO₃, 5.55mM D-Glucose and 10.00mg/L Phenol red pH 7.3
- ^I Sf-900 II SFM media (Invitrogen), 2% FBS, 25units/ml P/S
- ^J Insect cell phosphate-buffered saline (IPBS): 7.3mM NaH₂PO₄, 58mM KCl, 47mM NaCl, 5.0 mM CaCl₂ (pH 6.2)
- ^K Homogenization Buffer: 10mM Tris, 25mM NaCl, 10mM MgCl₂, 1mM EDTA, pH 8.0 with 1mM β-mercaptoethanol, 10µM GDP, 17µg/ml (0.1mM) phenylmethylsulfonyl fluoride, 20 µg/ml benzamidine, and 2µg/ml each of aprotinin, leupeptin, and pepstatin A
- ^L 50 mM HEPES, 140 mM NaCl pH 6.5
- ^M 50mM HEPES, 140 mM NaCl pH 7.2
- ^N 50mM Tris, 150mM NaCl, 0.88% OG pH 8.0. This Tris buffer is made from TRIZMA® Hydrochloride (T-5941) and TRIZMA® Base (T-6066) from Sigma chemicals
- ^O Hypotonic Buffer: 20 mM Sucrose, 25mM Tris and 1 mM EDTA (pH 7.4)
- ^P 10mM Tris-Cl, 25mM NaCl, 10mM MgCl₂, 1mM EDTA, 10µM GDP, 2% Brij 58, pH 8.0 with 1mM β-mercaptoethanol
- ^Q 50mM Tris-Cl, 100mM NaCl, 10mM MgCl₂, 1mM EDTA, 10µM GDP, 0.001 % Brij 58, pH 8.0 with 1mM β-mercaptoethanol
- ^R 0.1M Glycine, 100mM NaCl, 10mM MgCl₂, 1mM EDTA, 10µM GDP, 0.001% Brij 58 pH 4.0
- ^S 0.1M Glycine, 100mM NaCl, 10mM MgCl₂, 1mM EDTA, 10µM GDP, 0.001% Brij 58 pH 2.5
- ^T 1M Tris, 10mM MgCl₂, 1mM EDTA, 10µM GDP, 0.001% Brij 58 pH 8.0
- ^U 20mM Tris, 100mM NaCl, 1mM MgCl₂, 10µM GDP, 0.001 % Brij 58 pH 7.5 with 1mM β-mercaptoethanol

Table 2.10 List of constructs and stable cell lines created or used in this thesis.

For stable cell line clone #'s the first digit represents the concentration of G418 in mg/ml used for selection. All the clones were selected for maximal expression of receptor. NA: not applicable. *Glycine to serine mutation in 1D4 tag abolishes detection of protein on Western blot.

	Construct Name	Short name	Features	1D4 tag	Stable cells	Source
1	pMT3-GRM6-partial		Missing aminoacids 20 - 363 of human mGluR6	yes	NA	Dr. Phyllis Robinson
2	pMT3-GRM6		Full length human mGluR6	yes	NA	Dr. Phyllis Robinson
3	pMT3-KOZ-GRM6		pMT3-GRM6 with kozak sequence insertion at start codon	yes	NA	Kalyan Tirupula
4	pMT4-GRM6-516		No start codon; sequence for S583 to F845	yes	NA	Dr. Gulsum Anderson
5	pMT4-GRM6-585		No start codon; sequence for S583 to K877	yes	NA	Dr. Gulsum Anderson
6	pMT3-mGluR6:Rho (1-555:4-348)	chimera #2	expresses human mGluR6 (1-555) fused to Bovine opsin (4-348)	not needed	NA	Kalyan Tirupula
7	pMT3-mGluR6:Rho (1-574:23-348)	chimera #3	expresses human mGluR6 (1-574) fused to Bovine opsin (23-348)	not needed	NA	Kalyan Tirupula
8	pACMV-tetO-GRM6-516		No start codon; sequence for S583 to F845	yes	no	Dr. Gulsum Anderson
9	pACMV-tetO-GRM6-585		No start codon; sequence for S583 to F845	yes	no	Dr. Gulsum Anderson
10	pACMV-tetO-GRM6(1-877)	ACMV-mGluR6	Full length human mGluR6	yes	clone # 2-B	Kalyan Tirupula
11	pACMV-tetO-GRM6-(583-845)-7TM	7TM	Start codon followed by S583 to F845	*missense mutation	no	Kalyan Tirupula
12	pACMV-tetO-GRM6-(583-877)-7TMC	7TMC	Start codon followed by S583 to K877	yes	clone # 2-21	Kalyan Tirupula
13	pACMV-tetO-GRM6-XR-7TMC(575-877)	XR-7TMC	Start codon followed by P575 to K877	yes	clone # 3.3	Kalyan Tirupula
14	pACMV-tetO-GRM6-XR-7TMC(575-877) C754A	XR-7TMC C754A	same as XR-TMC but with C754A mutation	yes	no	Kalyan Tirupula
15	pACMV-tetO-GRM6-XR-7TMC(575-877) C765A	XR-7TMC C765A	same as XR-TMC but with C765A mutation	yes	no	Kalyan Tirupula
16	pACMV-tetO-GRM6-XR-7TMC(575-877) C793A	XR-7TMC C793A	same as XR-TMC but with C793A mutation	yes	no	Kalyan Tirupula
17	pACMV-tetO-GRM6-CRD-7TMC(516-877)	CRD	Start codon followed by P575 to K877	yes	clone # 3.3	Kalyan Tirupula
18	pACMV-tetO-GRM6(1-877) C754A	C754A	full length human mGluR6 with C754A mutation	yes	clone # 2.2	Kalyan Tirupula
19	pACMV-tetO-GRM6(1-877) C765A	C765A	full length human mGluR6 with C765A mutation	yes	clone # 2.2	Kalyan Tirupula
20	pACMV-tetO-GRM6(1-877) C793A	C793A	full length human mGluR6 with C793A mutation	yes	clone # 2.1	Kalyan Tirupula
21	pACMV-tetO-GRM6(1-877) C754A C765A	C754A C765A or 5465	full length human mGluR6 with C754A, C765A mutation	yes	clone # 1.6, 2.1	Kalyan Tirupula
22	pACMV-tetO-GRM6(1-877) C765A C793A	C765A C793A or 6593	full length human mGluR6 with C765A, C793A mutation	yes	clone # 2.7	Kalyan Tirupula
23	pACMV-tetO-GRM6(1-877) C754A C793A	C754A C793A or 6593	full length human mGluR6 with C754A, C793A mutation	yes	clone # 1.5	Kalyan Tirupula
24	pACMV-tetO-GRM6(1-877) C754A C765A C793A	C754A C765A C793A or 546593	full length human mGluR6 with C754A, C765A, C793A mutation	yes	clone # 2.9	Kalyan Tirupula
25	pACMV-tetO-Sall*-GRM6(1-877)		same as pACMV-tetO-GRM6(1-877) but has unique Sall site	yes	no	Kalyan Tirupula
26	pACMV-tetO-Sall*-GRM5	mGluR5	full length human mGluR5 isoform 1	yes	clone # 2.5	Kalyan Tirupula
27	pACMV-tetO-Sall*-mGluR2	mGluR2	full length human mGluR2	yes	clone # 2.1	Kalyan Tirupula
28	pACMV-tetO-Sall*-mGluR3	mGluR3	full length human mGluR3	yes	clone # 2.1	Kalyan Tirupula
29	pACMV-tetO-gp160(Co-89.6)	gp160	gp160 sequence of HIV-1 strain 89.6, Group M, subtype B (Q73372)	no	clone # 2.13a	Kalyan Tirupula
30	pIRESpuro2-human mGluR5 isoform 1			no	NA	Dr. Marlene Jacobson
31	pCR4-TOPO-mGluR2		IMAGE CLONE - 8322671	no	NA	Open biosystems
32	pBluescript-mGluR3		IMAGE CLONE - 4792430	no	NA	Open biosystems

3.0 ESTABLISHMENT OF MGLUR6 EXPRESSION SYSTEMS: LOCALIZATION AND FOLDING OF MGLUR6 AND COMPARISON TO RHODOPSIN

3.1 SUMMARY

Prior to my thesis work there was a lack of well-established stable cell expression system for mGluR6. I have, therefore, established a reproducible expression system in stable cell lines of HEK293S that express mGluR6 and its truncation mutants. In this chapter, I describe my efforts to determine whether mGluR6 and its mutants have properly folded in the HEK293S expression system. Membrane trafficking was used as probe to test folding. Rhodopsin was used as a positive control. Specifically, P23H and N15S mutants of rhodopsin were used as they had varying degrees of defects in misfolding and therefore trafficking. In particular, P23H does not traffick to the cell surface, while human N15S expressed in *Xenopus laevis* was previously shown to be localized both at the rod outer segments and as aggregated fractions in the Golgi membranes. Here, I show that two of the truncated mGluR6 mutants (CRD-7TMC and 7TMC) do not traffick to the cell surface similar to the rhodopsin P23H mutant. In contrast, ‘rhodopsin-like’ XR-7TMC construct has expression levels and trafficking pattern similar to wild-type mGluR6.

3.2 INTRACELLULAR LOCALIZATION OF WILD-TYPE RHODOPSIN AND ITS MUTANTS P23H AND N15S

3.2.1 Rationale

Rhodopsin is a well studied GPCR and several misfolding mutants of rhodopsin that causes the retinal degenerative disease retinitis pigmentosa (RP) have been reported (Kaushal and Khorana, 1994; Sung et al., 1991; Sung et al., 1993). Here the folding and localization of two such mutants P23H and N15S, expressed in COS-1 cells, were studied using confocal immunofluorescence. P23 and N15 are present in the amino terminal region and are shown to misfold (Kaushal and Khorana, 1994; Tam and Moritz, 2009) in cells. In this thesis, I studied trafficking and localization of the wild-type and RP mutants (P23H and N15S) of rhodopsin. The localization profiles of wild-type and mutant rhodopsin serve as controls to ascertain the folding and localization of wild-type and truncated mGluR6 mutants that lack the amino terminal ligand binding domain (ATD).

3.2.2 Localization results

Methods used in transient transfections of COS-1 cells and the immunofluorescence are described in chapter 2 see sections 2.2.2 and 2.4. The immunofluorescence results are shown in Figure 3.1. The cells were stained with antibody (1D4) against the carboxy terminus of rhodopsin (green), actin (red) and nucleus (blue). The actin and nucleus markers help to delineate the individual cells and their boundaries. The control cells which were transfected with empty vector (no rhodopsin) showed no expression of the receptor (panels A – C; Figure 3.1). The cells

transfected with wild-type rhodopsin show high levels of receptor expression which is distributed all over the cells. Rhodopsin is trafficked to the plasma membrane as evident from the characteristic orange color which is a result of the co-localization of the actin (red) and rhodopsin (green) at the cell boundaries (panels D – F; Figure 3.1). The localization of P23H is restricted to the cytoplasm confirming the previously suspected (Saliba et al., 2002) misfolding and trafficking problems of this mutant (panels G – I; Figure 3.1). The majority of P23H is localized adjacent to the nucleus similar to early reports where P23H was shown to aggregate in aggresomes (Saliba et al., 2002).

N15S mutant also shows aggregation as seen in the P23H mutant but with some fraction trafficked on to the membrane (panels J – L; Figure 3.1). The trafficking of Human N15S expressed in *Xenopus laevis* was previously shown to be localized both at the rod outer segments and as aggregated fractions in the Golgi membranes (Tam and Moritz, 2009). These expression profiles support simultaneous *in vitro* studies in our laboratory that suggest that misfolding, stability and glycosylation of N15S is significant but is less than that of P23H (Man, Balem, Klein-Seetharaman, unpublished data).

3.2.3 Consequences of rhodopsin results for mGluR6 studies

We demonstrated in the above section that there is correlation between folding and membrane trafficking by imaging wild-type rhodopsin and its mutants in the cells. Wild-type, N15S and P23H mutant rhodopsin represent fully folded, partial folded and totally misfolded states, thus providing a well defined set of controls to compare the folding of wild-type and mutant mGluR6.

As a general observation I noticed that transient transfection results in a heterogeneous population of cells which express the transfected protein at varied levels, resulting in difficulty to

analyze the results. For mGluR6 studies, inducible stable cells were used for localization studies to ensure homogenous expression of protein in all the cells.

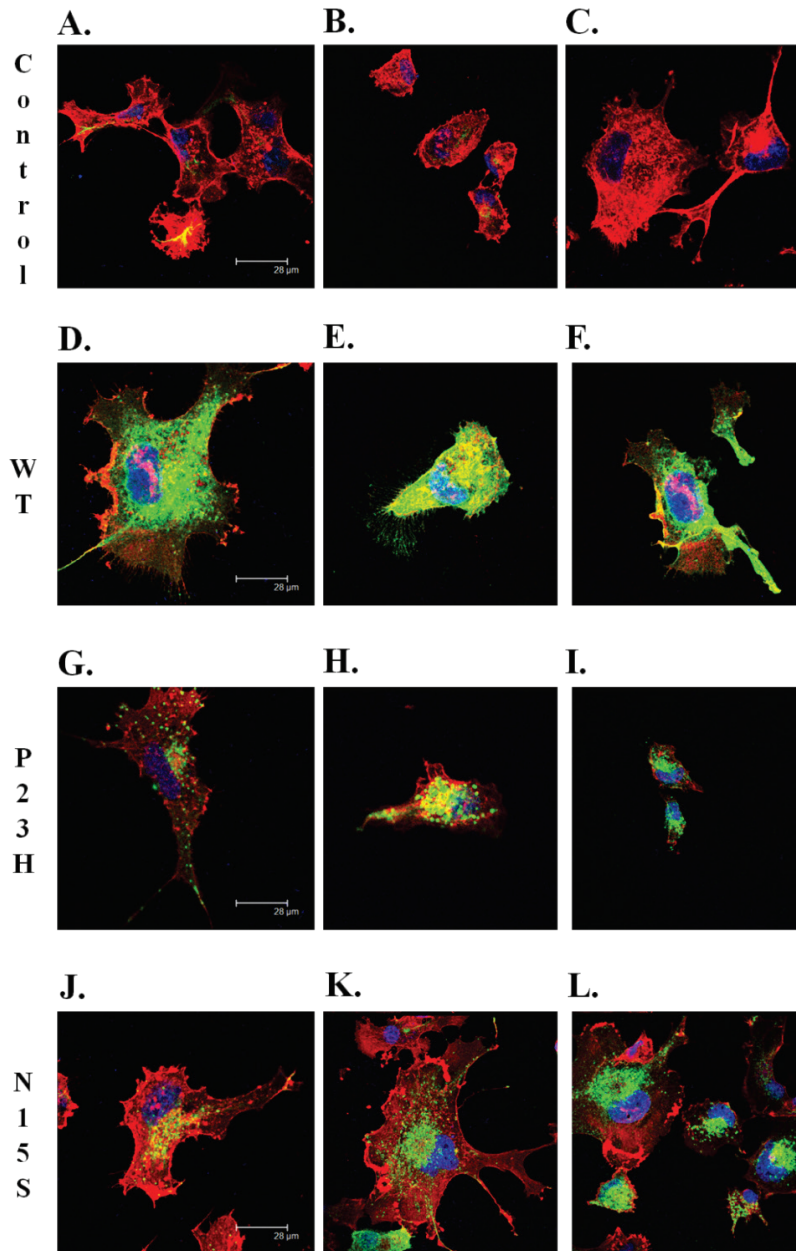


Figure 3.1 Localization of wild-type (WT) and mutant rhodopsin

COS-1 cells transfected with empty vector (panels A - C) and those transfected with wild-type (panels D - F), P23H (panels G - I) and N15S (panels J - L) rhodopsin mutants are stained with anti-rhodopsin antibody 1D4 (green;), actin marker (Red; and nuclear stain (Blue; Wild-type rhodopsin is observed only on the surface while P23H was only observed in aggresomes and N15S was present both on the surface and as aggresomes.

3.3 LOCALIZATION OF WILD-TYPE MGLUR6 AND TRUNCATION MUTANTS

3.3.1 Rationale

To allow a more detailed comparison of rhodopsin and mGluR6, a number of mGluR6 truncation mutants were created. The inspiration to create these mutants was derived from the studies where TM alone constructs of mGluR5 and mGluR2 lacking the amino terminal ligand binding domain (ATD) bound allosteric ligands and activated G proteins (Goudet et al., 2004; Rondard et al., 2006). The allosteric ligands that act as positive or negative modulators in full-length became agonists and antagonists in the absence of ATD, respectively (Goudet et al., 2004). Therefore, similar TM alone constructs of mGluR6 lacking the ATD were created here. The constructs are described below and in Figure 3.2.

- **Wild-type:** Full length sequence
- **7TMC:** ATD and CRD deleted
- **CRD-7TMC:** ATD deleted, but has cysteine rich and TM domain
- **XR-7TMC:** ATD and cysteine rich domain deleted, but slightly longer amino terminus compared to 7TMC

All mGluR6 constructs including wild-type were tagged with a 1D4 epitope at the carboxy terminus to enable Western blotting, immunofluorescence studies and immunoaffinity purification. Tetracycline inducible stable cell lines were established for wild-type and the truncated constructs.

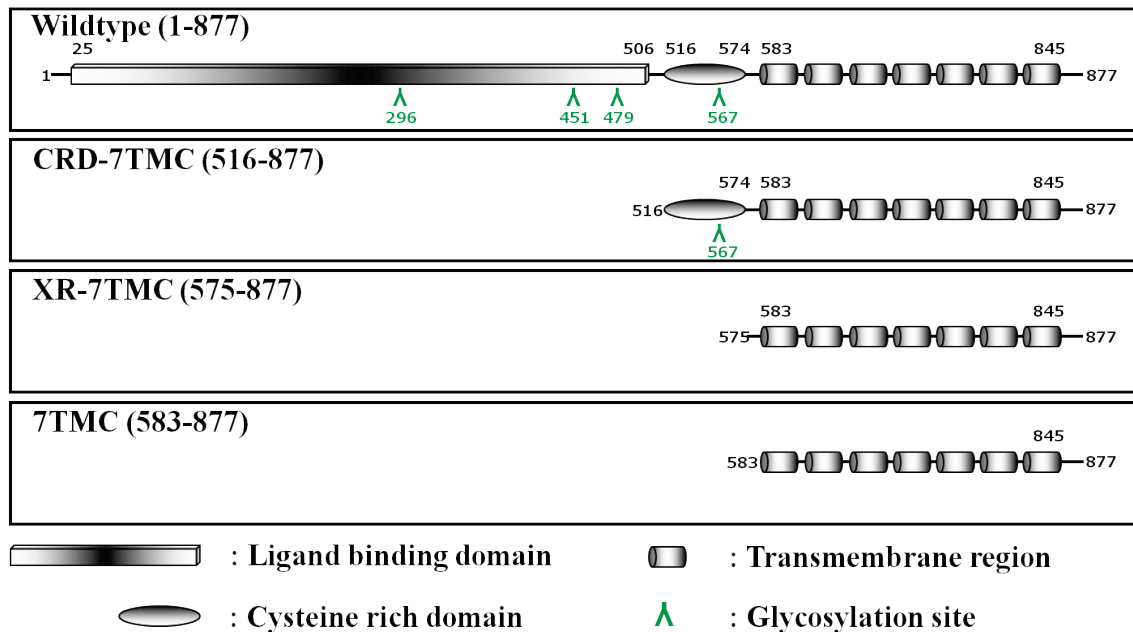


Figure 3.2 Schematic of different mGluR6 truncation mutants compared to wild-type

Shown in the top panel is wild-type mGluR6. The domain boundaries are extracted from the annotations of the human mGluR6 sequence (NP_000834.2) available at the NCBI. The numbers reflect the positions of amino acids in the human mGluR6 sequence. The truncated mutants were designed to lack the ligand binding domain. The three truncation mutants differ in their lengths of the amino terminus sequence before TM1. The CRD-7TMC mutant construct has the cysteine rich domain retained along with the TM region. The XR-7TMC and 7TMC contain only the TM regions with XR-7TMC containing a 7 amino acids longer amino terminus. All constructs have an amino terminus methionine and a carboxy terminus 1D4 tag. The putative glycosylation sites in mGluR6 were obtained from the UniProt database (sequence id O15303; <http://uniprot.org>).

3.3.2 Immunofluorescence studies of mGluR6 wild-type and 7TMC

Initial immunofluorescence studies were carried out for wild-type and 7TMC constructs. Negative controls without the primary antibody in samples and uninduced stable cells are included in these experiments to verify for back ground fluorescence and leaky expression in the cells respectively (Figure 3.3).

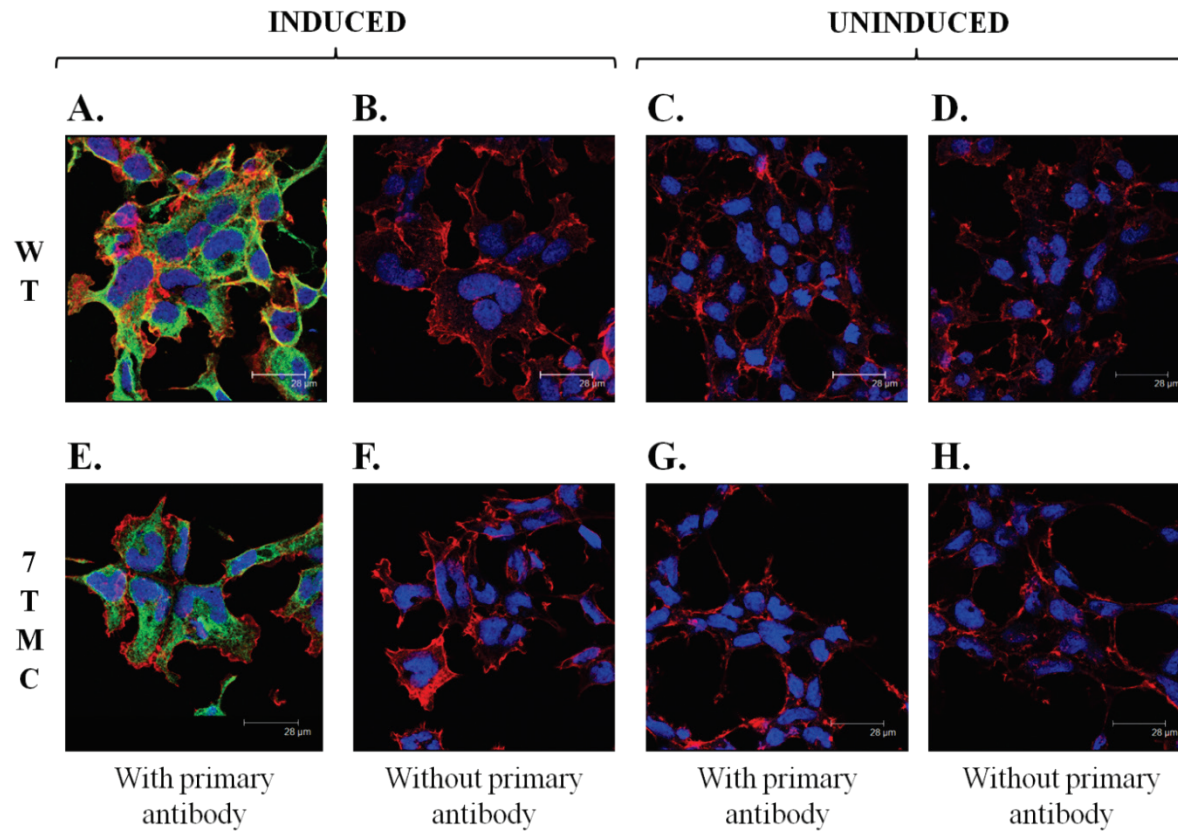


Figure 3.3 Localization of wild-type and 7TMC mGluR6 constructs in stable cell lines

Tetracycline inducible HEK293S stable cells for wild-type (panels A - D) and 7TMC (panels D - G) are shown. Cells in panels A, B, E and F are induced while those in panels C, D, G and H are uninduced. All samples are stained with actin marker (red) and nuclear stain (blue) while cells in panels A, C, E and G are additionally treated with antibody against 1D4 to detect the receptor (green). There is no receptor expression in uninduced cells and there is no background fluorescence in the green channel when the antibody against 1D4 is not added.

The localization and expression of wild-type and 7TMC mGluR6 were found to be different. Wild-type mGluR6 is present all over the cells and is trafficked to the plasma membrane as evident from the co-localization (orange) of action marker (red) and mGluR6 (green) at the cell boundaries (panel A; Figure 3.3). This is similar to WT rhodopsin (Figure 3.1) and indicates that the receptor is correctly folded.

In contrast to wild-type, the cell boundaries in 7TMC are stained only with actin marker (red) while the receptor is internalized in the cells (green) suggesting that 7TMC is not trafficked to the surface of the cells (panel E; Figure 3.3). This behavior is very similar to the P23H mutant of rhodopsin which is severely misfolded. There is no receptor expression in uninduced cells and there is no background fluorescence. There is no expression of wild-type and 7TMC mGluR6 in uninduced cells. Also there is no background fluorescence in green channel when the antibody against 1D4 is not added.

As a general observation, it appears that the stably transfected cells are homogenous for the expression of the heterologous proteins (mGluR6 and 7TMC in this case).

3.3.3 Localization results obtained with CRD-7TMC

The 7TMC construct showed that the sequence lacking the entire ATD and CRD domain does not fold and/or traffick correctly. Next we tested if retaining CRD would rescue folding. The result is shown in Figure 3.4. The expression and localization profile of CRD-7TMC is very similar to that of 7TMC. In both cases, there is no trafficking of mutant mGluR6 to the cell surface as evident from the lack of the co-localization signal (orange). Thus, CRD-7TMC and

7TMC both appear to be misfolded and localized inside the cells (panels B and D in Figure 3.4), analogous to the P23H mutant.

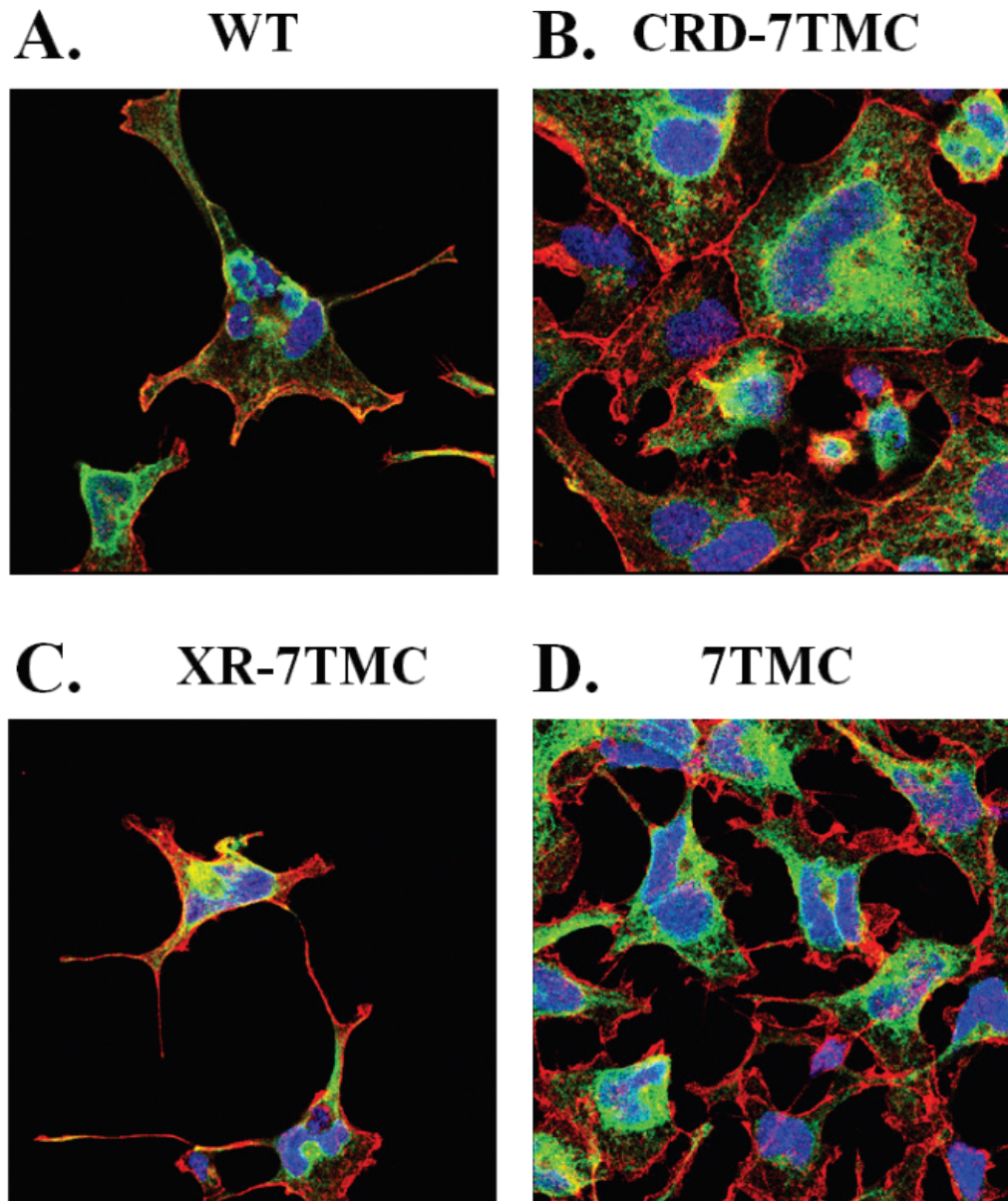


Figure 3.4 Localization of truncated mGluR6 constructs in stable cell lines

HEK293S stable cells expressing (A) wild-type, (B) CRD-7TMC, (C) XR-7TMC and (D) 7TMC immunostained with actin marker (red), nuclear stain (blue) and anti-1D4 antibody to detect the receptor (green). Among the truncated mutants only XR-7TMC construct has wild-type like expression and is trafficked to the membrane.

3.3.4 Localization of XR-7MC

Because previous truncation mutants were active (Goudet et al., 2004; Rondard et al., 2006), we then tested if part of TM was disrupted in our 7TMC construct by increasing the length at the N-terminus by 7 amino acids. The results are shown in (panel C, Figure 3.4). The XR-7TMC mutant, does show co-localization (orange) of actin (red) and mutant mGluR6 (green) suggesting that XR-TMC is trafficked to the cell membrane like the wild-type (panels A and C in Figure 3.4). Since CRD-7TMC, XR-7TMC and 7TMC differ only in their amino terminus (Figure 3.2). I speculate that CRD without the ATD is probably misfolded and hence CRD-7TMC does not traffic to the cell surface. In the case of 7TMC, the amino terminus is short compared to XR-7TMC and is probably missing key amino acids that are part of TM1, thus resulting in misfolding.

XR-7TMC is similar to the TM alone constructs reported for mGluR2 and mGluR5 (Goudet et al., 2004; Rondard et al., 2006), it is an ideal construct to identify and verify if allosteric modulators at mGluR6 can function as direct agonists or antagonists. XR-7TMC with only the TM region present is analogous to most class A GPCRs such as rhodopsin which lack ATDs and CRDs. Thus, XR-7MC allows for a direct comparison of XR-7TMC with rhodopsin.

4.0 DETERGENT SCREEN FOR SOLUBILIZATION AND PURIFICATION OF MGLUR6

4.1 SUMMARY

Having established that mGluR6 in mammalian cell expression system is properly folded (discussed in Chapter 3) and trafficked, the next step was to identify detergents that could optimally extract mGluR6 from cell membranes and reconstitute them into detergents while keeping the receptor function intact. Optimizing solubilization conditions is important to obtain medium to large quantities of mGluR6 from cells to enable structure-function studies. First, I setup a small-scale screen of 4 detergents during which I found that n-Octyl- β -D-glucoside (OG) is a suitable detergent that can maximally extract mGluR6 from cells. I then set up a large-scale detergent screen with 90 different detergents to identify solubilizing detergents potentially better than OG at extracting mGluR6 from membranes. Several detergents from ANAPOE® and CYMAL series were identified to be better or comparable to OG in solubilizing the membranes. Current efforts in this project are focused on identifying a suitable detergent that maintains the functionality of mGluR6 and its G protein partners. This is required to develop functional assays with purified receptor. I also optimized solubilization and purification conditions to purify mGluR6 from stable cell lines.

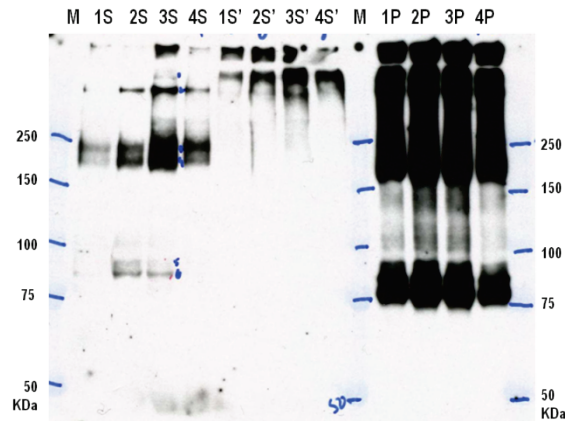
Using PNGase F, I confirmed that the glycosylation sites in mGluR6 are present in the ATD and CRD. I confirmed that wild-type mGluR6 is an obligate homodimer like other mGluRs. Though XR-7TMC lacks the ligand binding domain that harbors the cysteines that form inter subunit disulfide bond, it still forms dimers and higher order oligomers that are not disrupted under reducing conditions suggesting non-covalent association of XR-7TMC constructs.

4.2 DETERGENT SOLUBILIZATION OF MGLUR6

4.2.1 Preliminary solubilization experiments

In order to check the expression levels of mGluR6 in mammalian cells, mGluR6 was first expressed by transiently transfecting COS-1 cells (see section 2.2.2). To detect the protein yield, the conditions for extracting mGluR6 from cells was initially studied with 4 detergents. The detergents tested were CHAPS, n-Dodecyl- β -D-Maltopyranoside (DM), Triton X-100 and n-Octyl- β -D-glucoside (OG). CHAPS is a zwitterionic detergent while Triton X-100, DM and OG are non-ionic detergents. 1% DM is routinely used for extracting rhodopsin from cells (Reeves et al., 1996) while use of 4% OG can also extract rhodopsin successfully (Niu et al., 2002). 1% CHAPS has been used to solubilize mGluR6 from COS-7 cells (Weng et al., 1997). The critical micellar concentration (cmc) of Triton X-100 (0.0002mM) is extremely low compared to CHAPS, DM and OG (3mM, 0.17mM and 20mM respectively). I used 1% CHAPS, 1% DM, 4% OG and 1% Triton X-100 for solubilizing mGluR6.

Detergent was added to the harvested cells to reach the desired final concentration. The mixture was incubated at 4°C for 1-1.5 hours and then ultra-centrifuged at 50,000g for 30 min to separate supernatant and pellet. The supernatant fractions (with and without heating at 95°C for 5min) and pellet samples were separated on a SDS-PAGE gel followed by Western blot analysis (Figure 4.1).



Sample	Detergent [Conc]
1S, 1S', 1P	CHAPS [1%]
2S, 2S', 2P	n-Dodecyl-β-D-Maltopyranoside (DM) [1%]
3S, 3S', 3P	Triton X-100 [1%]
4S, 4S', 4P	n-Octyl-β-D-glucoside (OG) [4%]

S : Supernatant after solubilization in detergent
 S' : Sample S boiled at 95°C for 5min
 P : Pellet after solubilization in detergent

Figure 4.1 Preliminary solubilization experiments to extract mGluR6 from COS-1 cells.

Samples 1, 2, 3 and 4 represent mGluR6 solubilized with 1% CHAPS, 1% DM, 1% Triton and 4% OG, respectively. Lanes 1S – 4S, 1S' – 4S' and 1P – 4P represent supernatant, supernatant heat treated (at 95°C for 5min before loading on the gel) and pellet fractions, respectively. The predicted molecular weight for monomeric mGluR6 is 96.9KDa. The corresponding molecular weight for mGluR6 dimers is ~200KDa. The Western blot was probed with monoclonal mouse primary antibody against 1D4 epitope (at 1 to 25,000 dilution) and goat anti-mouse secondary antibody (at 1 to 50,000 dilution).

From Western blot analysis it was evident that the COS-1 cells expressed full length mGluR6 and there are monomeric, dimeric and tetrameric associations of mGluR6 (1S – 4S; Figure 4.1). The supernatant samples were heat-treated at 95°C for 5min before loading on the gel to disrupt dimers and to obtain monomer mGluR6 species on the blot (1S' – 4S'; Figure 4.1). However, heat treating resulted in aggregation of mGluR6. There is over loading of samples in cell pellet lanes (1P – 4P; Figure 4.1). The extent of solubilization comparing supernatants and pellets in decreasing order of efficiency was Triton X-100 > OG = DM > CHAPS. OG and DM solubilized the cells to the same extent. 4% OG appeared to cause less aggregation and was a milder detergent (since it has the highest cmc) as compared to CHAPS, Triton X-100 and DM.

4.2.2 Detergent screen

To identify better solubilizing detergents compared to OG, I next set up a large-scale detergent screen using 90 different detergents. The detergent screen kit with different detergents in a 96 well format was from Hampton research (Detergent Screen HT catalog # HR2-406). The detergents in the kit are provided as stocks at 10-fold cmc (10X). The kit was kindly provided by Dr. Guillermo Calero, University of Pittsburgh.

Frozen cell pellets of mGluR6 expressing HEK293S stable cell lines were used for screening detergents. For growing stable cells in spinner flasks, harvesting and storing cells see chapter two, section 2.2.4.1. A 250ml cell pellet was thawed on ice and resuspended in 6.5ml ice cold phosphate-buffered saline (PBS: 137mM NaCl, 2.7mM KCl, 1.8mM KH₂PO₄, 10mM Na₂HPO₄ pH 7.2) containing 0.7mM PMSF and 0.005% benzamidine. From this, 300µl cells were mixed with 100µl detergent from the kit (10X cmc) to obtain a final concentration of 2.5X cmc. The mixture was incubated at 4°C for 1-1.5 hours. The cells were then ultra-centrifuged at

50,000g for 30 min to extract solubilized supernatant. The solubilized samples were analyzed on a dot blot (see section 2.7.5) with 4% OG solubilized sample as a positive control (Figure 4.2).

NOTE: Most of the detergents in the kit are provided as stocks of 10X cmc. However, few detergents especially in the ANAPOE® series are provided as 10% w/v stocks. In our experiments, this resulted in higher concentrations for such detergents (greater than 2.5X cmc) (Table 4.1).

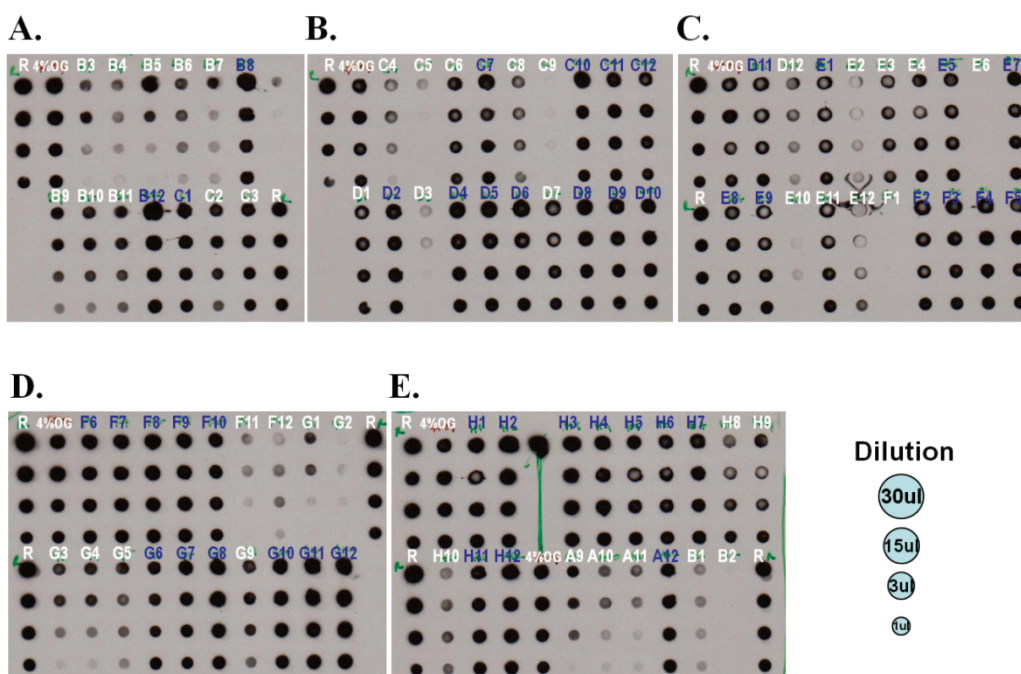


Figure 4.2 Detergent screen for solubilization of mGluR6

Dot blots (A – E) comparing solubilization of mGluR6 with different detergents. The dilution details for each sample are shown next to panel E. All the samples are identical except for the added detergents. The detergent concentration in the samples is 2.5X cmc. The samples are labeled by the well number in the 96 well plate detergent kit. 4% OG (mGluR6 solubilized in 4% n-Octyl- β -D-glucoside) and R (pure rhodopsin) in each blot are positive controls for comparing solubilization. The detergents with solubility better than 4% OG are highlighted in blue. See Table 4.1 and Table 4.2 for details on detergents and their names. A complete list of detergent names and details are available at <http://hamptonresearch.com/> (Detergent Screen HT catalog # HR2-406).

The solubilized supernatants were compared on a dot blot (Figure 4.2). There are several detergents that are better than 4% OG at extracting mGluR6 from cells. The detergents are listed in Table 4.1 for non ionic detergents and Table 4.2 for zwitterionic detergents and synthetic lipids.

Table 4.1 List of non ionic detergents that solubilize cells better than 4% OG.

Shown in the table are details of the detergents that are better solubilizers than 4% OG (n-Octyl- β -D-glucoside). The first column shows the location of detergents in 96 well plate. The detergents are added at 2.5X cmc except for ANAPOE® series of detergents (see text).

#	Well	Chemical name	Molecular weight (g)	Detergent type	[cmc] (mM)	[Stock]	Concentration in the screen [cmc] (X)
1	A12	ANAPOE®-58	1122.00	Non Ionic	0.004	10% w/v	5570.4
2	B8	ANAPOE®-C13E8	553.00	Non Ionic	0.1	10% w/v	452.1
3	C1	ANAPOE®-C12E10	627.00	Non Ionic	0.2	10% w/v	199.4
4	B12	ANAPOE®-X-114	536.00	Non Ionic	0.2	10% w/v	233.2
5	C7	ANAPOE®-C10E6	423.00	Non Ionic	0.9	10% w/v	65.7
6	C10	ANAPOE®-C10E9	555.00	Non Ionic	1.3	10% w/v	34.7
7	C11	Big CHAP, deoxy	862.10	Non Ionic	1.4	14 mM	2.5
8	C12	n-Decyl- β -D-maltoside	482.57	Non Ionic	1.8	18.0 mM	2.5
9	D2	n-Decanoylsucrose	496.55	Non Ionic	2.5	25.0 mM	2.5
10	D4	n-Nonyl- β -D-thiomaltoside	484.61	Non Ionic	3.2	32.0 mM	2.5
11	D5	CYMAL® -5	494.58	Non Ionic	5	50.0 mM	2.5
12	D6	n-Nonyl- β -D-maltoside	468.54	Non Ionic	6	60.0 mM	2.5
13	D8	HEGA® -10	379.50	Non Ionic	7	70.0 mM	2.5
14	D9	MEGA -10	349.47	Non Ionic	7	70.0 mM	2.5
15	D10	C8E5	350.50	Non Ionic	7.1	71.0 mM	2.5
16	D11	CYMAL® -4	480.55	Non Ionic	7.6	76.0 mM	2.5
17	E1	n-Octyl- β -D-thiomaltoside	470.58	Non Ionic	8.5	85.0 mM	2.5
18	E5	C-HEGA® -11	391.51	Non Ionic	11.5	115.0 mM	2.5
19	E7	HECAMEG®	335.40	Non Ionic	19.5	195.0 mM	2.5
20	E8	n-Octyl- β -D-glucoside	292.37	Non Ionic	20	200.0 mM	2.5
21	E9	n-Octanoylsucrose	468.50	Non Ionic	24.4	244.0 mM	2.5
22	F2	CYMAL® -3	466.53	Non Ionic	34.5	345.0 mM	2.5
23	F3	C-HEGA® -10	377.48	Non Ionic	35	350.0 mM	2.5
24	F4	HEGA® -9	365.47	Non Ionic	39	390.0 mM	2.5
25	F5	Dimethyloctylphosphine oxide	190.27	Non Ionic	40	400.0 mM	2.5
26	F6	MEGA-8	321.42	Non Ionic	79	790.0 mM	2.5
27	F7	C-HEGA® -9	363.45	Non Ionic	108	1.08 M	2.5
28	F8	HEGA® -8	351.44	Non Ionic	109	1.09 M	2.5
29	F9	CYMAL® -2	452.50	Non Ionic	120	1.20 M	2.5
30	F10	n-Hexyl- β -D-glucopyranoside	264.32	Non Ionic	250	2.50 M	2.5

From the detergent screens, it was evident that in general the ANAPOE® series of detergents and the CYMAL® series of detergents are better at solubilizing mGluR6 (Table 4.1). Solubilization is dependent on the cmc, chain length and on the charge of the head group. For example the CYMAL® series detergents have different chain lengths (CYMAL®-1 to CYMAL®-9) are present in the screen but only CYMAL®-5 to CYMAL®-2 are good solubilizing agents for mGluR6.

There are also zwitterionic detergents and synthetic lipids in the detergent kit and those that are better solubilizers are listed in Table 4.2.

Table 4.2 Synthetic lipids and ionic detergents that solubilize cells better than 4% OG.

Shown in the table are details of the detergents that are better solubilizers than 4% OG (n-Octyl-β-D-glucoside).

The first column shows the location of detergents in 96 well plate. The detergents are added at 2.5X cmc.

#	Well	Chemical name	Molecular weight (g)	Detergent type	[cmc] (mM)	[Stock]	Concentration in the screen [cmc] (X)
1	H11	LysoFos™ Choline 12	439.53	Synthetic Lipid	0.7	7.0 mM	2.5
2	H12	LysoFos™ Choline 10	411.48	Synthetic Lipid	7	70.0 mM	2.5
3	G6	ZWITTERGENT® 3-14	363.61	Zwitterionic	0.4	4.0 mM	2.5
4	G8	FOS-Choline®-12	351.47	Zwitterionic	1.5	15.0 mM	2.5
5	G7	n-Dodecyl-N,N-dimethylglycine	271.46	Zwitterionic	1.5	15.0 mM	2.5
6	G10	n-Undecyl-N,N-Dimethylamine-Oxide	215.38	Zwitterionic	3.21	32.10 mM	2.5
7	G11	ZWITTERGENT® 3-12	335.55	Zwitterionic	4	40.0 mM	2.5
8	G12	DDMAB	299.50	Zwitterionic	4.3	43.0 mM	2.5
9	H1	FOS-MEA®-10	295.36	Zwitterionic	5.25	52.5 mM	2.5
10	H3	CHAPSO	630.89	Zwitterionic	8	80.0 mM	2.5
11	H2	CHAPS	614.89	Zwitterionic	8	80.0 mM	2.5
12	H4	FOS-Choline®-10	323.41	Zwitterionic	11	110 mM	2.5
13	H5	n-Decyl-N,N-dimethylglycine	243.39	Zwitterionic	19	190 mM	2.5
14	H6	FOS-Choline®-9	309.39	Zwitterionic	39.5	395 mM	2.5
15	H7	ZWITTERGENT® 3-10	307.5	Zwitterionic	40	400 mM	2.5

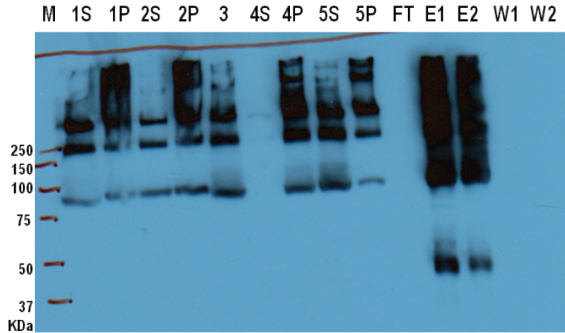
In summary, the detergent screens indicates that in general, the ANAPOE® series of detergents and the CYMAL series of detergents are the best solubilizing detergents for extracting mGluR6. ANAPOE® 58 (Brij® 58 from sigma) has the lowest cmc in the screen and is a good solubilizing agent. This detergent has been used to purify the G-protein heterotrimers from insect cells (see section 2.3.4). Moreover Brij® 58 is also inexpensive. Thus, Brij® 58 is a favorable choice for future studies, i.e. purifying and testing the function of mGluR6 in detergents.

4.3 IMMUNOAFFINITY PURIFICATION

I cloned mGluR6 with a 1D4 tag (ETSQVAPA) at the carboxy terminus to enable immunoaffinity purification (see section 2.1.1). In this section immunoaffinity purification of mGluR6 using the optimized protocol (see section 2.3.3.1) is described. For this purification 2g (wet weight) of cell pellet from spinner flask suspension culture (see section 2.2.4) was used. Aliquots of the samples were collected throughout the purification protocol and are analyzed on Western blot to monitor purification of mGluR6 (panel A, Figure 4.3). Before detergent solubilization, mGluR6 in the plasma membranes of the cells was separated from the nuclear components by osmotic shock with hypotonic buffer (see section 2.3.3.1; see lanes 1S, 1P, 2S, 2P, 3, 4S and 4P in panel A, Figure 4.3). The pellets containing mGluR6 in the membranes were then collected and solubilized in 1% DM (see lanes 4P, 5S and 5P in panel A, Figure 4.3). Supernatant collected after detergent solubilization was then incubated with 1D4 sepharose beads and the beads were collected in disposable plastic chromatographic column (see section 2.3.3). The flow through from the column and subsequent high salt and low salt washes were

collected. As observed on the Western blot (see lanes FT, W1 and W2 in panel A, Figure 4.3) there was no loss of mGluR6 in the flow through or the washes.

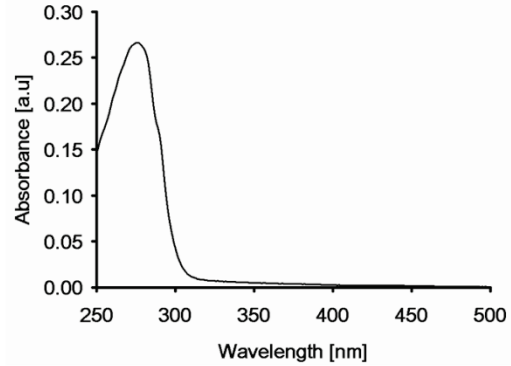
A. mGluR6 purification (Western blot)



Lane	Sample
1S, 1P	Cells in hypotonic buffer after 1000g spin
2S, 2P	1P in hypotonic buffer after 1000g spin
3	Pooled supernatants from (1S and 2S)
4S, 4P	Sample 3 after 100,000g spin
5S, 5P	Pellet from 4 solubilized in 1% DM
FT	Flow through
E1	Pooled peptide elutions
E2	Low pH elution
W1	High salt wash before elution
W2	Low salt wash after W1

S : Supernatant after solubilization in detergent
P : Pellet after solubilization in detergent

B. UV/Vis absorbance of mGluR6 elution



mGluR6	A ₂₈₀	Conc. [µg/ml]	Conc. [µM]	Yield
Elution (E1)	0.26	230	2.4	100µg / 2g cell pellet

Figure 4.3 Immunoaffinity purification of mGluR6 from HEK293 stable cells

Samples collected at various steps of the purification protocol were analyzed on (A) western blot. The predicted molecular weight for wild-type mGluR6 is 96.9KDa and mGluR6 dimers and trimers are expected at ~200KDa and ~300KDa. (B) Absorbance spectrum of mGluR6 elution. The concentration in the table below the figure was estimated from the absorbance values at 280nm using the molar extinction coefficient of 105480 M⁻¹cm⁻¹. Samples were separated on a 7.5% SDS-PAGE gel. The Western blot was probed with monoclonal mouse primary antibody against 1D4 epitope (at 1 to 25,000 dilution) and goat anti-mouse secondary antibody (at 1 to 50,000 dilution).

mGluR6 was then eluted into 5 column volumes of elution buffer with 1D4 peptide. All the elutions were pooled and analyzed on the Western blot (see lane E1 in panel A, Figure 4.3)

and by absorbance spectroscopy (panel B, Figure 4.3). From 2g of cell pellet I obtained ~100 μ g of purified protein at a concentration of 2.4 μ M (see table in panel B, Figure 4.3). The remaining mGluR6 from the column was eluted followed by low pH buffer (0.1M Glycine pH 2.0). The presence of mGluR6 at low pH suggests that the peptide elutions were incomplete.

4.4 CHARACTERIZATION OF GLYCOSYLATION

4.4.1 Glycosylation sites in rhodopsin and mGluR6

There are two glycosylation sites, N2 and N15, present at the amino terminus of rhodopsin (Hargrave, 1977). Mutations of these residues result in retinitis pigmentosa ((Saliba et al., 2002) and references within). Glycosylation at these sites in rhodopsin can be removed by PNGase F (Peptide: N-Glycosidase F) resulting in a measurable difference in apparent molecular weight on SDS-PAGE gels and Western blots (Iannaccone et al., 2006). We therefore used rhodopsin as a positive control in our studies to investigate the glycosylation sites in mGluR6 using PNGase F. There are four predicted glycosylation sites in mGluR6, at amino acid positions 296, 451, 471 and 567 as indicated in the UniProt database (sequence id O15303; <http://uniprot.org>). The glycosylation sites 296, 451 and 471 are located in the ATD, while 567 is present in the CRD. These glycosylation sites are absent in the truncated mutants XR-7TMC and 7TMC and there is only one glycosylation site present in the CRD-7TMC construct.

4.4.2 Deglycosylation studies of rhodopsin and mGluR6

Deglycosylation studies of wild-type and truncated mGluR6 was carried to experimentally verify the predicted glycosylation sites on mGluR6 (Figure 3.2 and Figure 4.4). Rhodopsin, wild-type and truncated mutants were expressed and purified from HEK293 stable cells. Comparable amounts of proteins for rhodopsin and mGluR6 was subjected to deglycosylation with PNGase F as described in section 2.6. As controls, samples were kept under identical conditions without PNGase F.

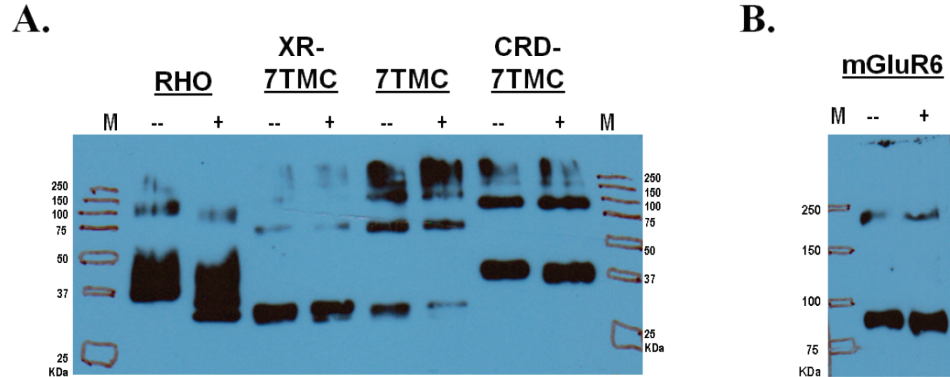


Figure 4.4 Glycosylation of wild-type and truncated mutants of mGluR6

Western blot of (A) rhodopsin (RHO) and truncated mGluR6 mutants (XR-7TMC, 7TMC and CRD-7TMC) and (B) wild-type mGluR6 (WT) from HEK293S stable cell lines. Protein concentrations were adjusted according to expression level and approximately 25ng was loaded per lane. For each mutant or the wild-type, equivalent amounts were analyzed before (--) and after (+) treatment with PNGase F. The predicted molecular weight for wild-type mGluR6, CRD-7TMC, XR-7TMC and 7TMC are 96.9KDa, 41.2KDa, 34.6KDa and 33.7KDa respectively. The Western blot was probed with monoclonal mouse primary antibody against the 1D4 epitope (at 1 to 25,000 dilution) and goat anti-mouse secondary antibody (at 1 to 50,000 dilution).

Upon deglycosylation, the apparent molecular weight of the rhodopsin control decreased as expected compared to fully glycosylated rhodopsin, as shown in the Western blot (panel A,

Figure 4.4). A decrease in molecular weight is observed for wild-type and CRD-7TMC mutants of mGluR6 indicating the presence of glycosylation in these receptors. In contrast, no difference in the molecular weight of XR-7TMC and 7TMC constructs was seen upon their deglycosylation indicating absence of glycosylation in these constructs. Our findings validate the predictions that the glycosylation sites in mGluR6 are present in the N-terminus, specifically in the ATD and potentially also in the CRD. The relatively similar decrease in wild-type and CRD-7TMC constructs along with our predictions indicates that may be only one glycosylation site in CRD (Figure 3.2 and Figure 4.4) but further studies are needed to test this hypothesis.

In the Western blots the truncated mutants appear to form dimers and higher order oligomers as evident from the high molecular weight bands. It is not clear if the observed results are a result of aggregation or if they are covalently linked dimers as seen in wild-type.

4.5 STUDIES ON OLIGOMERIZATION IN PURIFIED MGLUR6

4.5.1 Rationale

Wild-type mGluR6 is an obligate homodimer like other mGluRs where the individual sub units are covalently linked via a conserved disulfide bond in the ATD (Romano et al., 2001; Romano et al., 1996). In the deglycosylation studies, I noticed that there are dimers and oligomers present on the Western blots of truncated constructs of mGluR6. This is intriguing given that in truncated mutants, the ATD that harbors the cysteines involved in dimerization are absent. It has been shown earlier that mGluRs associate and form functional dimers even after the mutation of cysteine that disrupts the inter-subunit disulfide bond through non-covalent interactions (Romano

et al., 2001; Tsuji et al., 2000). Therefore, I tested if XR-7TMC (and cysteine mutants of XR-7TMC) formed dimers and oligomers like wild-type mGluR6 and if there was a role for cysteines in the TM in this process.

4.5.2 Results

Wild-type and XR-7TMC were expressed and purified from HEK293 stable cells. Comparable amounts of proteins were subjected to treatment with 20mM DTT (Dithiothreitol) to reduce disulfide bonds. The samples were incubated at room temperature for 1h (Cai et al., 2001) or for 3min at 60°C (Romano et al., 1996) as reported for rhodopsin and mGluR5, respectively.

In unreduced samples for wild-type and XR-7TMC there is a relatively smaller fraction of monomers as compared to reduced samples (Figure 4.5). On reduction with DTT at RT, wild-type mGluR6 predominantly resulted in a monomer species while monomer, dimer and trimer species are present for XR-7TMC. Wild-type mGluR6 significantly aggregates when incubated for 3min at 60°C without DTT. Under these conditions, even with DTT present predominantly oligomers are seen for wild-type mGluR6. In contrast XR-7TMC seems to react similarly to RT and 60°C treatments with DTT. Under both conditions all species (monomer, dimer, trimer and higher oligomers) are seen.

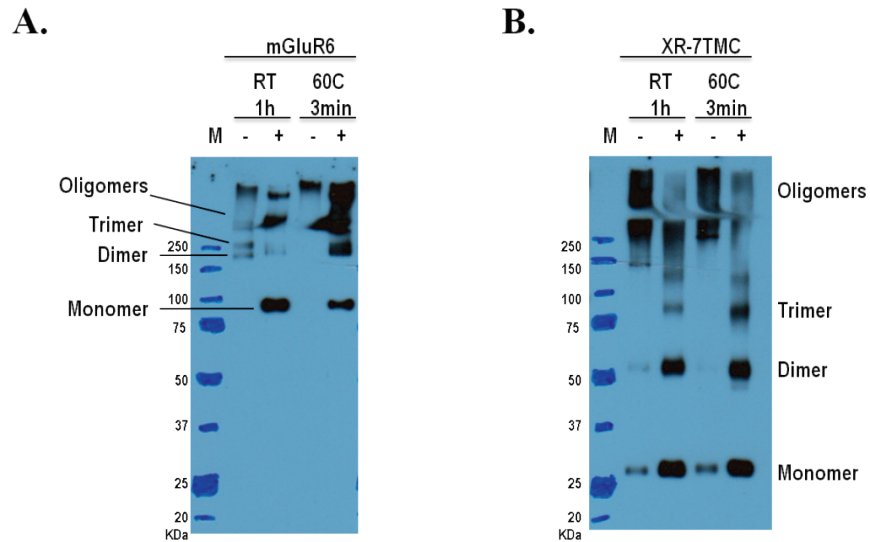


Figure 4.5 Dimerization and oligomerization of wild-type and XR-7TMC mGluR6

Western blots of (A) wild-type and (B) XR-7TMC mGluR6 from HEK293S stable cell lines. Both wild-type and XR-7TMC samples were analyzed before (-) and after (+) treatment with DTT (Dithiothreitol) to reduced disulfide bonds. The samples were reduced with DTT under two different conditions: incubation for 1h at room temperature (RT) or 3min at 60°C as reported in (Cai et al., 2001) and (Romano et al., 1996) respectively. The predicted molecular weight for wild-type mGluR6 and XR-7TMC is 96.9KDa and 34.6KDa respectively. For wild-type mGluR6, dimers and trimers are expected at ~200KDa and ~300KDa. In the case of XR-7TMC, dimers and trimers are expected at ~70KDa and ~105KDa, respectively. The Western blot was probed with monoclonal mouse primary antibody against 1D4 epitope (at 1 to 10,000 dilution) and goat anti-mouse secondary antibody (at 1 to 25,000 dilution).

4.5.3 Involvement of TM domain cysteines in oligomerization

To test if the cysteines in the TM domain of mGluR6 play a role in aggregation of XR-7TMC, we investigated oligomerization of cysteine mutants. There are three endogenous cysteines at positions 754, 765 and 793 in the TM domain of mGluR6 (Figure 9.1 and Figure 9.2). These

cysteines were mutated to alanine one at a time in the background of XR-7TMC, resulting in XR-7TMC:C754A, XR-7TMC:C765A and XR-7TMC:C793A constructs. These mutants were created in the tetracycline inducible vector pACMV-tetO (see section 2.1.3.5). Transient transfections in COS-1 cells were performed and their oligomerization was tested in membranes. Membranes were used in this case instead of purified proteins as the protein expression in COS-1 cells upon transiently transfected is very low as compared to HEK293 stable cell lines. The membranes containing XR-7TMC, XR-7TMC:C754A, XR-7TMC:C765A and XR-7TMC:C793A were treated without (-) and with (+) DTT (Dithiothreitol) for 1h at room temperature (Figure 4.6).

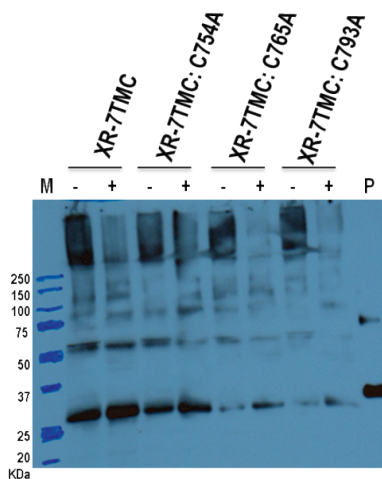


Figure 4.6 Dimerization and oligomerization of XR-7TMC cysteine mutants

Western blot of XR-7TMC and XR-7TMC cysteine mutants in membranes prepared from transiently transfected COS-1 cells. Samples were treated without (-) and with (+) DTT (Dithiothreitol) for 1h at room temperature to reduced disulfide bonds. 5 μ l of 25nM Rhodopsin (P) is also loaded to serve as a positive control on the Western blot. The Western blot was probed with monoclonal mouse primary antibody against 1D4 epitope (at 1 to 10,000 dilution) and goat anti-mouse secondary antibody (at 1 to 25,000 dilution).

In all the samples there is a small but visible increase in the extent of the monomer after treatment with DTT as compared to non-treated controls (Figure 4.6). Since this is the case in all mutants, each cysteine seems to contribute to oligomerization. Thus aggregation seems to involve TM cysteines relatively unspecifically. Since there is always a large fraction of oligomeric species present after DTT treatment, oligomers may be formed primarily through hydrophobic interactions.

5.0 OPTIMIZATION OF FUNCTIONAL ASSAYS FOR MGLUR6

5.1 SUMMARY

To initiate structure-function studies of mGluR6, I established human mGluR6 stable cell lines that are selected for overexpression of the receptors. I confirmed the expression and proper folding of mGluR6 in these cell lines as described in Chapters 3 and 4. In this chapter, I describe the functional characterization of mGluR6 in detergents, in membranes and in stable cell lines. Initial activation assays with purified mGluR6 in detergent micelles showed no activity of mGluR6. I therefore concentrated on optimizing mGluR6 activity in cells and membranes.

Two functional assays were established, a cAMP assay in cells and a GTP-Eu binding assay in membranes. cAMP assay is a well-established functional assay to characterize function of GPCRs but it required optimization for mGluR6 in our system. After optimization, I first showed that mGluR6 is constitutively active in cells using the cAMP assay. This finding led me to optimize buffer conditions for the cAMP assay to ensure complete removal of glutamate and eliminate constitutive activation of mGluR6 before the assay is performed.

In the membrane based GTP-Eu binding assay, the GTP analogue GTP-Eu was used and function of mGluR6 was determined by measuring fluorescence of bound GTP-Eu. A robust protocol for this assay for checking the function of mGluR6 in membranes was set up.

Using these two functional assays, I demonstrated the effects of the known agonists L-glutamate, L-AP4 and homoAMPA and antagonist LY341495 on the function of mGluR6. Our functional assay results were comparable to the values reported in literature using cAMP assays.

5.2 CELL BASED CAMP FUNCTIONAL ASSAY

mGluR6 as a $G\alpha_o$ coupled receptor negatively regulates adenylyl cyclase (Laurie et al., 1997; Nakajima et al., 1993). Typically, adenylyl cyclase catalyzes the production of cAMP from AMP upon stimulation with forskolin (FK). $G\alpha_o$ on activation by mGluR6 inhibits adenylyl cyclase activity and thus decreases cAMP levels. Activity of mGluR6 was assessed indirectly by measuring cAMP levels under different conditions.

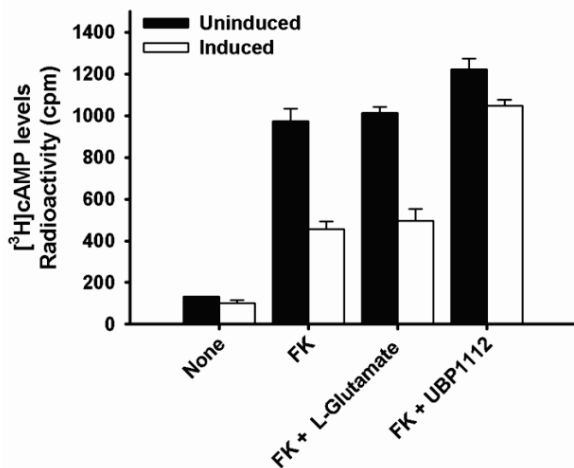
I used the inducible HEK293S stable cell lines that were selected for maximal expression, for measuring mGluR6 activity. In previous studies, function of mGluR6 had been reported mostly in CHO (Laurie et al., 1997; Nakajima et al., 1993) and RGT (Johnson et al., 1999) cells. The difference in my expression systems and those reported in the literature prevented direct application of the reported cAMP assays. Therefore, assay conditions were optimized for HEK293 cell lines to yield optimal response as described in the following section (section 5.2.1).

5.2.1 Optimization of cell culture and assay conditions

Initially, cAMP assays were set up as reported for mGluR4 (Flor et al., 1995) and mGluR6 (Nakajima et al., 1993). Uninduced cells were included as background controls in our assays. As expected, on addition of forskolin (FK) the cAMP levels were elevated to similar

extent in both induced and uninduced cells (panel A, Figure 5.2). Further in uninduced cells there was no change in the elevated cAMP levels on addition of agonist or antagonist which was expected as uninduced cells do not express mGluR6. In induced cells the FK stimulated cAMP levels were much lower than that of controls (uninduced cells) and there was no agonist response. However, the cAMP levels were elevated in the presence of the group III antagonist UBP1112 (panel A, Figure 5.2). These results indicated that in presence of UBP1112, there was positive modulation of adenylyl cyclase activity. An explanation that fit the key findings – (1) lack of elevated cAMP levels on FK stimulation, (2) absence of agonist response and (3) strong antagonist response, was that in induced cells mGluR6 was constitutively active. This hypothesis readily explains that in induced cells, active mGluR6 was inhibiting adenylyl cyclase activity. Since mGluR6 was already active there was no further response on adding agonist, while antagonist (UBP1112) inhibited its activity.

A.



B.

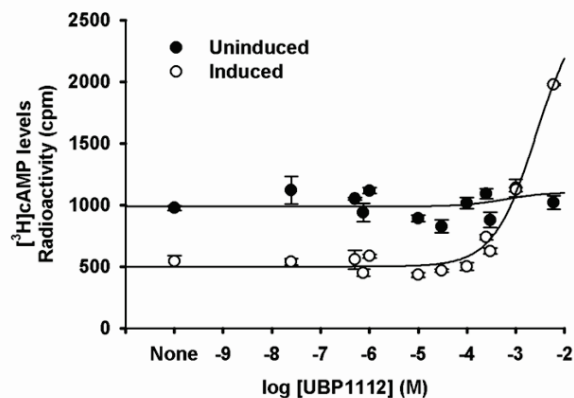


Figure 5.1 cAMP assay to test function of mGluR6 and UBP1112 (antagonist)

(A) cAMP assay measuring response of uninduced (filled bars) and induced (open bars) cells. The background cAMP levels (none) were similar in uninduced and induced cells. In uninduced cells there was elevation of cAMP levels on forskolin (FK; [10 μM]) stimulation. These elevated levels of cAMP were comparable in the presence of [6mM] agonist L-glutamate, and [1mM] antagonist UBP1112. For induced cells there was weak response to FK stimulation. Moreover there was no response to agonist but a strong response to antagonist. (B) UBP1112 dose-response curves for uninduced (filled circles), and induced cells (open circles). Uninduced cells show no response to UBP1112 while there was a sigmoidal dose-response in induced cells.

The constitutive activity of mGluR6 in cells could be attributed to the presence of high concentrations of L-glutamate (endogenous agonist) in the cell culture media. To test this hypothesis, I validated the resulting expectation that in the presence of increasing concentrations of antagonist UBP1112, the increase in cAMP levels should follow a simple sigmoidal dose-response (Motulsky and Christopoulos, 2003) demonstrating competitive antagonism. Shown in Figure 5.2 (panel B) is the cAMP dose-response curve for UBP1112. There was positive modulation of adenylyl cyclase activity by UBP1112 that follows sigmoidal dose dependence.

The cAMP levels in induced cells were lower than uninduced cells, but increase at higher concentrations of UBP1112. There was no effect of UBP1112 in uninduced cells. These results strongly indicated that mGluR6 is constitutively active in induced cells.

To further confirm that L-glutamate in the media was responsible for constitutive activity, I modified the assay protocol to remove L-glutamate from the media (section 2.5.2). To achieve this 48h after induction, cells were washed to remove media and were incubated in Hank's buffered saline solution as reported originally for 5-Hydroxytryptamine (5-HT, serotonin) 5-HT_{1B} receptors and later for mGluR6 (Laurie et al., 1997; Schoeffter et al., 1995). cAMP assay was also modified to include several washes. These washes and incubations were necessary to clear L-glutamate and to relieve activation of mGluR6. Additionally, to prevent loss of cells during washes the cell culture plates are coated with collagen. This modified protocol to test agonists, antagonists and allosteric ligand along with data analysis for cAMP are described in chapter 2 (section 2.5.2). mGluR6 function and its response to agonists and antagonist are described in the following sections 5.2.2 and 5.2.3, respectively.

5.2.2 Agonist response

cAMP levels in cells are decreased on mGluR6 activation with agonists such as L-glutamate, L-AP4 (Laurie et al., 1997) and homoAMPA (Ahmadian et al., 1997; Brauner-Osborne et al., 1996). I verified that L-AP4, L-glutamate and homoAMPA all produced a concentration dependent inhibition of forskolin stimulated cAMP accumulation with EC₅₀ values of $0.18 \pm 0.04 \mu\text{M}$, $4 \pm 1 \mu\text{M}$ and $13 \pm 2 \mu\text{M}$, respectively (Figure 5.2). In induced cells the cAMP levels were $54 \pm 3 \%$ (n = 7), $50 \pm 2 \%$ (n = 3) and $53 \pm 2 \%$ (n = 1) of forskolin stimulated levels, in the presence of L-AP4, L-glutamate and homoAMPA, respectively. In uninduced cells, the

cAMP levels in the presence of L-AP4, L-glutamate and homoAMPA was $77 \pm 7\%$ ($n = 2$), $85 \pm 3\%$ ($n = 3$) and $88 \pm 12\%$ ($n = 2$) of forskolin stimulated levels, respectively.

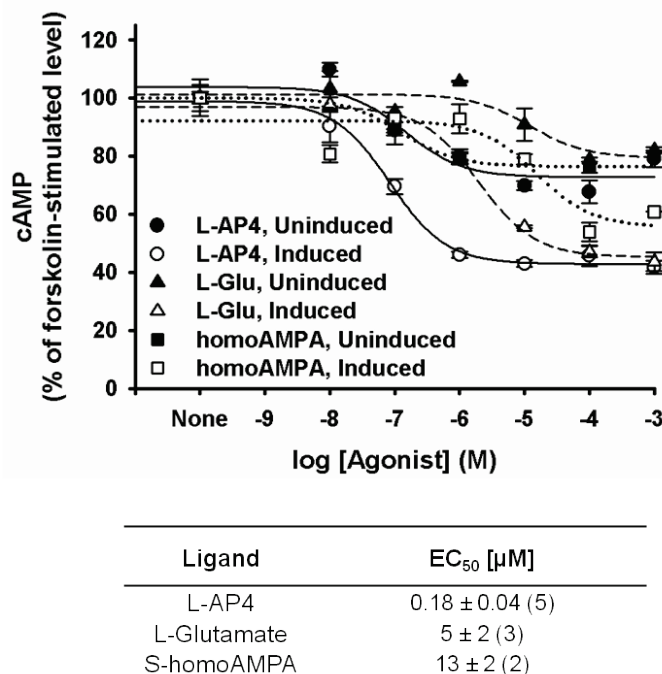


Figure 5.2 cAMP agonist dose-response curves for mGluR6 in cAMP assay

L-AP4 (circles), L-glutamate (triangles) and homoAMPA (squares) dose-response curves for mGluR6 in induced (open symbols) and uninduced (filled symbols) stable cells expressed as percent of forskolin (10μM) stimulated cAMP accumulation. EC₅₀ values (μM) were derived from the dose-response curves for induced cells and are listed in the table below. Data is represented as mean ± SEM (number of independent experiments).

The potency of agonists at mGluR6 was L-AP4 > L-glutamate > homoAMPA and the EC₅₀ values from our assays were comparable to those reported previously (Ahmadian et al., 1997; Brauner-Osborne et al., 1996; Laurie et al., 1997).

5.2.3 Antagonist response

The compound LY341495 is a potent group II mGluR antagonist and is also reported to have antagonist activity at group III mGluRs (Kingston et al., 1998). Specifically, LY341495 selectively displaces L-AP4 bound to human mGluR6 with reported K_d and B_{max} values of 31.6 ± 6.8 nM and 3.3 ± 0.7 pmol/mg protein (Wright et al., 2000). In mGluR6 stable cell line, LY341495 also produced a concentration dependent right-shift of the L-AP4 dose-response curves at 1, 10 and 100 μ M (panel A, Figure 5.3). Importantly, there was no effect of LY341495 in uninduced cells. Schild analysis (Arunlakshana and Schild, 1959) of the competitive dose-response curves was linear with a slope of 1.06 ± 0.03 , suggesting simple competitive antagonism. The pK_B estimate on constraining the slope to unity was 6.68 (corresponding to a LY341495 potency of 0.2 μ M) with a range of 6.5 to 6.8 at 95% confidence limits (panel A, Figure 5.3).

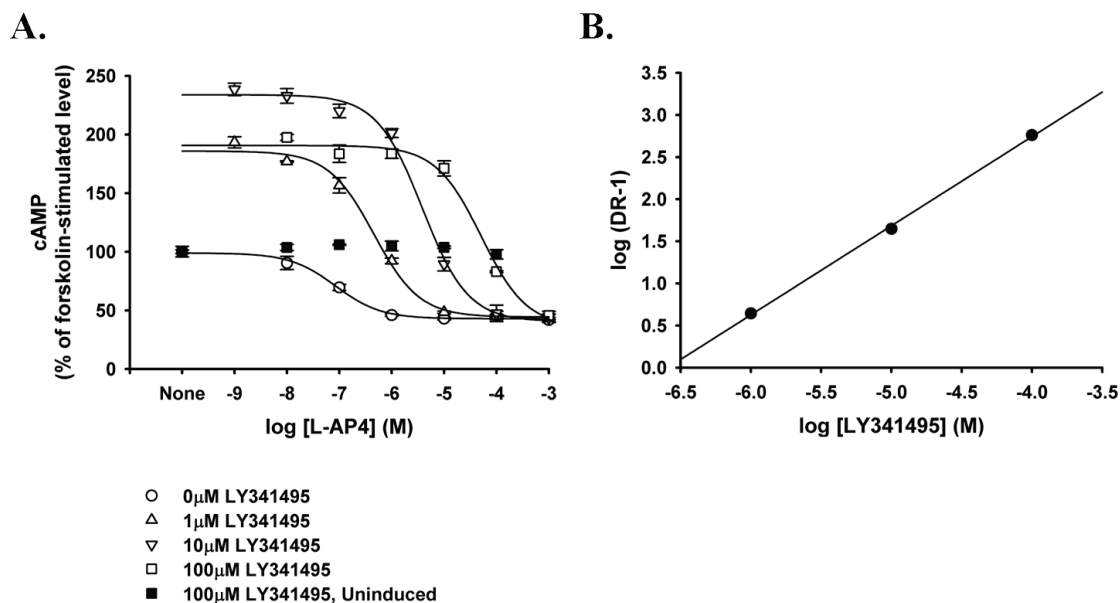


Figure 5.3 Competition dose-response curves for LY341495.

(A) Effect of LY341495 on L-AP4 dose-response curves. Cells were treated with 0, 1μM, 10μM and 100μM of LY341495. Note: The data point for LY341495 (100μM) at 1mM L-AP4 was not included in the experiment. In the figure and for calculating EC_{50} the counts at 1mM L-AP4 alone were substituted for this missing data point. Increasing concentrations of LY341495 right shifted the L-AP4 dose-response curves. There was no effect of LY341495 (100μM) in uninduced cells (B) Schild analysis of LY341495 competitive dose-response curves. The linear curve has a slope of 1.06 ± 0.03 and a pK_B estimate of 6.68 ($K_B = 0.2 \mu\text{M}$; constraining the slope to unity) with a range of 6.5 to 6.8 at 95% confidence limits. GraphPad Prism version 5.01 for Windows, GraphPad Software (San Diego, CA) is used for Schild analysis, while graphs are generated using SigmaPlot 10.0 scientific graphing software.

At 10μM concentration of LY341495, the increase in cAMP levels was $246 \pm 6 \%$ and $106 \pm 8 \%$ of forskolin stimulated levels for induced and uninduced cells, respectively (Table 1). Interestingly, I observed enhanced levels of cAMP (185%– 325% of forskolin stimulated levels) for WT and cysteine mutants, on addition of LY341495 (10μM), which is a known antagonist for mGluR6, in presence of forskolin. The effect of LY341495 (10μM) was completely reversed on

addition of L-AP4 (100 μ M) to the cAMP levels of 47 ± 1 % and 90 ± 1 % of forskolin stimulated levels for induced and uninduced cells, respectively (Table 1). There was no increase in cAMP levels on addition of LY341495 in the absence of forskolin, suggesting that LY341495 does not directly modulate adenylyl cyclase activity but acts on mGluR6 directly. A moderate increase in cAMP levels (122%– 143% of forskolin stimulated levels) in the presence of a 10-fold higher LY341495 concentration (100 μ M – 300 μ M) has also previously been reported for mGluR4, mGluR7 and mGluR8 (Kingston et al., 1998). The authors in that study discussed that LY341495 competes out the effect of endogenously formed glutamate in the assay which suppresses FK response by activating the receptor. In our assay system, I expected negligible levels of endogenous glutamate since I washed the cells twice with HBSS and further incubated the cells for 2h in HBSS before proceeding with cAMP assay. Moreover, I observed that there was an increase in cAMP levels on addition of LY341495 even for cysteine mutants which showed no response to the agonist (L-AP4, L-Glu). I speculate that in the presence of LY341495, mGluR6 is sequestering G proteins from other GPCRs. This would result in positive modulation of adenylyl cyclase activity, a phenomenon which is usually observed in highly overexpressing systems (Kenakin, 2004). In my system LY341495 addition is probably shifting the equilibrium of mGluR6 to antagonist and G-protein bound inactive complex, supporting the conclusion that LY341495 is an inverse agonist.

5.2.4 Effect of DMSO on cAMP assay

At high concentrations, ligands like LY341495 and PHCCC (allosteric ligand) were insoluble in aqueous buffers. So stocks of these were usually dissolved in DMSO as recommended by the supplier (Tocris Bioscience). For adding ligands in functional assays working stocks of these

ligands were first prepared in aqueous buffer and then added to the cells so that the final concentration of DMSO in the assay was never more than 1%. In this section the effect of DMSO at three different concentrations (0.1%, 1% and 10%) on the cAMP assay was investigated. As shown in Figure 5.4, addition of DMSO at 0.1% and 1% did not significantly alter the cAMP levels as compared to no DMSO control. But the addition of 10% DMSO significantly decreased the cAMP levels.

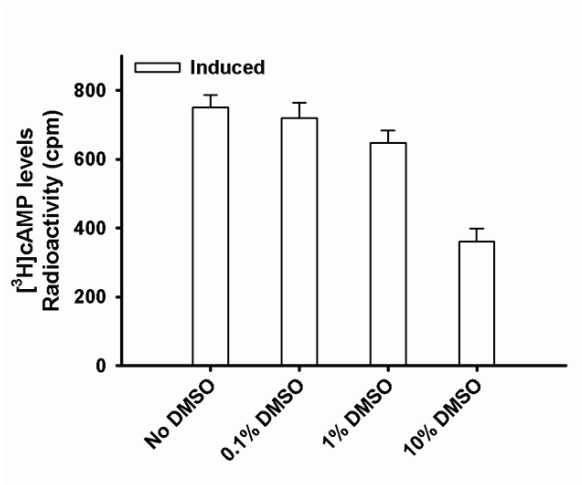


Figure 5.4 Effect of DMSO on the cAMP assay

DMSO was added to the cells at 0.1%, 1% and 10% (vol/vol) concentrations. Compared to the elevation of cAMP levels on forskolin ([10 μ M]) stimulation (No DMSO), addition of DMSO at 0.1% and 1% slightly decreased the cAMP levels. A significant decrease in cAMP levels was observed in presence of 10% DMSO.

For all functional assays described in this thesis, care was taken that the DMSO concentration was never >1% when ligands from DMSO stocks were added.

5.3 ACTIVATION ASSAY FOR MGLUR6 IN MEMBRANES

5.3.1 [³⁵S]GTPγS assay with mGluR6 in membranes and purified Gαβγ

GPCRs are coupled to G protein heterotrimer complexes. Activation of GPCRs triggers the conversion of GDP to GTP on the Gα partner of the heterotrimer complex. In *in vitro* activation assays, typically the non-hydrolysable GTP analogue [³⁵S]GTPγS is used to measure the activity of receptor by measuring radioactivity of the G protein bound [³⁵S]GTPγS.

Using cAMP assays I successfully demonstrated activity of mGluR6 in cells. Next, I tested the possibility of mGluR6 activating its cognate G protein heterotrimer in membranes. The G protein heterotrimer (Gα_oβ₃γ₁₃) was expressed and purified from insect cells (for details see chapter 2, sections 2.2.5 and 2.3.4). The activation assay was set up as reported for mGluR8 (Yamashita et al., 2004) and the assay protocol and buffers are described in chapter 2 (section 2.5.1.3). For the assay, membrane preparations containing mGluR6 were used instead of detergent purified mGluR6. The effect of mGluR6 agonist, L-AP4 and group III antagonist, UBP1112 (Miller et al., 2003) was tested with suitable controls as shown in Figure 5.5.

Signals from the negative controls - Gαβγ alone, Gαβγ with L-AP4, mGluR6 with Gαβγ and mGluR6 was not distinguishable from experiments with mGluR6, Gαβγ and ligands (L-AP4, UBP1112). A significant increase of Gαβγ activation by mGluR6 in the presence of agonist L-AP4 was expected. The lack of activity in these assays is possible due to following reasons: (1) purified Gαβγ is not active, (2) mGluR6 in preparations is inactive and (3) mGluR6 is constitutively active in membranes and hence does not respond to agonist. The high background activity observed in mGluR6 alone suggested plausible constitutive activity. These experiments were performed before adopting cAMP optimized cell culture conditions to prevent constitutive

activity of mGluR6 receptors. It is likely that the membranes used in these experiments contain constitutively active mGluR6 and hence there is no response in presence of agonist.

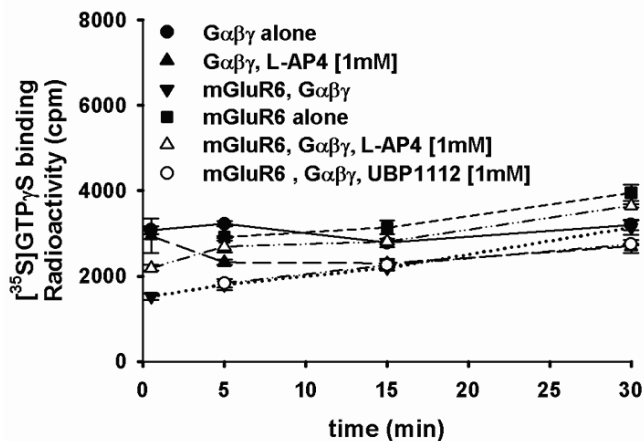


Figure 5.5 G protein heterotrimer ($G\alpha\beta\gamma$) activation by mGluR6

In vitro functional assay for testing activity of $G\alpha\beta\gamma$ and mGluR6 (in membrane preparations). The controls in the assay were: $G\alpha\beta\gamma$ alone (closed circles), $G\alpha\beta\gamma$ with L-AP4 (closed triangle), mGluR6 with $G\alpha\beta\gamma$ (closed inverted triangle) and mGluR6 alone (closed squares). The effect of $G\alpha\beta\gamma$ activation by mGluR6 in presence of L-AP4 (open triangles) and UBP1112 (open circles) is shown. Overall there was no significant difference between the controls and the experiments with ligands.

5.3.2 Development of GTP-Eu fluorescence assay

5.3.2.1 Rationale

To move towards more direct test of GPCR activity, I developed an assay that has a potential to be applicable to study activation of mGluR6 *in vitro*. A non-radioactive GTP-Eu activity assay which measures GTP/GDP exchange of the G protein was used. The assay is conceptually similar to the GTP γ S radioactive assay, but uses fluorescence as the read-out and is suitable for future high-throughput expansion.

The GTP-Eu reagent is available from PerkinElmer (catalog # AD0260). The concentrations of the reagents used in this assay were optimized for mGluR6 using DELFIA® GTP binding buffers (catalog # AD0261) following the instructions provided by PerkinElmer (http://las.perkinelmer.com/Content/relatedmaterials/posters/psh_automationoftrfbasedgtpbinding.pdf).

5.3.2.2 Optimization of conditions

The optimized protocol is described in chapter 2 section 2.5.3. The various steps involved in optimization are described in this section. As suggested by the supplier (PerkinElmer) the initial reaction was set up in standard buffer directions with 6µg membrane in 50mM HEPES, 10mM NaCl, 10mM MgCl₂ and 1µM GDP (pH 7.4) and with 100µM L-glutamate. Under these conditions there was an increase of 39% over basal fluorescence. All reactions were set up in 50mM HEPES (pH 7.4) for optimizing buffer components. As the first step of optimization the concentrations of MgCl₂ and GDP were screened for increasing the percent over basal fluorescence. Three and four different concentrations of MgCl₂ (1mM, 3mM and 10mM) and GDP (0.1µM, 1µM, 3µM and 10µM) were screened, respectively, as shown in Figure 5.6. The overall fluorescence counts decreased in presence of increasing concentrations of GDP. The maximal increase in fluorescence in presence of L-glutamate as compared to no ligand control was observed when the concentration of GDP and MgCl₂ were 3µM and 3mM, respectively (see panel C, Figure 5.6). The percent over basal fluorescence was 81% at 3µM and 3mM concentrations of GDP and MgCl₂, respectively.

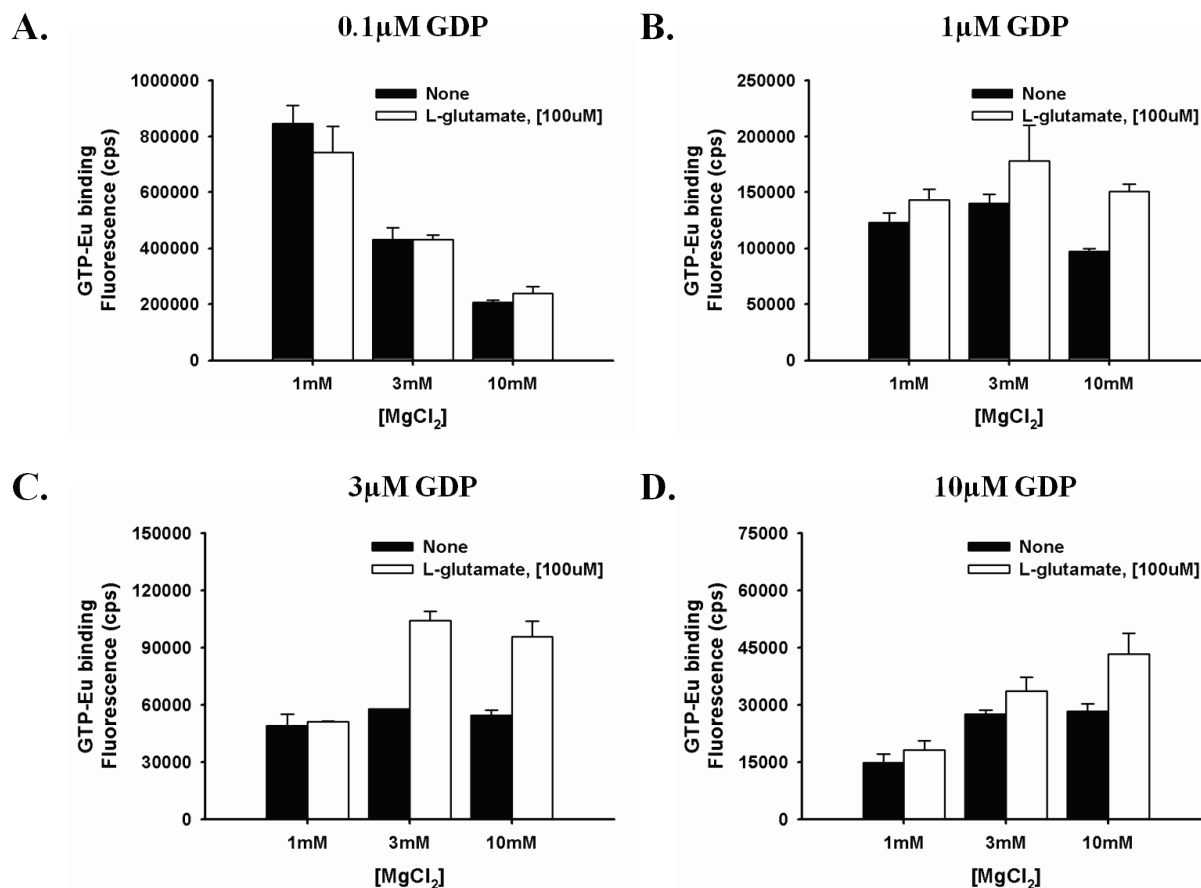


Figure 5.6 Screening of MgCl₂ and GDP for optimizing GTP-Eu assay

Fluorescence of trapped GTP-Eu was measured in the absence (filled bars) and presence (open bars) of L-glutamate [100 μM]. The concentrations of GDP tested were (A) 0.1 μM (B) 1 μM (C) 3 μM and (D) 10 μM. At set concentration of GDP (individual panels) three different concentrations of MgCl₂ (1 mM, 3 mM and 10 mM) were screened. The maximal increase in fluorescence was observed when the concentration of GDP and MgCl₂ were 3 μM and 3 mM, respectively. Data is represented as mean ± standard deviation.

Next, the concentrations of NaCl, saponin (detergent) and mGluR6 were optimized as shown in Figure 5.7. Among different concentrations of NaCl tested, at 20 mM there was maximal increase in fluorescence in presence of L-glutamate as compared to no ligand control (see panel A, Figure 5.7). The percent over basal fluorescence was 93% at this concentration.

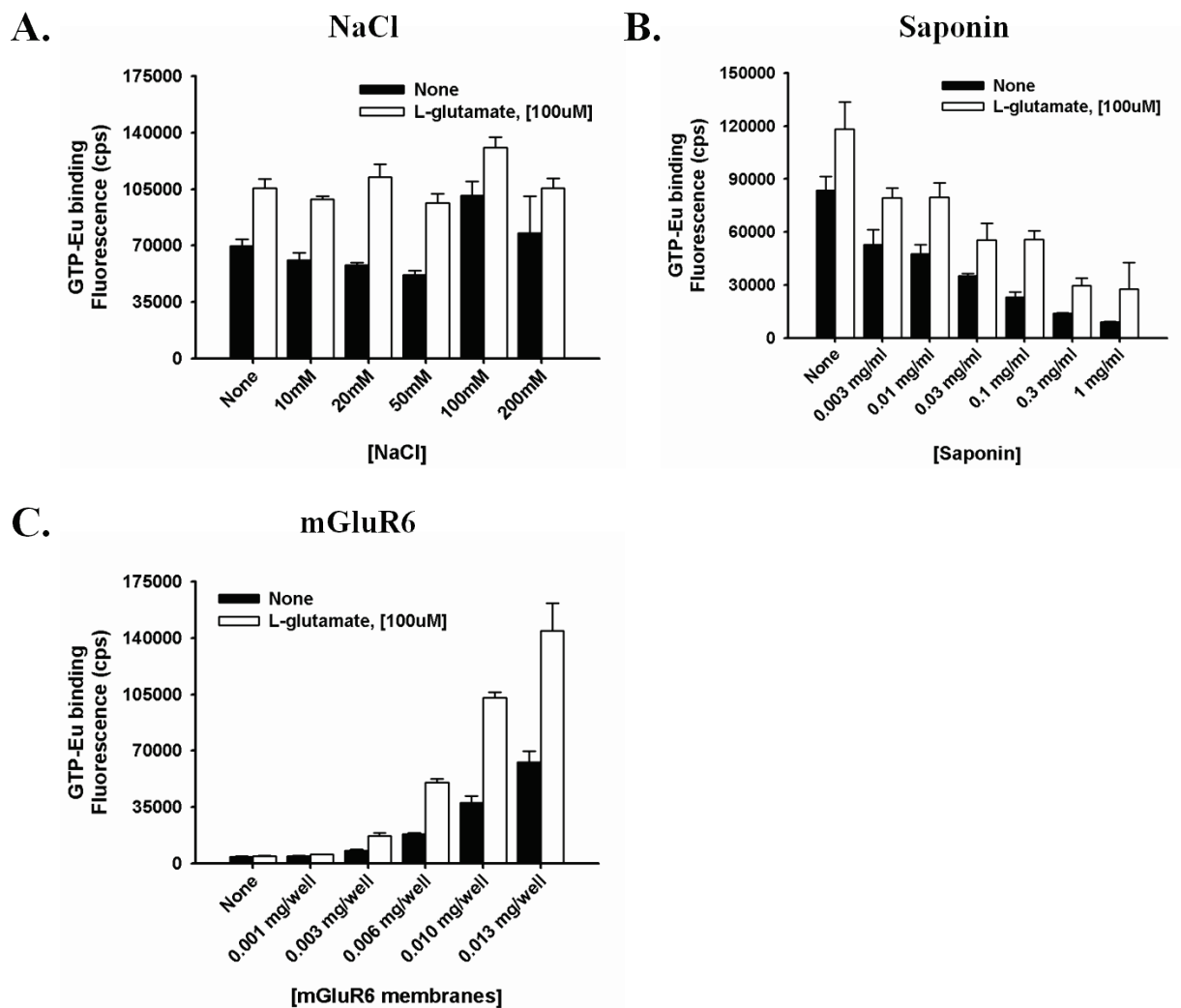


Figure 5.7 Screening of NaCl, saponin and mGluR6 membranes for optimizing GTP-Eu assay

Fluorescence of trapped GTP-Eu was measured in the absence (filled bars) and presence (open bars) of L-glutamate [100 μ M]. Buffer components that were screened are (A) NaCl, (B) Saponin and (C) mGluR6 membranes. Among the different concentrations measured maximal increase in fluorescence was observed at 20mM, 0.1 mg/ml and 0.006 mg/well of NaCl, saponin and mGluR6 membrane preparations, respectively. Data is represented as mean \pm standard deviation.

Among different concentrations of saponin tested there was maximal increase at 0.1mg/ml (see panel B, Figure 5.7). There was 140% increase in percent over basal fluorescence. Finally, different concentrations of mGluR6 membrane preparations were tested. Among different concentrations tested the maximal increase in fluorescence was observed at 0.006 mg/well or 6 μ g/well (see panel C, Figure 5.7) of mGluR6. There was 177% increase in percent over basal fluorescence after optimizing buffer conditions compared to 39% prior to optimization.

In summary the optimized buffer conditions that yield maximal GTP-Eu binding in presence of L-glutamate as compared to no ligand control are - 50mM HEPES (pH 7.4), 20mM NaCl, 3mM MgCl₂, 3 μ M GDP, 100 μ g/ml saponin and 6 μ g/well of mGluR6 membranes.

5.3.2.3 L-glutamate dose response

We tested the effect of L-glutamate to stimulate GTP-Eu binding in membrane preparations. The percent over basal binding dose-response curves for wild-type human mGluR6 in the presence of L-glutamate saturated at 198 ± 21 % with an EC₅₀ value of 5 ± 1 μ M (Figure 5.8). There was very minimal binding of GTP-Eu (2%) in membrane preparations from uninduced cells.

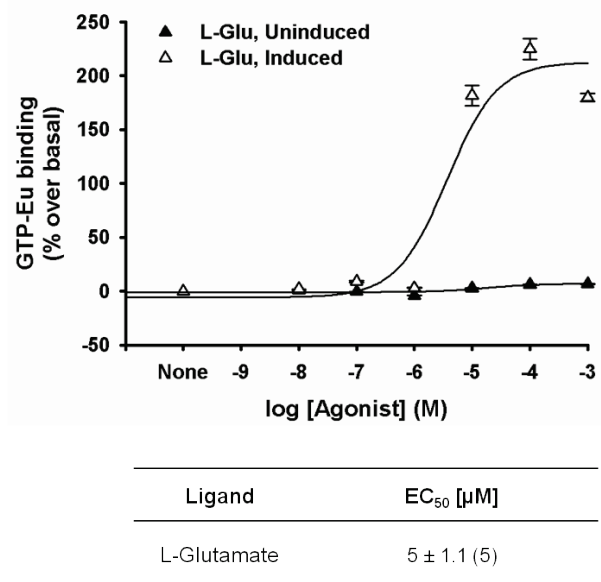


Figure 5.8 L-glutamate dose-response curves for mGluR6 (GTP-Eu binding)

L-glutamate dose-response curve measured as percent over basal (no ligand) binding of GTP-Eu for mGluR6 in membrane preparations from induced (open triangles) and uninduced (filled triangles) stable cells. EC₅₀ values (μM) were derived from the dose-response curves for induced cells and are listed in the table below. Data is represented as mean ± SEM (number of independent experiments).

Unfortunately, dose-response curves for L-AP4 using GTP-Eu binding assay could not be performed as the ligand interfered with the GTP-Eu fluorescence. Most likely, the phosphate group of L-AP4 chelates the Eu releasing it from its binding to the phosphate group in GTP.

5.4 *IN VITRO* FUNCTIONAL ASSAYS WITH PURIFIED RECEPTOR

5.4.1 [³⁵S]GTPγS assays in detergent micelles

5.4.1.1 Transducin (G_t) activation assay for rhodopsin and mGluR6

mGluR6 signaling is mediated through a G protein heterotrimer which is most likely composed of Gα_{o1}, Gβ_{3/4/5} and Gγ₁₃ (Dhingra et al., 2002; Huang et al., 2003; Morgans et al., 2007; Nawy, 1999; Vardi et al., 1993; Weng et al., 1997). It was reported that purified mGluR6 in reconstituted phospholipid vesicles promiscuously activated transducin (G_t; the G protein heterotrimer partner for rhodopsin) in *in vitro* assays (Weng et al., 1997). Use of G_t to set up *in vitro* assays is advantageous as this G protein can be purified in large quantities from bovine retina (Baehr et al., 1982).

With the aim of repeating the published experiments (Weng et al., 1997) I purified transducin (G_t; see section 2.3.5) and evaluated its function with rhodopsin as the control (panel A, Figure 5.9). Rhodopsin in DM micelles strongly activated G_t and the activation assays were set up as described in chapter 2 (see section 2.5.1.1) except that the concentrations of components in the reaction was as follows: 50mM Tris-HCl (pH 7.5), 150mM NaCl, 1mM MgCl₂, 1mM CaCl₂, 0.1mM EDTA, 1mM DTT, 0.01% DM (reaction buffer) and 2μM [³⁵S]GTPγS of radio ligand. There was an approximately 12-fold increase in activation of G_t by light-activated rhodopsin as compared to dark-adapted rhodopsin (panel A, open and closed circles, Figure 5.9) in 0.01% DM. The activation of rhodopsin was also tested in the presence of OG since our protein of interest, mGluR6, was purified in 0.88% OG. Rhodopsin activity was found to be compromised in the presence of 0.88% OG (panel A, open and closed triangles,

Figure 5.9). Having confirmed the activity of transducin with the positive control of rhodopsin, I tested mGluR6 activation.

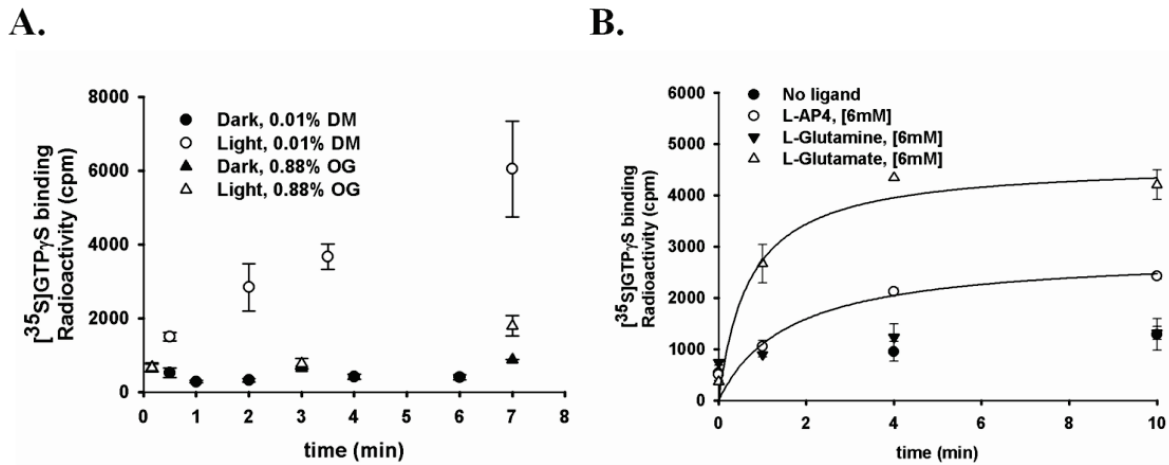


Figure 5.9 Transducin (G_t) activation by rhodopsin and mGluR6

The activity of rhodopsin and mGluR6 was tested by measuring $GTP\gamma S$ bound to G_t upon activation. **(A)** Light-induced activation of rhodopsin in the presence of DM (open and closed circles) and OG detergents (open and closed triangles). There was a 12-fold increase in activation of G_t by light activated rhodopsin compared to dark-adapted rhodopsin. **(B)** Activation of mGluR6 in the presence of L-glutamate (open triangles), L-AP4 (open circles) and L-Glutamine (closed triangles) is approximately 3-, 2- and 1-fold compared to no ligand control (closed circles). Conditions of mGluR6 activation are similar to that of rhodopsin in DM.

mGluR6 activity was tested *in vitro* by quantifying G_t activation as described previously (Weng et al., 1997) but instead of reconstituting the protein in lipid vesicles, purified mGluR6 was studied in DM micelles. The activation assay is described in chapter 2 section 2.5.1.2. mGluR6 activity was tested in the presence of the known agonists L-glutamate and L-AP4 that were previously reported in cell based functional assays (Laurie et al., 1997; Nakajima et al., 1993). As a negative control, L-Glutamine was also included (Frauli et al., 2006) (panel B, Figure 5.9). There was an approximately 3- and 2-fold activation of G_t by mGluR6 in the presence of L-glutamate (6mM) and L-AP4 (6mM), respectively compared to control in the

absence of ligand (panel B, Figure 5.9). However, no activation was observed in the presence of L-Glutamine (6mM).

However, the dose-response curves for L-glutamate under the same conditions were inconclusive. Upon close inspection, it was apparent that G_t activation was observed only in the presence of 6mM or higher concentrations of L-glutamate (panel A, Figure 5.10). I identified that the reason for G_t activation by mGluR6 in presence of L-glutamate and L-AP4 only at higher concentrations (6mM and above) was a pH induced artifact as described in the following section (5.4.1.2).

5.4.1.2 Activation of transducin (G_t) at low pH in the presence of high concentrations of glutamate

In the dose-response curves, activation of G_t by mGluR6 was only observed at unusually high concentrations (6mM and above) of L-glutamate (panel A, Figure 5.10). At these high concentrations of L-glutamate, the reaction buffer in the *in vitro* assay has an acidic pH (low) as shown in the table in panel A, Figure 5.10. It has been reported that G_t is constitutively active at low pH (Cohen et al., 1992). To verify that the observed activation was indeed due to low pH, I performed the same *in vitro* G_t assay by adding acetic acid to the reaction instead of L-glutamate (panel B, Figure 5.10). A pre-determined amount of acetic acid was added to lower the pH of reaction buffer as observed on addition of L-glutamate. There was a strong activation of G_t with decreasing pH which reached a maximum at pH 4 (panel B, Figure 5.10). Beyond pH 4 the activation levels dropped. A similar activation profile was observed in the presence of L-glutamate. Comparable levels of activation was observed in presence of 6mM L-glutamate and 7.5mM acetic acid both of which lower the pH to 3.47 (Figure 5.10). These results strongly

suggested that the observed G_t activation in the *in vitro* assays by mGluR6 (Figure 5.9) was a pH change induced artifact.

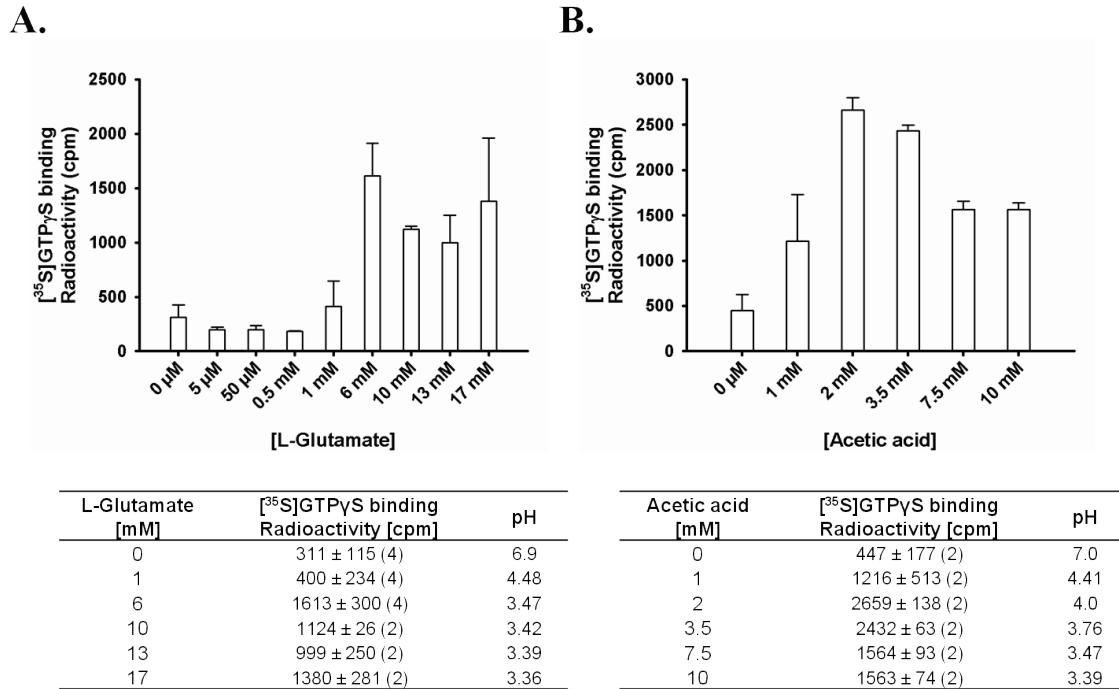


Figure 5.10 Low pH activation of transducin

Shown in the figure is the *in vitro* activation of G_t in the presence of mGluR6 and (A) L-glutamate and (B) acetic acid. The tables below the plots show the [³⁵S]GTPγS binding and the pH in the reaction buffer on addition of L-glutamate or acetic acid. In both cases the activation is correlated to the pH, suggesting constitutive activation of G_t at low pH.

To maintain the pH of the reaction buffer constant in subsequent assays, L-glutamate stock solutions (100mM) were prepared in 1 molar equivalent of sodium hydroxide (NaOH). L-glutamate dissolved easily in 1 molar equivalent of NaOH resulting in a solution that has close to neutral pH (~7). *In vitro* assays with G_t were then repeated with pH corrected L-glutamate. The activation of mGluR6 in presence of L-glutamate (6mM) was very low (~2-fold) and was similar to background levels as observed for rhodopsin control (Figure 5.11). Under the same conditions,

there was an approximately 12-fold activation of G_t (panel A, Figure 5.9) by light activated rhodopsin.

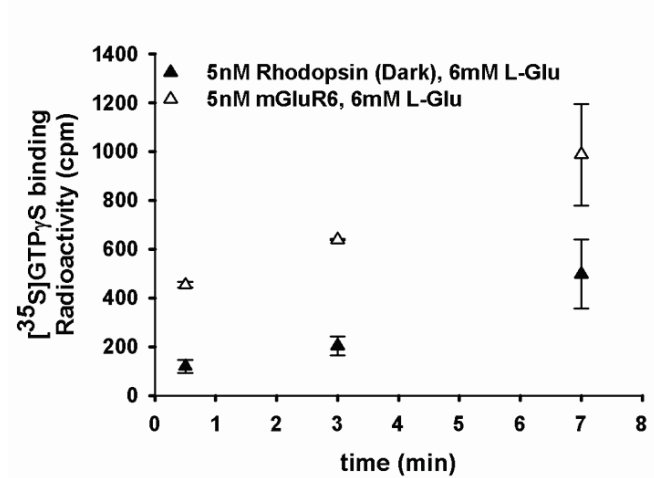


Figure 5.11 Transducin activation by mGluR6 in the presence of pH corrected L-glutamate

Activation of mGluR6 in the presence of glutamate (6mM) is shown in open triangles. Rhodopsin control in the presence of glutamate (6mM) was included to verify pH induced G_t activation (closed triangles). Activation of mGluR6 was ~2 fold but similar in extent to background levels as seen for inactive rhodopsin.

The activation levels of mGluR6 were close to background levels in the *in vitro* assays and this emphasized the need to pursue following options - (1) screen activity of mGluR6 in different detergents: It is possible that 0.08% OG used for purification of mGluR6 or the 0.01% DM used in the *in vitro* assays were not optimal for mGluR6 activation of G protein, (2) use endogenous G protein heterotrimer partners instead of G_t : It is possible that mGluR6 does not activate G_t and the reported promiscuous activity by (Weng et al., 1997) may be a pH induced artifact and (3) test for mGluR6 activity in a more physiological setting like cells and membranes. Option (1) can only be pursued after (2) or (3) are solved. I therefore pursued options (2) and (3) as described in sections 5.2 and 5.3.

6.0 EXTRACELLULAR ORTHOSTERIC LIGANDS

6.1 SUMMARY

mGluR6 is poorly characterized pharmacologically due to the lack of selective ligands. The aim here is to identify selective ligands for mGluR6 by adopting computational and experimental approaches. In chapters 3, 4 and 5, I discussed the establishment of expression system and production of properly folded and functional mGluR6. These were prerequisites for screening potential selective ligands for mGluR6 experimentally. Experimental characterization of ligand binding was preceded by computational approaches to identify potential selective ligands from a virtual library screen. For this, homology models of the ATD of mGluR6 were developed. These models and docking ligands to them using AutoDock Vina was combined in a two-step validation process. These validated models and approaches were used to screen a virtual library of ligands containing tetrazole and non-tetrazole molecules. In this screen, two hits, omega_352 and omega_345, were predicted to behave as selective ligands for mGluR6 based on their binding pockets. I also predicted the binding of dipeptides which have been shown earlier to modulate addiction in mice through glutamatergic systems (Cavun et al., 2005; Goktalay et al., 2006; Resch et al., 2005). These docking studies predicted that all three dipeptides may act as agonists. Based on docking energies and top-ranked poses, the predicted agonism decreases in this order cycloGly-Gln > Gly-Glu > Gly-Gln. The dipeptides and omega_352 were then tested

experimentally by functional assays to detect their effect on mGluR6 activity. In contrast to the predictions cycloGly-Gln did not show any effect on the activation of mGluR6. The predictions were successfully validated in terms of binding (although not agonism versus antagonism) Gly-Glu and Gly-Gln. Both molecules acted as inverse agonists. These findings for the first time provided direct evidence that dipeptides may act through mGluRs. The tetrazole molecule omega_352 tested was found to be less stable during synthesis and therefore its effect on mGluR6 could not be tested conclusively. Efforts are in process for designing a more stable omega_352. To test the effect of dipeptides and ligands from virtual screens I also established inducible stable cell expression systems for mGluR2, mGluR3 and mGluR5.

6.2 HOMOLOGY MODELS OF EXTRACELLULAR AMINO TERMINAL LIGAND BINDING DOMAIN OF MGLUR6

The extracellular amino terminal ligand binding (ATD) domain of mGluRs generally exists in an agonist bound closed conformation or antagonist bound open conformation, while the ligand free form is thought to be in equilibrium between open and closed conformations independent of bound ligand (Kunishima et al., 2000; Muto et al., 2007; Tsuchiya et al., 2002). For these studies, I generated closed (agonist preferred) and open (antagonist preferred) structures of ATD for mGluR6 as described in chapter 2 (section 2.8.4.1).

6.3 VALIDATION OF THE DOCKING APPROACH

AutoDock Vina (Trott and Olson, 2010) was used to dock orthosteric ligands to closed and open structures of ATD. The preparation of structure and ligand files for docking and the docking protocol is described in chapter 2 (see section 2.8.5). Before setting up of virtual screens, I did a two-step validation of our models and the docking approach. The primary validation was done to optimize the ligand binding pocket in the structural model of mGluR6. The secondary validation was done to determine the success rate of docking of known ligands in a small library screening using the current docking approach.

6.3.1 Primary validation

6.3.1.1 Validation of the docking approach for closed mGluR structures and optimization of the mGluR6 ligand binding pocket

As a positive control, L-glutamate was docked to mGluR1 and mGluR3 agonist bound closed crystal structures after removing the ligand from the structure files. AutoDock Vina successfully recapitulated L-glutamate binding to mGluR1 and mGluR3 as observed in the crystal structures with a predicted binding affinity of -6.2 kcal/mol (Figure 6.1).

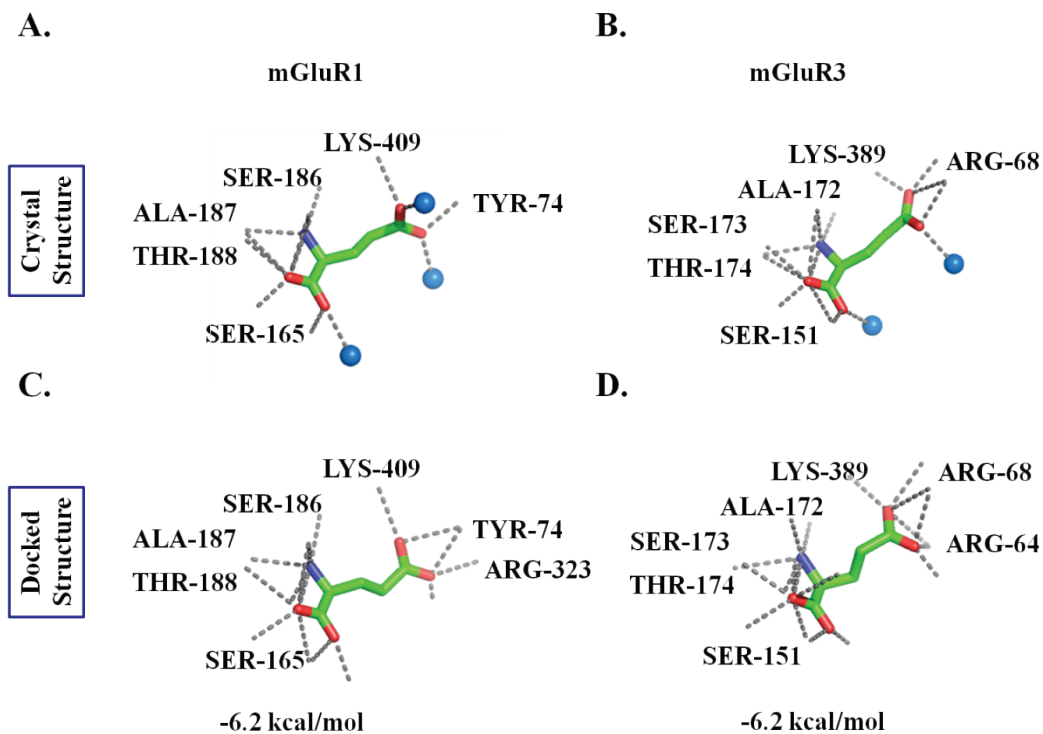


Figure 6.1 Primary validation of docking approach for agonist bound close conformation of ATD

L-glutamate binding poses in crystal structures of (A) mGluR1 (PDB: 1EWK, chain A) and (B) mGluR3 (PDB: 2E4U, chain A). To validate the docking approach, L-glutamate was removed from these structure files and was docked computationally using AutoDock Vina. The docked L-glutamate poses for (C) mGluR1 and (D) mGluR3 are very similar to the poses seen in crystal structures. Also shown in the figure are residues within 5Å of L-glutamate. L-glutamate is represented as sticks. Water molecules in the binding pocket of crystal structures are shown as blue spheres. The images are generated using PyMOL (Version 0.99rc6; <http://pymol.org/pymol>).

However L-glutamate docked to the homology model (closed conformation) of mGluR6 in a different orientation as compared to that in the positive controls (panel A, Figure 6.2). The binding energy in the docked structure was -5.8 kcal/mol compared to that in the positive controls where the binding energy was -6.2 kcal/mol (Figure 6.1). Therefore, to optimize L-glutamate binding to mGluR6 several rounds of docking were carried out, each time keeping the side chains of different amino acids in the binding pocket flexible. In the optimized binding

pocket, I obtained a binding pose and docking energy of -6.2 kcal/mol for L-glutamate similar to that seen for mGluR1 and mGluR3 (panel B, Figure 6.2). This mGluR6 homology model with an optimized binding pocket for L-glutamate was used for all subsequent docking experiments

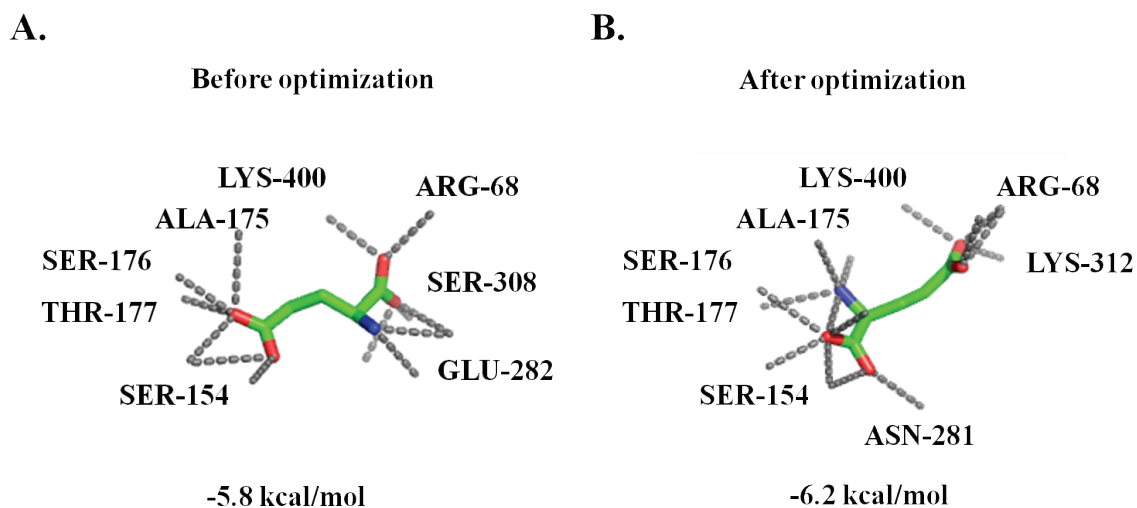


Figure 6.2 Comparison of L-glutamate binding pose in mGluR6 before and after optimization

Docking pose of L-glutamate in (A) original homology model and (B) optimized homology model. The binding pose of L-glutamate after optimization of the binding pocket resembles L-glutamate binding in crystal structures of mGluR1 and mGluR3 (panels A and B; Figure 6.1) and has an improved binding energy of -6.2 kcal/mol. Also shown in the figure are residues within 5Å of L-glutamate. L-glutamate is represented as sticks. The images were generated using PyMOL (Version 0.99rc6; <http://pymol.org/pymol>).

6.3.1.2 Validation of the docking approach for open mGluR structures

The open conformation crystal structures of only mGluR1 were used, since only other mGluRs with open conformation when we carried out our studies was that of mGluR7 and it had poor resolution (see Table 1.3 for more details). The crystal structures of open conformations were free (no ligand), L-glutamate (agonist) or S-MCPG (antagonist) bound. As positive controls, using AutoDock Vina, L-glutamate and S-MCPG were docked to their respective crystal structures. The docking results were not in agreement with those reported in the crystal

structures. In the L-glutamate bound open mGluR1 crystal structure, the ligand is engaged in key water mediated contacts with amino acids (panel A; Figure 6.3).

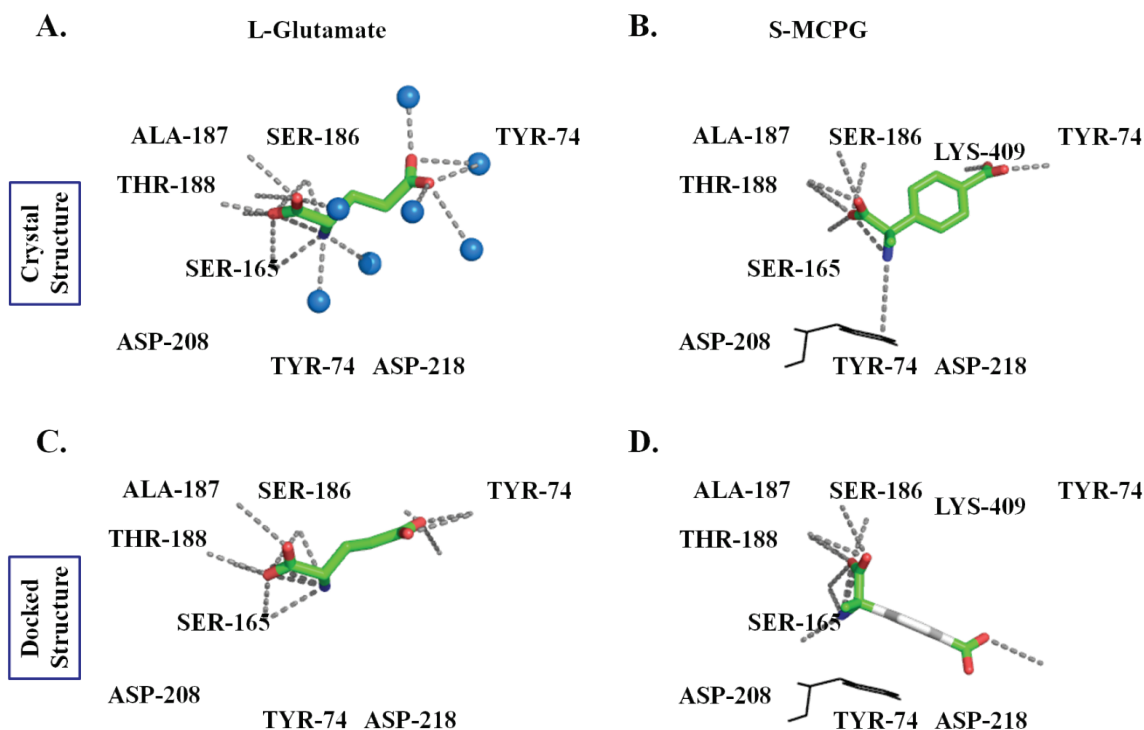


Figure 6.3 Primary validation of the docking approach for agonist bound close conformation of the ATD

Binding poses of (A) L-glutamate and (B) S-MCPG in crystal structures of mGluR1 (PDB: 1EWK, chain B and 1ISS, chain A). To validate the docking approach, ligands were removed from these structure files and were docked computationally using AutoDock Vina software. The docked ligand poses of (C) L-glutamate and (D) S-MCPG are different from crystal structures. The binding of L-glutamate in the docked structure was close its pose in the crystal structure. But, unlike in the crystal structure, L-glutamate in the docked structure lacked key water mediated contacts while S-MCPG is incorrectly docked. Also shown in the figure are residues within 5Å of ligands. Ligands are represented as sticks. Water molecules in the binding pocket of crystal structures are shown as blue spheres. The images were generated using PyMOL (Version 0.99rc6; <http://pymol.org/pymol>).

In my docked structures, L-glutamate docking successfully recapitulated the binding pose as observed in the crystal structure (panel C; Figure 6.3). However, L-glutamate was missing key

water-mediated contacts in the binding pocket due to the absence of water molecules in the docking protocol (panel C; Figure 6.3). This also led to the absence of contacts with some residues in the binding pocket which were observed in the crystal structure. To accurately mimic the L-glutamate binding in the open ligand pocket, the presence of water during docking appears to be important. However, this could not be done due to complexity arising from placing water molecules in the homology model since the position of the water molecules would be dependent on the position of the bound ligand.

In the case of docking S-MCPG, the molecule bound in the correct binding pocket but failed to recapitulate the docking pose seen in the crystal structure (panels B and D; Figure 6.3). S-MCPG docking was very different from the one observed in crystal structure (panels B and D; Figure 6.3). Especially the key cation-pi interactions between ligand and amino acid TYR-74 is missing. The current docking approach failed to dock ligands for open structures and therefore open structures were not used for library screening studies.

6.3.2 Secondary validation

Secondary validation of the docking approach was carried out by using a larger number of known ligands compared to the primary validation. For this, a comprehensive list of ligands that have been reported by experimental data to bind to mGluR1, mGluR3 or mGluR6 was prepared. The complete list of ligands along with the experimental binding data and docking results for mGluR1, mGluR3 and mGluR6 is shown in Appendix A. This list contains 61 ligands that are agonists, antagonists and molecules that have been reported to have no effect. These ligands were docked to the closed crystal structures of mGluR1 and mGluR3 and the homology model of mGluR6. I expected that agonists will preferentially dock to the closed structures as

opposed to antagonists, since it is known from crystal structures that in general, agonists and antagonists bind to closed and open conformations respectively (Kunishima et al., 2000; Muto et al., 2007; Tsuchiya et al., 2002). A summary of the docking results is shown in Table 6.1. For mGluR1 and mGluR3, 86% and 100% of the known agonists (positive control) docked respectively. In contrast, none of the antagonists (negative control) and only 14% of the antagonists docked to mGluR1 and mGluR3 respectively. For mGluR6, 67% of the known agonists docked while only 8% of antagonists showed binding. This demonstrates that our docking approach can be successfully used for large-scale virtual screening for mGluR6.

Table 6.1 Summary of results from secondary validation

The ligands were docked to the 1EWK (chain A) and 2E4U (chain A) crystal structures of mGluR1 and mGluR3, respectively. In case of mGluR6, homology model (closed conformation) with the optimized binding pocket was used for docking. Only the top hit with lowest energy was analyzed to verify docking.

Receptor	Activity of ligands	Total	Docked	Not Docked	Docked (%)
mGluR1	Agonists	14	12	2	86
	Antagonists	10	0	10	0
	No effect	35	9	26	26
	No data	2			
mGluR3	Agonists	15	15	0	100
	Antagonists	14	2	12	14
	No effect	23	9	14	39
	No data	9			
mGluR6	Agonists	21	14	7	67
	Antagonists	13	1	12	8
	No effect	17	5	12	29
	No data	11			

6.4 VIRTUAL LIGAND SCREENING OF SELECTIVE AGONISTS FOR MGLUR6

6.4.1 Library creation

A library of 2,630 molecules was generated *in silico* by Dr. Alexander Dömling, University of Pittsburgh. This library contains 1,395 molecules with tetrazole rings. The tetrazole ring on the tetrazole molecules has chemical properties similar to the carboxylic functional group. The non-tetrazole molecules consisted of pyrrole and furan rings. The tetrazole and non-tetrazole molecules were separately screened against mGluR6 to discover potential selective agonists. mGluR6 homology model (closed conformation) with the optimized binding pocket (as described in section 6.3.1.1) was used for docking.

6.4.1.1 Non-tetrazole containing molecules

A total of 69 molecules out of 1,235 molecules docked in the glutamate binding pocket of mGluR6. The molecule with the lowest binding energy was omega_646 (-7.5 kcal/mol) which is similar to that of known agonist ACPD (panels C and F; Figure 6.4). Other known agonists in the top scoring hits omega_622 and omega_614 were similar to L-glutamate (panels B and E; Figure 6.4) and S-3C4HPG (panels A and D; Figure 6.4), respectively. These known agonist molecules were present in the library as part of *in silico* library development and were not added with prior knowledge of their binding to mGluR6. These results are therefore a further validation of our docking approach.

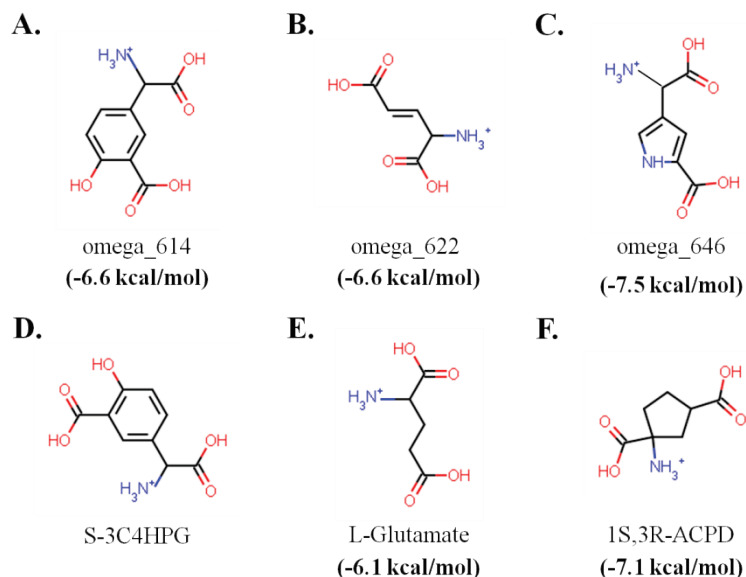


Figure 6.4 Top and interesting hits from of non-tetrazole library screening

Shown in A-C are interesting hits from the screening. Omega_614, shown in (A) is identical to known mGluR6 agonist S-3C4HPG shown in (D). Omega_622, shown in (B) is similar to L-glutamate shown in (E) except for the double bond in the side chain. The top hit omega_646 shown in (C) is similar to 1S,3R-ACPD shown in (F) except for the additional double bonds in the ring.

6.4.1.2 Tetrazole containing molecules

The tetrazole ring mimics the carboxylic acid functional group as present in L-glutamate. Thus, tetrazole containing molecules were of great interest in virtual screening. Out of 1395 molecules, 32 molecules docked in the L-glutamate binding pocket. The molecule with lowest binding energy was omega_830 (-7.5 kcal/mol) which docked similar in pose to L-glutamate. Interestingly, the tetrazole ring of this molecule (and its stereoisomer omega_829) was seen to occupy the same space making similar contacts with the receptor as the carboxylic acid functional group of L-glutamate (Figure 6.5).

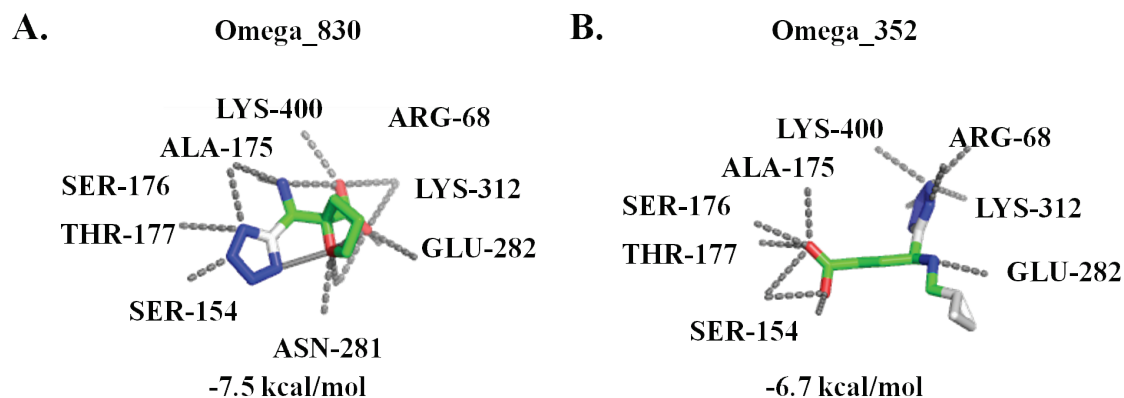
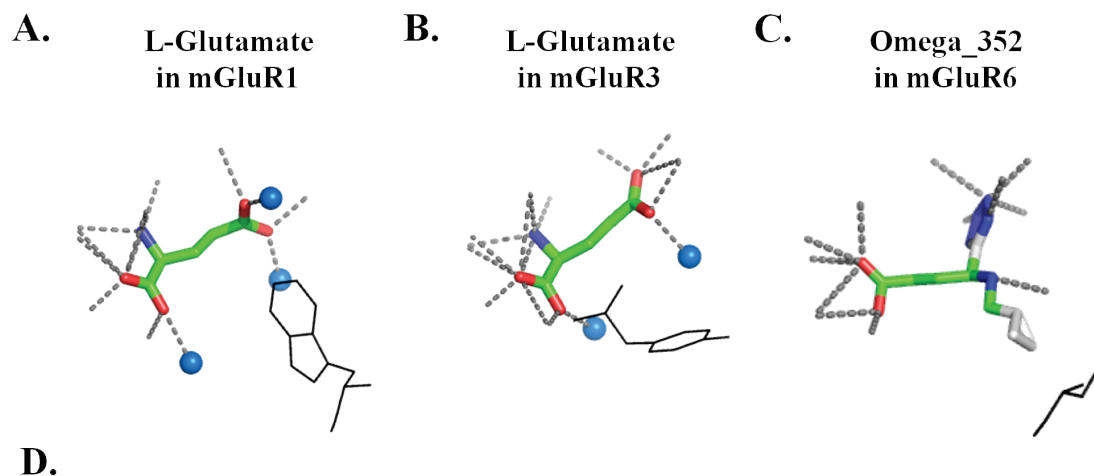


Figure 6.5 Top-ranked and interesting hits from the tetrazole library screening

(A) Omega_830 has a very low docking energy (-7.5 kcal/mol) and binds in a pose similar to L-glutamate. (B) Omega_352 is a possible selective agonist as it has a side-chain that binds in the extended binding pocket of mGluR6. Ligands are represented as sticks. The images were generated using PyMOL (Version 0.99rc6; <http://pymol.org/pymol>).

Other interesting stereoisomer hits were omega_352 (-6.7 kcal/mol) and omega_345 (-6.1 kcal/mol) which have an attached three-membered carbon ring that occupies a cavity in glutamate binding pocket (panel B; Figure 6.5). This cavity is unique to group III mGluRs indicating that omega_352 and omega_345 has a potential to be a selective ligand for group III mGluRs (Figure 6.6). For experimental validation of the selectivity of these ligands, our collaborator Dr. Doemling is in the process of synthesizing the omega_352 molecule. Since the starting materials for the synthesis of omega_345 were not readily available, we focused our efforts on omega_352.



GROUP I		GROUP II		GROUP III			
mGluR1	mGluR5	mGluR2	mGluR3	mGluR4	mGluR6	mGluR7	mGluR8
W_110	W_100	S_93	S_100	S_110	S_94	S_110	S_107
S_164	S_150	Y_144	Y_150	G_158	A_147	G_158	A_155

Figure 6.6 Comparison of ligand binding pockets of mGluR1, mGluR3 and mGluR6

L-glutamate binding poses in crystal structures of (A) mGluR1 (PDB: 1EWK, chain A) and (B) mGluR3 (PDB: 2E4U, chain A) compared to (C) Omega_352 docking in the homology model of mGluR6. Also shown in lines are the bulky aromatic groups present in mGluR1 and mGluR3. These bulky groups are absent in mGluR6 and the resulting cavity as result of their absence is occupied by the side chain of Omega_352. The bulky residues across different mGluRs are shown in (D). The bulky groups were absent in group III mGluRs. The images are generated using PyMOL (Version 0.99rc6; <http://pymol.org/pymol>).

6.5 DOCKING OF DIPEPTIDES TO MGLURS

Apart from the virtual library screening, I also tested *in silico* binding of dipeptides Gly-Glu, Gly-Gln and cyclo-Gly-Gln to mGluR6. The dipeptides dipeptides Gly-Glu and Gly-Gln were previously shown to decrease the propensity of addiction to a variety of drugs by the laboratory

of W.R. Millington and coworkers (Cavun et al., 2005; Goktalay et al., 2006; Resch et al., 2005). But, the actual receptor target(s) of these dipeptides are so far unknown. Moreover, mGluR6 and mGluR8 have been implicated in playing a role in addiction (Fonseca et al., 2010; Nielsen et al., 2008). Given these evidences, we wanted to test if dipeptides bind to mGluRs. These ligands were tested for docking to homology model of mGluR6 and to crystal structures of mGluR1 and mGluR3. The docking results are summarized in Table 6.2. Among the dipeptides, cyclo-Gly-Gln docked with a binding affinity of -6.7 kcal/mol to mGluR6. For Gly-Glu although the top one hit was not present in the binding pocket the second best hit was in the binding pocket. Gly-Gln also docked in the binding pocket but was not in the top two hits and has a predicted binding energy of -5.8 kcal/mol.

Table 6.2 Summary of dipeptide docking results

Dipeptides are docked to the optimized homology model of mGluR6 and crystal structures of mGluR1 (PDB: 1EWK, chain A) and mGluR3 (PDB: 2E4U, chain A). Top 10 docked poses were analyzed and docking pose that was not the top hit is listed along with the corresponding rank.

Dipeptide	Docking to closed structures (agonists)		
	mGluR6	mGluR1	mGluR3
Gly-Glu	YES -6.0 kcal/mol; (top 2 hit)	YES -6.1 kcal/mol; (top 2 hit)	YES -6.6 kcal/mol
Gly-Gln	YES -5.8 kcal/mol; (top 6 hit)	YES -6.2 kcal/mol	YES -7.0 kcal/mol
cycloGly-Gln	YES -6.7 kcal/mol	YES -6.4 kcal/mol	YES -6.8 kcal/mol

In the case of mGluR1, all three dipeptides docked, while cycloGly-Gln and Gly-Gln were the top hits, Gly-Glu was the top 2 hit. In the case on mGluR3, all three dipeptides docked

with much lower energies (>6.6 kcal/mol) compared to mGluR6 and mGluR1. At mGluR1, mGluR3 and mGluR6, docking results predict that dipeptides act as agonists.

6.6 EXPERIMENTAL TESTING OF POTENTIAL LIGANDS

We identified two classes of interesting hits during *in silico* experiments of ligand binding to mGluR6: dipeptides and tetrazole containing molecules. I tested the effects of dipeptides Gly-Glu, Gly-Gln and cyclo-Gly-Gln and omega_352 on the function of mGluR6 by using the cAMP assay. For details of cAMP assay please refer to section 2.5.2.

Results of the functional assay for these ligands are shown in Figure 6.7. I found that cycloGly-Gln showed no effect on cAMP levels whereas Gly-Gln and Gly-Glu slightly elevated cAMP levels above that of the induced cells at high concentrations of ligand (1mM) indicating that they act as weak inverse agonists (panel A; Figure 6.7). The dipeptides were not able to compete out the effect of agonist L-AP4 (panel B; Figure 6.7) even at a concentration of 1mM, suggesting that they had antagonist action. The observed inverse agonism though not strong hinted at possible binding and consequent modulation of mGluR6 activity by these dipeptides, therefore encouraging us to test their effect on other mGluRs. The dipeptides are also predicted to bind mGluR1 (group I mGluR) and mGluR3 (group II mGluR). To test the binding of these dipeptides at different types of mGluRs, I cloned and established inducible stable cell lines for group II (mGluR 2 and mGluR3) and group I (mGluR5) mGluRs. These mGluRs have been implicated to have a possible role in modulating addiction (Cavun et al., 2005; Goktalay et al., 2006; Resch et al., 2005).

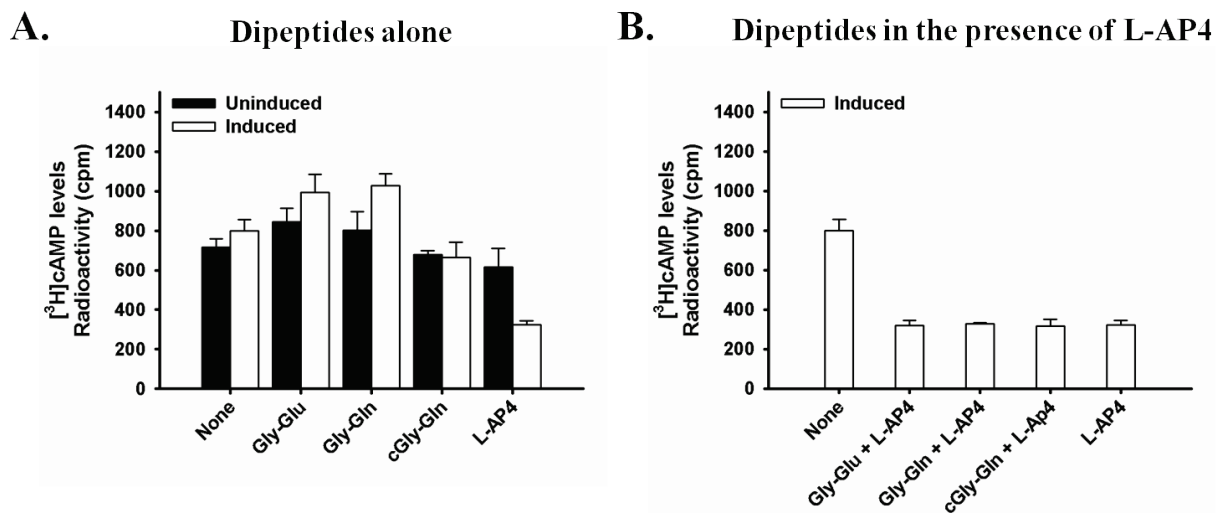


Figure 6.7 cAMP assay to test the effect of dipeptides on the function of mGluR6

cAMP assay measuring response of uninduced (filled bars) and induced (open bars) cells. (A) Dipeptides are tested for agonism at mGluR6. Compared to the elevation of cAMP levels on forskolin (FK; [10 μ M]) stimulation (none), addition of dipeptides Gly-Glu [1mM] and Gly-Gln [1mM] slightly elevated the cAMP levels demonstrating inverse agonism. Addition of cycloGly-Gln (cGly-Gln) [1mM] does not affect cAMP levels compared to FK alone control (none). L-AP4 [10 μ M] is included in the experiment as a positive control of agonism. (B) Testing for antagonism of dipeptides. Addition of dipeptides each at 1mM do not compete out the L-AP4 [10 μ M] induced decrease in cAMP levels compared to FK alone [10 μ M] control. The dipeptides do not have antagonistic activity.

We tested the effect of omega_352, which was synthesized by Dr. Dömling's group (University of Pittsburgh, PA), on mGluR6 activity and found that it neither acts as an agonist or as an inverse agonist in cAMP assays as shown in Figure 6.8. However, further characterization of this molecule by Dr. Dömling's group showed that this compound was not stable and cyclized spontaneously during synthesis. Current efforts are in progress for synthesizing a more stable omega_352 compound so that it can be used for functional assays.

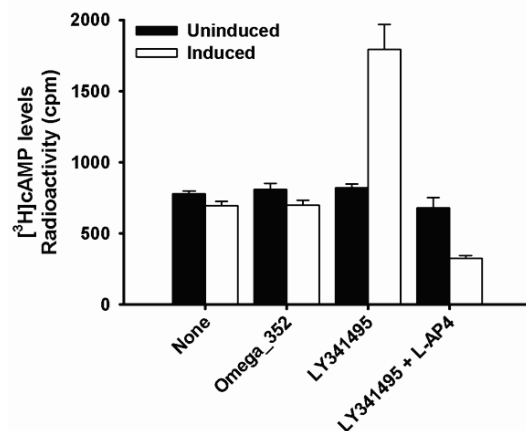


Figure 6.8 cAMP assay to test the effect of virtual screen hit Omega_352 on mGluR6 function

cAMP assay measuring response of uninduced (filled bars) and induced (open bars) cells. Addition of Omega_352 [10 μ M] does not change the cAMP levels compared to forskolin (FK; [10 μ M]) stimulation (none) alone controls. Also included in the experiment are positive controls for inverse agonism (LY341495 [10 μ M]) and agonism (LY341495 [10 μ M] / L-AP4 [100 μ M]; at this high concentration L-AP4 response is predominant).

7.0 TRANSMEMBRANE ALLOSTERIC LIGANDS

7.1 SUMMARY

In chapter 6, we reported both computational and experimental efforts to identify novel, selective orthosteric ligands for mGluR6, that bind in the binding pocket located in the ATD. Computational methods were used to generate homology models of the ATD of mGluR6 and for screening virtual libraries while experimental methods were focused on testing the virtual screen hits. In this chapter, similar efforts are reported to identify allosteric ligands for mGluR6 that bind in the TM domain. In general, most of the known allosteric ligands for mGluRs do not function directly but they either positively or negatively modulate the agonist-induced activity. However, there are no allosteric ligands reported for mGluR6 except for contradictory reports that PHCCC, a known allosteric ligand for mGluR4, may also bind mGluR6.

In contrast to the ATD of mGluRs, there is no structural information available for the TM regions. Therefore, we prepared homology models of inactive and active structures for TM regions of all eight different subtypes of mGluRs based on the crystal structure of dark-adapted inactive rhodopsin and a computationally derived model of active rhodopsin. We validated the homology models and docking approach by comparing the predicted binding energies of known positive and negative modulators bound to active and inactive TM models of mGluRs. We observed that – (1) there is preferential binding of positive modulators to active structures and

negative modulators to inactive structures and (2) the residues indentified in the predicted ligand binding pockets correlate with the residues that are shown experimentally to be critical for allosteric ligand function. These findings validate our homology models and docking approach.

To identify allosteric ligands for mGluR6, we initially docked known allosteric ligands to both active and inactive models of mGluR6. We found that MPEP did not dock while 3,3'-DFB binds to both the active and inactive conformation with low energy. CPCCOEt, PHCCC and all-*trans*-retinal docked only to active models with PHCCC having the lowest binding energy. When tested experimentally by cAMP assays, only PHCCC had an effect on mGluR6 activity. Additional experimental analysis showed that PHCCC acts as a direct inverse agonist at mGluR6, a first such ligand for this receptor. From these studies it appears that PHCCC selectively binds to inactive mGluR6. Furthermore, PHCCC showed no effect on the 'rhodopsin-like' XR-7TMC construct; one possible explanation is that this construct may be constitutively active.

7.2 ALLOSTERIC LIGANDS FOR MGLURS

Therapeutic potential of drugs targeting mGluRs has been demonstrated in number of conditions, including pain, epilepsy, Parkinson's disease, cognitive disorders, drug abuse, anxiety and schizophrenia (Conn and Pin, 1997; Kew, 2004). mGluRs are well studied due to their involvement in a variety of neuronal disorders. This has also led to the discovery of different glutamate competitors as well as allosteric ligands (Kew, 2004). Detailed experimental mutagenesis and chimera studies, in conjunction with modeling have revealed that the allosteric ligands bind to the TM domain of mGluRs (Hermans et al., 1998; Litschig et al., 1999; Pagano et

al., 2000; Varney et al., 1999). Typically, these ligands positively or negatively modulate the effects of binding of glutamate or glutamate analogs to a receptor. A summary of ligands for mGluRs that have been reported so far are listed in Table 1.4. Unfortunately, no allosteric ligands have been discovered so far for mGluR6. However, PHCCC which is a positive allosteric modulator for mGluR4 was recently proposed to act as a direct agonist for mGluR6 (Beqollari and Kammermeier, 2008). This was in contrast to earlier studies that reported the discovery of this molecule and claimed that it had no effect on mGluR6 signaling (Maj et al., 2003). Discovery of allosteric ligands would enable pharmacological characterization of mGluR6 and subsequent drug development, which is extremely important given the roles of mGluR6 in night vision (Nakajima et al., 1993; Nomura et al., 1994) and possibly in addiction (Fonseca et al., 2010; Nielsen et al., 2008).

7.3 HOMOLOGY MODELS OF TRANSMEMBRANE REGIONS

Crystal structures are available only for the ATD region of mGluRs. Obtaining crystal structures of the TM region is a difficult endeavor (see 1.1.3.1) and until recently the only crystal structure available among any GPCR was for the inactive structure of rhodopsin. In GPCRs, the two major TM conformations are (1) active and (2) inactive; although, intermediate activation states have also been observed. Active conformation is the structure that can activate the G protein while the inactive conformation is the inverse agonist or the antagonist bound structure that cannot activate the G protein. Inactive TM domain homology models of mGluRs were prepared using the inactive crystal structure of rhodopsin (Palczewski et al., 2000). There were no active structures available of any GPCRs when we did this study. The active TM models of mGluR6 were

therefore generated using an anisotropic network model (ANM) of rhodopsin (Isin et al., 2006) which represents the light-activated state, as template. The homology models for active and inactive conformations were created for all subtypes of mGluRs including mGluR6 (Yanamala, 2009). These homology models were used for docking allosteric ligands.

7.4 VALIDATION OF DOCKING

7.4.1 Preferential binding of allosteric ligands to active and inactive TM structures of mGluRs

The homology models of the TM domains and the docking studies with known allosteric ligands were created in our laboratory and are described in detail in the Ph.D. thesis of Naveena Yanamala (Yanamala, 2009) and are published in (Yanamala et al., 2008). For validating the docking approach, a list of 24 ligands from the literature were pooled and docked to inactive and active homology models using AutoDock (Goodsell et al., 1996) and ArgusLab (Thompson ArgusLab 4.0.1) softwares. Docking results from both docking programs were compared (Figure 7.1). From the rank-ordered list of docked structures in each case the ligand that was most buried and had minimum energy conformation was considered as a positive hit and was included in further analysis. Among these 24 ligands, a total of 9 ligands were experimentally shown to act as positive modulators of specific subtypes, 14 ligands were negative modulators and one ligand was neutral. In general, the positive modulators bound with more favorable energy to the model of the active mGluR conformation, while the negative modulators bound with more favorable energy to the model of the inactive mGluR conformation (Figure 7.1). ArgusLab

predicted 12 of the 14 (86%) negative modulators to bind with more favorable energy to the inactive model and 8 of 9 (89%) positive modulators to bind to the active model, while the numbers for the Auto-Dock results were less well correlated: 10 out of 14 (71%) and 7 out of 9 (78%) for negative and positive modulators, respectively. There were also more incidences in which AutoDock was not able to predict binding for the ligands at all. Five of the predictions for negative modulators and one positive modulator obtained with AutoDock were near or beyond the capability of AutoDock as judged by the error obtained when multiple independent docking experiments were carried out. In contrast, in the case of ArgusLab only one difference between docking to active and inactive models was at the noise level. We conclude that the relative difference between the binding energies of the docked ligands for the active and inactive models is highly predictive of the nature of the modulator, positive or negative (Figure 7.1). Positive modulators in most cases appear to strongly prefer the active conformation over the inactive conformation and negative modulators vice versa.

We found that the allosteric ligand binding pockets of mGluRs are overlapping with the retinal binding pocket of rhodopsin, and that ligands have strong preferences for the active and inactive states depending on their modulatory nature. Additionally, the residues identified in the predicted ligand binding pocket correlate with the residues that are shown to be critical for allosteric ligand function.

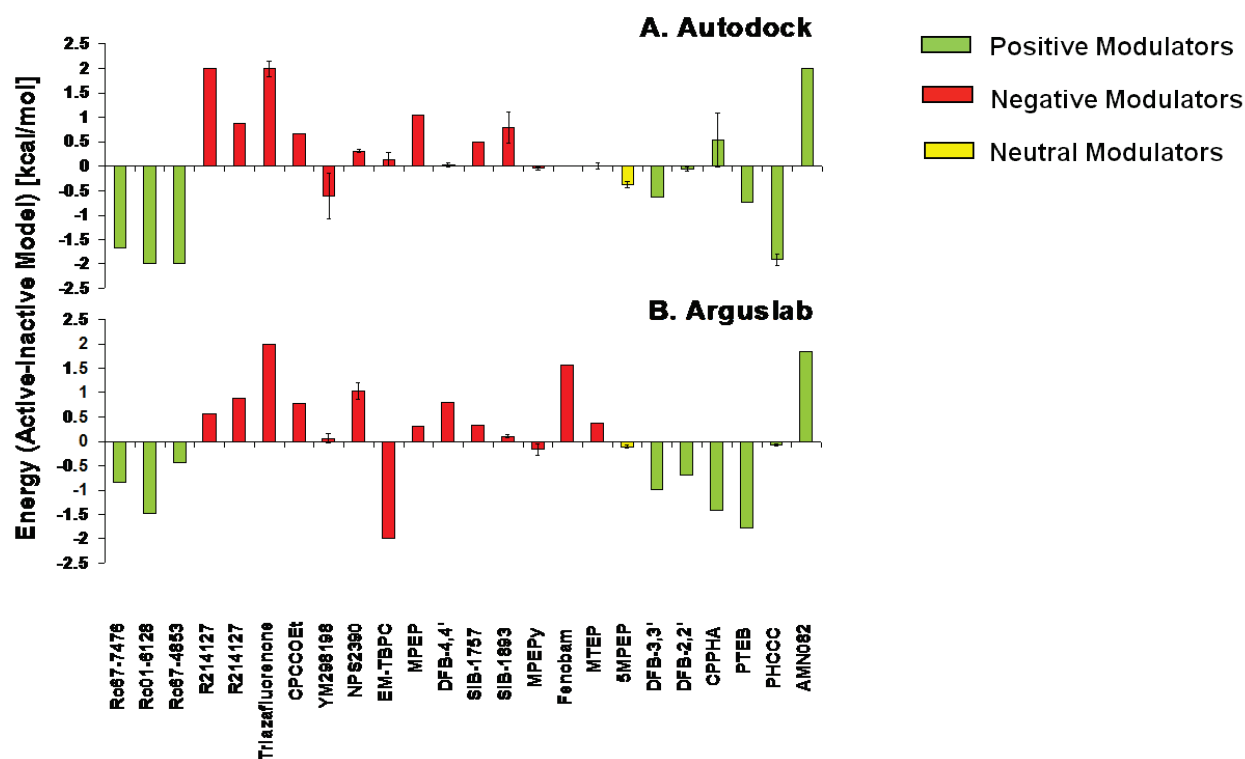


Figure 7.1 Differences in energy between allosteric ligands docked to active and inactive models of mGluRs.

This figure is a courtesy of Dr. Naveena Yanamala. Green bars indicate positive modulators, red bars negative modulators and the yellow bar represents a neutral ligand. Where values of 2 are shown, the ligand did not dock to the active model, where values of -2 are shown; the ligand did not dock to the inactive model. Error bars indicate standard deviation in three docking experiments each for the respective active and inactive models. If an error bar is placed at a -2 or 2 bar, the error represents the standard deviation of the ligand and model combination where docking was observed. (A) Results from docking with AutoDock software. (B) Results from docking with ArgusLab software.

7.4.2 Prediction of allosteric ligands for mGluR6

As described in section 7.4.1, we validated that positive and negative modulators of mGluRs dock respectively to active and inactive homology models of the receptor with better binding energies (Yanamala et al., 2008). Using the same methodology active and inactive

homology models were developed for mGluR6. There are no allosteric ligands reported for mGluR6 previously. Since, in our computational studies we observed that the allosteric ligand binding pockets of mGluRs significantly overlap with each other and with the analogous binding pocket in rhodopsin, we hypothesized that we may be able to use the mGluR6 homology model to predict putative mGluR6 candidates. Given the overlap in the allosteric binding pockets among mGluRs and the sequence identity of 70% within subtypes and 40% between subtypes we set to test if the allosteric ligands reported for other mGluRs dock to mGluR6 models. Amongst the allosteric ligands we docked the following based on commercial availability - CPCCOEt, 3,3'-DFB, MPEP, PHCCC and the rhodopsin ligand all-*trans*-retinal - to mGluR6. Interestingly, these allosteric ligands selectively docked to active and inactive models of mGluR6 with the predicted energies listed in (Table 7.1).

Table 7.1 Docking of allosteric ligands to active and inactive models of mGluR6

^aDocking scores from AutoDock Vina; ^bPAM: Positive allosteric modulator; ^cNAM: Negative allosteric modulator

Ligand	mGluR6			Cognate mGluR receptor		
	Active (kcal/mol)	Inactive (kcal/mol)	Prediction	Active (kcal/mol)	Inactive (kcal/mol)	Experimental
CPCCOEt	-6.8 ^a	Does not dock ^a	PAM ^b	-6.8 (mGluR1)	-7.46 (mGluR1)	NAM ^c
3,3'-DFB	-6.72	-5.42	PAM	-7.06 (mGluR5)	-6.43 (mGluR5)	PAM
MPEP	Does not dock	Does not dock	Does not bind	-6.73 (mGluR5)	-7.77 (mGluR5)	NAM
PHCCC	-9.22 ^a	Does not dock ^a	PAM	-8.07 (mGluR4)	-6.16 (mGluR4)	PAM
all-<i>trans</i>-retinal	-9.11	Does not dock	PAM	--	--	--

MPEP did not dock to any structure while 3,3'-DFB is predicted to bind both active and inactive conformation. CPCCOEt, PHCCC and all-*trans*-retinal docked only to active models

with PHCCC having the lowest binding energy. We tested these predictions experimentally as described below (section 7.5).

7.5 EXPERIMENTAL TESTING OF POTENTIAL ALLOSTERIC LIGANDS ON MGLUR6 FUNCTION

We tested the effects of CPCCOEt, 3,3'-DFB, MPEP, PHCCC and all-*trans*-retinal on the function of mGluR6 by using the cAMP assay as all of them except MPEP were predicted to act as agonists of mGluR6 (Table 7.1). For details of cAMP assay please refer to section 2.5.2. All the ligands were tested at a concentration of 10 μ M and the results of the functional assay are shown in Figure 7.2. We found that none of the ligands showed any effect on cAMP levels.

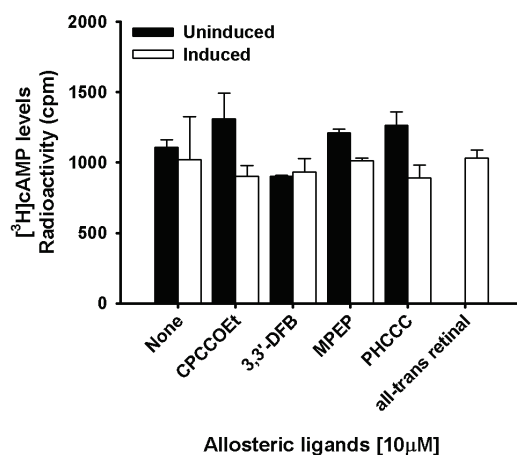


Figure 7.2 cAMP assay to test the effect of predicted allosteric ligands on the function of mGluR6

Allosteric ligands were tested for their effect on mGluR6 activity in both uninduced (filled bars) and induced (open bars) cells. Compared to the elevation of cAMP levels on forskolin (FK; [10 μ M]) stimulation (none), addition of allosteric ligands [10 μ M] does not affect cAMP levels.

In the case of MPEP there was no change in cAMP levels as predicted by docking which also indicated no binding to mGluR6. However, CPCCOEt, 3,3'-DFB, PHCCC and all-*trans*-retinal were computationally predicted to be agonists and likewise did not show any effect at 10 μ M concentrations. The negative result for PHCCC was in line with an earlier report on PHCCC which indicated that it has no effect on mGluR6 (Maj et al., 2003). In contrast, a more recent study suggested that PHCCC acts as a direct agonist at PHCCC at an elevated concentrations of 50 - 100 μ M (Beqollari and Kammermeier, 2008). I therefore tested the effect of PHCCC at 100 μ M concentration. At this increased concentration, there was indeed a strong increase in the cAMP levels in the cells expressing mGluR6 indicating that PHCCC is acting as an inverse agonist. The cAMP results for the allosteric ligands are compared with the docking predictions in Table 7.2.

Table 7.2 Comparison of docking predictions and cAMP assay results for allosteric ligands

^aPAM: Postive allosteric modulator; ^bNo effect at 10 μ M

Ligand	Docking prediction	Reported action at mGluR6 from literature	Response in cAMP assay [ligand concentration]
CPCCOEt	PAM ^a	--	No effect [10 μ M]
3,3'-DFB	PAM	--	No effect [10 μ M]
MPEP	Does not bind	--	No effect [10 μ M]
PHCCC	PAM	No effect / agonist	Inverse agonist [100 μ M] ^b
all-<i>trans</i> retinal	PAM	--	No effect [10 μ M]

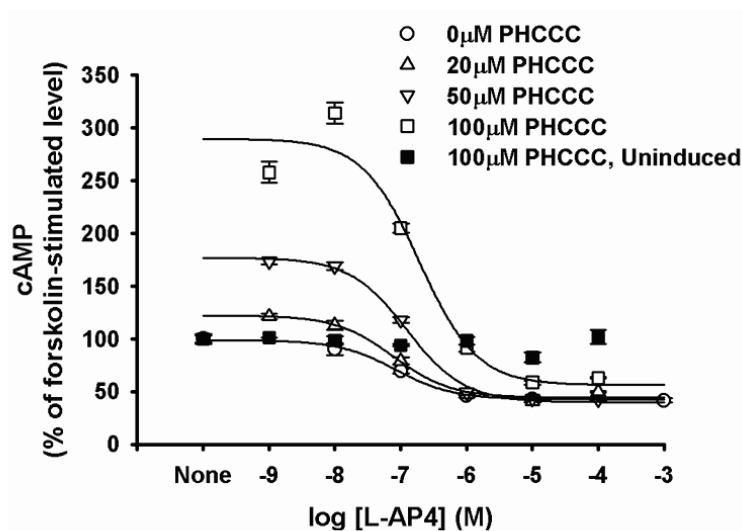
7.5.1 Demonstration of direct inverse agonism of PHCCC

At 0 μ M, 10 μ M, 20 μ M, 50 μ M and 100 μ M concentration of PHCCC, the cAMP levels were 100 \pm 3% , 99 \pm 2% , 123 \pm 4% , 173 \pm 4% and 258 \pm 17% of forskolin alone stimulated levels, respectively (Figure 7.3). There was no effect of PHCCC in uninduced cells at the highest concentration tested (100 μ M). The effect of PHCCC was completely reversed on addition of L-AP4 in a dose-dependent manner (Figure 7.3).

L-AP4 inhibited the PHCCC response in a dose-dependent manner with no shift in EC₅₀ values (panel A, Figure 7.3). The EC₅₀ values of the L-AP4 dose-response in the presence of 20 μ M, 50 μ M and 100 μ M PHCCC were 0.07 μ M, 0.12 μ M and 0.19 μ M, respectively (panel B, Figure 7.3). Note that the EC₅₀ for L-AP4 was 0.18 \pm 0.04 μ M. Generally, in competitive dose-response curves addition of competitive antagonists increases the EC₅₀ values of agonist dose-response (Kenakin, 2006). The apparent EC₅₀ values for L-AP4 dose-response curves were comparable to that of L-AP4 alone suggesting non-competitive (allosteric) mode of action for PHCCC. Further, from our experimental results we conclude that PHCCC preferably binds inactive TM since in the presence of L-AP4 (active TM conformation as L-AP4 is an agonist) the PHCCC effect is mitigated.

The inverse agonism of PHCCC in our studies is in contradiction to both findings from the literature that report no action and direct agonist action. It is hard to explain the inconsistencies but it is tempting to speculate that the differences could arise because of differences in expression systems and functional assays used (Hall et al., 1999; Rajagopal et al., 2010).

A.



B.

PHCCC [μ M]	cAMP (% of forskolin stimulated level)		Apparent EC_{50} [μ M] of L-AP4 dose-response in presence of PHCCC
	PHCCC alone control		
0	100 \pm 3 (3)		0.18 \pm 0.04 (5)
10	99 \pm 2 (3)		-
20	123 \pm 4 (3)		0.20 (1)
50	173 \pm 4 (3)		0.13 (1)
100	258 \pm 17 (3)		0.08 (1)

Figure 7.3 Competition dose-response curves for PHCCC

(A) Effect of PHCCC on L-AP4 dose-response curves. Cells were treated with 0, 20 μ M, 50 μ M and 100 μ M of PHCCC. There was no effect of PHCCC (100 μ M) in uninduced cells. L-AP4 reversed the effect of PHCCC without any right ward shift in the dose-response curves. (B) Table with increase in cAMP levels of cells when PHCCC alone was added and the apparent EC_{50} values for L-AP4 in presence of PHCCC. These apparent EC_{50} values for L-AP4 dose-response curves are comparable to the L-AP4 alone dose-response.

7.5.2 Effect of PHCCC on activity of XR-7TMC

The experimental finding that PHCCC is an allosteric inverse agonist for mGluR6 suggests that PHCCC binds to the TM domain of mGluRs as predicted. Our docking studies and previous work on mGluR4 (Maj et al., 2003) both imply that PHCCC binds in the TM region. To test this hypothesis we tested the functional effect of PHCCC on ‘rhodopsin-like’, TM alone construct - XR-7TMC (see 2.1.3.4) of mGluR6. I described in chapter 3 that XR-7MC has wild-type like expression and trafficking (see 3.3.3) indicating that this protein is likely to be folded. However, in cAMP assays, there was no effect of PHCCC on XR-7TMC at any of the concentrations tested (10nM - 10 μ M; Figure 7.4). There was no difference between induced and uninduced cells. It remains to be tested, if PHCCC has an effect at higher concentrations.

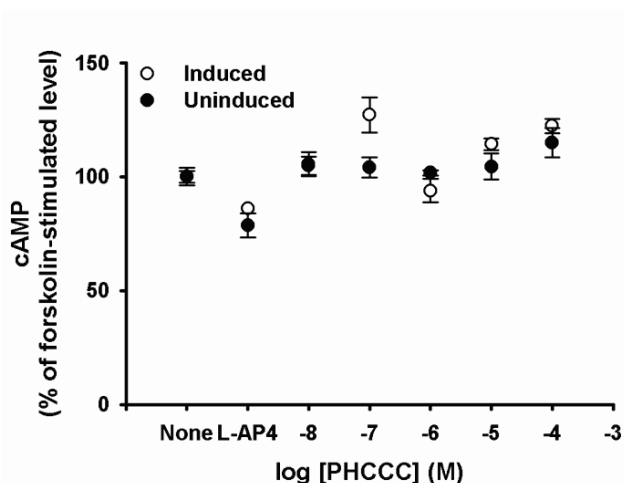


Figure 7.4 cAMP assay to test function of PHCCC on the XR-7MC construct of mGluR6

PHCCC dose-response curves for uninduced (filled circles) and induced cells (open circles). Both uninduced and induced cells show no response to PHCCC over the concentration range studied. L-AP4 was included in the experiment as a negative control.

From the current results it appears that full length mGluR6 may be necessary for PHCCC function. It is also possible that XR-7MC is constitutively active in the absence of the ATD as reported for a similar TM alone construct for mGluR5 (Goudet et al., 2004). As seen in the wild-type, PHCCC response is lost in presence of active mGluR6 (Figure 7.3).

8.0 CYTOPLASMIC ALLOSTERIC LIGANDS

8.1 SUMMARY

Having identified and characterized the binding of ATD and TM domain ligands to mGluR6 in Chapters 6 and 7, I describe here the effect of allosteric ligands that are shown to bind in the IC domain of rhodopsin. The ligands that we re-tested belong to the chemical classes of anthocyanins and porphyrins. These compounds are phyto-chemicals that are readily available as part of our diet and are components in several dietary supplements. Anthocyanin (Cyanidin-3-glucoside (C3G)) and porphyrin (Chlorin e6 (Ce6)) have been shown to modulate vision. Rhodopsin has been identified as a primary target of these ligands so far but a molecular characterization of the binding of these ligands to rhodopsin and their effect on rhodopsin function has not been carried out. Like rhodopsin, mGluR6 is uniquely expressed in the retina and plays a key role in night vision. Therefore, I tested the hypothesis that mGluR6 is a putative target. In this chapter, we discuss characterization of the binding properties of C3G and Ce6 to rhodopsin and determine their effect on rhodopsin function. I tested the effect of these ligands on the function of mGluR6.

Docking studies with rhodopsin predicted that C3G and Ce6 bind in the cytoplasmic domain of inactive and light-activated (Meta II) rhodopsin. Further, ^{19}F and ^1H NMR experiments indicated that the binding of both Ce6 and C3G modulate the structure of the IC

domain, which is a key functional region in rhodopsin, thus, validating the docking predictions. As observed previously, in rod outer segments (Matsumoto et al., 2003), regeneration of purified rhodopsin in detergent micelles accelerated in the presence of C3G without any effect on G-protein activation. In contrast, Ce6 strongly inhibited G-protein activation. Similar to rhodopsin, C3G had no effect on mGluR6 function while Ce6 inhibits its activity as seen in the cAMP assay. Inhibition of G-protein activation by Ce6 on binding to both rhodopsin and mGluR6 provides evidence for to the hypothesis that the TM domain function during activation may be conserved across class A and C GPCRs.

8.2 EFFECT OF ANTHOCYANINS AND PORPHYRINS IN VISION

Anthocyanins and porphyrins are both phytochemicals that are part of our regular diet. Anthocyanins confer color to flowers, fruits, vegetables and leaves and they are shown to have numerous health benefits, including improved vision. Recent studies have shown that the anthocyanin cyanidin-3-O-glucoside (C3G) increases the regeneration of the dim-light photoreceptor rhodopsin (Matsumoto et al., 2003). A member of the porphyrin compounds chlorine e6 (Ce6), a chlorophyll-derivative, also appeared to have role in modulating vision (Douglas et al., 1998; Isayama et al., 2006; Washington et al., 2004; Washington et al., 2007). However, until recently, there was no data on the molecular determinants and consequences of binding of these molecules on the function of photoreceptors.

Both rhodopsin and mGluR6 are important for night vision. Rhodopsin is a primary photoreceptor for night vision and was our primary target for testing the modulatory effects of C3G and Ce6. Like rhodopsin, mGluR6 is uniquely expressed in retina and disruption of

mGluR6 causes night blindness. These facts imply that mGluR6 may also be a suitable target for C3G and Ce6 in modulating night vision. mGluR6 is expressed in the ON bipolar cells that directly communicate with rod cells which express rhodopsin. Together rhodopsin and mGluR6 are critical in the first two steps of dim-light vision and thus small molecules that modulate dim-light vision may target not only rhodopsin but also mGluR6.

8.3 EFFECT OF ANTHOCYANINS AND PORPHYRINS ON RHODOPSIN FUNCTION

Computational and experimental binding studies and effects of binding of C3G and Ce6 on the function of rhodopsin were previously done in our laboratory and are described in detail in the Ph.D. thesis of Naveena Yanamala (Yanamala, 2009). The results for C3G are published in (Tirupula et al., 2009; Yanamala et al., 2009). Here, I have summarized the results of these studies and describe the experiments that I contributed to this work.

8.3.1 Binding studies of C3G and Ce6 to rhodopsin by docking

Docking studies of C3G and Ce6 were carried out with the inactive crystal structure (PDB: 1L9H) and computationally derived active conformation (Meta II) of rhodopsin (Isin et al., 2006; Okada et al., 2002) using AutoDock software (Morris et al., 1996) by Naveena Yanamala (Yanamala, 2009). Both C3G and Ce6 docked to the cytoplasmic face of rhodopsin. I verified the existence of different chemical species of C3G at different pH by absorption spectroscopy (Figure 8.1). At pH 6.0, C3G exists in equilibrium between chalcone and quinoidal

forms (Figure 8.1). Thus, both chalcone and quinoidal species were docked to rhodopsin. The chalcone form was found to bind with high energy to the inactive state of rhodopsin. In contrast, the quinoidal species exhibited the highest binding energy when docked to the Meta II model of rhodopsin. Similar to C3G, Ce6 also docked in the cytoplasmic domain and to both the inactive and Meta II states.

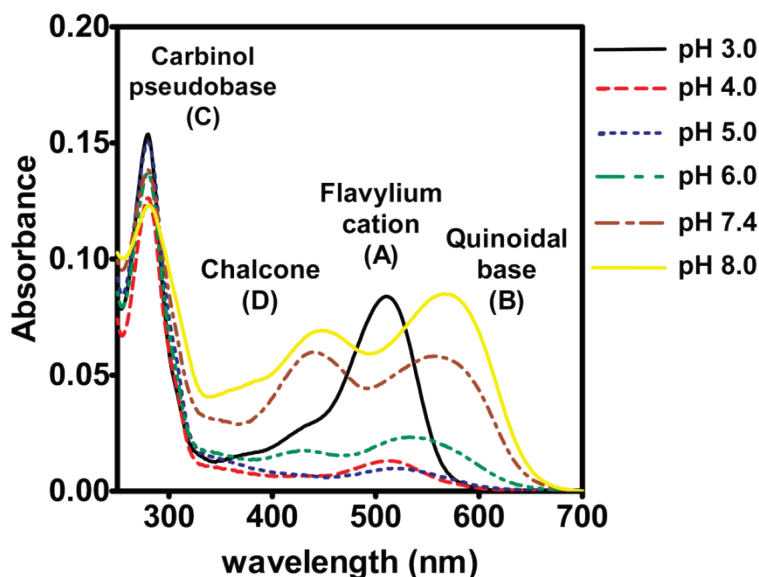


Figure 8.1 Absorption spectra of C3G alone at different pH conditions

The figure shows the absorption spectrum of 5 μ M C3G at different pH values. In the spectrum at pH 3, the predominant species is the flavylium cation with absorbance in visual range (514nm). At pH values of 4 and 5, the flavylium cation disappears and there is little absorption in the visible range. At pH 6 and 7.4, two new peaks at 440nm and 550nm are predominant which indicate ionized chalcone and anhydrobase (quinoidal) respectively. At pH 8 (and above) the 550 peak shifts towards 600nm which is typical of ionized anhydrobase (Levi et al., 2004).

8.3.2 Binding studies of C3G and Ce6 to rhodopsin by NMR

To complement the docking studies, Naveena Yanamala studied binding of different C3G species to inactive and Meta II states of rhodopsin by ^1H NMR. One-dimensional selective excitation ^1H NMR spectra without and with C3G were recorded. The ligand peaks of C3G observed in the inactive and Meta II states were different suggesting that different species (chalcone and quinoidal) of C3G bind to different states of rhodopsin. This finding fits well with the docking predictions. Moreover, an overall decrease in the peak intensities arising from the flexible cytoplasmic residues of rhodopsin was observed in the presence of C3G when bound to the Meta II state as compared to the inactive state. These results indicated that the binding of C3G to rhodopsin may occur at the IC domain, in support of the predictions. Similar to C3G, ^1H NMR studies were used to determine binding of Ce6 to rhodopsin. Additionally, ^{19}F NMR spectra of rhodopsin, with ^{19}F labels on the cysteines at positions 140 and 316 in the cytoplasmic domain, were carried out in the presence and absence of Ce6. Distinct changes in the NMR spectra were observed for both inactive and Meta II rhodopsin samples in the presence and absence of Ce6 (Yanamala, 2009). These findings suggest that Ce6 binds at and affects the local environment of both cysteines in the cytoplasmic face of rhodopsin, in the inactive and Meta II states supporting the docking studies.

8.3.3 Effect of C3G and Ce6 on function of rhodopsin

The molecular effects of C3G and Ce6 binding on the function of rhodopsin were investigated in our laboratory using three different functional assays: rhodopsin chromophore regeneration, G protein activation and Meta II decay (see chapter 2 for experimental details). The results indicated that C3G modulates rhodopsin function by increasing its rate of regeneration while Ce6 acts by directly inhibiting G protein (transducin) activation, as described in detail, below.

8.3.3.1 C3G enhances regeneration rate of rhodopsin

Absorbance spectrum of rhodopsin is characterized by a 500nm peak that arises due to the bound 11-*cis*-retinal. On light activation of rhodopsin, 11-*cis*-retinal isomerizes to all-*trans*-retinal and the 500nm peak shifts to 380nm. The reverse can be observed on addition of 11-*cis*-retinal to photoactivated state and this can be used to quantify regeneration of rhodopsin. The increase in 500nm absorbance by addition of 11-*cis*-retinal after light-activation was followed using UV/Visible spectroscopy. The normalized change in absorbance at 500nm of rhodopsin at pH 6 in the presence of 11-*cis*-retinal after illumination and in the absence (filled circles) and presence of C3G (open circles) is shown in (panel A; Figure 8.2). The regeneration rates for rhodopsin in the absence and presence of C3G are $0.072 \pm 0.009 \text{ min}^{-1}$ and $0.119 \pm 0.008 \text{ min}^{-1}$, respectively. In the presence of C3G, the rate of regeneration increased by 1.65-fold as compared to rhodopsin alone, in agreement with previous studies (Matsumoto et al., 2003). Additionally, we also found that the presence of C3G not only changed the rate but also the extent of regeneration. C3G decreased the total amount of rhodopsin regenerated by ~10% as compared to rhodopsin alone at pH 6.

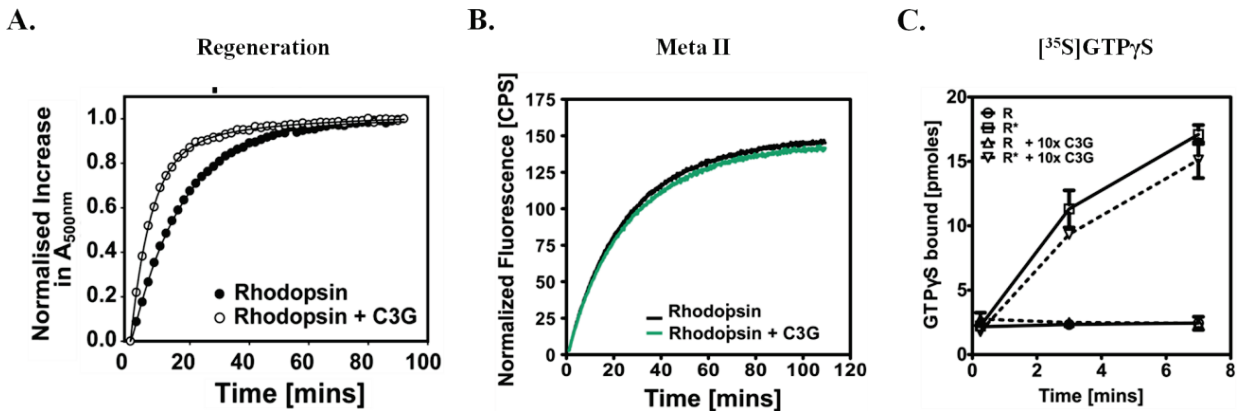


Figure 8.2 Effect of C3G on function of rhodopsin

(A) Regeneration of rhodopsin ($0.5\mu\text{M}$) in the absence (filled circles) and presence (open circles) of C3G ($0.5\mu\text{M}$) at pH 6. The total amount of increase in absorbance at 500nm in the presence and absence of C3G was normalized to 100%. The detergent content in the samples was 0.6%. (B) Effect of C3G on rhodopsin Meta II decay at concentrations and conditions similar to the regeneration assay (panel A). Rhodopsin alone fluorescence is represented by a black line, while the fluorescence in presence of C3G is represented by green line. (3) Functional assay to determine effect of C3G on rhodopsin activity. The activity is tested by measuring the $[^{35}\text{S}]\text{GTP}\gamma\text{S}$ bound to the G protein transducin. Dark state rhodopsin (R) and light activated rhodopsin (R*) are shown as solid lines with open circles and open squares respectively. Identical reactions but with C3G are shown as dashed lines with open triangles. Each experiment was performed in duplicate. Rhodopsin concentration is 5nM while the C3G concentration is 50nM (10X). Figure in panel A is courtesy of Dr. Naveena Yanamala.

8.3.3.2 C3G has no effect on Meta II decay

Meta II decay refers to the rate at which all-*trans*-retinal leaves activated rhodopsin and results in ligand-free opsin, an obligatory step in the regeneration process. The rate of Meta II decay can be conveniently measured with fluorescence (Farrens and Khorana, 1995). On light-activation there is a mono-exponential increase in fluorescence resulting from tryptophan residues that are no longer quenched by retinal. The Meta II assay was carried out under similar experimental conditions and concentrations of C3G and rhodopsin as in the regeneration assays

(panel B, Figure 8.2). The half-life of Meta II decay ($t_{1/2}$) in the absence and presence of C3G was 17.6min versus 18min, respectively. This corresponds to a rate in the absence and presence of C3G of 0.039min^{-1} versus 0.0384min^{-1} , respectively (panel B, Figure 8.2). These results indicate that there is no significant effect of C3G binding on Meta II decay. Further, there was no significant change in the fluorescence saturation levels and half-lives in presence and absence of C3G.

8.3.3.3 C3G slightly inhibits G protein activation

Next, we checked if C3G binding affects rhodopsin activity. Upon light incidence, rhodopsin catalyzes the exchange of GDP to GTP on the G protein transducin (G_t). The GTP-bound G_t can be quantified *in vitro* by [^{35}S]GTP γ S filter binding assays. The activation of G_t by rhodopsin is measured as the increase in [^{35}S]GTP γ S-bound G_t . Compared to rhodopsin in the dark, there is a 12-fold increase in G_t activation by Meta II rhodopsin (panel C, Figure 8.2). In the presence of a 10-fold excess (50nM) of C3G, there is a slight decrease in the activation of G_t (panel C, Figure 8.2). The magnitude of the decrease is on the order of the error in the experiment suggesting C3G may not influence rhodopsin activation. For rhodopsin activation experiments at increased C3G (1mM; ~200,000 excess) concentrations, the average fold increase in activity (illuminated versus dark) for rhodopsin alone and rhodopsin with 1mM C3G was 2.2 ± 0.3 ($n = 4$) and 1.5 ± 0.1 ($n = 4$) respectively. Thus, even at these very elevated concentrations of C3G, there was only a modest decrease (32%) in G_t activation and this effect may be due to direct effects on G_t rather than rhodopsin. This suggests that C3G binding may affect G_t activation only slightly, if at all.

8.3.3.4 Ce6 inhibits G protein activation

In order to study the effect of Ce6 on rhodopsin function, similar to C3G, we set up a G protein activation assay. A time course of light-dependent activation of G_t was measured in the presence and absence of a 25-fold excess Ce6 (Figure 8.3). At 120 seconds post-illumination, rhodopsin without Ce6 displayed near saturation in activation, whereas an identical sample containing 25-fold excess Ce6 displayed no activation as compared to dark controls (Figure 8.3).

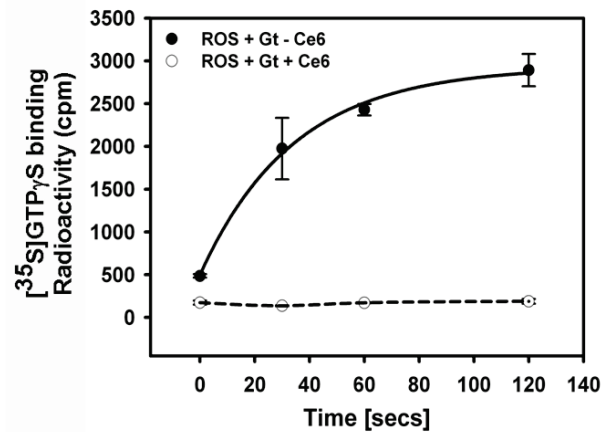


Figure 8.3 Transducin (G_t) activation assay in presence of Ce6

This figure is a courtesy of Dr. Naveena Yanamala. Shown in the figure is G_t activation by illuminated rhodopsin in the absence (filled circles) and presence of a 25-fold excess of Ce6 [$6.25\mu\text{M}$] (open circles) measured at different time points. The rhodopsin concentration used was $0.25\mu\text{M}$.

These results along with the data from binding studies indicate that Ce6 probably competes with G_t for binding in the cytoplasmic domain.

8.4 EFFECT OF ANTHOCYANINS AND PORPHYRINS ON MGLUR6 FUNCTION

Next, I investigated the effect of anthocyanins (C3G and Cyanidin-3-O-rutinoside (C3R)) and porphyrins (Ce6) on the function of mGluR6. I tested the effect of these compounds on mGluR6 using the cAMP assay that I optimized for the inducible stable cell lines (section 2.5.2).

8.4.1 Effect of anthocyanins on function of mGluR6

I tested the effect of two different anthocyanins (C3G and C3R) on mGluR6 function using cAMP assay. cAMP levels were measured in cells expressing mGluR6 when these compounds were added directly (testing for agonism) or in the presence of L-AP4 (testing for antagonism). On C3G and C3R addition, there was no change in cAMP levels as compared to forskolin (FK; [10 μ M]) stimulation alone (Figure 8.4). On addition of L-AP4, the cAMP levels were 55 ± 4 % and 49 ± 4 % of FK alone controls for C3G and C3R respectively. These levels were comparable to L-AP4 alone response (see section 5.2.2) of 54 ± 3 %. These results suggest that there is no effect of anthocyanins on the function of mGluR6.

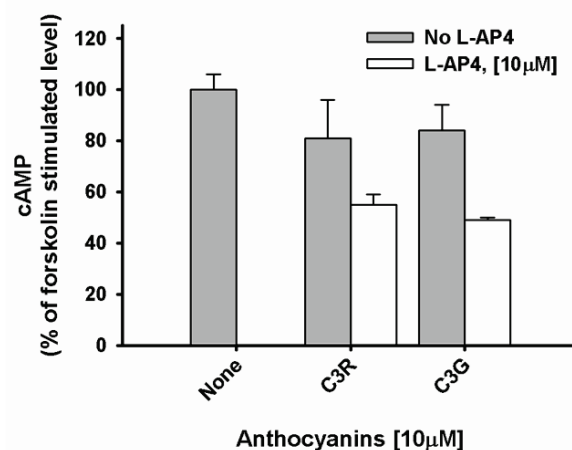


Figure 8.4 cAMP assay to test effect of C3G, C3R on the function of mGluR6

cAMP assay measuring the response of induced cells in the absence (filled bars) and presence (open bars) of C3G [10µM] C3G [10µM] and Ce6 [10µM]. Compared to the elevation of cAMP levels on forskolin (FK; [10µM]) alone stimulation (none), addition of C3G or C3R does not affect the cAMP levels. The decrease of cAMP levels on addition of L-AP4 [10µM] in the presence of C3R and C3G were 55 ± 4 % and 49 ± 4 %. The data is represented as mean \pm standard deviation.

8.4.2 Effect of Ce6 on function of mGluR6

Unlike C3G, the addition of Ce6 significantly elevated the cAMP levels both in uninduced and induced cells to 225 ± 13 % and 253 ± 9 % of FK stimulated controls, respectively (Figure 8.5). This increase in cAMP levels was absent when FK was not added suggesting that this is an adenylyl cyclase mediated response (Figure 8.5) which is typical of the cAMP assay. However, addition of L-AP4 decreases the cAMP levels to 171 ± 8 % of FK stimulated controls (none). This corresponds to only 81 ± 9 % of the cAMP levels of Ce6 alone controls. However, in presence of L-AP4 alone the cAMP levels were typically 54 ± 3 % (see section 5.2.2) of the FK stimulated controls. Thus, the addition of Ce6 maintains higher cAMP levels even in the

presence of L-AP4, suggesting that Ce6 is inhibiting the agonist response. This finding is similar to the lack of G protein activation by light-activated rhodopsin in presence of Ce6.

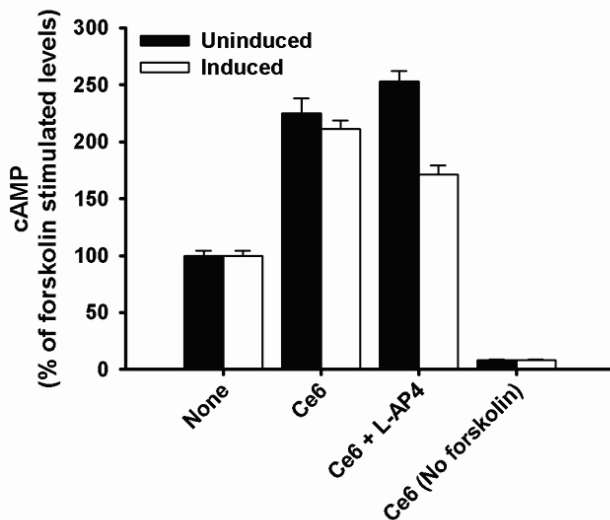


Figure 8.5 cAMP assay to test an effect of Ce6 on cAMP levels in induced and uninduced cells

Shown in the figure is the cAMP assay measuring the effect of Ce6 on uninduced (filled bars) and induced (open bars) cells. Compared to the elevation of cAMP levels on forskolin (FK; [10 μ M]) stimulation (none), the addition of Ce6 significantly elevated the cAMP levels to 225 ± 13 % and 211 ± 8 % of FK stimulated levels in uninduced and induced cells, respectively. This increase is forskolin mediated (see no forskolin control). In the presence of L-AP4 [10 μ M], the cAMP levels were decreased in induced cells (171 ± 8 % of FK stimulated levels) but not in uninduced cells (253 ± 9 % of FK stimulated levels). Data is represented as mean \pm standard deviation.

This similarity in the effects observed with mGluR6 and rhodopsin suggests that this effect may be general for GPCRs. There is conservation of the G protein binding site in the cytoplasmic domain of GPCR, allowing a few number of different G proteins to bind the diverse range of receptors. This conservation appears strong enough to allow binding of Ce6 to both, rhodopsin and mGluR.

9.0 ROLE OF TM CYSTEINES IN MGLUR6 ACTIVATION

9.1 SUMMARY

Metabotropic glutamate receptor subtype 6 (mGluR6) is a Class C type G protein coupled receptor uniquely expressed on retinal bipolar cells. mGluR6 plays a key role in night vision but little is known about its structure and function. Here, we characterized the role of the three free transmembrane (TM) cysteines in activation through site-directed mutagenesis. Signaling function of the mutants in cells and membranes was assayed via cAMP and G protein activation, respectively. Mutants with cysteine replacements in TM helix V, C765^{5.57}A and C754^{5.46}A, display slightly elevated activity as compared to wild type, while C754^{5.46}A/C765^{5.57}A is active at levels comparable to that of wild type. In contrast, all mGluR6 proteins carrying the mutation in TM helix VI, namely C793^{6.45}, C754^{5.46}A/C793^{6.45}A, C765^{5.57}A/C793^{6.45}A and cys-less, lack activity. These results suggest that all three TM cysteines are important for mGluR6 activity, with C793^{6.45} being critical. Since all three cysteines are predicted to be in close proximity, we hypothesize that they form part of a microdomain on TM5 and TM6 involved in receptor activation.

9.2 RATIONALE

Current knowledge of GPCR activation is derived primarily from studies on rhodopsin, and to lesser extent from other class A GPCRs such as adrenergic, dopamine and chemokine receptors. However, class C GPCR sequences show very low identity to Class A sequences and are furthermore distinguished from other GPCRs by their unique, ATD and CRD additions. Models for activation of mGluRs are controversial (see Introduction, section 1.3.6).

In this chapter, I describe the first structure-function studies carried out for mGluR6 to date. I characterized the role of conserved cysteines in the TM for activation and find experimental support for the generality hypothesis, stating that class A and class C GPCR activation mechanism are fundamentally conserved. In particular, my studies highlight the importance of importance of TM helix 6 for activation.

9.3 IMPORTANCE OF TM CYSTEINES

9.3.1 Identification of conserved cysteines in TM of mGluRs

There are a total of 22 cysteines in human mGluR6 – eight in the ATD, nine in the CRD and five in the TM region. Crystal structures of the ATD and CRD of rat mGluR1, mGluR3 and mGluR7 suggest that all cysteines in these domains form disulfide bonds (Kunishima et al., 2000; Tsuchiya et al., 2002). A conservation profile from a sequence alignment of 92 mGluRs from different subtypes and organisms highlighting the remaining five cysteines is shown in Figure

9.1. C650 and C744 are located at the EC end of helix III and the second EC loop connecting TM helices IV and V (Figure 9.2), respectively. They are conserved in all mGluRs and are presumed to form a disulfide bond (Gether, 2000; Pin et al., 2003) that is conserved throughout much of the GPCR family, corresponding to the disulfide bond between C110 and C187 in rhodopsin (Rader et al., 2004). Thus, the only cysteines that are not predicted to be involved in disulfide bonds are C754^{5.46}, C765^{5.57} and C793^{6.45}, all of which are located in the TM region (Figure 9.1). C765^{5.57} and C793^{6.45} are conserved in all mGluRs, while C754^{5.46} is conserved only in mGluR6 (Figure 9.1). Other members of group III mGluRs have a cysteine at position 753^{5.45} instead of 754^{5.46}.

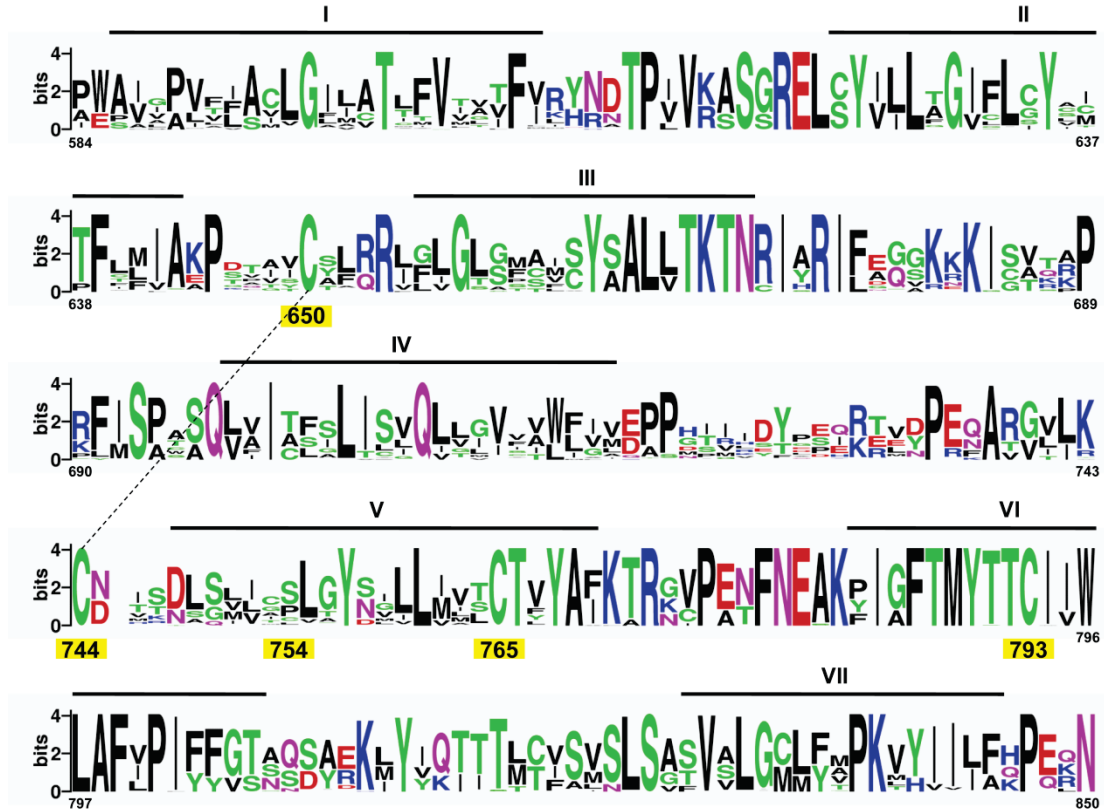


Figure 9.1 Multiple sequence alignment of transmembrane region of mGluRs

The sequences of mGluRs were obtained from NCBI. The amino terminal domain (ATD) and cysteine rich domain (CRD) were removed and only the TM regions were included in the alignment for clarity. mGluR TM regions from different organisms were aligned using ClustalW and for easy visualization the logo of the alignment was generated using Weblogo (<http://weblogo.berkeley.edu>) (see 2.8.1). The amino acid numbering is based on the positions of human mGluR6 (NCBI Reference Sequence: NP_000834). The positions of conserved cysteines are highlighted in yellow. The individual letter height of amino acid(s) at each position indicates their relative frequencies and conservation in the alignment. C650 and C744 form a disulfide bond which is conserved in most of the G protein coupled receptors (Rader et al., 2004). C765^{5,57} and C793^{6,45} are conserved in all mGluRs, while C754^{5,46} is conserved only in mGluR6. The TM helices are indicated as lines above the sequence.

9.3.2 Structural modeling of the cluster of cysteines in TM 5 and 6

There is no structural data available for the TM regions of any mGluR. I therefore conducted homology model predictions. The result is shown in panel B, Figure 9.2. In the structural model, C754^{5.46}, C765^{5.57} and C793^{6.45} are clustered with C β -C β distances ranging from 14Å to 18Å, on helices TM5 and TM6 (panel B, Figure 9.2). C754^{5.46} and C793^{6.45} are located in the middle of these helices. In other GPCRs, this region plays an important role for ligand binding and receptor activation as described in more detail below (section 9.3.3). Thus, the location in the predicted mGluR6 structure together with the conservation in sequence suggests that these cysteines may play a role for mGluR6 functional activation.

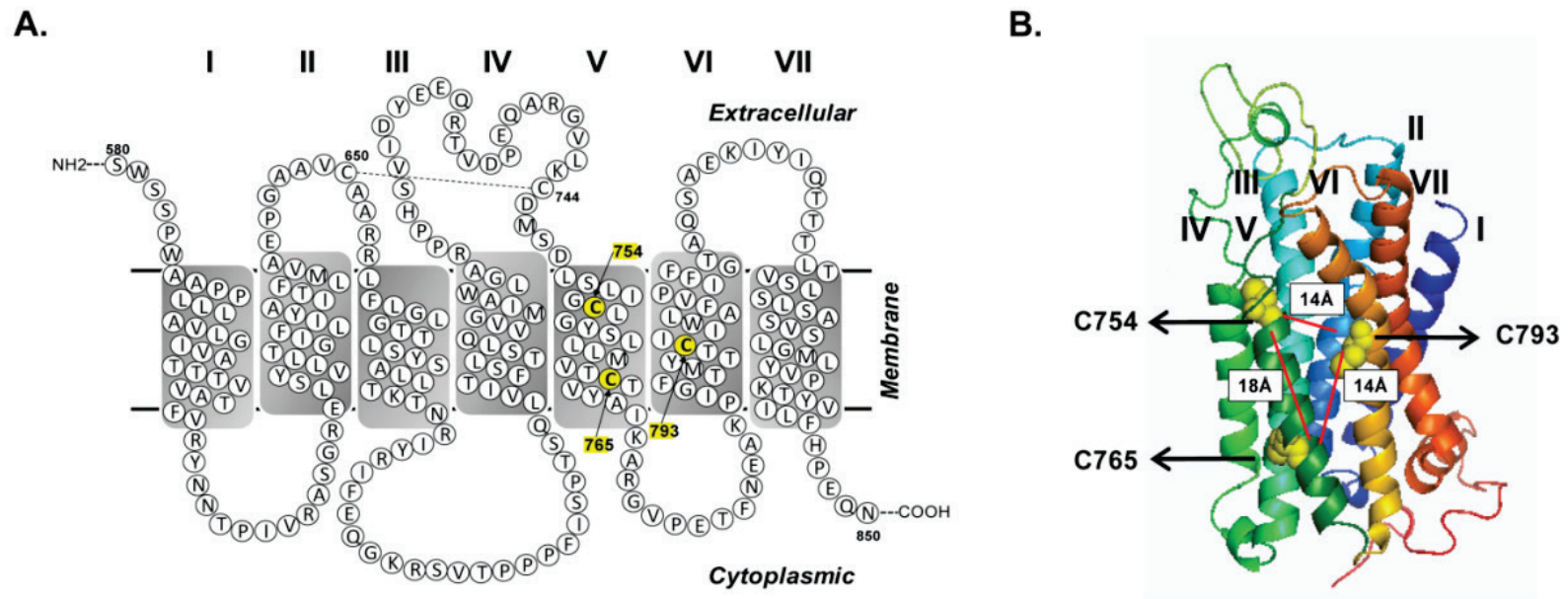


Figure 9.2 Location of transmembrane (TM) domain cysteines

The location of cysteines 754^{5,46}, 765^{5,57} and 793^{6,45} is highlighted in (A) the secondary structure snake-plot model which was created using the TM annotations of the human mGluR6 sequence (NP_000834.2) available at NCBI. (B) Tertiary structure homology model generated using known GPCR structures (see section 2.8.4.2). Also shown are the distances between C β -C β atoms of cysteines in angstroms (Å). The cysteines are clustered on TM helices V and VI.

9.3.3 Comparison of mGluR6 with rhodopsin and other mGluRs

In the prototypical GPCR rhodopsin the activation mechanism is well studied. Light triggered retinal isomerization induces conformational changes of multiple ‘switches’ involving residues from TM5 and TM6 that ultimately lead to activation of the receptor (Ahuja and Smith, 2009). Rhodopsin TM5 residues M207^{5.42}, F208^{5.43}, H211^{5.46}, F212^{5.47} and TM6 residues F261^{6.44}, W265^{6.48}, Y268^{6.51} and A269^{6.52} are most involved in retinal packing (Palczewski et al., 2000). On TM5 and TM6 retinal isomerization results in the rotation of W265^{6.48} (rotamer toggle switch), and in reorientation of H211^{5.46}, Y223^{5.58}, M257^{6.40} and Y268^{6.51} residues that results in the outward rotation of TM5 on the extracellular side and TM6 in intracellular side and the breaking of ionic lock (Ahuja and Smith, 2009; Patel et al., 2005). Thus TM5 and TM6 play a key role in rhodopsin activation.

2006). This finding suggests that like in rhodopsin TM5 and TM6 play a key role in the activation of mGluRs (Malherbe et al., 2006; Muhlemann et al., 2006; Noeske et al., 2006; Yanagawa et al., 2009). The TM6 region is more strongly conserved in mGluRs as compared to the conservation of TM5. To investigate the roles of these two helices in mGluR6 activation, we systematically mutated the cysteines in both, the TM5 and TM6 regions. To date, there were no structure-function studies performed with mGluR6. Moreover, human mGluR6 has no additional cysteines in TM regions other than those located in TM5 and TM6. Thus, the analysis of cysteine mutants provides us with an opportunity to evaluate the role of TM5 and TM6 in receptor activation.

9.4 COMPARISON OF EXPRESSION LEVELS OF WILD-TYPE AND CYSTEINE MUTANTS

We verified the relative expression levels of wild-type and mutant receptors in order to rule out the possibility that differences in activity was because of variable expression levels of the receptors in stable cells.

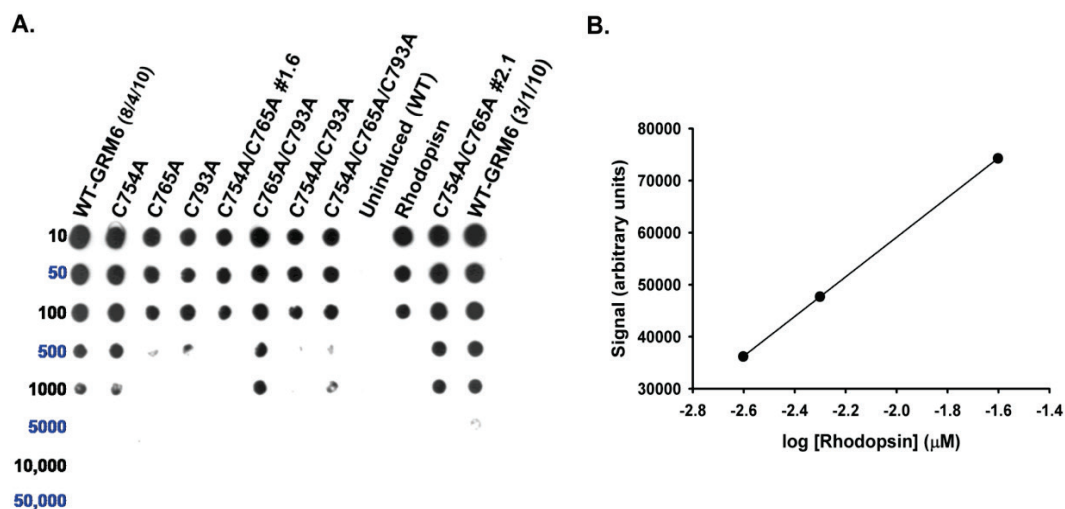


Figure 9.4 Quantifying expression levels Wild-type and mutant mGluR6 membranes

(A) Dot blot with serial dilutions of membranes for wild-type and cysteine mutants. Two independent ten-fold dilutions were loaded on the dot blot starting with 10-fold dilution (in black font) and 50-fold dilution (in blue font). Known quantities of rhodopsin were loaded as a positive control. (B) Standard curve representing signal dot intensity in arbitrary units versus concentration of rhodopsin from dot blots. The linear regression equation which fits this data best is: $y = 38073x + 13526$; $R^2 = 1$. The concentrations in μM as derived from the standard curve are: WT (8/4/10): 0.56, C754^{5.46}A: 0.68, C765^{5.57}A: 0.23, C793^{6.45}A: 0.37, C754^{5.46}A/C765^{5.57}A #1.6: 0.16, C765^{5.57}A/C793^{6.45}A: 0.51, C754^{5.46}A/C793^{6.45}A: 0.18, C754^{5.46}A/C765^{5.57}A/C793^{6.45}A: 0.24, C754^{5.46}A/C765^{5.57}A #2.1: 0.69, WT (3/1/10): 0.77. Two different stable cell line clones (clones #2.1 and #1.6) are characterized for C754^{5.46}A/C765^{5.57}A mutant. For cell line information of wild-type and other mutants see Table 2.10.

Membrane preparations of WT and mutant mGluR6 are shown in dot blots in Figure 9.4. Receptor expression levels vary between 0.16 μM - 0.77 μM suggesting comparable levels of expression across mutants. As expected, no expression of receptors was observed when the cells were uninduced. Membranes prepared on different days and debanked separately show reproducible levels of receptor expression (compare 0.56 μM versus 0.77 μM for wild-type mGluR6; (Figure 9.4)). The uninduced cells were used as controls for evaluating background responses in functional assays in the absence of receptor.

9.5 ACTIVATION STUDIES

To experimentally test the hypothesis from sequence and structural modeling that the three cysteines in the TM domain may be involved in mGluR6 activation, we systematically mutated them to alanines, one at a time and in all possible permutations. There are a total of seven cysteine mutants that are categorized into double (C754^{5.46}A, C765^{5.57}A, C793^{6.45}A), single (C754^{5.46}A/C765^{5.57}A, C765^{5.57}A/C793^{6.45}A, C754^{5.46}A/C793^{6.45}A) and cys-less (C754^{5.46}A/C765^{5.57}A/C793^{6.45}A) mutants, referring to the presence of two, one or no native cysteines in the TM domains of these mutants, respectively. For both the WT and cysteine mutants tetracycline inducible stable cell lines were established that were selected for maximal receptor expression. Receptor expression is under tetracycline inducible promoter which prevents any adverse effects of constitutive over expression that could be toxic.

9.5.1 Agonist response

9.5.1.1 Forskolin stimulated cAMP formation in cells

We evaluated the response of double, single and cys-less mutants to L-AP4 (10 μ M) in induced and uninduced cells (Figure 9.5 and Table 9.4). In the cAMP assay, the background activity in the presence of ligands was between 75% and 110% of the forskolin stimulated cAMP levels. The highest activity in the presence of L-AP4 was observed for double cysteine mutants C754^{5.46}A and C765^{5.57}A (38 \pm 1 % and 37 \pm 2 %), followed by WT (54 \pm 3 %). The activity of single cysteine mutant C754^{5.46}A/C765^{5.57}A was like WT (52 \pm 5 %). Also, the EC₅₀ value for the L-AP4 dose-response for C754^{5.46}A/C765^{5.57}A was 0.18 \pm 0.04 μ M similar to WT (Table 9.2). The double cysteine mutant C793^{6.45}A has no response to L-AP4 (107 \pm 6 %). Similarly all other

cysteine mutants carrying the C793^{6.45}A mutation were inactive. The cAMP data thus strongly suggests that C793^{6.45} is critical for activation. Similar response of WT, single and cys-less mutants was observed with L-glutamate (Table 9.1). Also, the EC₅₀ value for the L-glutamate dose-response for C754^{5.46}A/C765^{5.57}A was similar to WT (Table 9.2).

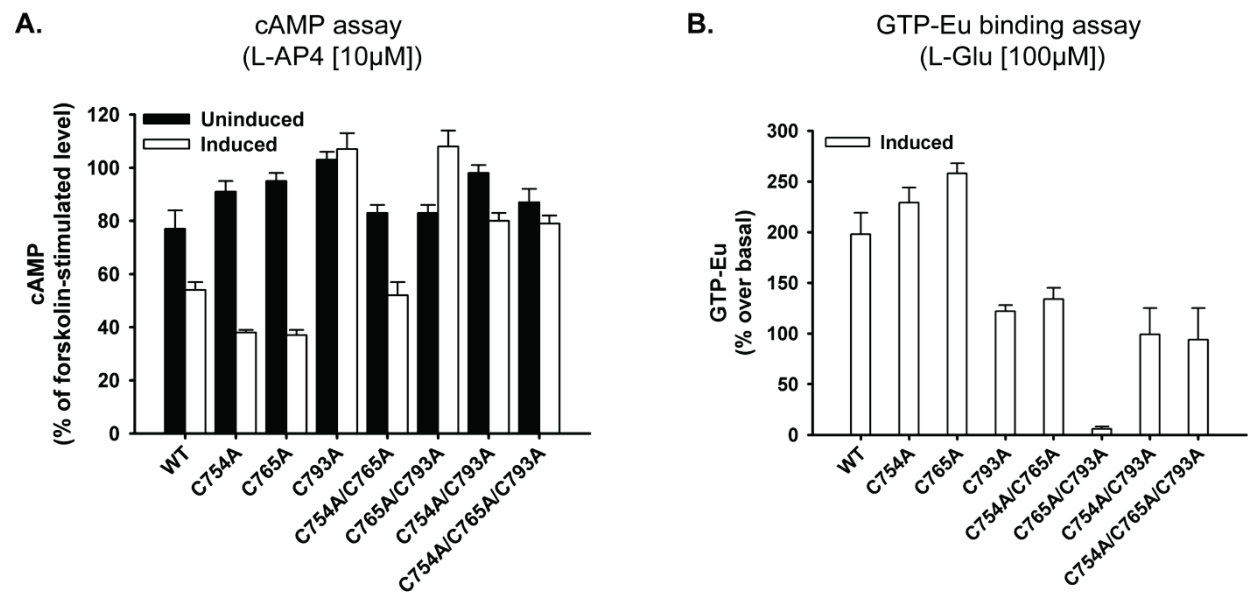


Figure 9.5 Comparison of agonist induced activity in different cysteine mutants

Effect of transmembrane domain cysteine mutants on (A) inhibition of forskolin (10μM) stimulated cAMP accumulation in the presence of L-AP4 (10μM) and (B) percent over basal increase of GTP-Eu fluorescence in the presence of L-glutamate (100μM) in induced (filled bars) cells. Data for uninduced cells in GTP-Eu is omitted as the % over basal counts was very low. Data for C754^{5.46}A/C765^{5.57}A mutant in cAMP and GTP-Eu assays is average of stable cell line clones #2.1 and #1.6 (see Table 9.4 and Table 9.3).

Table 9.1 L-glutamate induced response for WT and cysteine mutants (cAMP formation)Data is represented as mean \pm SEM (number of independent experiments)

Receptor construct	L-Glutamate [100 μ M]	
	Induced	Uninduced
WT	50 \pm 2 (3)	85 \pm 3 (3)
Single cysteine mutants		
C754A/C765A	57 \pm 1 (2)	82 \pm 4 (2)
C765A/C793A	85 (1)	60 (1)
C754A/C793A	81 (1)	75 (1)
Cys-less mutant		
C754A/C765A/C793A	76 (1)	82 (1)

Table 9.2 EC₅₀ [μ M] values for agonists at active cysteine mutants compared to WTData is represented as mean \pm SEM (number of independent experiments)

Receptor construct	EC ₅₀ (μ M)		
	L-Glutamate		L-AP4
	Eu-GTP	cAMP	cAMP
WT	5 \pm 1.1 (5)	4 \pm 2 (3)	0.18 \pm 0.04 (5)
C754A	3 \pm 0.2 (3)		
C765A	6 \pm 1.9 (2)		
C754A/C765A	5 \pm 1.2 (5)	5 (1)	0.22 \pm 0.1 (2)

9.5.1.2 GTP-Eu binding in membranes

The effect of L-glutamate was tested at double, single and cys-less mutants (Figure 9.5 and Table 9.3). Dose-response curves for L-AP4 using GTP-Eu binding assay could not be performed as the ligand interfered with the GTP-Eu fluorescence. Therefore, L-glutamate was added instead of L-AP4 in this assay. I verified (see section 5.2) that 10 μ M L-AP4 and 100 μ M L-glutamate show comparable decrease in cAMP levels to 54 \pm 3 % (n = 7) and 50 \pm 2 % (n = 3) of forskolin stimulated levels, respectively, suggesting comparable levels of G protein activation.

Among the double cysteine mutants, C754^{5.46}A (229 \pm 15 % over basal) and C765^{5.57}A (258 \pm 10 % over basal) showed enhanced binding of GTP-Eu compared to WT (198 \pm 21 %

over basal). C793^{6.45}A displayed relatively low binding (122 ± 6 %) compared to WT. The single cysteine mutant C754^{5.46}A/C765^{5.57}A also has a lower GTP-Eu binding (134 ± 11 %) compared to wild-type. The remaining single cysteine mutants and the cys-less mutants have very low percent over basal GTP-Eu binding. The relative activities (E_{\max}) of cysteine mutants compared to WT (set at 100%) are in this order: C765^{5.57}A (130%) > C754^{5.46}A (116%) > WT (100%) > C754^{5.46}A/C765^{5.57}A (68%) > C793^{6.45}A (62%) > C754^{5.46}A/C793^{6.45}A (50%) > C754^{5.46}A/C765^{5.57}A/C793^{6.45}A (47%) > C765^{5.57}A/C793^{6.45}A (3%). The EC_{50} values as estimated from this assay for L-glutamate are 3 ± 0.2 μ M, 6 ± 1.9 μ M and 5 ± 1.2 μ M for C754^{5.46}A, C765^{5.57}A and C754^{5.46}A/C765^{5.57}A mutants respectively (Table 9.2).

Table 9.3 L-glutamate induced response for WT and cysteine mutants (GTP-Eu binding)

Data for C754^{5.46}A/C765^{5.57}A mutant is average of 154 ± 17 (2) and 121 ± 7 (3) % over basal binding for stable cell line clones #2.1 and #1.6, respectively. Data is represented as mean \pm SEM (number of independent experiments).

Receptor construct	Maximal binding (% over basal at 100 μ M L-Glu)	E_{\max} [% of wildtype]
Wild type	198 \pm 21 (6)	100
Double cysteine mutants		
C754A	229 \pm 15 (3)	116
C765A	258 \pm 10 (3)	130
C793A	122 \pm 6 (4)	62
Single cysteine mutants		
C754A/C765A	134 \pm 11 (5)	68
C765A/C793A	6 \pm 2 (3)	3
C754A/C793A	99 \pm 26 (2)	50
Cys-less mutant		
C754A/C765A/C793A	94 \pm 31 (2)	47

9.5.1.3 Comparison of cAMP and GTP-Eu results

GTP-Eu binding in general complements the results observed with the cAMP assays. C754^{5.46}A and C765^{5.57}A which have maximal inhibition of cAMP levels (beyond those

observed with the WT) also show elevated levels of GTP-Eu binding. C754^{5.46}A/C765^{5.57}A which has similar activity as WT in cAMP assays shows less GTP-Eu binding compared to WT, suggesting that this mutant probably is not as active as WT. cAMP assay measures cAMP levels in cells which is a downstream amplified response and may therefore might not be as sensitive to receptor defects as the GTP-Eu assay. Furthermore, the cAMP assay can be affected by processes such as regulation of activation, internalization, degradation, and desensitization in cell based cAMP assay (Kim et al., 2005). All the mutants with the C793^{6.45}A mutation have no activity in cAMP assays and similarly show drastically reduced levels of GTP-Eu binding. The strongest reduction was observed for C765^{5.57}A/C793^{6.45}A, which has binding levels similar to negative controls (membranes prepared from uninduced cells). These results show that C754^{5.46} and C765^{5.57} on TM5 result in slightly increased activity, while C793^{6.45} in the middle of the TM6 results in loss of activity suggesting that all three cysteines play a role in receptor activation in cells.

9.5.2 Antagonist response (cAMP formation in cells)

Next, we evaluated the response of double, single and cys-less mutants to LY341495 (10 μ M) alone and in the presence of L-AP4 (100 μ M) in induced and uninduced cells (Figure 9.5 and Table 9.4). LY341495 is a potent agonist at group II mGluRs with reported antagonism at mGluRs6. Antagonists (neutral) when added alone do not alter the cAMP levels in cells in FK stimulation. The function of antagonist is usually measured as a competition assay in presence of agonist where antagonist decreases ('antagonizes') agonist response. Hence we carried out cAMP assays with LY341495 in presence and absence of L-AP4.

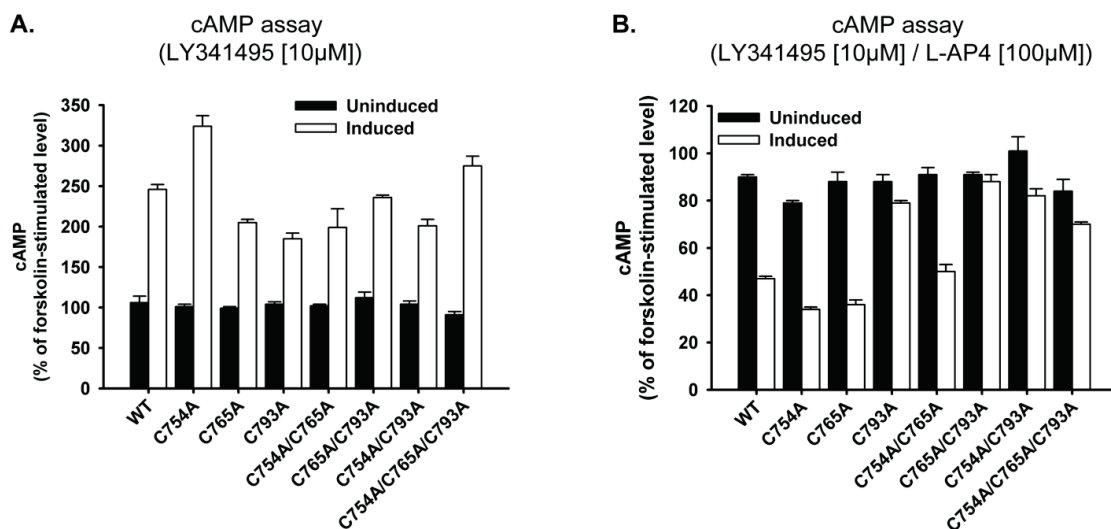


Figure 9.6 Effect of LY341495 on the activity of WT and cysteine mutants of mGluR6

(A) In presence of LY341495 (10µM) there is increased levels of cAMP accumulation in induced (open bars) compared to uninduced (filled bars) cells. (B) The effect of LY341495 (10µM) is reversed on addition of L-AP4 (100µM). LY341495 seems to act as an inverse agonist which can be competed out by adding excess L-AP4. Data for C754^{5.46}A/C765^{5.57}A mutant is average of stable cell line clones #2.1 and #1.6 (see Table 9.4).

Like WT, both C754^{5.46}A and C793^{6.45}A demonstrate enhanced cAMP levels in the presence of LY341495 (324 ± 13 % and 205 ± 4 % of FK stimulated levels, respectively) which were reversed in the presence of L-AP4 (34 ± 1 % and 36 ± 2 % of FK stimulated levels, respectively). The double cysteine mutant C793^{6.45}A has no response to L-AP4 but shows response to LY341495 (185 ± 7 %), although at lower levels than that of wild-type. LY341495 responses are abolished (79 ± 1 %) in the presence of L-AP4 for the C793^{6.45}A mutant. Among single cysteine mutants, only C754^{5.46}A/C765^{5.57}A displays a WT-like response to LY341495 (199 ± 23 %) and L-AP4/LY341495 (50 ± 3 %). The remaining two single cysteine mutants and the cys-less mutant shared activity profiles similar to C793^{6.45}A mutant; there was positive response to LY341495 which was reversed upon L-AP4 addition. LY341495 exhibited inverse agonism both at wild-type and cysteine mutants. It is possible that the cysteine mutants,

especially those involving C793^{6,45}A do not affect conformation changes triggered by the binding of inverse agonist.

Table 9.4 L-AP4 and LY341495 induced response for WT and cysteine mutants (cAMP formation)

Data for C754^{5,46}A/C765^{5,57}A mutant is average of stable cell line clones #2.1 and #1.6 whose individual values are reported in the sub-table below. Data is represented as mean \pm SEM (number of independent experiments)

Receptor construct	cAMP formation (% of forskolin stimulated cAMP levels)					
	L-AP4 [10 μ M]		LY341495 [10 μ M]		LY341495 [10 μ M] / L-AP4 [100 μ M]	
	Induced	Uninduced	Induced	Uninduced	Induced	Uninduced
Wild type	54 \pm 3 (7)	77 \pm 7 (2)	246 \pm 6 (4)	106 \pm 8 (3)	47 \pm 1 (3)	90 \pm 1 (3)
Double cysteine mutants						
C754A	38 \pm 1 (5)	91 \pm 4 (3)	324 \pm 13 (3)	101 \pm 3 (3)	34 \pm 1 (3)	79 \pm 1 (3)
C765A	37 \pm 2 (5)	95 \pm 3 (3)	205 \pm 4 (3)	99 \pm 2 (3)	36 \pm 2 (3)	88 \pm 4 (3)
C793A	107 \pm 6 (5)	103 \pm 3 (3)	185 \pm 7 (3)	104 \pm 3 (3)	79 \pm 1 (3)	88 \pm 3 (3)
Single cysteine mutants						
C754A/C765A*	52 \pm 5 (6)	83 \pm 3 (8)	199 \pm 23 (6)	102 \pm 2 (6)	50 \pm 3 (6)	91 \pm 3 (6)
C765A/C793A	108 \pm 6 (2)	83 \pm 3 (3)	236 \pm 3 (3)	112 \pm 7 (3)	88 \pm 3 (3)	91 \pm 1 (3)
C754A/C793A	80 \pm 3 (4)	98 \pm 3 (3)	201 \pm 8 (3)	104 \pm 4 (3)	82 \pm 3 (3)	101 \pm 6 (3)
Cys-less mutant						
C754A/C765A/C793A	79 \pm 3 (5)	87 \pm 5 (4)	275 \pm 12 (3)	91 \pm 4 (3)	70 \pm 1 (3)	84 \pm 5 (3)
* Data for individual clones of C754A/C765A mutant						
C754A/C765A #2.1	59 \pm 3 (4)	80 \pm 3 (6)	250 \pm 3 (3)	101 \pm 1 (3)	56 \pm 1 (3)	87 \pm 3 (3)
C754A/C765A #1.6	36 \pm 5 (2)	94 \pm 1 (2)	147 \pm 9 (3)	103 \pm 5 (3)	44 \pm 1 (3)	95 \pm 3 (3)

9.5.3 Allosteric ligands

The TM cysteines in mGluR6 are present on TM5 and TM6 in the vicinity of the allosteric binding pocket (Figure 9.3). PHCCC is a known allosteric ligand at mGluR4 (Beqollari and Kammermeier, 2008). In chapter 7, I predicted that PHCCC binds to the TM region of mGluR6 (section 7.4.2) and showed experimental evidence that PHCCC acts as a direct inverse agonist (see section 7.5.1 and Table 9.5) at wild-type mGluR6. I performed cAMP assays to see if

double cysteine mutants had any effect on the inverse agonism of PHCCC. The double cysteine mutants showed slightly higher levels of cAMP compared to uninduced cells, but it was difficult to arrive at conclusions as the standard error was large (Table 9.5). The problem working with PHCCC was insolubility of the compound in aqueous buffers. The large standard errors were probably a result of insolubility issues.

Table 9.5 Effect of PHCCC on WT and double cysteine mutants activity (cAMP assay)

Data is represented as mean \pm SEM (number of independent experiments)

Construct	L-AP4 (10uM)		PHCCC (50uM)		PHCCC (50uM) / L-AP4 (10uM)	
	Induced	Uninduced	Induced	Uninduced	Induced	Uninduced
WT	54 \pm 3 (7)	77 \pm 7 (2)	142 \pm 18 (3)	No effect at 100uM	56 \pm 6 (3)	
C754A	38 \pm 1 (5)	91 \pm 4 (3)	104 \pm 24 (2)		39 \pm 2 (2)	
C765A	37 \pm 2 (5)	95 \pm 3 (3)	115 \pm 28 (2)		47 \pm 3 (2)	
C793A	107 \pm 6 (5)	103 \pm 3 (3)	123 \pm 13 (2)		127 \pm 25 (2)	

9.6 CONCLUSIONS: CONTRIBUTION OF CYSTEINES IN ACTIVATION OF MGLUR6

The comparative sequence alignment of TM5 and TM6 regions of mGluR6, rhodopsin, mGluR1 and mGluR5 (Figure 9.3) shows that residues C754^{5.46} and C793^{6.45} are adjacent to critical residues that are part of the ligand binding pocket in the TM. The analogous residue for C765^{5.57} is also cysteine (C222^{5.57}) in rhodopsin. Meta II studies of the C222^{5.57}S mutation in rhodopsin showed no effect on the decay rate compared to WT rhodopsin (Isin et al., 2006). T764^{5.58} in mGluR8, which is adjacent to C763^{5.57} (analogous residue to C765^{5.57} in mGluR6), was

extensively mutated (Yanagawa et al., 2009). The 19 point mutations at T764^{5.58} resulted in low expression of protein except for T764^{5.58}W and T764^{5.58}A. All mutant proteins displayed increased basal activity, with T764^{5.58}W losing response to agonist while T764^{5.58}A did not. Loss of agonist response in T764^{5.58}W was rescued by Y663^{3.40}A point mutation in TM3, suggesting that TM3 and TM5 interactions are important in maintaining the inactive state of the receptor.

The analogous residue to C754^{5.46} in rhodopsin is H211^{5.46}. H211^{5.46} is part of the TM3 and TM5 interaction in the inactive state that is broken on activation (Patel et al., 2005). The analogous residue of C754^{5.46} in mGluR5 is P742^{5.46}. We predicted that this residue is part of the allosteric ligand binding pocket in our earlier study (Yanamala et al., 2008) (chapter 7.0). So far, no mutational studies of analogous residues in this position have been reported for any of the mGluRs.

C793^{6.45} is part of the TM6 stretch that has important residues that are conserved across all GPCRs like W265^{6.48} in rhodopsin. The analogous residue L262^{6.45} in rhodopsin has not been studied directly. In mGluR8 the analogous residue for C793^{6.45} is C791^{6.45}, which when mutated to alanine (C791^{6.45}A) resulted in the elevation of basal activity (Yanagawa et al., 2009).

Taken together, my results provide strong evidence supporting the conclusion that C793^{6.45}A compromises agonist response. Furthermore, C754^{5.46}A and C765^{5.57}A slightly enhance activation. In rhodopsin, TM5 forms hydrogen bond interactions with TM3 (Ahuja and Smith, 2009) and it is possible that the C754^{5.46}A and C765^{5.57}A mutations in mGluR6 stabilize TM3-TM5 interactions in the activated state. On the other hand TM6 does not pack closely with any helices except at the ionic lock (Ahuja and Smith, 2009; Patel et al., 2005) and is the major moving helix in activation of rhodopsin and other GPCRs (Farrens et al., 1996; Park et al., 2008; Scheerer et al., 2008). In mGluR6, the C793^{6.45}A mutation is located in the middle of TM6 and

thus probably compromises the movements in TM6 necessary for activation. This suggests that the rotamer toggle switch of W265^{6,48} in rhodopsin known to be a key element in the activation for many GPCRs may prevail in mGluR6. Helix 6 is the most conserved helix in mGluRs and our findings strongly support the generality hypothesis that this helix plays a major role in activation of Class A and Class C GPCRs alike.

10.0 RHODOPSIN-MGLUR6 CHIMERAS

10.1 SUMMARY

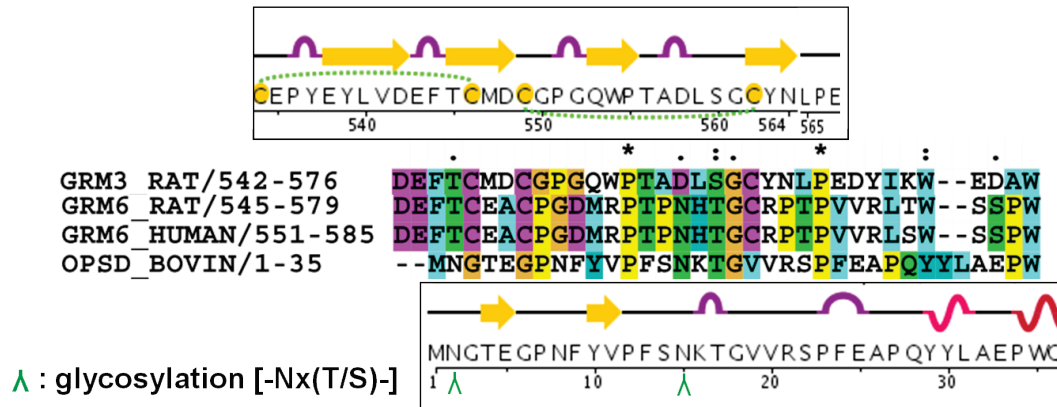
Functional assays with TM cysteine mutants of mGluR6 showed that TM6 plays a crucial role in the activation mechanism of mGluR6 (discussed in Chapter 9) in direct analogy to the role of this helix for rhodopsin. Here, I describe another approach to demonstrate the functional similarity between the TM domains of the two proteins by swapping the TM domain of mGluR6 with that of rhodopsin. Rhodopsin was chosen as the TM domain surrogate for mGluR6 because of its model system role and ease of handling such as solubilization and purification. TM ligand binding is simply investigated by absorbance spectroscopy, which also provides a simple assay for correct folding. I found that the chimeras could bind to the natural ligands of rhodopsin 11-*cis*-retinal and 9-*cis*-retinal, when added to cells during their expression. This indicates that the binding pocket of the retinal in the TM domain of the chimera is not perturbed by the presence of the ATD of mGluR6. This opens the door to future studies validating the analogy between the TM domains of rhodopsin and mGluR6.

10.2 RATIONALE AND CONSTRUCTS

Like all mGluRs, mGluR6 has three main structural domains, the ATD (~510 residues), followed by the CRD (~70 residues) and the TM (~300 residues). The TM domain is thermally unstable when removed from membrane environment. Obtaining functional mGluR6 in detergent micelles has been challenging. We propose that this limitation could be overcome by designing chimeric proteins where the TM domain of mGluR6 is switched with that of rhodopsin. Due to the well-established protocols available for purification of rhodopsin and extensive structure-function studies reported, these approaches when used with the chimeric protein would help in better understanding of mGluR6 function and would enable structure-function studies. Furthermore, such a chimera could be used to study similarities between rhodopsin and mGluR6.

Three chimeras were designed as shown in Figure 10.1. For designing these chimeras, the sequences of the C-terminal end of CRD of mGluR3 (rat) and mGluR6 (rat and human) and the N-terminal region of rhodopsin were positioned to allow alignment. These regions exhibited conservation in sequence, secondary structure and glycosylation sites (panel A, Figure 10.1). This conserved region was selected as the site of intersection of TM domain of rhodopsin and CRD of mGluR6 giving rise to three different chimeric proteins (#1, #2 and #3) with variable N-terminus lengths of rhodopsin. Experimentally, I only created chimera #2 and chimera #3 and verified the expression and possible retinal binding of these constructs. Chimera #2 contains mGluR6 fragment from 1 – 555 amino acids followed by the rhodopsin fragment from 4 – 348 amino acids (panel B, Figure 10.1). Chimera #3 contains mGluR6 fragment from 1 – 574 amino acids followed by the rhodopsin fragment from 23 – 348 amino acids (panel B, Figure 10.1). These chimeras were constructed in the pMT3 vector and were used for transient transfections in COS-1 cells as shown in chapter 2 (sections 2.1.4 and 2.2.2).

A.



B.

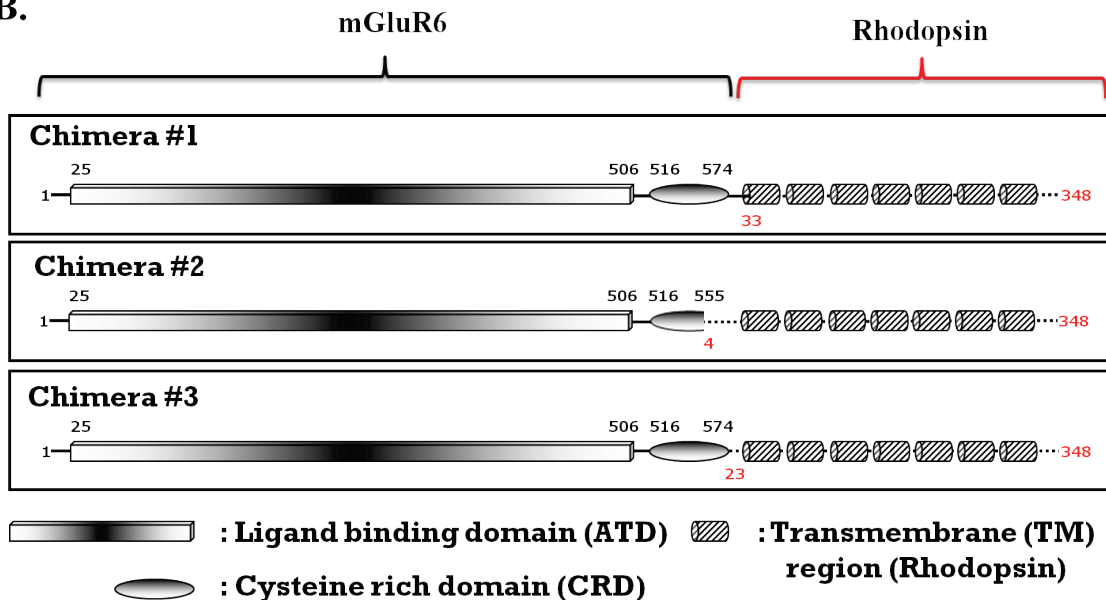


Figure 10.1 Design of mGluR6: Rhodopsin chimera

(A) Alignment of secondary structures in boxes (for mGluR3 (PDB: 2E4U) and rhodopsin (1F88)) and sequence alignment of the C-terminus end [544-567] of the cysteine rich domain (CRD) of mGluR3, mGluR6 (rat and human) with the N-terminus [1-24] of rhodopsin. As shown in the figure the C-terminus of CRD and N-terminus of rhodopsin share sequence and structure homology including glycosylation sites. (B) Domain organization of mGluR6: Rhodopsin chimeras. Residue numbering for mGluR6 and rhodopsin is in black and red font respectively. The chimeras have variable lengths of the rhodopsin N-terminus and corresponding changes at the C-terminus of CRD of mGluR6.

10.3 RETINAL BINDING

11-*cis*-retinal is the natural ligand for rhodopsin. Since the TM domain of rhodopsin is retained in the chimeras, retinal binding in the presence of ATD of mGluR6 was tested. In general for rhodopsin, cells expressing opsin, the apo form of rhodopsin, is harvested and incubated with 11-*cis*-retinal to generate rhodopsin. The extent of rhodopsin regeneration is estimated by formation of a 500nm peak in the absorption spectra (see methods section 2.7.1.1). 11-*cis*-retinal binding to chimeras was tested by adding it to the harvested cells, membrane preparations and detergent purified chimera samples. Under all these conditions there was no binding of 11-*cis* retinal to chimeras.

Based on studies involving rescue of mis-folded rhodopsin (Krebs et al., 2010), I then added retinal directly to the growth medium immediately after transfection. Instead of 11-*cis*-retinal, the less expensive analog 9-*cis*-retinal was added to the cell culture plates at a concentration of 20 μ M total, immediately (2h) and 24h after transfections. The cells were harvested 48h after transfections and were tested for retinal binding. Retinal binding was observed in rhodopsin and chimeras (Figure 10.2).

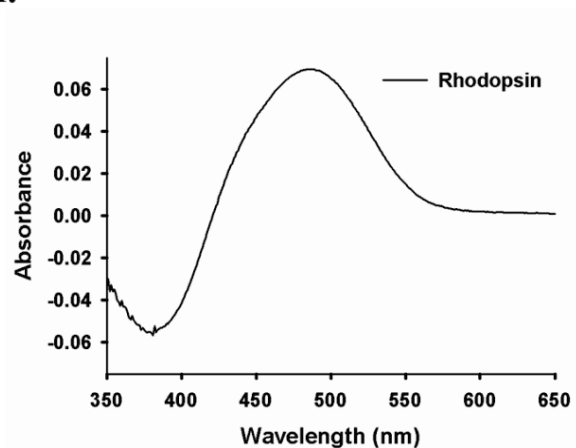
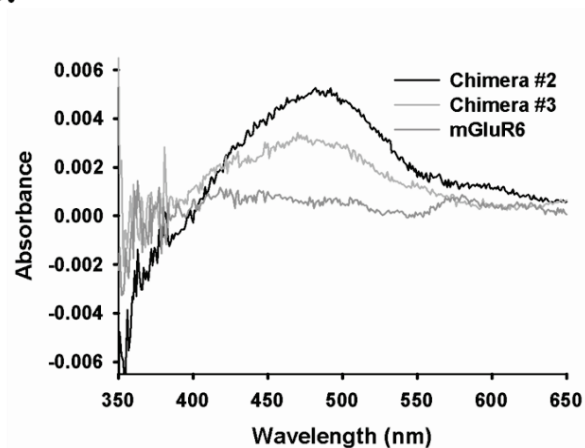
A.**B.**

Figure 10.2 Retinal binding to rhodopsin and chimera

Difference absorption spectra measured for (A) rhodopsin and (B) chimeras. *9-cis*-retinal Retinal binding is evident from the ~500nm peak. Rhodopsin and mGluR6 are included as positive and negative controls in each experiment. The yields from one 15cm plate (transiently transfected COS-1 cells with 15ug DNA per plate) as estimated from the 500nm peak are: Rhodopsin (94 μ g), Chimera #2 (16 μ g), Chimera #3 (9 μ g) and mGluR6 (0 μ g).

The amount of retinal bound protein in the chimeras was 6 – 9 fold lower compared to rhodopsin. It remains to be tested if this is due to lower expression levels or lower binding of the retinal. Within the chimeras, chimera #2 appears to form more retinal bound protein than chimera #3. The protein yields as estimated from 500nm peak are 94 μ g, 16 μ g, 9 μ g and 0 μ g for rhodopsin, Chimera #2, Chimera #3 and mGluR6, respectively.

Our finding, that rhodopsin when expressed as a fusion protein with the ATD of mGluR6 retains retinal binding ability, suggests that within the chimera the integrity of the retinal binding pocket is retained. This provides preliminary evidence for conservation of TM domain function between class A and class C GPCRs. This is a particularly exciting finding that opens the door to further studies aimed at finding out if there are any contacts formed between the ATD and the TM domains and if yes, if there is communication possible across the interface.

11.0 IDENTIFICATION OF ALLOSTERIC COUPLING SITES IN GPCRS

11.1 SUMMARY

G protein coupled receptors (GPCRs) are membrane proteins that function as signal transducers. GPCRs are characterized by a seven helical transmembrane domain (TM), an extracellular domain (EC) and an intracellular domain (IC). Binding of different ligands in the EC or TM regions triggers conformational changes that propagate to the IC where it ultimately results in the activation of cognate G proteins and other signaling cascades in the cells. The relay of allosteric communication between the ligand binding site and the G protein binding site is poorly understood. Sequence analysis techniques that tease out pairs of amino acid positions that have co-evolved can be provide insight into communication in proteins. In this chapter, Generative REgularized ModeLs of proteins (GREMLIN) (Balakrishnan et al., 2010), was used to identify the allosteric network of residues involved in activation of class A GPCRs. Allosteric communication was analyzed in all seven GPCRs that have been crystallized to date. GREMLIN significantly enriched the edges containing residues that are part of the ligand binding pocket when compared to a control distribution of edges drawn from a random graph. The fold enrichment across receptors was comparable, suggesting a common set of residues in the binding pockets. A minimal binding pocket with four residues - T118^{3.33}, M207^{5.42}, Y268^{6.51} and A292^{7.39} (residue numbering refers to bovine rhodopsin and Ballesteros-Weinstein convention in

superscript) was identified that resulted in maximal enrichment of edges across all seven GPCRs that were analyzed. A set of top 10 ranked residues - A117^{3.32}, A272^{6.55}, E113^{3.28}, H211^{5.46}, S186^{EC2}, A292^{7.39}, E122^{3.37}, G90^{2.57}, G114^{3.29} and M207^{5.42} were identified based on the number of long-range interactions they were involved in. Out of these 10 residues 9 of them are part of the retinal binding domain of rhodopsin. We also identified that 32 out of the 34 long-range interactions mediated by the top 10 residues involved residues in the retinal binding pocket. This is very much in line with our understanding that receptor activation is initiated by conformational changes in the disruption of the immediate vicinity of the retinal after isomerization. Several of the residues from these long-range couplings are part of experimentally determined ‘microdomains’ and ‘activation switches’ in rhodopsin. Furthermore on mapping these statistically significant long-range interactions onto rhodopsin, we find that ligand binding domain mediates the interactions between extracellular and intracellular residues, a novel finding just based on sequence analysis alone using GREMLIN.

Moreover, the top 10 ranked residues identified in class A GPCRs are shown to be involved in long-range interactions significantly overlap with the allosteric ligand binding pocket of mGluRs. This finding further supports the hypothesis that the activation mechanism is conserved between class A (rhodopsin) and class C (mGluRs) GPCRs.

This work was done in collaboration with Subhodeep Moitra.

11.2 IMPORTANCE OF ALLOSTERIC COMMUNICATION

In GPCRs, the binding of ligand in the EC or TM domain causes a signal to be propagated to the IC domain wherein different effectors such as the G protein heterotrimer, GPCR receptor kinases

(GRK) and β -arrestin bind. The activation of rhodopsin and other class A GPCRs is thought to be conserved because of the existence of structural microdomains (Ballesteros et al., 2001b). Conformational changes of multiple ‘switches’ in tandem activate the receptor (Ahuja and Smith, 2009). These long-range interactions between distant residues are not only within soluble (EC, IC) and membrane (TM) portions but also between soluble and membrane portions. Such changes are important for the function of receptors and are also closely involved in folding and structural stability (Klein-Seetharaman, 2005; Rader et al., 2004). Identifying the residues involved in the propagation of signals within the protein is important to understand mechanism of activation and specificity of ligand recognition. While much information can be directly extracted from crystal structures, allosteric interactions are dynamic and implicit in nature and thus are not directly observable in static crystal structures. Experimental methods for investigating dynamics, such as nuclear magnetic resonance, are presently incapable of resolving allosteric interactions in large membrane proteins, such as GPCRs.

To reveal this allosteric communication between residues in the proteins computational and statistical sequence analysis tools such as Hidden Markov Models (HMMs) (Finn et al., 2010), Statistical Coupling Analysis (SCA) (Lockless and Ranganathan, 1999; Suel et al., 2003), Explicit Likelihood of Subset Co-variation (ELSC) (Dekker et al., 2004), Graphical Models for Residue Coupling (GMRC) (Thomas et al., 2008) and Generative REGularized ModeLS of proteins (GREMLIN) (Balakrishnan et al., 2010) are employed.

The basic notion on which these approaches are based is that amino acid sites in the protein that are communicating with each other will be evolutionarily constrained and co-evolve with each other (Marcotte et al., 1999; Suel et al., 2003). These co-evolving sites can be identified as statistical couplings from the sequence data. A common practice is to use a multiple

sequence alignment (MSA) to align a family of protein sequences according to some global optimization criteria (Chenna et al., 2003) in order to calculate sequence statistics. A variety of methods try to characterize the properties of a protein family given an MSA of the protein family. Each method tries to learn a model that describes the constraints governing a protein family either implicitly through the parameters of the model, or explicitly by enumerating the observed statistical couplings.

I will discuss two of these methods SCA (Suel et al., 2003) and GMRC (Thomas et al., 2008). The class A GPCR multiple sequence alignment (MSA) generated by (Suel et al., 2003) in SCA studies was also used in GMRC (Thomas et al., 2008) studies and by us for analysis with GREMLIN.

11.3 PRIOR WORK IN GPCR RESIDUE COUPLING ANALYSIS

11.3.1 Statistical Coupling Analysis (SCA)

Ranganathan and colleagues (Lockless and Ranganathan, 1999; Suel et al., 2003) developed a correlated mutation method - Statistical Coupling Analysis (SCA) for finding allosteric couplings among residues from the multiple sequence alignment (MSA). This method calculates a variant of the mutual information (MI) score for pairs of columns in the MSA. In a sufficiently large MSA with diverse sequences, amino acid frequencies at a specific site would represent their background distribution in all proteins unless there is some evolutionary constraint at that position that dictates the function or folding of the protein. The extent of deviation from the background distributions can be quantified providing a measure of conservation at that site. If

two such sites are functionally coupled, then choosing a subset of sequences from the MSA such that it alters the amino acid distribution at one site would also result in the alteration of distribution of amino acids at the coupled site, which can be measured as a statistical coupling energy.

The authors who conducted the SCA study (Suel et al., 2003) obtained the class A GPCR alignment from the GPCRDB (Horn et al., 1998) and TinyGRAP (Beukers et al., 1999) databases and manually adjusted the sequences using structure-based sequence alignments. The final MSA has 940 sequences and 348 residue positions covering the entire length of bovine rhodopsin without any gaps (Figure 11.1).

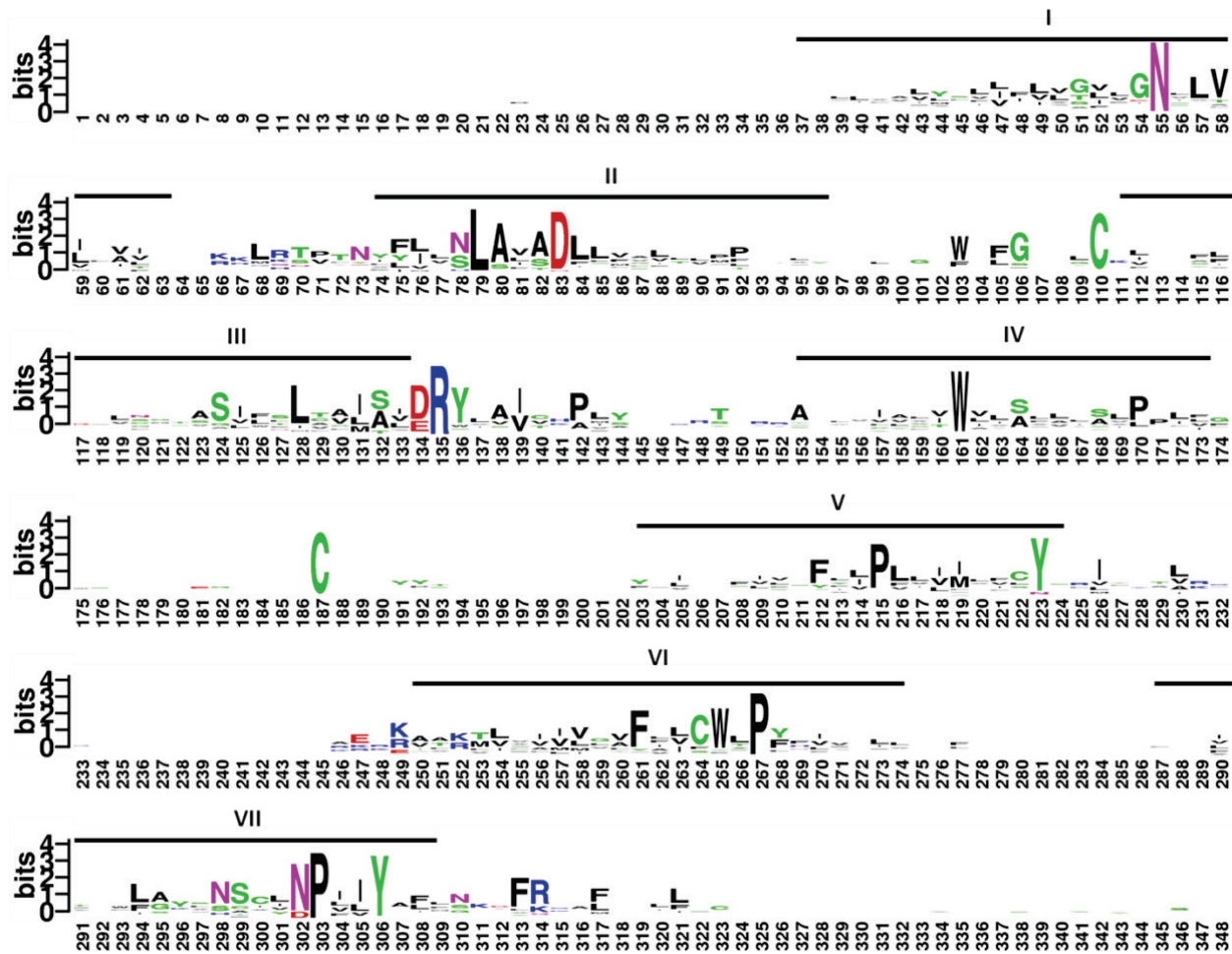


Figure 11.1 Multiple sequence alignment of class A GPCRs

For easy visualization the logo of the MSA alignment is generated using Weblogo (<http://weblogo.berkeley.edu>). The amino acids numbering is based on the positions of bovine opsin (NCBI Reference Sequence: NP_001014890.1). The individual letter height of amino acid(s) at each position indicates their relative frequencies and conservation in the alignment. The TM helices are indicated as lines above the sequence. Most of the conserved regions are restricted to TM regions.

The authors focused on a critical residue at position 296 corresponding to a lysine (K296) in bovine rhodopsin which is involved in direct ligand interaction (Ballesteros et al., 2001b;

Gether, 2000). Three classes of residues were found to be statistically coupled to K296. The three classes and corresponding residues are:

- **Immediate neighbors:** F293, L294, A295, A299, F91, E113
- **Linked network:** F261, W265, Y268, F212
- **Sparse but contiguous network:** G121, I123, L125, I219, F261, S298, A299, N302

These categories were formulated on mapping the residues onto the rhodopsin structure. Residues in the immediate neighbor category are in the vicinity of K296 and are mainly involved in helix packing interactions except for E113. E113 forms a salt bridge interaction with the protonated Schiff base. The linked network residues are parallel to the plasma membrane and form an aromatic cluster around the β -ionone ring of retinal in rhodopsin. The residues in the sparse but contiguous network are distant from 296 and form helix packing interactions toward the IC side. There are critical residues including N302 which is part of the NPxxY motif. Over 14% of all residues and 22% of residues buried in the core of rhodopsin are coupled to K296. The authors qualitatively propose that there is signal flow from the ligand binding pocket to the G protein coupling site through these networks.

11.3.2 Graphical Models for Residue Coupling (GMRC)

Bailey-Kellogg and colleagues developed a method called GMRC (Thomas et al., 2008), which employs a Markov random field (MRF) for learning a graphical model for a family of protein sequences. This method uses conditional mutual information metric for defining the strength of the correlations and provides a probabilistic basis for sequence covariation. This method allows

for distinguishing between coupling and conservation of a particular site. Moreover it can identify residues that are conserved only in a sub-class within the given MSA.

The authors in GMRC study (Thomas et al., 2008) assigned the MSA from (Suel et al., 2003) (see 11.3.1) into different sub-classes based on the ligand binding data. A total of 16 subclasses were defined of which the amine (196 sequences), peptide (333 sequences) and rhodopsin (143 sequences) represent the bulk of the sequences. The authors in this study identified the pairs L57 – A82, F313 – R314, I305 – Y306, N302 – I304 and C264 – S299 as the most significant couplings for the combined amine, peptide and rhodopsin sub-classes.

11.4 GREMLIN RESULTS

11.4.1 General observation

We took a sequence based approach, GREMLIN (Balakrishnan et al., 2010), to examine statistical couplings between amino acids in a protein. The methodology is described in chapter 2 (section 2.8.6.1). In brief, this is a graphical model similar to GMRC but uses a L1-regularized structure learning approach to determine the structure of a Markov random field (MRF). Unlike SCA and GMRC, GREMLIN does not use any mutual information but instead formulates a convex optimization problem which is guaranteed to learn the optimal model on convergence. This is a generative model that allows for both sampling and classification tasks for any new sequence, though our focus here is mainly on the results from the structure learning task. The topology of our graphical model provides information about the network of interacting residues and can distinguish between direct and indirect couplings.

We used the same MSA from (Suel et al., 2003) (see 11.3.1) to gain insight into the correlated mutations in class A GPCRs. In our models an edge penalty of 38 or higher gives statistically significant couplings (see section 2.8.6.1). We used bovine rhodopsin as template to evaluate the edges (couplings) and used the PDB structure 1U19 (Okada et al., 2004) to map these edges. Our preliminary observations (at penalty 38) indicated that many edges involved residues in the ligand (retinal; RT) binding pocket (extracted from rhodopsin structure 1F88) as compared to those edges between or within the residues belonging to extracellular EC, IC and TM domains (Figure 11.2).

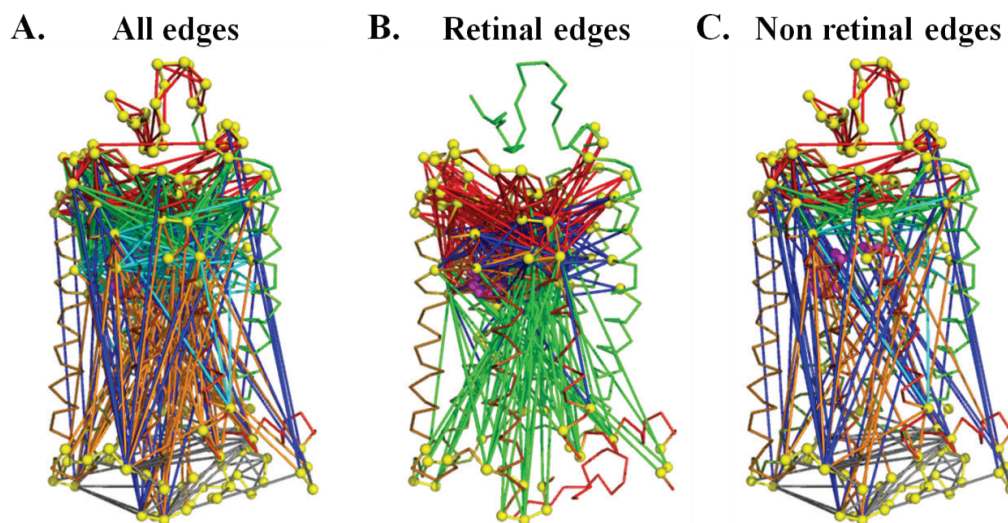


Figure 11.2 Distribution of GREMLIN edges between different domains

Mapping of (A) all (B) retinal and (C) non retinal edges identified by GREMLIN (at edge cutoff penalty 38) mapped onto the bovine rhodopsin structure (1U19). The edges are **EC-EC** (red), **EC-TM** (green), **EC-IC** (blue), **TM-TM** (cyan), **IC-TM** (orange), **IC-IC** (grey), **EC-RT** (red), **RT-TM** (blue), **IC-RT** (green) and **RT-RT** (orange) where EC, IC, TM and RT represent residues in extracellular, intracellular, transmembrane and retinal (ligand binding) domains.

11.4.2 Enumeration of domain edges

To quantify the observation that there appear to be differences in the number of edges connecting different domains (EC, IC, TM and RT), we enumerated the GREMLIN edges and compared them to the control set, which included all possible edges (a total of 60378 edges) involving all the 348 amino acids in rhodopsin. The results are summarized in Table 11.1. We find that there is a significant enrichment of edges involving retinal residues compared to the null distribution or control set (46.48% for GREMLIN versus 13.87% for control; p-value of ~ 0). Similar enrichment was observed in the relative distributions of EC-EC (23.8% for GREMLIN versus 6.78% for control; p-value of ~ 0) and IC-IC (14.93% versus 7.24%, p-value ~ 0). There was significant under representation of edges in EC-IC (7.89% versus 14.17%, p-value ~ 0), EC-TM (21.55% versus 24.57%, p-value ~ 0.026) and IC-TM (11.41% versus 25.38%, p-value ~ 0). There was no significant difference in TM-TM contacts (20.42% versus 21.87%, p-value ~ 0.16). These results are statistically significant at a significance level of $\alpha = 0.05$.

Table 11.1 Comparison of edge distribution from null set (control) and GREMLIN

Categories	Null Distribution (Control set)		GREMLIN (at penalty 38)		GREMLIN > Null	GREMLIN < Null
	Total edges	% of edges	Total edges	% of edges	p value	p value
EC-EC	4095	6.78	169	23.80	0	1
EC-TM	14833	24.57	153	21.55	0.97	0.03
EC-IC	8554	14.17	56	7.89	1	0
TM-TM	13203	21.87	145	20.42	0.84	0.16
IC-TM	15322	25.38	81	11.41	1	0
IC-IC	4371	7.24	106	14.93	0	1
TOTAL	60378	100.00	710	100.00		
EC-RT	2125	3.52	114	16.06	0	1
RT-TM	3600	5.96	98	13.80	0	1
IC-RT	2350	3.89	67	9.44	0	1
RT-RT	300	0.50	51	7.18	0	1
SUB-TOTAL	8375	13.87	330	46.48		

The finding that there is significant enrichment in the EC-EC and IC-IC contacts and that there is an under-representation of EC-IC domain contacts is biologically meaningful, because EC-IC interactions would be mediated via the TM domain, structurally. Interestingly, there is a lack of significant enrichment of edges within the TM domain and a slight under-representation of EC-TM and TM-IC edges. A lack of TM enrichment is in line with the general view of the TM helices as rigid bodies in the GPCR field (Altenbach et al., 2008; Farrens et al., 1996; Sakmar et al., 2002) and supported by the recent GPCR structures (see section 1.2.4). GPCR structures are stabilized in the membrane through backbone hydrogen bonds. The primary evolutionary pressure in the TM region is to ensure that hydrophobic residues face the lipid bilayer. However, it was puzzling that EC-TM and TM-IC contacts are under-represented since we would expect to find long-range couplings between EC and IC domains to be mediated via the intermediate TM domain. We therefore hypothesized that the EC-IC long-range contacts are more specifically mediated through a subset of TM residues in RT. Indeed, 20 residues out of 27 in the RT pocket are in TM regions. We therefore analyzed the edges involving RT binding pocket residues in more detail.

11.4.3 Long-range couplings involving the ligand binding pockets

The RT edges were further classified into EC-RT, RT-TM, IC-RT and RT-RT groups and were compared with similar distributions with the control set. There is significant enrichment in EC-RT, RT-IC and all other groups compared to the control set (see Table 11.1). These findings also suggest that the EC-IC long-range couplings are probably mediated via RT. This is in line with our current understanding of rhodopsin activation, as the initial conformational changes triggered

on activation of the receptor are in the ligand binding domain which is ultimately propagated to the IC domain.

As described in experimental methods (section 2.8.6.3) we defined a common binding pocket for each GPCR with known structure: bovine rhodopsin (BR), squid rhodopsin (SR), turkey β_1 adrenergic receptor (β_1 AR), human β_2 adrenergic receptor (β_2 AR), human A_{2A} adenosine receptor (A2A), human chemokine receptor CXCR4 and human dopamine D3 receptor (D3R). Additionally, two more binding pockets for CXCR4 were defined: CXCR4-pep and CXCR4-c to distinguish between peptide bound and small molecule bound pockets respectively, as the peptide binding pocket is considerably large (39 residues versus 18; Figure 11.4). We compared the percentage of edges formed by the residues in these pockets to that of the null distribution and against each other. The percent of edges involving binding pocket residues for the null set decreased linearly from 21% to 8% with decreasing number of residues in the pocket, i.e. pocket size (Figure 11.3). The percentage of edges for the receptor binding pockets plateaus between 47% - 51% independent of pocket size except for CXCR4-c and A2A, which had lower values of 31% and 20% respectively (Figure 11.3). The fold enrichment of edges for receptor binding pockets over the null set varied between 2.4 to 3.8.

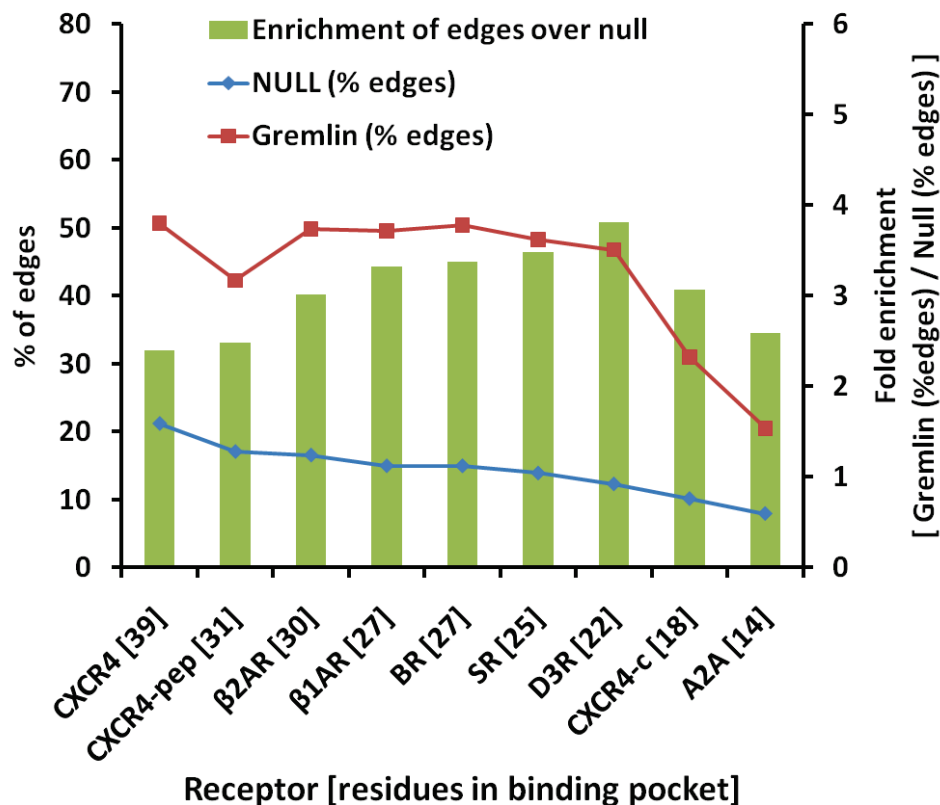


Figure 11.3 Edge distributions in the common ligand binding pockets (GREMLIN vs. null set)

The percentage of edges for GREMLIN (squares) and null set (diamonds) are plotted against the common ligand binding pockets sorted by their size. The bars indicate fold enrichment (values on secondary y-axis) of edges in GREMLIN over the null set.

Thus, GREMLIN significantly enriches edges containing ligand binding pocket residues compared to null distribution set. Importantly, the plateau observed in the percentage of edges for CXCR4, β2AR, β1AR, BR, SR and D3R suggests that there is a conserved ligand binding pocket shared between these receptors. The lower percentage of edges for CXCR4-c and A2A suggest that their binding pockets are possible outliers. Upon closer inspection, we find that the small molecule ligands IT1t and ZM241385 in CXCR4 and A2A, respectively, bind more towards the EC side compared to the position of ligands of other GPCRs (Figure 11.4) in the binding pocket. Additionally, the ligand in A2A (ZM241385) and CXCR4-c (IT1t) are parallel to

the TM helical bundle unlike ligands in other receptors in which are relatively perpendicular in orientation to TM. Nonetheless, both ligands still share a set of residue contacts. These findings suggest that there is a minimal binding pocket common to all GPCRs crystallized to date.

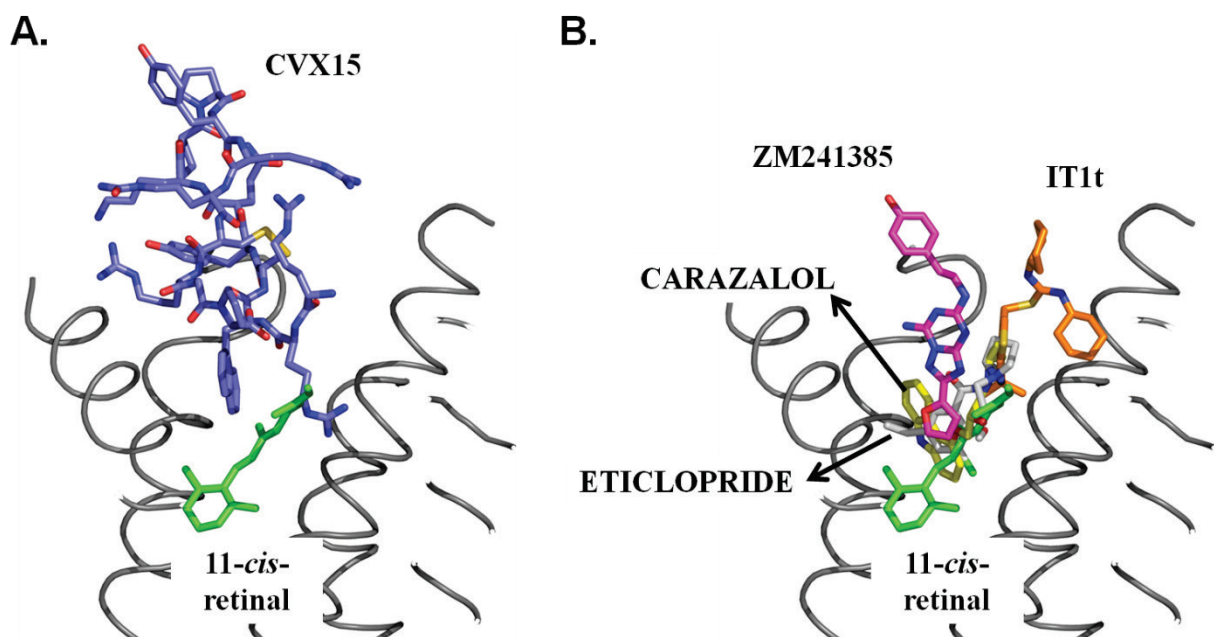


Figure 11.4 Peptide (CVX15) and different small molecule ligand-binding mapped onto rhodopsin

Ligands from other GPCRs are mapped onto rhodopsin by structure alignment. The alignment and images were generated using PyMOL (Version 0.99rc6; <http://pymol.org/pymol>). For clarity loop regions and parts of TM regions of rhodopsin (in grey; PDB id 1U19) are not shown in the images, the bound retinal is in green. (A) Comparison of the ligand-binding modes for CVX15 (blue) with retinal (green). CVX15 is a large molecule extending beyond the EC domain. (B) The small-molecule ligand-binding modes IT1t (for CXCR4; in orange), ZM241385 (for A2A; in magenta), carazolol (for β 2AR; in yellow) and eticlopride (for D3R; white) as mapped on to rhodopsin. ZM241385 and IT1t are binding modes do not overlap significantly with retinal and other ligands. The PDB is used in the images are 3OE0 (for peptide bound CXCR4), 3ODU (for IT1t bound CXCR4), 3EML (for A2A), 2RH1 (for β 2AR) and 3PBL (for D3R).

11.4.4 A minimal ligand binding pocket

We hypothesized that if there is a minimal binding pocket common to the seven known GPCRs, then GREMLIN would significantly enrich the percentage edges for this pocket of residues compared to the null distribution set. To test this hypothesis we first defined (section 2.8.6.3) ligand binding pockets B1, B2, B3, B4, B5, B6 and B7 representing residues common to at least one, two, three, four, five, six and seven receptor ligand binding pockets, respectively. We compared the percentage of edges formed by the residues in these pockets to that of the null distribution set and against each other. The percent edges for the null set decreased linearly from 32% to 2% with decreasing pocket size (Figure 11.5). The percentage edges over the same range for GREMLIN decreased 69% to 10% as expected because of the decreasing pocket size (Figure 11.5). But interestingly, the fold enrichment of edges for GREMLIN over null set increased from 2.2 – 5.2 for pockets B1 – B6. The fold enrichment for B7 slightly decreased to 4.3 (Figure 11.5) which is expected given that the pocket is small with only 4 residues (T118^{3.33}, M207^{5.42}, Y268^{6.51} and A292^{7.39}).

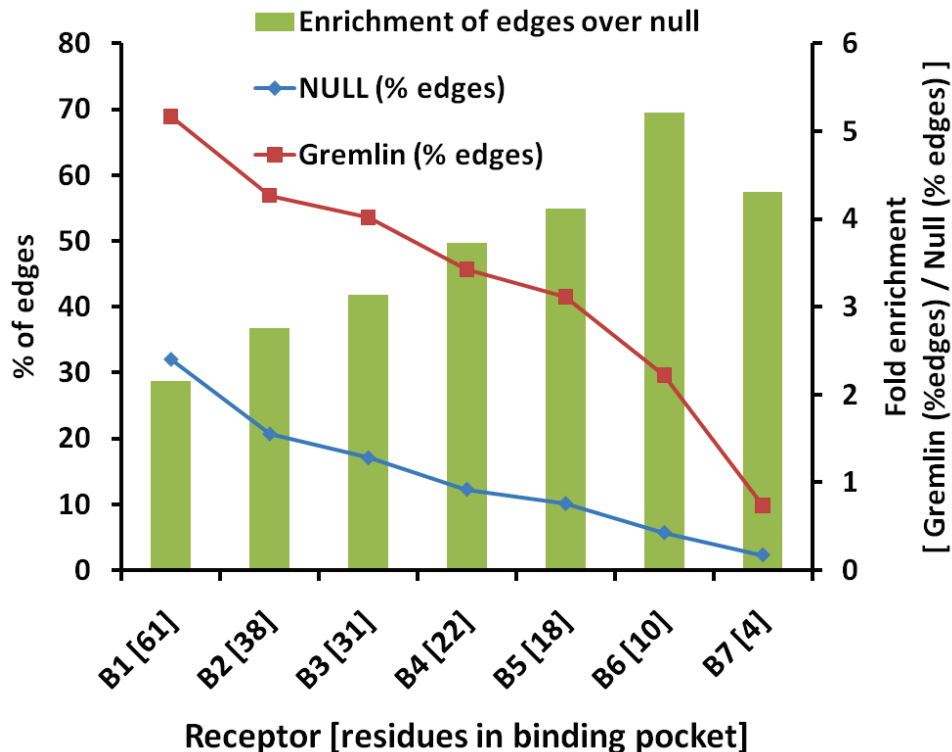


Figure 11.5 Edge distributions in the minimal ligand binding pockets (GREMLIN vs. null set)

The percentage of edges for GREMLIN (squares) and null set (diamonds) are plotted against the minimal ligand binding pockets sorted by their size. The bars indicate fold enrichment (values on secondary y-axis) of edges in GREMLIN over the null set.

The four residues in B7 (T118^{3.33}, M207^{5.42}, Y268^{6.51} and A292^{7.39}) are uniquely positioned around the ligand (retinal in rhodopsin; Figure 11.6). These residues make key interactions that stabilize the retinal (Okada et al., 2004; Palczewski et al., 2000). On the other hand, the B7 pocket has the maximum enrichment of GREMLIN edges over the control null set. There are 6 additional residues in B6 (total 10 residues; E113^{3.28}, G114^{3.29}, A117^{3.32}, T118^{3.33}, M207^{5.42}, W265^{6.48}, Y268^{6.51}, A269^{6.52}, A272^{6.55}, A292^{7.39}) compared to B7 that seem to make contacts with retinal towards the EC and IC side. These residues are known to stabilize ligand binding and are part of micro-domains that are involved in rhodopsin activation (Ahuja and

Smith, 2009; Ballesteros et al., 2001b; Okada et al., 2004; Palczewski et al., 2000). Thus, these results suggest that residues in B7 form the minimal GPCR pocket and the expanded set of residues in B6 represents a meaningful pocket for many GPCRs.

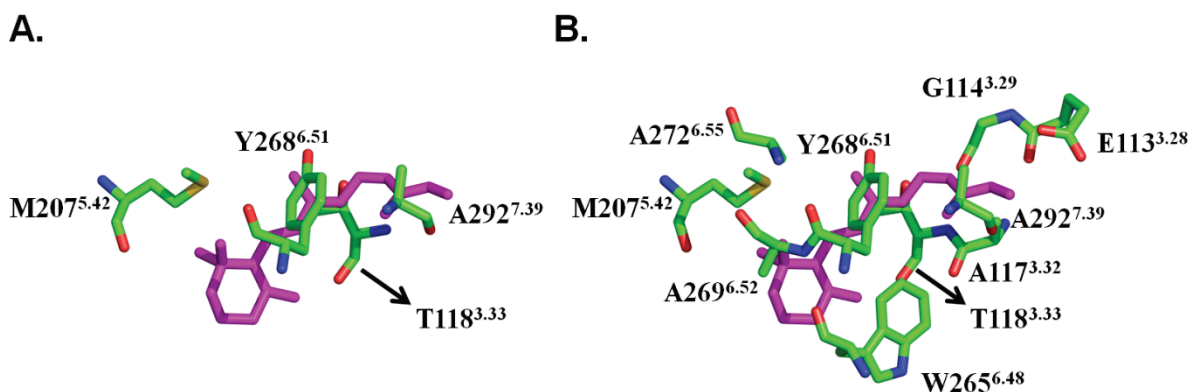


Figure 11.6 Location of minimal ligand binding pocket residues in rhodopsin structure

The spatial organization of residues in the minimal binding pocket (A) B7 and the larger pocket (B) B6 as present in the rhodopsin structure (PDB id 1U19). Rhodopsin numbering along with Ballesteros-Weinstein numbering (superscript) is given for comparison with other GPCRs. For clarity only the binding pocket residues are shown along with bound retinal (in magenta). The images were generated using PyMOL (Version 0.99rc6; <http://pymol.org/pymol>).

11.4.5 Identification of top ranked long-range interactions in rhodopsin

We enumerated the number of edges each residue was part of at penalty 38 and ranked the residues such that the-top ranked one has the highest number of edges. The highest number of edges shown in the set of top 10 residues is shown in Table 11.2. Nine of these top ten residues (A117^{3.32}, A272^{6.55}, E113^{3.28}, H211^{5.46}, S186^{EC2}, A292^{7.39}, E122^{3.37}, G90^{2.57}, G114^{3.29} and M207^{5.42}) are part of the retinal binding pocket and are involved in packing and stabilizing the

retinal (Okada et al., 2004; Palczewski et al., 2000). Of these nine residues eight are from TM regions while S186^{EC2} is from the EC region. S186^{EC2} has been shown to be involved in EC2 loop movement and its mutation to alanine alters the kinetics of activation (Ahuja et al., 2009; Yan et al., 2007). The remaining residue G90^{2.57} though not directly part of the retinal binding pocket is nonetheless an important residue. The naturally occurring mutation G90^{2.57}D in the retinal degeneration disease, retinitis pigmentosa, results in the constitutive activity of the receptor (Rao et al., 1994).

Table 11.2 List of top ranked residues and the most persistent edges.

Residues in bold are part of the retinal binding pocket extracted from the rhodopsin structure (PDB ID: 1U19). The residues which are part of the EC and the IC regions are underlined. The Ballesteros-Weinstein numbering (superscript) is given for comparison with other GPCRs. Only long-range edges are reported i.e. the edges formed with neighboring residues (8 amino acids on either side) are filtered out.

Rank	Position	Number of Edges (at penalty 38)	Most persistent pair position (edges at penalty 140)
1	A117 ^{3.32}	41	G90 ^{2.57} , E247 ^{IC3} , F293 ^{7.40} , K296 ^{7.43}
2	A272 ^{6.55}	30	L72 ^{IC1} , G114 ^{3.29} , S176 ^{EC2} , Y178 ^{EC2}
3	E113 ^{3.28}	29	M44 ^{1.39} , L72 ^{IC1} , W126 ^{3.41} , Q237 ^{IC3} , F293 ^{7.40}
4	H211 ^{5.46}	29	F91 ^{2.58} , C140 ^{IC2} , F148 ^{IC2}
5	A292 ^{7.39}	28	Y29 ^{EC (N-terminus)}
6	S186 ^{EC2}	27	K67 ^{IC1} , Q244 ^{IC3} , P291 ^{7.38}
7	E122 ^{3.37}	26	I48 ^{1.43} , G90 ^{2.57} , E196 ^{EC3} , M207 ^{5.42} , A269 ^{6.52} , F293 ^{7.40} , C316 ^{IC (C-terminus)}
8	G90 ^{2.57}	23	A117 ^{3.32} , G120 ^{3.35} , E122 ^{3.37} , M207 ^{5.42} , Q237 ^{IC3} , A269 ^{6.52} , F293 ^{7.40}
9	G114 ^{3.29}	22	S176 ^{EC2} , A272 ^{6.55} , Y178 ^{EC2}
10	M207 ^{5.42}	22	G90 ^{2.57} , E122 ^{3.37} , C316 ^{IC (C-terminus)}

We found the most persistent long-range edges (where long-range is defined to be between residues forming the edge to be separated by at least 8 amino acids in the primary

sequence) for all these residues at a very high penalty of 140 (Table 11.2). We particularly focused on long-range interactions as these are known to be critical for receptor folding and signaling (Klein-Seetharaman, 2005).

These persistent edges were then categorized based on the long-range contacts between the EC, IC and TM domains. The resulting 34 long-range contacts are shown in Table 11.3. From the categories it is evident that the long contacts are present between the domains of EC – TM, TM – IC and EC – IC with the exception of TM – TM, suggesting that inter-domain contacts are critical. On sub-categorizing the persistent edges (see Table 11.3) we find that 32 of the 34 edges involve residues in the retinal binding residues. These findings indicate that the retinal pocket is central to these long-range interactions. This is very much in line with our understanding that receptor activation is initiated by conformational changes in the disruption of the immediate vicinity of the retinal after isomerization.

Table 11.3 Persistent edges categorized based on the long-range contacts between different domains.

Categorization of edges based on the long-range contacts between the EC, IC and TM domains. The number of edges are in each category are given in the parenthesis. There are a total of 34 edges formed by top 10 ranking residues at penalty 140. There are no edges in the EC – EC and IC – IC categories. In the second column, the edges are sub-categorized to include the retinal domain. Ballesteros-Weinstein numbering (superscript) is given for comparison with other GPCRs. Only long-range edges are reported. These are edges where neighboring residues (8 amino acids on either side) are filtered out.

Edge categories [total edges]	Sub categories of edges containing RT residues [total edges]
EC – TM [7]	EC – RT [7]: A272 ^{6.55} - S176 ^{EC2} , A272 ^{6.55} - Y178 ^{EC2} , A292 ^{7.39} - Y29 ^{EC (N-terminus)} , S186 ^{EC2} - P291 ^{7.38} , E122 ^{3.37} - E196 ^{EC3} , G114 ^{3.29} - S176 ^{EC2} , G114 ^{3.29} - Y178 ^{EC2}
TM – TM [17]	G90 ^{2.57} - G120 ^{3.35} RT – TM [10]: A117 ^{3.32} - G90 ^{2.57} , E113 ^{3.28} - M44 ^{1.39} , E113 ^{3.28} - W126 ^{3.41} , H211 ^{5.46} - F91 ^{2.58} , E122 ^{3.37} - I48 ^{1.43} , E122 ^{3.37} - G90 ^{2.57} , E122 ^{3.37} - M207 ^{5.42} , G90 ^{2.57} - M207 ^{5.42} , G90 ^{2.57} - A269 ^{6.52} , G90 ^{2.57} - F293 ^{7.40} RT – RT [6]: A117 ^{3.32} - F293 ^{7.40} , A117 ^{3.32} - K296 ^{7.43} , A272 ^{6.55} - G114 ^{3.29} , E113 ^{3.28} - F293 ^{7.40} , E122 ^{3.37} - A269 ^{6.52} , E122 ^{3.37} - F293 ^{7.40}
TM – IC [8]	G90 ^{2.57} - Q237 ^{IC3} RT – IC [7]: A117 ^{3.32} - E247 ^{IC3} , A272 ^{6.55} - L72 ^{IC1} , E113 ^{3.28} - L72 ^{IC1} , H211 ^{5.46} - C140 ^{IC2} , H211 ^{5.46} - F148 ^{IC2} , E122 ^{3.37} - C316 ^{IC (C-terminus)} , M207 ^{5.42} - C316 ^{IC (C-terminus)}
EC – IC [2]	RT – IC [2]: S186 ^{EC2} - K67 ^{IC1} , S186 ^{EC2} - Q244 ^{IC3}

11.4.6 Involvement of long-range interactions in activation of rhodopsin

The retinal pocket forms a central hub for the long-range edges (see Figure 11.7) suggesting that conformational changes in the retinal pocket, as a result of activation are communicated to EC, TM and IC regions. Several of the residues and edges identified in our study are part of known ‘microdomains’ and ‘activation switches’ present in rhodopsin (Ahuja and Smith, 2009; Ballesteros et al., 2001b).

11.4.6.1 Edges involving EC and TM domain

K296^{7.43} which is part of the top persistent edge (A117^{3.32} - K296^{7.43}, only edge at penalty 280) is covalently linked to 11-*cis*-retinal through a protonated Schiff base in inactive rhodopsin and it is also a key determinant for ligand specificity in different GPCR families (Ballesteros et al., 2001b; Gether, 2000). The counter-ion of the Schiff base is E113^{3.28} (Sakmar et al., 1989) which is one of the top-ranked residues in our study. The imine moiety of the retinal Schiff base is surrounded by several amino acids of which M44^{1.39} and F293^{7.40} are identified in our edge list (Sakmar et al., 2002). The major event on light-activation is the isomerization of 11-*cis*-retinal to all-*trans*-retinal which results in the rotation of the C20 methyl group towards the EC2 loop (Nakamichi and Okada, 2006a). This rotation results in movements of the EC2 loop and rotation of the Schiff base to a more hydrophobic interior (Ahuja and Smith, 2009). The EC2 loop displacement is one of the molecular switches in rhodopsin activation (Ahuja and Smith, 2009). Three important residues on this loop S176^{EC2}, Y178^{EC2} and S186^{EC2} are identified in our study.

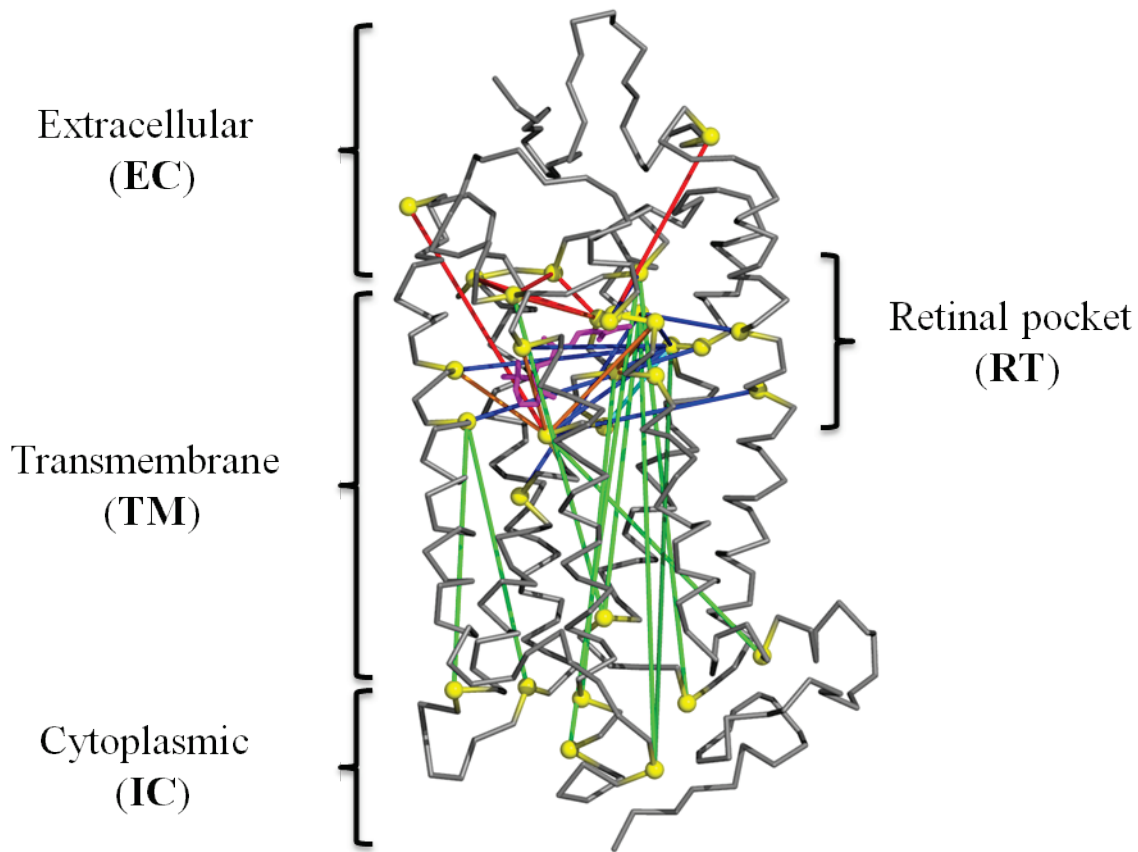


Figure 11.7 Persistent long-range contacts mapped onto structure of rhodopsin.

Persistent edges at penalty 140 for the top 10 residues (see Table 11.2) are mapped onto the rhodopsin structure (PDB id: 1U19). The residues forming the edges are represented as yellow spheres. The edges are **TM-TM** (cyan), **IC-TM** (dark green), **EC-RT** (red), **RT-TM** (blue), **IC-RT** (green) and **RT-RT** (orange), where EC, IC, TM and RT represent residues in extracellular, intracellular, transmembrane and retinal (ligand binding) domains. The images are generated using PyMOL (Version 0.99rc6; <http://pymol.org/pymol>).

Movement of EC2 is coupled to the outward rotation of the extracellular end TM5. The shift in the retinal β -ionone ring towards M207^{5.42} on TM5 results in a rearrangement of the hydrogen bonding network involving TM3 and TM5 (Ahuja and Smith, 2009). Residue H211^{5.46} interacts with E122^{3.37} and W126^{3.41} and this interaction is important for Meta II activation. Point mutation studies of these residues affect Meta II activation and stability (Lewis et al., 2006; Lin

and Sakmar, 1996). Other residues that are important for Meta II stability on TM3 and identified in our study are E113^{3.28}, G114^{3.29}, A117^{3.32}, G120^{3.35}, E122^{3.37} and W126^{3.41}. Cysteine mutations of G114^{3.29} and W126^{3.41} completely failed to bind retinal (Ou et al., 2011). E113^{3.28}C mutation bound retinal where the absorption maximum of the chromophore was shifted to 380nm instead of 500nm. Cysteine mutants of A117^{3.32}, G120^{3.35} and E122^{3.37} had altered stability of Meta II (Ou et al., 2011). Retinal isomerization also results in the rotation of W265^{6.48} (rotamer toggle switch) which along with the rearrangement of hydrogen bonding network between TM3 and TM5 results in reorientation of Y223^{5.58}, M257^{6.40} and Y268^{6.51} on TM6 (Ahuja and Smith, 2009; Patel et al., 2005). These movements ultimately result in the breaking of the conserved ionic lock involving the above discussed E/DRY motif at the cytoplasmic end (Ballesteros et al., 2001a; Park et al., 2008; Scheerer et al., 2008). Note, that R135^{3.50}, Y223^{5.58} (residues of the ionic lock) and rotamer toggle switch W265^{6.48} which is part of the CWxP motif (Shi et al., 2002) did not appear in our edge lists as GREMLIN does not pick highly conserved residues (see 2.8.6.1). For the same reason, absent from our lists are residues from the highly conserved NPxxY motif (Fritze et al., 2003) that are involved in the TM6 motions on the cytoplasmic side. However, E247^{IC3} from the ionic lock which is not highly conserved is present in our list forming an edge with A117^{3.32}. Other important residues that are present in our edge list are A269^{6.52}, A272^{6.55} on TM6 and A292^{7.39} on TM7 which are part of the retinal binding pocket (Okada et al., 2004; Palczewski et al., 2000). In addition, A269^{6.52} in rhodopsin is usually substituted by phenylalanine in other GPCRs and is considered an extension of the conserved aromatic cluster on TM6. F^{6.52} in other ligand-activated GPCRs is thought to act as ‘ligand-sensor’ and acts in concert with the CWxP motif (Weinstein, 2005).

11.4.6.2 Edges involving IC domain

Several key cytoplasmic residues (K67^{IC1}, L72^{IC1}, C140^{IC2}, F148^{IC2}, Q237^{IC3}, Q244^{IC3}, E247^{IC3}, and C316^{IC (C-terminus)}) form edges with the top ten residues that have the highest number of edges (Table 11.3). The conformational changes in the IC domain of rhodopsin have been extensively investigated by cysteine mutagenesis (Altenbach et al., 2001a; Altenbach et al., 2001b; Cai et al., 1999a; Cai et al., 1999b; Klein-Seetharaman et al., 1999). Both K67^{IC1}C and L72^{IC1}C have normal Meta II activity but K67^{IC1}C has decreased G_t activation compared to wild-type while L72^{IC1}C has no effect on activation (Klein-Seetharaman et al., 1999). Moreover, solvent accessibility studies have shown that L72^{IC1}C undergoes the largest conformational change in IC1 upon activation whereby it becomes more solvent exposed than in the dark state (Klein-Seetharaman et al., 1999). L72^{IC1} in the crystal structure of opsin makes van der Waals contacts with the G_t peptide (Scheerer et al., 2008). C140^{IC2}S shows wild-type G_t activation while F148^{IC2}C shows significantly reduced G_t activation (Farahbakhsh et al., 1995; Ridge et al., 1995). EPR studies show an increase in mobility of C140^{IC2} on photoactivation but no change in mobility is seen at F148^{IC2}C (Farahbakhsh et al., 1995; Ridge et al., 1995). E247^{IC3} is a critical residue that forms a salt bridge with the conserved ionic lock motif and undergoes major conformational changes during activation leading to the formation of the G_t binding pocket (Scheerer et al., 2008). Previous studies of mutants Q237^{IC3}C and E247^{IC3}C exhibit normal G_t activity while Q244^{IC3}C shows reduced activity indicating that Q244^{IC3}C probably interacts with G_t. Further, upon activation, Q244^{IC3}C shows a significant increase in mobility on activation while no such changes are seen for Q237^{IC3}C and E247^{IC3}C indicating that Q244^{IC3}C plays a role in activation (Altenbach et al., 1996; Yang et al., 1996). C316 in the carboxy terminus is identified as a persistent edge in our studies. EPR studies have shown previously that an increase

in mobility occurs upon activation at this site. However, no change in G_t activation was seen upon mutation of this residue to serine indicating no direct interaction with G_t (Altenbach et al., 1999; Cai et al., 1999a).

11.5 EXTENDING FINDINGS TO CLASS C GPCRS

There is significant overlap of residues which are part of persistent edges of rhodopsin and key amino acids that are shown to be critical for allosteric ligand binding in mGluR1 and mGluR5 (Figure 11.8) (Fukuda et al., 2009; Malherbe et al., 2006; Muhlemann et al., 2006; Yanamala et al., 2008). The overlap of these residues suggests that like in rhodopsin, long-range contacts are probably mediated by allosteric ligand binding domain (analogous to retinal binding domain) in mGluRs. This finding provides evidence that the activation mechanism between rhodopsin (class A GPCRs) and (class C GPCRs) is possibly conserved.

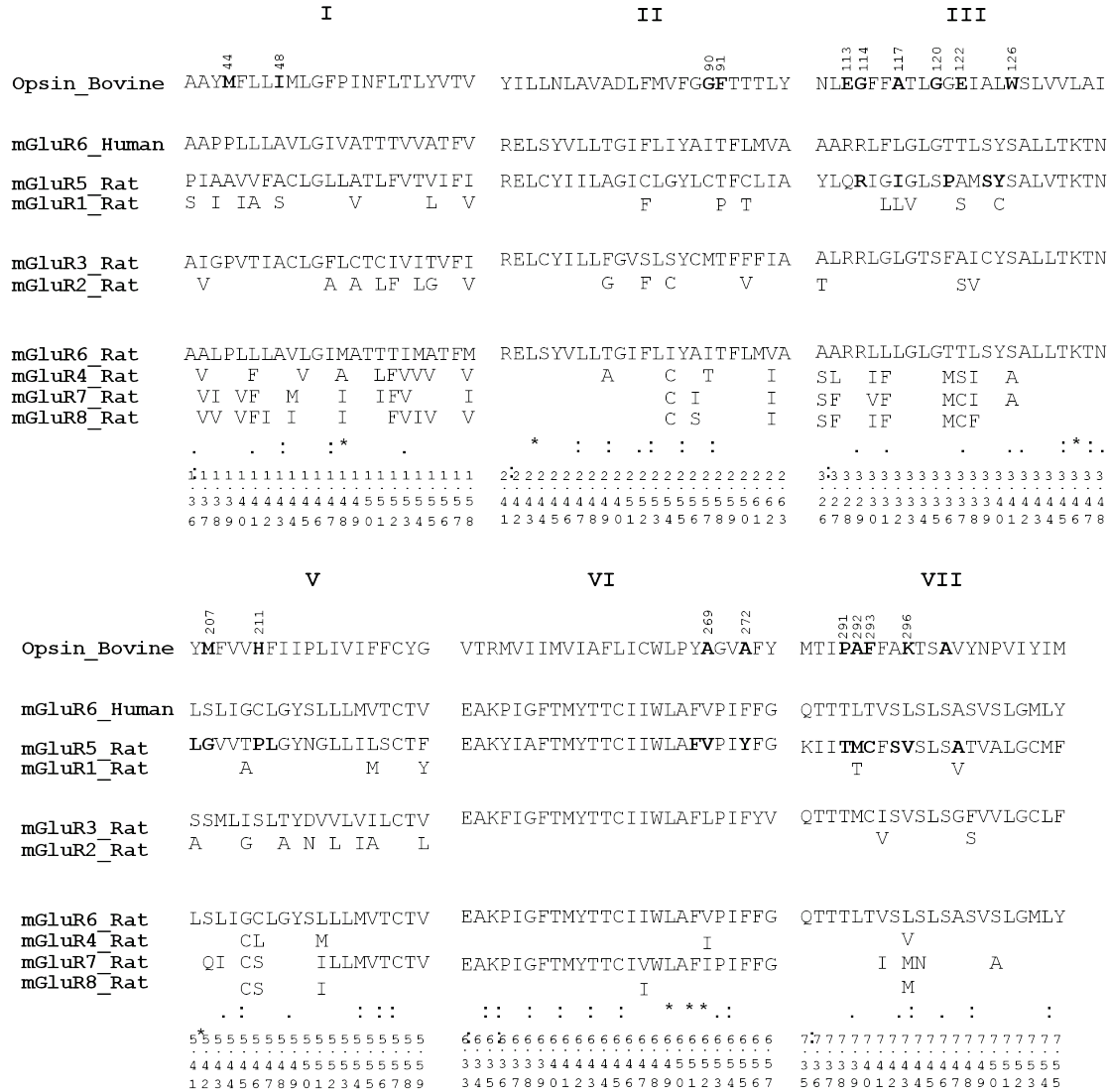


Figure 11.8 Alignment of amino acid residues of TM involved in persistent edges

The TM regions of rat mGluR1 - mGluR 8 and human mGluR6 are aligned with TM regions of rhodopsin that contain persistent edges. mGluR alignment is subdivided into group I, II and III. Within each group the top sequence is the representative sequence for which complete sequence is given. For other members within the group only amino acids that are not conserved are shown. Persistent edges identified in rhodopsin are in bold. Residues experimentally shown to be critical for allosteric ligand binding in mGluR1 and mGluR 5 are also in bold (Fukuda et al., 2009; Malherbe et al., 2006; Muhlemann et al., 2006). Additional residues that are predicted to be within 5Å of allosteric ligand binding pocket in mGluR5 are also in bold (Yanamala et al., 2008). At the bottom of the alignment Ballesteros Weinstein numbering scheme of the amino acids is provided.

12.0 SUMMARY

G protein coupled receptors are proteins on the cell surface that sense diverse environmental stimuli and communicate them into the cells. Sensing the environment is key to maintain homeostasis of the cells and dysfunction of GPCRs is often pathological. Thus, GPCRs are important pharmacological targets. Among GPCRs we are interested in structure-function studies of rhodopsin and mGluR6, both of which are critical for dim light vision. Rhodopsin is a prototypical class A GPCR and mGluR6 belongs to the family of class C GPCRs. The classification of GPCRs is primarily based on sequence similarity among the receptors. Although class A GPCRs share very low sequence similarity they all contain a structurally conserved seven helical transmembrane (TM) domain. In rhodopsin the endogenous ligand (11-*cis*-retinal) binds in the TM domain and activates the receptor in response to light. The mechanism of activation in rhodopsin is a result of structural changes in the TM domain which are very well understood. However, in mGluR6 the binding of endogenous agonist (L-glutamate) in an extracellular region activates the receptor by previously unknown conformational changes in the TM domain. In this thesis, I hypothesized that the mechanism of activation is conserved between in rhodopsin (class A GPCR) and mGluR6 (class C GPCR). mGluR6 is structurally and functionally poorly characterized and there are no known selective ligands. Aims in this thesis are (1) to enable structure-function studies of mGluR6 (2) to identify selective ligands for

mGluR6 and (3) to characterize structure-function relationships in mGluR6 and compare them to rhodopsin.

Towards enabling structure-function studies: I established mammalian stable cell lines expressing high levels of mGluR6 and its mutants to aid any structure-function studies of this receptor. I showed that mGluR6 and some of its mutants are trafficked to the cell membrane and are properly folded inside the cell, while others are mis-folded and retain inside the cell. I next developed robust functional assays in cellular and membrane environments to characterize the function of mGluR6. In order to establish functional assays for mgluR6 in detergents, a detergent screen was carried out to extract mGluR6 from the stable cells.

Towards discovering orthosteric (selective) and allosteric ligands for mGluR6: Ligand binding studies to identify potential selective ligands for mGluR6 were carried out both computationally and experimentally. Broadly, three different types of ligands were tested based on the location of their binding pocket: ATD (orthosteric), TM (allosteric) and IC (allosteric). Computational approaches included designing homology models of mGluR6 followed by screening of a virtual library of ligands. Experimental characterization involved using the optimized functional assays for mGluR6 in cells and membranes. Among orthosteric ligands, a tetrazole containing molecule (Omega_352) was identified to be a selective agonist for mGluR6 based on analysis of its binding pocket but experimental confirmation awaits improvements in ligand stability.

I also tested binding of dipeptides which have been shown earlier to modulate addiction in mice through glutamatergic systems (Cavun et al., 2005; Goktalay et al., 2006; Resch et al., 2005). Docking studies predicted the dipeptides act as agonists with decreasing strength in this order cycloGly-Gln > Gly-Glu > Gly-Gln. Although cycloGly-Gln bound to mGluR6 with low

binding affinity it did not show any effect on mGluR6 function, while Gly-Gln and Gly-Glu behaved as weak inverse agonists.

Among different TM allosteric ligands predicted to bind (all-trans retinal, DFB, PHCCC and CPCCOEt) only PHCCC which was predicted to dock to active conformation of mGluR6 showed direct inverse agonism when tested experimentally. This is the first time that such a direct effect of an allosteric ligand, which usually has a modulatory effect on the bound orthosteric ligand, on mGluR6 function has been shown.

Two different IC allosteric ligands were tested, anthocyanins (C3G) and porphyrins (Ce6), which were known to enhance night vision (Matsumoto et al., 2003; Washington et al., 2004). My work contributed to the demonstration of direct binding of these compounds to rhodopsin. C3G did not show a pronounced effect on rhodopsin function but it altered the stability of rhodopsin and enhanced its regeneration. I was part of the work demonstrating that Ce6 inhibits function of rhodopsin by preventing G protein activation. Anthocyanins showed no effect on G protein activation while Ce6 inhibited agonist (L-AP4) response when tested in cAMP assays. Further studies are required to characterize the physiological implications of binding of anthocyanins and porphyrins to rhodopsin and mGluR6.

Towards structure-function studies: In order to characterize the activation mechanism of mGluR6, conserved endogenous cysteines on TM5 and TM6 were systematically mutated to alanine and the resulting functional changes in the receptor were probed. I found that TM6 plays a key role in the activation of mGluR6 based on assays of the cysteine mutants. This is in agreement with our understanding that TM6 plays a key role in activation mechanism of the distant GPCR, rhodopsin. This finding suggests a conserved activation mechanism between class C (mGluR6) and class A (rhodopsin) GPCRs.

I also designed another way to characterize the role of the TM domain in activation. mGluR6:Rhodopsin chimeras where the TM domain of mGluR6 was switched with that of rhodopsin were constructed and expressed. Preliminary characterization of these chimeras showed that retinal, which is a ligand of rhodopsin, bound to the chimeras upon its addition to cells directly during expression of these constructs. This provides additional support for the hypothesis that the function of TM domains is conserved between class A and C GPCRs.

Finally, the involvement of long-range interactions in the activation mechanism of rhodopsin was identified by a sequence-based computational approach. Rhodopsin served as a model system for testing this approach since structure-function relationships of rhodopsin are well established. In collaboration with Subhdeep Moitra, I identified long-range interactions in rhodopsin, which were mediated via residues that are part of the retinal binding domain. A set of top 10 ranked residues were identified in rhodopsin that are predicted to be important in these long-range interactions. These top 10 residues significantly overlap with the allosteric ligand binding pocket of mGluRs. This finding further supports the hypothesis that the activation mechanism is conserved between class A (rhodopsin) and class C (mGluRs) GPCRs.

13.0 FUTURE RESEARCH DIRECTIONS

13.1 IMMEDIATE GOALS

13.1.1 Test the effect of PHCCC on the activity of C754A, C765A and C793A double cysteine mutants

I have established that PHCCC (a known positive allosteric modulator of mGluR4) acts as a direct inverse agonist for mGluR6 (Chapter 7, section 7.5). Direct evidence that PHCCC is bound to an allosteric site was suggested by the competition dose-response curves with L-AP4 (see Figure 7.3). The actual binding site of PHCCC yet remains to be clearly determined. To verify if PHCCC binds in the TM domain of mGluR6, I checked its effect on the activity of the ‘rhodopsin-like’ TM alone construct of mGluR6, XR-7TMC. There was no difference in cAMP levels between control (no receptor) cells and XR-7TMC expressing cells. Since, there is no positive control to evaluate the function of XR-7TMC; the lack of effect of PHCCC on this construct cannot be unambiguously interpreted as a lack of binding. However, we have double cysteine constructs of mGluR6 with endogenous TM cysteines C754, C765 and C793 mutated to alanine. These TM cysteines in mGluR6 are present in TM5 and TM6 in the vicinity of the allosteric binding pocket (Figure 9.3). I performed cAMP assays to see if double cysteine mutants had any effect on the inverse agonism of PHCCC but it was difficult to arrive at

conclusions because of the small sample size of experiments (n=2) and large standard errors (Table 9.5). The problem working with PHCCC was insolubility of the compound in aqueous buffers. The large standard errors were probably a result of insolubility issues. These experiments have to be repeated carefully taking into consideration solubility issues of PHCCC to obtain a functional activity profile of PHCCC with the double cysteine mutants.

13.1.2 Optimization of functional assays for mGluR2, mGluR3 and mGluR5 to evaluate selectivity and specificity of binding of dipeptides and other ligands

In studies of class C GPCRS, I focused my efforts on mGluR6 which is a group III mGluR. In order to extend my study to members of other groups of mGluRs, I cloned and established inducible stable cell lines for mGluR5 to represent group I and both mGluR2 and mGluR3 to represent group II mGluRs. This will allow investigating selectivity and specificity of ligand binding to mGluRs in the future.

mGluR2 and mGluR3 were previously shown to decrease forskolin stimulated cAMP levels in cells (Tanabe et al., 1992; Tanabe et al., 1993). I tested whether the function of mGluR2 and mGluR3 are retained in the inducible stable cell lines. The cAMP assay was performed under similar conditions as optimized for mGluR6 (see sections 5.2 and 2.5.2). Under these conditions there was no response for the agonist (L-glutamate) while the antagonist (LY341495) behaved as an inverse agonist. This observation of lack of agonist response, while maintaining antagonist response suggested constitutive activity of receptors. Such constitutive activity was also seen for mGluR6 prior to optimization of the cAMP assay. Therefore, these results suggest the need for optimization of the cAMP assay for both mGluR2 and mGluR3. The important steps that are needed for optimization are the number of times and extent of washes to be carried out to

remove media and the length of incubation of cells in Hank's buffered saline solution to eliminate constitutive activity of receptors (see sections 5.2 and 2.5.2).

The GTP-Eu assay is a more generic assay compared to the cAMP assay and can be used to evaluate function of any GPCR. I therefore also tested function of mGluR2, mGluR3 and mGluR5 using the GTP-Eu assay. To perform GTP-Eu assays, I made membrane preparations using the same protocol as for mGluR6. Preliminary single point L-glutamate dose response obtained under the conditions optimized for mGluR6 showed very weak functional responses of mGluR2, mGluR3 and mGluR5. To obtain a robust signal, the assay conditions need to be optimized for mGluR2, mGluR3 and mGluR5 following the optimization protocol as described for mGluR6 in chapter 2 (see section 2.5.3).

Once the functional assays are optimized the activity of dipeptides (Gly-Glu, Gly-Gln and cycloGly-Gln) can be evaluated. Our predictions indicate that these dipeptides are agonists for mGluR2, mGluR3 and mGluR5. Additionally, potential selective ligands for mGluR6 (like Omega_352) can be verified for selective binding, by comparison of mGluR6 results with mGluR2, mGluR3 and mGluR5.

13.1.3 Evaluate effect of DMSO on GTP-Eu binding assay

At high concentrations, ligands like LY341495 and PHCCC (allosteric ligand) are insoluble in aqueous buffers. So stocks of these are usually dissolved in DMSO as recommended by the supplier (Tocris Bioscience). As described in section 5.2.4 elevated DMSO concentrations (10%) inhibit cAMP assay. Therefore, DMSO titration has to be carried to estimate the concentration of DMSO that can be tolerated by GTP-Eu binding assay before evaluating any ligands whose stocks are prepared in DMSO. In our assays, working stocks of the ligands are first prepared in

aqueous buffer and then added to the cells so that the final concentration of DMSO in the assay was never more than 1%. I recommend that the effect of different DMSO concentrations (0.01%, 0.1%, 1%, 5% and 10%) has to be tested, to evaluate DMSO tolerance for GTP-Eu binding assay.

13.1.4 Imaging mGluR6 trafficking in cells under optimized cell culture conditions that prevent its constitutive activation

mGluR6 imaging studies reported in chapter 3 (see sections 3.3.2 and 3.3.3) were carried out in cells in which mGluR6 was constitutively active because of the presence of L-glutamate in the media. In these studies, I observed that mGluR6 is present both on the membranes and inside the cells. It is possible that a significant amount of mGluR6 present in the cells is due to internalization as a result of constitutive stimulation of mGluR6 by L-glutamate. The internalization of mGluR6 after activation has not yet been reported. The imaging studies need to be repeated under optimized cell culture conditions (which are reported in chapter 5, section 5.2.1) to verify if mGluR6 levels are enriched on membranes and depleted inside the cells. This would be an important contribution to understand the fate of mGluR6 after activation.

Additionally, the use of specific internal markers for intracellular compartments like β -COP or anti-Golgin 97 to stain Golgi bodies and Calnexin or anti-PDI to stain the endoplasmic reticulum would be beneficial to precisely identify the localization of mGluR6 within the cells. Imaging with specific internal markers also need to be carried out to identify the localization of truncated misfolding mutants of mGluR6 (mutants described in chapter 3, section 3.3.3).

13.1.5 Development of an *in vitro* functional assay for purified mGluR6 in detergent micelles

In order to understand the activation mechanism of mGluR6 by biophysical characterization, it is necessary to produce functional mGluR6 in detergent micelles so that the total size of the protein-detergent complex does not interfere with biophysical experiments. For this, development of a robust *in vitro* functional assay with purified mGluR6 and G protein heterotrimer in detergents is a prerequisite. I performed a large-scale detergent screen and identified detergents (Table 4.1) from Anapoe® and Cymal series as good solubilizers to extract mGluR6 from cells. Additionally, I optimized expression and purification of the G protein heterotrimer ($G\alpha_0\beta_3\gamma_{13}$) using the baculovirus expression system in insect cells (see section 2.3.4). The next step towards developing an *in vitro* functional assay is to systematically screen the detergents identified in our screen (shown in Table 4.1) for (1) purifying properly folded mGluR6 from cells using the optimized protocol (2.3.3.1) and for (2) testing the activity of purified mGluR6 and G protein heterotrimer using [³⁵S]GTP γ S or GTP-Eu filter binding assays (section 2.5.1.3 and 2.5.3).

13.1.6 Docking validation of antagonists to open mGluR structures

As described in sections 6.3.1.1 and 6.4, I have successfully validated the docking approach and screened a virtual library and identified selective agonists for mGluR6. However, the docking approach could not be validated to screen antagonist as described in section 6.3.1.2.

In order to validate the docking approach for screening antagonists and to serve as positive controls, L-glutamate and S-MCPG ligands were removed from the open conformation

structure files of mGluR1 (PDB: 1EWK, chain B and 1ISS, chain A) and were docked using AutoDock Vina software (see section 6.3.1.2). The docking results were not in agreement with those observed in the crystal structures. In the case of L-glutamate docking, L-glutamate successfully recapitulated the binding pose as observed in the crystal structure, but was missing the water mediated contacts in the binding pocket as the water molecules were not included in the docking procedure (panels A and C; Figure 6.3). In the case of S-MCPG, the molecule docked in the correct binding pocket but failed to recapitulate the docking pose seen in the crystal structure as the key cation-pi interaction between S-MCPG and the ligand binding pocket residues was missing (panels B and D; Figure 6.3).

In order to accurately mimic the L-glutamate, the presence of water during docking appears to be important. But, the placement of water molecules in the binding pocket would be dependent on the position of the bound ligand and hence including water molecules in the docking procedure is not favorable for screening novel ligands. However, L-glutamate is an endogenous agonist and probably binds to the open conformation of mGluR1 as a transient intermediate. This is evident from the crystal structure where L-glutamate makes very few direct contacts with the ligand binding pocket residues (Kunishima et al., 2000). Therefore L-glutamate is probably not an ideal positive control to validate docking approaches for antagonist screening. On the other hand in the co-crystal structure of S-MCPG and the ATD of mGluR1 (Tsuchiya et al., 2002), S-MCPG interacts with most of the ligand binding pocket residues and also forms a key cation-pi interaction that positions it as a wedge that maintains the open conformation of ATD. Therefore, I recommend docking of S-MCPG to mGluR1 open structure to validate docking approaches for antagonist screening.

To obtain crystal structure pose for S-MCPG in docking, I speculate that the scoring function of AutoDock Vina might have to be altered to bias it in favor of electrostatic interactions (cation- π interactions). Altering the scoring function of the docking procedure is not straight forward and requires extensive optimization and testing (Jain, 2006; Rajamani and Good, 2007). Before attempting to alter the scoring function I would recommend using alternative docking methods such as AutoDock (Goodsell et al., 1996), ArgusLab (Thompson ArgusLab 4.0.1), GOLD (Jones et al., 1997) and GLIDE (Friesner et al., 2004). These programs use different force fields and scoring functions (Oda et al., 2006) to dock molecules, thus, increasing the probability to obtain S-MCPG docking pose as seen in the crystal structure. The docking programs that successfully recapitulate the crystal structure of S-MCPG can be used to screen small molecules to identify novel antagonists.

13.2 LONG TERM GOALS

13.2.1 Large scale virtual and experimental screens to identify ligands for mGluR6

In this thesis I adopted an integrated approach involving computational and experimental tools to identify novel ligands for mGluR6. I demonstrated use of homology models to virtually screen small molecule libraries and experimentally tested the predicted ligands using optimized cell and membrane based functional assays.

Typically for experimental screening of drug-like molecules initially a primary assay is set up to screen hundreds to a few thousands of compounds and positive hits from this screen are further validated using secondary assays where EC_{50} and IC_{50} are determined (An and Tolliday,

2009). In line with this, to screen ligands for mGluR6, I developed a high-throughput membrane based (GTP-Eu fluorescence; section 5.3.2) and a cell based (cAMP assay; section 5.2) functional assay that act as primary and secondary screening assays, respectively. Moreover, selectivity and specificity of these ligands can be tested as described in section 13.1.2.

I screened a virtual library with 3000 molecules and was able to identify a putative selective ligand for mGluR6. The library screens can be extended to virtually screen thousands or millions of compounds to identify molecules that could be selective agonists or antagonists for mGluR6. Similar to the screening of agonists and antagonists, small molecule libraries can be virtually screened to identify allosteric ligands. For this purpose active and inactive structure models of mGluR6 can be used for screening positive and negative modulators, respectively. For initial screens, use of small molecule libraries of commercially available compounds like ZINC (Irwin and Shoichet, 2005) would be advantageous, since positive hits from the screens can be readily obtained and experimentally tested.

13.2.2 Functional characterization of chimeras

In order to take advantage of the well-established detergent reconstituted functional assays for rhodopsin, mGluR6: Rhodopsin chimeras where the TM domain of mGluR6 is switched with that of rhodopsin were created. I designed three different chimeras which differ in length of the amino-terminus region of rhodopsin. Among these three chimeras, I successfully cloned chimera #2 which has an mGluR6 fragment from amino acids 1 – 555 followed by amino acids 4 – 348 of rhodopsin and chimera #3 that has an mGluR6 fragment from amino acids 1 – 574 followed by amino acids 23 – 348 of rhodopsin. Preliminary characterization of these chimeras suggests that these chimeras bind retinal (ligand for rhodopsin) weakly upon its direct addition to cells during

expression. To increase the yield of retinal-bound fractions, the timing and amount of retinal added to the cultures can be varied. If sufficient quantities of the retinal bound chimera constructs can be obtained these can then be studied using different biophysical approaches that are well established for rhodopsin to address structure-function relationships in mGluRs. For example, the stability of retinal-protein interactions in the TM region can be measured in relation to agonist or antagonist binding in the extracellular L-glutamate binding pocket.

13.2.3 Cysteine accessibility and EPR studies of mGluR6

In mGluRs, ligand binding in the ATD activates the cytoplasmic domain via the TM regions. However, the actual conformational changes in the TM domain during activation are not yet identified. Based on models derived from the crystal structures of ATD, within the mGluR homodimer, TM regions are thought to associate/dimerize only in the active (A) but not in the inactive/resting (R) states (Kunishima et al., 2000; Muto et al., 2007; Tsuchiya et al., 2002). It is hypothesized that there is an equilibrium between A and R states where the addition of agonist shifts the equilibrium to the A state and the antagonist to the R state. In an alternate activation model, TM regions are suggested to be in association both in inactive and active states with only inter-subunit rearrangement of cytoplasmic regions observed on activation based on fluorescence resonance energy transfer (FRET) studies (Tateyama et al., 2004). Both models from crystal structures and FRET studies suggest that dimerization of TM region of mGluRs is essential for activation, though the models differ in the dynamics of dimerization. We can study the conformational dynamics of dimerization using the wild-type and TM domain cysteine mutants of mGluR6.

For biophysical characterization, we need to first establish a robust *in vitro* functional assay (see section 13.1.5 above). Once established, the cysteines in the TM region of wild-type or the active cysteine mutants C754A, C765A and C754A/C765A can be probed for solvent accessibility using the cysteine derivatizing reagent 4,4'-dithiopyridine (PDS) in the presence and absence of both orthosteric (L-glutamate, dipeptides, Omega_352) and allosteric ligands (PHCCC). Cysteine accessibility studies will provide qualitative information about the conformational dynamics in the TM5 and TM6 before and after activation. Further, the single cysteine mutant C754A/C765A which has wild-type like activity would be a suitable construct for electron paramagnetic resonance (EPR) studies as one can chemically derivatize the single cysteine (with free sulfhydryl group) in the TM domain. EPR can be used for distance measurements and/or solvent accessibility measurements that can be used to detect the presence or absence of dimerization and/or conformational changes during activation thus providing data for supporting or refuting the existing models. In general these findings will help better understand the activation mechanism of mGluRs.

13.2.4 Comparison of GREMLIN analysis with other sequence analysis methods and extension of GREMLIN analysis to Class C GPCRs

In chapter 11, I identified the long-range interactions involved in activation of rhodopsin, a class A GPCR using a recently reported method of sequence analysis, GREMLIN. Using this method, I identified that the long-range interactions between extracellular and intracellular regions are mediated through the ligand binding pocket in transmembrane domain. Long-range interactions in class A GPCRs have also been identified previously using different sequence analysis methods like Statistical Coupling Analysis (SCA) (Suel et al., 2003) and Graphical Models for

Residue Coupling (GMRC) (Thomas et al., 2008). A multiple sequence alignment (MSA) is required for such sequence analysis studies. The alignment we used for GREMLIN studies was used in both the SCA (Suel et al., 2003) and GMRC studies (Thomas et al., 2008). The use of the same MSA by different methods to determine long-range interactions in GPCRs enables an unbiased comparison of the findings between these three methods. Such a comparison of results obtained from GREMLIN, SCA and GMRC would aid in evaluating the strengths and weaknesses of the individual methods as applicable to GPCR sequence analysis. This in turn would enable design/construction of superior sequence analysis methods.

Compared to class A GPCRs, in class C GPCRs the extracellular domains are larger and contain the endogenous ligand binding pocket. Ligand binding in the extracellular domain of mGluRs initiates activation of G protein inside the cells. The actual activation mechanism is currently not understood. To gain insights into the involvement of long-range interactions, GREMLIN analysis can be performed on the multiple sequence alignment of class C GPCRs. It is possible that L-glutamate binding in the extracellular domain of mGluRs is communicated to the intracellular domain via the allosteric ligand binding domain in the transmembrane region.

APPENDIX A. LIST OF ORTHOSTERIC LIGANDS FOR MGLUR1, 3 AND 6

Orthosteric ligands for mGluR1, 3 and 6 collected from literature are used in secondary validation. Top ranked docking results in agreement and disagreement with literature are shown in green and red boxes, respectively. Yellow boxes indicate ligands for which binding data is not reported.

#	ligands	mGluR6 (closed model)	mGluR1 (PDB: 1EWK_A)	mGluR3 (PDB: 2E4U_A)
1.	ABHxD I	Agonist (EC50 5.3uM)	Agonist (EC50 1.6uM)	Agonist (2.2uM)
2.	ABHxD II	Agonist (EC50 800 uM)	Agonist (EC50 121uM)	No effect (EC50 -1000uM)
3.	ABHxD III	No effect (EC50 >1000uM)	Agonist (EC50 232uM)	No effect (EC50 -1000uM)
4.	ABHxD IV	No effect (EC50 >1000uM)	No effect (EC50 >1000uM)	No effect (EC50 -1000uM)
5.	1R_3R_ACPD	No data/ No binding	No effect (EC50 >1000uM)	No effect ?
6.	1S_3S_ACPD	No data/ No binding	Agonist (>300uM)	Agonist (30uM)
7.	1R_3S_ACPD	Agonist (trans ACPD: 82uM)	Agonist (EC50 126uM)	No effect (trans ACPD: 40uM)
8.	1S_3R_ACPD	Agonist (EC50 20uM @ HUMAN)	Agonist (EC50 8-42uM)	Agonist (5uM @ mGluR2)
9.	1_Bn_APDC	Agonist (EC50 20uM)	No effect (EC50 >1000uM)	Antagonist (200 uM at mGluR2)
10.	2R_4R_APDC	Agonist (EC50 110uM)	Agonist (EC50 100uM)	Agonist (0.4 uM)
11.	AFBD	No effect	No effect	Agonist (0.08 uM)
12.	MGS0028	No effect	No effect	Agonist (0.002 uM)
13.	LY354740	Agonist (EC50 3uM)	No effect (EC50 >100-300uM)	Agonist (0.02 0.06 uM)
14.	HYDIA	No effect (at GRM4/7)	No effect	Antagonist (Ki 0.08)
15.	MCCG	No effect	No effect	Antagonist (87.5 uM)
16.	L_CCG_I	Agonist (EC50 0.57uM @ HUMAN)	Agonist (1.9uM)	Agonist (0.44 uM)
17.	DCG_IV	Antagonist (39.6 uM)	Antagonist (389 uM)	Agonist (0.09 uM)
18.	Ibotenate	No effect (>100uM)	Agonist (2.3-11.3uM)	No data/ No binding
19.	S AMPA	Agonist (220uM)	No effect (Ki 450uM)	No effect (@ mGluR2 EC50 >1000uM)
20.	R AMPA	No effect (>1000uM)	No effect (EC50 >1000uM)	No effect (@ mGluR2 EC50 >1000uM)
21.	S homo AMPA	Agonist (58uM)	No effect (EC50 >1000uM)	No effect (>1000uM)
22.	R homo AMPA	No effect (>1000uM)	No effect (EC50 >1000uM)	No effect (>1000uM)
23.	L Quisqualate	Agonist (EC50 15.7uM @ HUMAN)	Agonist (Kd=22nM)	No data/ No binding
24.	L SOP	Agonist (EC50 0.4uM @ HUMAN)	No effect / No data?	No effect / No data?
25.	MSOP	Antagonist (@ group II)	No effect	No effect (@ group II)
26.	MAP4	No effect (>100uM)	No effect	No effect (@ group II)
27.	L AP4	Agonist (EC50 0.18uM @ HUMAN)	No effect (EC50 >1000uM)	No effect (>1000uM)
28.	L Glu	Agonist (EC50 1.6uM @ HUMAN)	Agonist (1-20uM)	Agonist (2 -10uM)
29.	L GLA	Agonist (Partial EC50 60uM)	No effect	Antagonist (337uM)
30.	S Amino Adipicacid	Agonist (EC50 140uM @ HUMAN)	No effect (EC50 >1000uM)	Agonist (35uM @ mGluR2)
31.	LY341495	Antagonist (Kd 31nM @ human)	Antagonist (IC50 6.8 uM @ human)	Antagonist (IC50 0.014 uM @ human)
32.	S 3 5 DHPG	Agonist (Weak)	Agonist (3.5uM)	No effect @ mGluR2 (selective grp I)
33.	S 4CPG	No effect (>100uM)	Antagonist (40uM)	Agonist @ mGluR2
34.	S 4C3HPG	No effect	Antagonist (30uM)	Agonist @ mGluR2
35.	S 3C4HPG	Agonist	Antagonist (400uM)	Agonist @ mGluR2
36.	R 3C4HPG	No data/ No binding	No effect	Agonist @ mGluR2
37.	S CHPG	No data/ No binding	Agonist (RS mixture: >1000uM)	No data/ No binding
38.	R CHPG	No data/ No binding	Agonist (RS mixture: >1000uM)	No data/ No binding
39.	S DCPG	Agonist (EC50 3.6uM @ HUMAN)	Antagonist (IC50 32uM @ human)	No effect
40.	R DCPG	No data/ No binding	No data / No Binding	No data/ No binding
41.	S MCPG	No effect	Antagonist (70 uM)	No effect (grp II and mGluR2)
42.	R MCPG	No effect	No effect	Antagonist @ mGluR2 400uM
43.	S 2MeCPG	No data/ No binding	Antagonist (RS mixture Ki 0.7uM)	No data/ No binding
44.	R 2MeCPG	No data/ No binding	Antagonist (RS mixture Ki 0.7uM)	No data/ No binding
45.	AIDA	No data/ No binding	Antagonist (250 uM)	No data/ No binding
46.	S PPG	Agonist (EC50 1.6uM @ HUMAN RS mix)	No effect (>500 IC50 @ human)	No effect (@ mGluR2 EC and IC50 >300uM)
47.	R PPG	Agonist (EC50 1.6uM @ HUMAN RS mix)	No effect (>500 IC50 @ human)	No effect (@ mGluR2 EC and IC50 >300uM)
48.	S MPPG	Antagonist (weak @ human RS mix)	No effect at group I	Antagonist (@ grpII and mGluR2 11uM RX mixture)
49.	R MPPG	Antagonist (weak @ human RS mix)	No effect at group I	Antagonist (@ grpII and mGluR2 11uM RX mixture)
50.	S CPPG	No effect	No effect	No effect
51.	R CPPG	No effect	No effect	No effect
52.	S UBPI113	No effect (@ grp III)	No effect	No effect
53.	R UBPI113	No effect (@ grp III)	No effect	No effect
54.	S UBPI110	Antagonist (at grp III)	No effect	Antagonist (@ grpII RS mixture)
55.	R UBPI110	Antagonist (at grp III)	No effect	Antagonist (@ grpII RS mixture)
56.	S UBPI111	Antagonist (at grp III)	No effect	Antagonist (@ grpII RS mixture)
57.	R UBPI111	Antagonist (at grp III)	No effect	Antagonist (@ grpII RS mixture)
58.	S UBPI112	Antagonist (at grp III)	No effect (selective grp III)	Antagonist (@ grpII RS mixture)
59.	R UBPI112	Antagonist (at grp III)	No effect (selective grp III)	Antagonist (@ grpII RS mixture)
60.	S UBPI130	Antagonist (at grp III)	No effect	No effect
61.	R UBPI130	Antagonist (at grp III)	No effect	No effect

APPENDIX B. PUBLICATIONS

B.1 MANUSCRIPTS PUBLISHED

1. Dutta A, **Tirupula KC**, Alexiev U, Klein-Seetharaman J: Characterization of Membrane Protein Non-native States. 1. Extent of Unfolding and Aggregation of Rhodopsin in the Presence of Chemical Denaturants. *Biochemistry* 2010, 49(30):6317-6328.
2. Qi Y, Dhiman HK, Bhola N, Budyak I, Kar S, Man D, Dutta A, **Tirupula K**, Carr BI, Grandis J, Bar-Joseph Z, Klein-Seetharaman J: Systematic prediction of human membrane receptor interactions. *Proteomics* 2009, 9(23):5243-5255.
3. **Tirupula KC**[†], Balem F[†], Yanamala N, Klein-Seetharaman J: pH-dependent interaction of rhodopsin with cyanidin-3-glucoside. 2. Functional aspects. *Photochemistry and photobiology* 2009, 85(2):463-470. [†]These authors contributed equally to this manuscript.
4. Yanamala N[†], **Tirupula KC**[†], Balem F, Klein-Seetharaman J: pH-dependent interaction of rhodopsin with cyanidin-3-glucoside. 1. Structural aspects. *Photochemistry and photobiology* 2009, 85(2):454-462. [†]These authors contributed equally to this manuscript.

5. Yanamala N, **Tirupula KC**, Klein-Seetharaman J: Preferential binding of allosteric modulators to active and inactive conformational states of metabotropic glutamate receptors. BMC bioinformatics 2008, 9 Suppl 1:S16.

B.2 MANUSCRIPTS IN PREPARATION

1. Isin B, **Tirupula KC**, Oltvai Z, Klein-Seetharaman J, Bahar I: Identification of motions in membrane proteins by Elastic Network Models and their experimental validation. Methods in molecular biology 2011. (Submitted)
2. **Tirupula KC**, Dhiman HK, Murthy L, Bisello A, Klein-Seetharaman J: Role of conserved transmembrane domain cysteines in activation of metabotropic glutamate receptor type 6.
3. Moitra S[†], **Tirupula KC**[†], Klein-Seetharaman J, Langmead CJ: Identification of long-range couplings in G protein coupled receptors. [†]These authors contributed equally to this manuscript.

BIBLIOGRAPHY

- Ahmadian, H., Nielsen, B., Brauner-Osborne, H., Johansen, T. N., Stensbol, T. B., Slok, F. A., Sekiyama, N., Nakanishi, S., Krogsgaard-Larsen, P., Madsen, U., 1997. (S)-homo-AMPA, a specific agonist at the mGlu6 subtype of metabotropic glutamic acid receptors. *J Med Chem* 40, 3700-3705.
- Ahuja, S., Hornak, V., Yan, E. C., Syrett, N., Goncalves, J. A., Hirshfeld, A., Ziliox, M., Sakmar, T. P., Sheves, M., Reeves, P. J., Smith, S. O., Eilers, M., 2009. Helix movement is coupled to displacement of the second extracellular loop in rhodopsin activation. *Nat Struct Mol Biol* 16, 168-175.
- Ahuja, S., Smith, S. O., 2009. Multiple switches in G protein-coupled receptor activation. *Trends Pharmacol Sci* 30, 494-502.
- Altenbach, C., Cai, K., Khorana, H. G., Hubbell, W. L., 1999. Structural features and light-dependent changes in the sequence 306-322 extending from helix VII to the palmitoylation sites in rhodopsin: a site-directed spin-labeling study. *Biochemistry* 38, 7931-7937.
- Altenbach, C., Cai, K., Klein-Seetharaman, J., Khorana, H. G., Hubbell, W. L., 2001a. Structure and function in rhodopsin: mapping light-dependent changes in distance between residue 65 in helix TM1 and residues in the sequence 306-319 at the cytoplasmic end of helix TM7 and in helix H8. *Biochemistry* 40, 15483-15492.
- Altenbach, C., Klein-Seetharaman, J., Cai, K., Khorana, H. G., Hubbell, W. L., 2001b. Structure and function in rhodopsin: mapping light-dependent changes in distance between residue 316 in helix 8 and residues in the sequence 60-75, covering the cytoplasmic end of helices TM1 and TM2 and their connection loop CL1. *Biochemistry* 40, 15493-15500.
- Altenbach, C., Kusnetzow, A. K., Ernst, O. P., Hofmann, K. P., Hubbell, W. L., 2008. High-resolution distance mapping in rhodopsin reveals the pattern of helix movement due to activation. *Proc Natl Acad Sci U S A* 105, 7439-7444.
- Altenbach, C., Yang, K., Farrens, D. L., Farahbakhsh, Z. T., Khorana, H. G., Hubbell, W. L., 1996. Structural features and light-dependent changes in the cytoplasmic interhelical E-F loop region of rhodopsin: a site-directed spin-labeling study. *Biochemistry* 35, 12470-12478.

- An, W. F., Tolliday, N. J., 2009. Introduction: cell-based assays for high-throughput screening. *Methods in molecular biology* 486, 1-12.
- Archer, E., Maigret, B., Escrieut, C., Pradayrol, L., Fourmy, D., 2003. Rhodopsin crystal: new template yielding realistic models of G-protein-coupled receptors? *Trends Pharmacol Sci* 24, 36-40.
- Arunlakshana, O., Schild, H. O., 1959. Some quantitative uses of drug antagonists. *Br J Pharmacol Chemother* 14, 48-58.
- Baehr, W., Morita, E. A., Swanson, R. J., Applebury, M. L., 1982. Characterization of bovine rod outer segment G-protein. *J Biol Chem* 257, 6452-6460.
- Balakrishnan, S., Kamisetty, H., Carbonell, J. G., Lee, S. I., Langmead, C. J., 2010. Learning generative models for protein fold families. *Proteins*.
- Ballesteros, J. A., Jensen, A. D., Liapakis, G., Rasmussen, S. G., Shi, L., Gether, U., Javitch, J. A., 2001a. Activation of the beta 2-adrenergic receptor involves disruption of an ionic lock between the cytoplasmic ends of transmembrane segments 3 and 6. *J Biol Chem* 276, 29171-29177.
- Ballesteros, J. A., Shi, L., Javitch, J. A., 2001b. Structural mimicry in G protein-coupled receptors: implications of the high-resolution structure of rhodopsin for structure-function analysis of rhodopsin-like receptors. *Mol Pharmacol* 60, 1-19.
- Baylor, D., 1996. How photons start vision. *Proc Natl Acad Sci U S A* 93, 560-565.
- Bellone, R. R., Brooks, S. A., Sandmeyer, L., Murphy, B. A., Forsyth, G., Archer, S., Bailey, E., Grahn, B., 2008. Differential gene expression of TRPM1, the potential cause of congenital stationary night blindness and coat spotting patterns (LP) in the Appaloosa horse (*Equus caballus*). *Genetics* 179, 1861-1870.
- Beqollari, D., Kammermeier, P. J., 2008. The mGlu(4) receptor allosteric modulator N-phenyl-7-(hydroxyimino)cyclopropa[b]chromen-1a-carboxamide acts as a direct agonist at mGlu(6) receptors. *Eur J Pharmacol* 589, 49-52.
- Beukers, M. W., Kristiansen, I., AP, I. J., Edvardsen, I., 1999. TinyGRAP database: a bioinformatics tool to mine G-protein-coupled receptor mutant data. *Trends Pharmacol Sci* 20, 475-477.
- Birdsall, B., King, R. W., Wheeler, M. R., Lewis, C. A., Jr., Goode, S. R., Dunlap, R. B., Roberts, G. C., 1983. Correction for light absorption in fluorescence studies of protein-ligand interactions. *Anal Biochem* 132, 353-361.
- Blake, B. L., Wing, M. R., Zhou, J. Y., Lei, Q., Hillmann, J. R., Behe, C. I., Morris, R. A., Harden, T. K., Bayliss, D. A., Miller, R. J., Siderovski, D. P., 2001. G beta association and effector interaction selectivities of the divergent G gamma subunit G gamma(13). *J Biol Chem* 276, 49267-49274.

- Bleakman, D., Lodge, D., 1998. Neuropharmacology of AMPA and kainate receptors. *Neuropharmacology* 37, 1187-1204.
- Bockaert, J., Marin, P., Dumuis, A., Fagni, L., 2003. The 'magic tail' of G protein-coupled receptors: an anchorage for functional protein networks. *FEBS Lett* 546, 65-72.
- Bockaert, J., Pin, J. P., 1999. Molecular tinkering of G protein-coupled receptors: an evolutionary success. *Embo J* 18, 1723-1729.
- Bokoch, M. P., Zou, Y., Rasmussen, S. G., Liu, C. W., Nygaard, R., Rosenbaum, D. M., Fung, J. J., Choi, H. J., Thian, F. S., Kobilka, T. S., Puglisi, J. D., Weis, W. I., Pardo, L., Prosser, R. S., Mueller, L., Kobilka, B. K., 2010. Ligand-specific regulation of the extracellular surface of a G-protein-coupled receptor. *Nature* 463, 108-112.
- Bourne, H. R., Sanders, D. A., McCormick, F., 1991. The GTPase superfamily: conserved structure and molecular mechanism. *Nature* 349, 117-127.
- Bownds, D., 1967. Site of attachment of retinal in rhodopsin. *Nature* 216, 1178-1181.
- Brauner-Osborne, H., Slok, F. A., Skjaerbaek, N., Ebert, B., Sekiyama, N., Nakanishi, S., Krogsgaard-Larsen, P., 1996. A new highly selective metabotropic excitatory amino acid agonist: 2-amino-4-(3-hydroxy-5-methylisoxazol-4-yl)butyric acid. *J Med Chem* 39, 3188-3194.
- Cai, K., Klein-Seetharaman, J., Altenbach, C., Hubbell, W. L., Khorana, H. G., 2001. Probing the dark state tertiary structure in the cytoplasmic domain of rhodopsin: proximities between amino acids deduced from spontaneous disulfide bond formation between cysteine pairs engineered in cytoplasmic loops 1, 3, and 4. *Biochemistry* 40, 12479-12485.
- Cai, K., Klein-Seetharaman, J., Farrens, D., Zhang, C., Altenbach, C., Hubbell, W. L., Khorana, H. G., 1999a. Single-cysteine substitution mutants at amino acid positions 306-321 in rhodopsin, the sequence between the cytoplasmic end of helix VII and the palmitoylation sites: sulfhydryl reactivity and transducin activation reveal a tertiary structure. *Biochemistry* 38, 7925-7930.
- Cai, K., Klein-Seetharaman, J., Hwa, J., Hubbell, W. L., Khorana, H. G., 1999b. Structure and function in rhodopsin: effects of disulfide cross-links in the cytoplasmic face of rhodopsin on transducin activation and phosphorylation by rhodopsin kinase. *Biochemistry* 38, 12893-12898.
- Cavun, S., Goktalay, G., Millington, W. R., 2005. Glycyl-glutamine, an endogenous beta-endorphin-derived peptide, inhibits morphine-induced conditioned place preference, tolerance, dependence, and withdrawal. *J Pharmacol Exp Ther* 315, 949-958.
- Chang, M. W., Ayeni, C., Breuer, S., Torbett, B. E., 2010. Virtual screening for HIV protease inhibitors: a comparison of AutoDock 4 and Vina. *PLoS One* 5, e11955.

- Chen, C., Okayama, H., 1987. High-efficiency transformation of mammalian cells by plasmid DNA. *Mol Cell Biol* 7, 2745-2752.
- Chen, C. K., 2005. The vertebrate phototransduction cascade: amplification and termination mechanisms. *Rev Physiol Biochem Pharmacol* 154, 101-121.
- Chenna, R., Sugawara, H., Koike, T., Lopez, R., Gibson, T. J., Higgins, D. G., Thompson, J. D., 2003. Multiple sequence alignment with the Clustal series of programs. *Nucleic Acids Res* 31, 3497-3500.
- Cherezov, V., Rosenbaum, D. M., Hanson, M. A., Rasmussen, S. G., Thian, F. S., Kobilka, T. S., Choi, H. J., Kuhn, P., Weis, W. I., Kobilka, B. K., Stevens, R. C., 2007. High-resolution crystal structure of an engineered human beta2-adrenergic G protein-coupled receptor. *Science* 318, 1258-1265.
- Chien, E. Y., Liu, W., Zhao, Q., Katritch, V., Han, G. W., Hanson, M. A., Shi, L., Newman, A. H., Javitch, J. A., Cherezov, V., Stevens, R. C., 2010. Structure of the human dopamine D3 receptor in complex with a D2/D3 selective antagonist. *Science* 330, 1091-1095.
- Choe, H.-W., Kim, Y. J., Park, J. H., Morizumi, T., Pai, E. F., Krausz, N., Hofmann, K. P., Scheerer, P., Ernst, O. P., 2011a. Crystal structure of metarhodopsin II. *Nature advance online publication*.
- Choe, H. W., Park, J. H., Kim, Y. J., Ernst, O. P., 2011b. Transmembrane signaling by GPCRs: insight from rhodopsin and opsin structures. *Neuropharmacology* 60, 52-57.
- Choi, G., Landin, J., Galan, J. F., Birge, R. R., Albert, A. D., Yeagle, P. L., 2002. Structural studies of metarhodopsin II, the activated form of the G-protein coupled receptor, rhodopsin. *Biochemistry* 41, 7318-7324.
- Cohen, G. B., Oprian, D. D., Robinson, P. R., 1992. Mechanism of activation and inactivation of opsin: role of Glu113 and Lys296. *Biochemistry* 31, 12592-12601.
- Collingridge, G. L., Singer, W., 1990. Excitatory amino acid receptors and synaptic plasticity. *Trends Pharmacol Sci* 11, 290-296.
- Congreve, M., Marshall, F., 2010. The impact of GPCR structures on pharmacology and structure-based drug design. *Br J Pharmacol* 159, 986-996.
- Conn, P. J., Pin, J., 1997. Pharmacology and functions of metabotropic glutamate receptors. *Annu. Rev. Pharmacol. Toxicol.* 37, 205-237.
- Crooks, G. E., Hon, G., Chandonia, J. M., Brenner, S. E., 2004. WebLogo: a sequence logo generator. *Genome Res* 14, 1188-1190.
- Davies, M. N., Secker, A., Freitas, A. A., Mendao, M., Timmis, J., Flower, D. R., 2007. On the hierarchical classification of G protein-coupled receptors. *Bioinformatics* 23, 3113-3118.

- de la Villa, P., Kurahashi, T., Kaneko, A., 1995. L-glutamate-induced responses and cGMP-activated channels in three subtypes of retinal bipolar cells dissociated from the cat. *J Neurosci* 15, 3571-3582.
- Dekker, J. P., Fodor, A., Aldrich, R. W., Yellen, G., 2004. A perturbation-based method for calculating explicit likelihood of evolutionary co-variance in multiple sequence alignments. *Bioinformatics* 20, 1565-1572.
- Demas, J., Sagdullaev, B. T., Green, E., Jaubert-Miazza, L., McCall, M. A., Gregg, R. G., Wong, R. O., Guido, W., 2006. Failure to maintain eye-specific segregation in nob, a mutant with abnormally patterned retinal activity. *Neuron* 50, 247-259.
- Dhingra, A., Jiang, M., Wang, T. L., Lyubarsky, A., Savchenko, A., Bar-Yehuda, T., Sterling, P., Birnbaumer, L., Vardi, N., 2002. Light response of retinal ON bipolar cells requires a specific splice variant of Galpha(o). *J Neurosci* 22, 4878-4884.
- Dhingra, A., Lyubarsky, A., Jiang, M., Pugh, E. N., Jr., Birnbaumer, L., Sterling, P., Vardi, N., 2000. The light response of ON bipolar neurons requires G[alpha]o. *J Neurosci* 20, 9053-9058.
- Doi, T., Molday, R. S., Khorana, H. G., 1990. Role of the intradiscal domain in rhodopsin assembly and function. *Proc Natl Acad Sci U S A* 87, 4991-4995.
- Douglas, R. H., Partridge, J. C., Dulai, K., Hunt, D., Mullineaux, C. W., Tauber, A. Y., Hynninen, P. H., 1998. Dragon fish see using chlorophyll. *Nature* 393, 423-424.
- Dryja, T. P., McGee, T. L., Berson, E. L., Fishman, G. A., Sandberg, M. A., Alexander, K. R., Derlacki, D. J., Rajagopalan, A. S., 2005. Night blindness and abnormal cone electroretinogram ON responses in patients with mutations in the GRM6 gene encoding mGluR6. *Proc Natl Acad Sci U S A* 102, 4884-4889.
- Duvoisin, R. M., Morgans, C. W., Taylor, W. R., 2005. The mGluR6 receptors in the retina: Analysis of a unique G-protein signaling pathway. *Cellscience* 2.
- Enz, R., 2007. The trick of the tail: protein-protein interactions of metabotropic glutamate receptors. *Bioessays* 29, 60-73.
- Eswar, N., Eramian, D., Webb, B., Shen, M. Y., Sali, A., 2008. Protein structure modeling with MODELLER. *Methods Mol Biol* 426, 145-159.
- Eswar, N., Webb, B., Marti-Renom, M. A., Madhusudhan, M. S., Eramian, D., Shen, M. Y., Pieper, U., Sali, A., 2007. Comparative protein structure modeling using MODELLER. *Curr Protoc Protein Sci Chapter 2, Unit 2 9*.
- Farahbakhsh, Z. T., Ridge, K. D., Khorana, H. G., Hubbell, W. L., 1995. Mapping light-dependent structural changes in the cytoplasmic loop connecting helices C and D in rhodopsin: a site-directed spin labeling study. *Biochemistry* 34, 8812-8819.

- Farrens, D. L., Altenbach, C., Yang, K., Hubbell, W. L., Khorana, H. G., 1996. Requirement of rigid-body motion of transmembrane helices for light activation of rhodopsin. *Science* 274, 768-770.
- Farrens, D. L., Khorana, H. G., 1995. Structure and function in rhodopsin. Measurement of the rate of metarhodopsin II decay by fluorescence spectroscopy. *J Biol Chem* 270, 5073-5076.
- Filipek, S., Teller, D. C., Palczewski, K., Stenkamp, R., 2003. The crystallographic model of rhodopsin and its use in studies of other G protein-coupled receptors. *Annu Rev Biophys Biomol Struct* 32, 375-397.
- Finn, R. D., Mistry, J., Tate, J., Coghill, P., Heger, A., Pollington, J. E., Gavin, O. L., Gunasekaran, P., Ceric, G., Forslund, K., Holm, L., Sonnhammer, E. L., Eddy, S. R., Bateman, A., 2010. The Pfam protein families database. *Nucleic Acids Res* 38, D211-222.
- Fishkin, N., Berova, N., Nakanishi, K., 2004. Primary events in dim light vision: a chemical and spectroscopic approach toward understanding protein/chromophore interactions in rhodopsin. *Chem Rec* 4, 120-135.
- Flor, P. J., Lukic, S., Ruegg, D., Leonhardt, T., Knopfel, T., Kuhn, R., 1995. Molecular cloning, functional expression and pharmacological characterization of the human metabotropic glutamate receptor type 4. *Neuropharmacology* 34, 149-155.
- Fonseca, F., Gratacos, M., Escaramis, G., De Cid, R., Martin-Santos, R., Fernandez-Espejo, E., Estivill, X., Torrens, M., 2010. Response to methadone maintenance treatment is associated with the MYOCD and GRM6 genes. *Mol Diagn Ther* 14, 171-178.
- Frauli, M., Neuville, P., Vol, C., Pin, J. P., Prezeau, L., 2006. Among the twenty classical L-amino acids, only glutamate directly activates metabotropic glutamate receptors. *Neuropharmacology* 50, 245-253.
- Fredriksson, R., Lagerstrom, M. C., Lundin, L. G., Schioth, H. B., 2003. The G-protein-coupled receptors in the human genome form five main families. Phylogenetic analysis, paralogon groups, and fingerprints. *Mol Pharmacol* 63, 1256-1272.
- Friesner, R. A., Banks, J. L., Murphy, R. B., Halgren, T. A., Klicic, J. J., Mainz, D. T., Repasky, M. P., Knoll, E. H., Shelley, M., Perry, J. K., Shaw, D. E., Francis, P., Shenkin, P. S., 2004. Glide: a new approach for rapid, accurate docking and scoring. 1. Method and assessment of docking accuracy. *Journal of medicinal chemistry* 47, 1739-1749.
- Fritze, O., Filipek, S., Kuksa, V., Palczewski, K., Hofmann, K. P., Ernst, O. P., 2003. Role of the conserved NPxxY(x)5,6F motif in the rhodopsin ground state and during activation. *Proc Natl Acad Sci U S A* 100, 2290-2295.
- Fukuda, J., Suzuki, G., Kimura, T., Nagatomi, Y., Ito, S., Kawamoto, H., Ozaki, S., Ohta, H., 2009. Identification of a novel transmembrane domain involved in the negative

- modulation of mGluR1 using a newly discovered allosteric mGluR1 antagonist, 3-cyclohexyl-5-fluoro-6-methyl-7-(2-morpholin-4-ylethoxy)-4H-chromen-4-one. *Neuropharmacology* 57, 438-445.
- Gether, U., 2000. Uncovering molecular mechanisms involved in activation of G protein-coupled receptors. *Endocr Rev* 21, 90-113.
- Ghosh, K. K., Bujan, S., Haverkamp, S., Feigenspan, A., Wassle, H., 2004. Types of bipolar cells in the mouse retina. *J Comp Neurol* 469, 70-82.
- Goktalay, G., Cavun, S., Levendusky, M. C., Hamilton, J. R., Millington, W. R., 2006. Glycyl-glutamine inhibits nicotine conditioned place preference and withdrawal. *Eur J Pharmacol* 530, 95-102.
- Goodsell, D. S., Morris, G. M., Olson, A. J., 1996. Automated docking of flexible ligands: applications of AutoDock. *J Mol Recognit* 9, 1-5.
- Goudet, C., Gaven, F., Kniazeff, J., Vol, C., Liu, J., Cohen-Gonsaud, M., Acher, F., Prezeau, L., Pin, J. P., 2004. Heptahelical domain of metabotropic glutamate receptor 5 behaves like rhodopsin-like receptors. *Proc Natl Acad Sci U S A* 101, 378-383.
- Graber, S. G., Figler, R. A., Garrison, J. C., 1992a. Expression and purification of functional G protein alpha subunits using a baculovirus expression system. *J Biol Chem* 267, 1271-1278.
- Graber, S. G., Figler, R. A., Garrison, J. C., 1994. Expression and purification of G-protein alpha subunits using baculovirus expression system. *Methods Enzymol* 237, 212-226.
- Graber, S. G., Figler, R. A., Kalman-Maltese, V. K., Robishaw, J. D., Garrison, J. C., 1992b. Expression of functional G protein beta gamma dimers of defined subunit composition using a baculovirus expression system. *J Biol Chem* 267, 13123-13126.
- Guex, N., Peitsch, M. C., 1997. SWISS-MODEL and the Swiss-PdbViewer: an environment for comparative protein modeling. *Electrophoresis* 18, 2714-2723.
- Hall, R. A., Premont, R. T., Lefkowitz, R. J., 1999. Heptahelical receptor signaling: beyond the G protein paradigm. *J Cell Biol* 145, 927-932.
- Hamm, H. E., 1998. The many faces of G protein signaling. *J Biol Chem* 273, 669-672.
- Hanson, M. A., Cherezov, V., Griffith, M. T., Roth, C. B., Jaakola, V. P., Chien, E. Y., Velasquez, J., Kuhn, P., Stevens, R. C., 2008. A specific cholesterol binding site is established by the 2.8 Å structure of the human beta2-adrenergic receptor. *Structure* 16, 897-905.
- Hargrave, P. A., 1977. The amino-terminal tryptic peptide of bovine rhodopsin. A glycopeptide containing two sites of oligosaccharide attachment. *Biochim Biophys Acta* 492, 83-94.

- Hartong, D. T., Berson, E. L., Dryja, T. P., 2006. Retinitis pigmentosa. *Lancet* 368, 1795-1809.
- Hermans, E., Nahorski, S. R., Challiss, R. A., 1998. Reversible and non-competitive antagonist profile of CPCCOEt at the human type 1alpha metabotropic glutamate receptor. *Neuropharmacology* 37, 1645-1647.
- Hollmann, M., Heinemann, S., 1994. Cloned glutamate receptors. *Annu. Rev. Neurosci.* 17, 31-108.
- Horn, F., Weare, J., Beukers, M. W., Horsch, S., Bairoch, A., Chen, W., Edvardsen, O., Campagne, F., Vriend, G., 1998. GPCRDB: an information system for G protein-coupled receptors. *Nucleic Acids Res* 26, 275-279.
- Huang, L., Max, M., Margolskee, R. F., Su, H., Masland, R. H., Euler, T., 2003. G protein subunit G gamma 13 is coexpressed with G alpha o, G beta 3, and G beta 4 in retinal ON bipolar cells. *J Comp Neurol* 455, 1-10.
- Hubbell, W. L., Altenbach, C., Hubbell, C. M., Khorana, H. G., 2003. Rhodopsin structure, dynamics, and activation: a perspective from crystallography, site-directed spin labeling, sulfhydryl reactivity, and disulfide cross-linking. *Adv Protein Chem* 63, 243-290.
- Iannaccone, A., Man, D., Waseem, N., Jennings, B. J., Ganapathiraju, M., Gallaher, K., Reese, E., Bhattacharya, S. S., Klein-Seetharaman, J., 2006. Retinitis pigmentosa associated with rhodopsin mutations: Correlation between phenotypic variability and molecular effects. *Vision Res* 46, 4556-4567.
- Irwin, J. J., Shoichet, B. K., 2005. ZINC--a free database of commercially available compounds for virtual screening. *J Chem Inf Model* 45, 177-182.
- Isayama, T., Alexeev, D., Makino, C. L., Washington, I., Nakanishi, K., Turro, N. J., 2006. An accessory chromophore in red vision. *Nature* 443, 649.
- Isin, B., Rader, A. J., Dhiman, H. K., Klein-Seetharaman, J., Bahar, I., 2006. Predisposition of the dark state of rhodopsin to functional changes in structure. *Proteins* 65, 970-983.
- Jaakola, V. P., Griffith, M. T., Hanson, M. A., Cherezov, V., Chien, E. Y., Lane, J. R., Ijzerman, A. P., Stevens, R. C., 2008. The 2.6 angstrom crystal structure of a human A2A adenosine receptor bound to an antagonist. *Science* 322, 1211-1217.
- Jain, A. N., 2006. Scoring functions for protein-ligand docking. *Current protein & peptide science* 7, 407-420.
- Johnson, B. G., Wright, R. A., Arnold, M. B., Wheeler, W. J., Ornstein, P. L., Schoepp, D. D., 1999. [3H]-LY341495 as a novel antagonist radioligand for group II metabotropic glutamate (mGlu) receptors: characterization of binding to membranes of mGlu receptor subtype expressing cells. *Neuropharmacology* 38, 1519-1529.

- Jones, G., Willett, P., Glen, R. C., Leach, A. R., Taylor, R., 1997. Development and validation of a genetic algorithm for flexible docking. *Journal of molecular biology* 267, 727-748.
- Kalivas, P. W., Duffy, P., 1998. Repeated cocaine administration alters extracellular glutamate in the ventral tegmental area. *J Neurochem* 70, 1497-1502.
- Kaushal, S., Khorana, H. G., 1994. Structure and function in rhodopsin. 7. Point mutations associated with autosomal dominant retinitis pigmentosa. *Biochemistry* 33, 6121-6128.
- Kenakin, T., 2004. Principles: receptor theory in pharmacology. *Trends Pharmacol Sci* 25, 186-192.
- Kenakin, T. P., 2006. A pharmacology primer : theory, applications, and methods. Academic, Amsterdam ; London.
- Kenny, P. J., Gasparini, F., Markou, A., 2003a. Group II metabotropic and alpha-amino-3-hydroxy-5-methyl-4-isoxazole propionate (AMPA)/kainate glutamate receptors regulate the deficit in brain reward function associated with nicotine withdrawal in rats. *J Pharmacol Exp Ther* 306, 1068-1076.
- Kenny, P. J., Markou, A., 2004. The ups and downs of addiction: role of metabotropic glutamate receptors. *Trends Pharmacol Sci* 25, 265-272.
- Kenny, P. J., Paterson, N. E., Boutrel, B., Semenova, S., Harrison, A. A., Gasparini, F., Koob, G. F., Skoubis, P. D., Markou, A., 2003b. Metabotropic glutamate 5 receptor antagonist MPEP decreased nicotine and cocaine self-administration but not nicotine and cocaine-induced facilitation of brain reward function in rats. *Ann N Y Acad Sci* 1003, 415-418.
- Kew, J. N., 2004. Positive and negative allosteric modulation of metabotropic glutamate receptors: emerging therapeutic potential. *Pharmacol Ther* 104, 233-244.
- Kim, J. M., Hwa, J., Garriga, P., Reeves, P. J., RajBhandary, U. L., Khorana, H. G., 2005. Light-driven activation of beta 2-adrenergic receptor signaling by a chimeric rhodopsin containing the beta 2-adrenergic receptor cytoplasmic loops. *Biochemistry* 44, 2284-2292.
- Kingston, A. E., Ornstein, P. L., Wright, R. A., Johnson, B. G., Mayne, N. G., Burnett, J. P., Belagaje, R., Wu, S., Schoepp, D. D., 1998. LY341495 is a nanomolar potent and selective antagonist of group II metabotropic glutamate receptors. *Neuropharmacology* 37, 1-12.
- Klein-Seetharaman, J., 2002. Dynamics in rhodopsin. *Chembiochem* 3, 981-986.
- Klein-Seetharaman, J., 2005. Dual role of interactions between membranous and soluble portions of helical membrane receptors for folding and signaling. *Trends Pharmacol Sci* 26, 183-189.

- Klein-Seetharaman, J., Hwa, J., Cai, K., Altenbach, C., Hubbell, W. L., Khorana, H. G., 1999. Single-cysteine substitution mutants at amino acid positions 55-75, the sequence connecting the cytoplasmic ends of helices I and II in rhodopsin: reactivity of the sulfhydryl groups and their derivatives identifies a tertiary structure that changes upon light-activation. *Biochemistry* 38, 7938-7944.
- Kohn, J., Wilchek, M., 1978. A colorimetric method for monitoring activation of Sepharose by cyanogen bromide. *Biochem Biophys Res Commun* 84, 7-14.
- Koike, C., Obara, T., Uriu, Y., Numata, T., Sanuki, R., Miyata, K., Koyasu, T., Ueno, S., Funabiki, K., Tani, A., Ueda, H., Kondo, M., Mori, Y., Tachibana, M., Furukawa, T., 2010. TRPM1 is a component of the retinal ON bipolar cell transduction channel in the mGluR6 cascade. *Proc Natl Acad Sci U S A* 107, 332-337.
- Kolb, P., Rosenbaum, D. M., Irwin, J. J., Fung, J. J., Kobilka, B. K., Shoichet, B. K., 2009. Structure-based discovery of beta2-adrenergic receptor ligands. *Proc Natl Acad Sci U S A* 106, 6843-6848.
- Kozak, M., 1987. At least six nucleotides preceding the AUG initiator codon enhance translation in mammalian cells. *J Mol Biol* 196, 947-950.
- Krebs, M. P., Holden, D. C., Joshi, P., Clark, C. L., 3rd, Lee, A. H., Kaushal, S., 2010. Molecular mechanisms of rhodopsin retinitis pigmentosa and the efficacy of pharmacological rescue. *J Mol Biol* 395, 1063-1078.
- Kristiansen, K., 2004. Molecular mechanisms of ligand binding, signaling, and regulation within the superfamily of G-protein-coupled receptors: molecular modeling and mutagenesis approaches to receptor structure and function. *Pharmacol Ther* 103, 21-80.
- Kumel, G., Daus, H., Mauch, H., 1979. Improved method for the cyanogen bromide activation of agarose beads. *J Chromatogr* 172, 221-226.
- Kunishima, N., Shimada, Y., Tsuji, Y., Sato, T., Yamamoto, M., Kumasaka, T., Nakanishi, S., Jingami, H., Morikawa, K., 2000. Structural basis of glutamate recognition by a dimeric metabotropic glutamate receptor. *Nature* 407, 971-977.
- Laemmli, U. K., 1970. Cleavage of structural proteins during the assembly of the head of bacteriophage T4. *Nature* 227, 680-685.
- Larkin, M. A., Blackshields, G., Brown, N. P., Chenna, R., McGettigan, P. A., McWilliam, H., Valentin, F., Wallace, I. M., Wilm, A., Lopez, R., Thompson, J. D., Gibson, T. J., Higgins, D. G., 2007. Clustal W and Clustal X version 2.0. *Bioinformatics* 23, 2947-2948.
- Laskowski, R. A., MacArthur, M. W., Moss, D. S., Thornton, J. M., 1993. PROCHECK: a program to check the stereochemical quality of protein structures. *Journal of Applied Crystallography* 26, 283-291.

- Laurie, D. J., Schoeffter, P., Wiederhold, K. H., Sommer, B., 1997. Cloning, distribution and functional expression of the human mGlu6 metabotropic glutamate receptor. *Neuropharmacology* 36, 145-152.
- Lavreysen, H., Dautzenberg, F. M., 2008. Therapeutic potential of group III metabotropic glutamate receptors. *Curr Med Chem* 15, 671-684.
- Levi, M. A. B., Scarminio, I. S., Poppi, R. J., Trevisan, M. G., 2004. Three-way chemometric method study and UV-Vis absorbance for the study of simultaneous degradation of anthocyanins in flowers of the *Hibiscus rosa-sinensis* species. *Talanta* 62, 299-305.
- Lewis, J. W., Szundi, I., Kazmi, M. A., Sakmar, T. P., Kliger, D. S., 2006. Proton movement and photointermediate kinetics in rhodopsin mutants. *Biochemistry* 45, 5430-5439.
- Li, J., Codina, J., Petroske, E., Werle, M. J., DuBose, T. D., Jr., 2004a. The carboxy terminus of the colonic H(+), K(+)-ATPase alpha-subunit is required for stable beta subunit assembly and function. *Kidney Int* 65, 1301-1310.
- Li, J., Edwards, P. C., Burghammer, M., Villa, C., Schertler, G. F., 2004b. Structure of bovine rhodopsin in a trigonal crystal form. *J Mol Biol* 343, 1409-1438.
- Lin, S. W., Sakmar, T. P., 1996. Specific tryptophan UV-absorbance changes are probes of the transition of rhodopsin to its active state. *Biochemistry* 35, 11149-11159.
- Litschig, S., Gasparini, F., Rueegg, D., Stoehr, N., Flor, P. J., Vranesic, I., Prezeau, L., Pin, J. P., Thomsen, C., Kuhn, R., 1999. CPCCOEt, a noncompetitive metabotropic glutamate receptor 1 antagonist, inhibits receptor signaling without affecting glutamate binding. *Mol Pharmacol* 55, 453-461.
- Lockless, S. W., Ranganathan, R., 1999. Evolutionarily conserved pathways of energetic connectivity in protein families. *Science* 286, 295-299.
- Maj, M., Bruno, V., Dragic, Z., Yamamoto, R., Battaglia, G., Inderbitzin, W., Stoehr, N., Stein, T., Gasparini, F., Vranesic, I., Kuhn, R., Nicoletti, F., Flor, P. J., 2003. (-)-PHCCC, a positive allosteric modulator of mGluR4: characterization, mechanism of action, and neuroprotection. *Neuropharmacology* 45, 895-906.
- Malherbe, P., Kratochwil, N., Knoflach, F., Zenner, M. T., Kew, J. N., Kratzeisen, C., Maerki, H. P., Adam, G., Mutel, V., 2003a. Mutational analysis and molecular modeling of the allosteric binding site of a novel, selective, noncompetitive antagonist of the metabotropic glutamate 1 receptor. *J Biol Chem* 278, 8340-8347.
- Malherbe, P., Kratochwil, N., Muhlemann, A., Zenner, M. T., Fischer, C., Stahl, M., Gerber, P. R., Jaeschke, G., Porter, R. H., 2006. Comparison of the binding pockets of two chemically unrelated allosteric antagonists of the mGlu5 receptor and identification of crucial residues involved in the inverse agonism of MPEP. *J Neurochem* 98, 601-615.

- Malherbe, P., Kratochwil, N., Zenner, M. T., Piussi, J., Diener, C., Kratzeisen, C., Fischer, C., Porter, R. H., 2003b. Mutational analysis and molecular modeling of the binding pocket of the metabotropic glutamate 5 receptor negative modulator 2-methyl-6-(phenylethynyl)-pyridine. *Mol Pharmacol* 64, 823-832.
- Marcotte, E. M., Pellegrini, M., Ng, H. L., Rice, D. W., Yeates, T. O., Eisenberg, D., 1999. Detecting protein function and protein-protein interactions from genome sequences. *Science* 285, 751-753.
- Masu, M., Iwakabe, H., Tagawa, Y., Miyoshi, T., Yamashita, M., Fukuda, Y., Sasaki, H., Hiroi, K., Nakamura, Y., Shigemoto, R., et al., 1995. Specific deficit of the ON response in visual transmission by targeted disruption of the mGluR6 gene. *Cell* 80, 757-765.
- Matsumoto, H., Nakamura, Y., Tachibanaki, S., Kawamura, S., Hirayama, M., 2003. Stimulatory effect of cyanidin 3-glycosides on the regeneration of rhodopsin. *J Agric Food Chem* 51, 3560-3563.
- Meldrum, B. S., 2000. Glutamate as a neurotransmitter in the brain: review of physiology and pathology. *J Nutr* 130, 1007S-1015S.
- Meldrum, B. S., Akbar, M. T., Chapman, A. G., 1999. Glutamate receptors and transporters in genetic and acquired models of epilepsy. *Epilepsy Res* 36, 189-204.
- Mendes, H. F., van der Spuy, J., Chapple, J. P., Cheetham, M. E., 2005. Mechanisms of cell death in rhodopsin retinitis pigmentosa: implications for therapy. *Trends Mol Med* 11, 177-185.
- Miller, J. C., Howson, P. A., Conway, S. J., Williams, R. V., Clark, B. P., Jane, D. E., 2003. Phenylglycine derivatives as antagonists of group III metabotropic glutamate receptors expressed on neonatal rat primary afferent terminals. *Br J Pharmacol* 139, 1523-1531.
- Minakami, R., Katsuki, F., Sugiyama, H., 1993. A variant of metabotropic glutamate receptor subtype 5: an evolutionally conserved insertion with no termination codon. *Biochem Biophys Res Commun* 194, 622-627.
- Monaghan, D. T., Bridges, R. J., Cotman, C. W., 1989. The excitatory amino acid receptors: their classes, pharmacology, and distinct properties in the function of the central nervous system. *Annu Rev Pharmacol Toxicol* 29, 365-402.
- Morgans, C. W., Brown, R. L., Duvoisin, R. M., 2010. TRPM1: the endpoint of the mGluR6 signal transduction cascade in retinal ON-bipolar cells. *Bioessays* 32, 609-614.
- Morgans, C. W., Wensel, T. G., Brown, R. L., Perez-Leon, J. A., Bearnot, B., Duvoisin, R. M., 2007. Gbeta5-RGS complexes co-localize with mGluR6 in retinal ON-bipolar cells. *Eur J Neurosci* 26, 2899-2905.

- Morgans, C. W., Zhang, J., Jeffrey, B. G., Nelson, S. M., Burke, N. S., Duvoisin, R. M., Brown, R. L., 2009. TRPM1 is required for the depolarizing light response in retinal ON-bipolar cells. *Proc Natl Acad Sci U S A* 106, 19174-19178.
- Morris, G. M., Goodsell, D. S., Halliday, R. S., Huey, R., Hart, W. E., Belew, R. K., Olson, A. J., 1998. Automated docking using a Lamarckian genetic algorithm and an empirical binding free energy function. *J Comput Chem* 19, 1639-1662.
- Morris, G. M., Goodsell, D. S., Huey, R., Olson, A. J., 1996. Distributed automated docking of flexible ligands to proteins: parallel applications of AutoDock 2.4. *J Comput Aided Mol Des* 10, 293-304.
- Motulsky, H. J., Christopoulos, A., 2003. Fitting models to biological data using linear and nonlinear regression. A practical guide to curve fitting. GraphPad Software Inc., San Diego, CA.
- Muhlemann, A., Ward, N. A., Kratochwil, N., Diener, C., Fischer, C., Stucki, A., Jaeschke, G., Malherbe, P., Porter, R. H., 2006. Determination of key amino acids implicated in the actions of allosteric modulation by 3,3'-difluorobenzaldazine on rat mGlu5 receptors. *Eur J Pharmacol* 529, 95-104.
- Murakami, M., Kouyama, T., 2008. Crystal structure of squid rhodopsin. *Nature* 453, 363-367.
- Muto, T., Tsuchiya, D., Morikawa, K., Jingami, H., 2007. Structures of the extracellular regions of the group II/III metabotropic glutamate receptors. *Proc Natl Acad Sci U S A* 104, 3759-3764.
- Nakajima, Y., Iwakabe, H., Akazawa, C., Nawa, H., Shigemoto, R., Mizuno, N., Nakanishi, S., 1993. Molecular characterization of a novel retinal metabotropic glutamate receptor mGluR6 with a high agonist selectivity for L-2-amino-4-phosphonobutyrate. *J Biol Chem* 268, 11868-11873.
- Nakamichi, H., Buss, V., Okada, T., 2007. Photoisomerization mechanism of rhodopsin and 9-cis-rhodopsin revealed by x-ray crystallography. *Biophys J* 92, L106-108.
- Nakamichi, H., Okada, T., 2006a. Crystallographic analysis of primary visual photochemistry. *Angew Chem Int Ed Engl* 45, 4270-4273.
- Nakamichi, H., Okada, T., 2006b. Local peptide movement in the photoreaction intermediate of rhodopsin. *Proc Natl Acad Sci U S A* 103, 12729-12734.
- Nakamura, M., Sanuki, R., Yasuma, T. R., Onishi, A., Nishiguchi, K. M., Koike, C., Kadowaki, M., Kondo, M., Miyake, Y., Furukawa, T., 2010. TRPM1 mutations are associated with the complete form of congenital stationary night blindness. *Mol Vis* 16, 425-437.
- Nakanishi, S., 1994. Metabotropic glutamate receptors: synaptic transmission, modulation, and plasticity. *Neuron* 13, 1031-1037.

- Nawy, S., 1999. The metabotropic receptor mGluR6 may signal through G(o), but not phosphodiesterase, in retinal bipolar cells. *J Neurosci* 19, 2938-2944.
- Nawy, S., Jahr, C. E., 1990a. Suppression by glutamate of cGMP-activated conductance in retinal bipolar cells. *Nature* 346, 269-271.
- Nawy, S., Jahr, C. E., 1990b. Time-dependent reduction of glutamate current in retinal bipolar cells. *Neurosci Lett* 108, 279-283.
- Nielsen, D. A., Ji, F., Yuferov, V., Ho, A., Chen, A., Levran, O., Ott, J., Kreek, M. J., 2008. Genotype patterns that contribute to increased risk for or protection from developing heroin addiction. *Mol Psychiatry* 13, 417-428.
- Niswender, C. M., Conn, P. J., 2010. Metabotropic glutamate receptors: physiology, pharmacology, and disease. *Annu Rev Pharmacol Toxicol* 50, 295-322.
- Niu, L., Kim, J. M., Khorana, H. G., 2002. Structure and function in rhodopsin: asymmetric reconstitution of rhodopsin in liposomes. *Proc Natl Acad Sci U S A* 99, 13409-13412.
- Noeske, T., Gutcaits, A., Parsons, C. J., Weil, T., 2006. Allosteric Modulation of Family 3 GPCRs. *QSAR & Combinatorial Science* 25, 134-146.
- Nomura, A., Shigemoto, R., Nakamura, Y., Okamoto, N., Mizuno, N., Nakanishi, S., 1994. Developmentally regulated postsynaptic localization of a metabotropic glutamate receptor in rat rod bipolar cells. *Cell* 77, 361-369.
- O'Boyle, N. M., Morley, C., Hutchison, G. R., 2008. Pybel: a Python wrapper for the OpenBabel cheminformatics toolkit. *Chem Cent J* 2, 5.
- O'Brien, J. A., Lemaire, W., Chen, T. B., Chang, R. S., Jacobson, M. A., Ha, S. N., Lindsley, C. W., Schaffhauser, H. J., Sur, C., Pettibone, D. J., Conn, P. J., Williams, D. L., Jr., 2003. A family of highly selective allosteric modulators of the metabotropic glutamate receptor subtype 5. *Mol Pharmacol* 64, 731-740.
- O'Connor, E., Allen, L. E., Bradshaw, K., Boylan, J., Moore, A. T., Trump, D., 2006. Congenital stationary night blindness associated with mutations in GRM6 encoding glutamate receptor MGLuR6. *Br J Ophthalmol* 90, 653-654.
- O'Hara, P. J., Sheppard, P. O., Thogersen, H., Venezia, D., Haldeman, B. A., McGrane, V., Houamed, K. M., Thomsen, C., Gilbert, T. L., Mulvihill, E. R., 1993. The ligand-binding domain in metabotropic glutamate receptors is related to bacterial periplasmic binding proteins. *Neuron* 11, 41-52.
- O'Mahoney, J. V., Adams, T. E., 1994. Optimization of experimental variables influencing reporter gene expression in hepatoma cells following calcium phosphate transfection. *DNA Cell Biol* 13, 1227-1232.

- Oda, A., Tsuchida, K., Takakura, T., Yamaotsu, N., Hirono, S., 2006. Comparison of consensus scoring strategies for evaluating computational models of protein-ligand complexes. *Journal of chemical information and modeling* 46, 380-391.
- Okada, T., Fujiyoshi, Y., Silow, M., Navarro, J., Landau, E. M., Shichida, Y., 2002. Functional role of internal water molecules in rhodopsin revealed by X-ray crystallography. *Proc Natl Acad Sci U S A* 99, 5982-5987.
- Okada, T., Sugihara, M., Bondar, A. N., Elstner, M., Entel, P., Buss, V., 2004. The retinal conformation and its environment in rhodopsin in light of a new 2.2 Å crystal structure. *J Mol Biol* 342, 571-583.
- Okamoto, T., Sekiyama, N., Otsu, M., Shimada, Y., Sato, A., Nakanishi, S., Jingami, H., 1998. Expression and purification of the extracellular ligand binding region of metabotropic glutamate receptor subtype 1. *J Biol Chem* 273, 13089-13096.
- Oprian, D. D., Molday, R. S., Kaufman, R. J., Khorana, H. G., 1987. Expression of a synthetic bovine rhodopsin gene in monkey kidney cells. *Proc Natl Acad Sci U S A* 84, 8874-8878.
- Ou, W. B., Yi, T., Kim, J. M., Khorana, H. G., 2011. The Roles of Transmembrane Domain Helix-III during Rhodopsin Photoactivation. *PLoS ONE* 6, e17398.
- Overington, J. P., Al-Lazikani, B., Hopkins, A. L., 2006. How many drug targets are there? *Nat Rev Drug Discov* 5, 993-996.
- Pagano, A., Ruegg, D., Litschig, S., Stoehr, N., Stierlin, C., Heinrich, M., Floersheim, P., Prezeau, L., Carroll, F., Pin, J. P., Cambria, A., Vranesic, I., Flor, P. J., Gasparini, F., Kuhn, R., 2000. The non-competitive antagonists 2-methyl-6-(phenylethynyl)pyridine and 7-hydroxyiminocyclopropan[b]chromen-1a-carboxylic acid ethyl ester interact with overlapping binding pockets in the transmembrane region of group I metabotropic glutamate receptors. *J Biol Chem* 275, 33750-33758.
- Palczewski, K., 2006. G protein-coupled receptor rhodopsin. *Annu Rev Biochem* 75, 743-767.
- Palczewski, K., Kumasaka, T., Hori, T., Behnke, C. A., Motoshima, H., Fox, B. A., Le Trong, I., Teller, D. C., Okada, T., Stenkamp, R. E., Yamamoto, M., Miyano, M., 2000. Crystal structure of rhodopsin: A G protein-coupled receptor. *Science* 289, 739-745.
- Park, J. H., Scheerer, P., Hofmann, K. P., Choe, H. W., Ernst, O. P., 2008. Crystal structure of the ligand-free G-protein-coupled receptor opsin. *Nature* 454, 183-187.
- Parker, C., A., 1968. *Photoluminescence of solutions*. Elsevier, New York.
- Patel, A. B., Crocker, E., Reeves, P. J., Getmanova, E. V., Eilers, M., Khorana, H. G., Smith, S. O., 2005. Changes in interhelical hydrogen bonding upon rhodopsin activation. *J Mol Biol* 347, 803-812.

- Pierce, K. L., Premont, R. T., Lefkowitz, R. J., 2002. Seven-transmembrane receptors. *Nat Rev Mol Cell Biol* 3, 639-650.
- Pignatelli, V., Strettoi, E., 2004. Bipolar cells of the mouse retina: a gene gun, morphological study. *J Comp Neurol* 476, 254-266.
- Pin, J. P., Duvoisin, R., 1995. The metabotropic glutamate receptors: structure and functions. *Neuropharmacology* 34, 1-26.
- Pin, J. P., Galvez, T., Prezeau, L., 2003. Evolution, structure, and activation mechanism of family 3/C G-protein-coupled receptors. *Pharmacol Ther* 98, 325-354.
- Pin, J. P., Kniazeff, J., Goudet, C., Bessis, A. S., Liu, J., Galvez, T., Acher, F., Rondard, P., Prezeau, L., 2004. The activation mechanism of class-C G-protein coupled receptors. *Biol Cell* 96, 335-342.
- Pin, J. P., Waeber, C., Prezeau, L., Bockaert, J., Heinemann, S. F., 1992. Alternative splicing generates metabotropic glutamate receptors inducing different patterns of calcium release in *Xenopus* oocytes. *Proc Natl Acad Sci U S A* 89, 10331-10335.
- Protti, D. A., Flores-Herr, N., Li, W., Massey, S. C., Wassle, H., 2005. Light signaling in scotopic conditions in the rabbit, mouse and rat retina: a physiological and anatomical study. *J Neurophysiol* 93, 3479-3488.
- Rader, A. J., Anderson, G., Isin, B., Khorana, H. G., Bahar, I., Klein-Seetharaman, J., 2004. Identification of core amino acids stabilizing rhodopsin. *Proc Natl Acad Sci U S A* 101, 7246-7251.
- Rajagopal, K., Lefkowitz, R. J., Rockman, H. A., 2005. When 7 transmembrane receptors are not G protein-coupled receptors. *J Clin Invest* 115, 2971-2974.
- Rajagopal, S., Rajagopal, K., Lefkowitz, R. J., 2010. Teaching old receptors new tricks: biasing seven-transmembrane receptors. *Nat Rev Drug Discov* 9, 373-386.
- Rajamani, R., Good, A. C., 2007. Ranking poses in structure-based lead discovery and optimization: current trends in scoring function development. *Current opinion in drug discovery & development* 10, 308-315.
- Rao, V. R., Cohen, G. B., Oprian, D. D., 1994. Rhodopsin mutation G90D and a molecular mechanism for congenital night blindness. *Nature* 367, 639-642.
- Rasmussen, S. G., Choi, H. J., Fung, J. J., Pardon, E., Casarosa, P., Chae, P. S., Devree, B. T., Rosenbaum, D. M., Thian, F. S., Kobilka, T. S., Schnapp, A., Konetzki, I., Sunahara, R. K., Gellman, S. H., Pautsch, A., Steyaert, J., Weis, W. I., Kobilka, B. K., 2011. Structure of a nanobody-stabilized active state of the beta(2) adrenoceptor. *Nature* 469, 175-180.
- Rasmussen, S. G., Choi, H. J., Rosenbaum, D. M., Kobilka, T. S., Thian, F. S., Edwards, P. C., Burghammer, M., Ratnala, V. R., Sanishvili, R., Fischetti, R. F., Schertler, G. F., Weis,

- W. I., Kobilka, B. K., 2007. Crystal structure of the human beta2 adrenergic G-protein-coupled receptor. *Nature* 450, 383-387.
- Reeves, P. J., Kim, J. M., Khorana, H. G., 2002. Structure and function in rhodopsin: a tetracycline-inducible system in stable mammalian cell lines for high-level expression of opsin mutants. *Proc Natl Acad Sci U S A* 99, 13413-13418.
- Reeves, P. J., Thurmond, R. L., Khorana, H. G., 1996. Structure and function in rhodopsin: high level expression of a synthetic bovine opsin gene and its mutants in stable mammalian cell lines. *Proc Natl Acad Sci U S A* 93, 11487-11492.
- Resch, G. E., Shridharani, S., Millington, W. R., Garris, D. R., Simpson, C. W., 2005. Glycyl-glutamine in nucleus accumbens reduces ethanol intake in alcohol preferring (P) rats. *Brain Res* 1058, 73-81.
- Ridge, K. D., Zhang, C., Khorana, H. G., 1995. Mapping of the amino acids in the cytoplasmic loop connecting helices C and D in rhodopsin. Chemical reactivity in the dark state following single cysteine replacements. *Biochemistry* 34, 8804-8811.
- Romano, C., Miller, J. K., Hyrc, K., Dikranian, S., Mennerick, S., Takeuchi, Y., Goldberg, M. P., O'Malley, K. L., 2001. Covalent and noncovalent interactions mediate metabotropic glutamate receptor mGlu5 dimerization. *Mol Pharmacol* 59, 46-53.
- Romano, C., Yang, W. L., O'Malley, K. L., 1996. Metabotropic glutamate receptor 5 is a disulfide-linked dimer. *J Biol Chem* 271, 28612-28616.
- Rondard, P., Goudet, C., Kniazeff, J., Pin, J. P., Prezeau, L., 2011. The complexity of their activation mechanism opens new possibilities for the modulation of mGlu and GABAB class C G protein-coupled receptors. *Neuropharmacology* 60, 82-92.
- Rondard, P., Liu, J., Huang, S., Malhaire, F., Vol, C., Pinault, A., Labesse, G., Pin, J. P., 2006. Coupling of agonist binding to effector domain activation in metabotropic glutamate-like receptors. *J Biol Chem* 281, 24653-24661.
- Rosenbaum, D. M., Rasmussen, S. G., Kobilka, B. K., 2009. The structure and function of G-protein-coupled receptors. *Nature* 459, 356-363.
- Rosenbaum, D. M., Zhang, C., Lyons, J. A., Holl, R., Aragao, D., Arlow, D. H., Rasmussen, S. G., Choi, H. J., Devree, B. T., Sunahara, R. K., Chae, P. S., Gellman, S. H., Dror, R. O., Shaw, D. E., Weis, W. I., Caffrey, M., Gmeiner, P., Kobilka, B. K., 2011. Structure and function of an irreversible agonist-beta(2) adrenoceptor complex. *Nature* 469, 236-240.
- Sack, J. S., Saper, M. A., Quioco, F. A., 1989. Periplasmic binding protein structure and function. Refined X-ray structures of the leucine/isoleucine/valine-binding protein and its complex with leucine. *J Mol Biol* 206, 171-191.
- Sakmar, T. P., Franke, R. R., Khorana, H. G., 1989. Glutamic acid-113 serves as the retinylidene Schiff base counterion in bovine rhodopsin. *Proc Natl Acad Sci U S A* 86, 8309-8313.

- Sakmar, T. P., Menon, S. T., Marin, E. P., Awad, E. S., 2002. Rhodopsin: insights from recent structural studies. *Annu Rev Biophys Biomol Struct* 31, 443-484.
- Sali, A., Blundell, T. L., 1993. Comparative protein modelling by satisfaction of spatial restraints. *J Mol Biol* 234, 779-815.
- Saliba, R. S., Munro, P. M., Luthert, P. J., Cheetham, M. E., 2002. The cellular fate of mutant rhodopsin: quality control, degradation and aggresome formation. *J Cell Sci* 115, 2907-2918.
- Salom, D., Lodowski, D. T., Stenkamp, R. E., Le Trong, I., Golczak, M., Jastrzebska, B., Harris, T., Ballesteros, J. A., Palczewski, K., 2006. Crystal structure of a photoactivated deprotonated intermediate of rhodopsin. *Proc Natl Acad Sci U S A* 103, 16123-16128.
- Salomon, Y., Londos, C., Rodbell, M., 1974. A highly sensitive adenylate cyclase assay. *Anal Biochem* 58, 541-548.
- Sanner, M. F., 1999. Python: a programming language for software integration and development. *J Mol Graph Model* 17, 57-61.
- Scheerer, P., Park, J. H., Hildebrand, P. W., Kim, Y. J., Krauss, N., Choe, H. W., Hofmann, K. P., Ernst, O. P., 2008. Crystal structure of opsin in its G-protein-interacting conformation. *Nature* 455, 497-502.
- Schmidt, M., Murphy, K., Fung, G., Rosales, R., 2008. Structure learning in random fields for heart motion abnormality detection. *Computer Vision and Pattern Recognition, 2008. CVPR 2008. IEEE Conference on*, pp. 1-8.
- Schoeffter, P., Pfeilschifter, J., Bobirnac, I., 1995. 5-Hydroxytryptamine 5-HT_{1B} receptors inhibiting cyclic AMP accumulation in rat renal mesangial cells. *Naunyn Schmiedebergs Arch Pharmacol* 351, 35-39.
- Schuttelkopf, A. W., van Aalten, D. M., 2004. PRODRG: a tool for high-throughput crystallography of protein-ligand complexes. *Acta Crystallogr D Biol Crystallogr* 60, 1355-1363.
- Schwartz, T. W., Frimurer, T. M., Holst, B., Rosenkilde, M. M., Elling, C. E., 2006. Molecular mechanism of 7TM receptor activation--a global toggle switch model. *Annu Rev Pharmacol Toxicol* 46, 481-519.
- Sharman, J. L., Mpamhanga, C. P., Spedding, M., Germain, P., Staels, B., Dacquet, C., Laudet, V., Harmar, A. J., 2011. IUPHAR-DB: new receptors and tools for easy searching and visualization of pharmacological data. *Nucleic Acids Res* 39, D534-538.
- Shen, M. Y., Sali, A., 2006. Statistical potential for assessment and prediction of protein structures. *Protein Sci* 15, 2507-2524.

- Shen, Y., Heimel, J. A., Kamermans, M., Peachey, N. S., Gregg, R. G., Nawy, S., 2009. A transient receptor potential-like channel mediates synaptic transmission in rod bipolar cells. *J Neurosci* 29, 6088-6093.
- Shi, L., Liapakis, G., Xu, R., Guarnieri, F., Ballesteros, J. A., Javitch, J. A., 2002. Beta2 adrenergic receptor activation. Modulation of the proline kink in transmembrane 6 by a rotamer toggle switch. *J Biol Chem* 277, 40989-40996.
- Shi, L., Simpson, M. M., Ballesteros, J. A., Javitch, J. A., 2001. The first transmembrane segment of the dopamine D2 receptor: accessibility in the binding-site crevice and position in the transmembrane bundle. *Biochemistry* 40, 12339-12348.
- Shiells, R. A., Falk, G., 1990. Glutamate receptors of rod bipolar cells are linked to a cyclic GMP cascade via a G-protein. *Proc Biol Sci* 242, 91-94.
- Shimamura, T., Hiraki, K., Takahashi, N., Hori, T., Ago, H., Masuda, K., Takio, K., Ishiguro, M., Miyano, M., 2008. Crystal structure of squid rhodopsin with intracellularly extended cytoplasmic region. *J Biol Chem* 283, 17753-17756.
- Soudijn, W., Van Wijngaarden, I., AP, I. J., 2004. Allosteric modulation of G protein-coupled receptors: perspectives and recent developments. *Drug Discov Today* 9, 752-758.
- Sprang, S. R., 2011. Cell signalling: Binding the receptor at both ends. *Nature* 469, 172-173.
- Standfuss, J., Edwards, P. C., D'Antona, A., Fransen, M., Xie, G., Oprian, D. D., Schertler, G. F. X., 2011. The structural basis of agonist-induced activation in constitutively active rhodopsin. *Nature advance online publication*.
- Standfuss, J., Xie, G., Edwards, P. C., Burghammer, M., Oprian, D. D., Schertler, G. F., 2007. Crystal structure of a thermally stable rhodopsin mutant. *J Mol Biol* 372, 1179-1188.
- Stenkamp, R. E., 2008. Alternative models for two crystal structures of bovine rhodopsin. *Acta Crystallogr D Biol Crystallogr* D64, 902-904.
- Sternweis, P. C., Robishaw, J. D., 1984. Isolation of two proteins with high affinity for guanine nucleotides from membranes of bovine brain. *J Biol Chem* 259, 13806-13813.
- Suel, G. M., Lockless, S. W., Wall, M. A., Ranganathan, R., 2003. Evolutionarily conserved networks of residues mediate allosteric communication in proteins. *Nat Struct Biol* 10, 59-69.
- Sung, C. H., Davenport, C. M., Hennessey, J. C., Maumenee, I. H., Jacobson, S. G., Heckenlively, J. R., Nowakowski, R., Fishman, G., Gouras, P., Nathans, J., 1991. Rhodopsin mutations in autosomal dominant retinitis pigmentosa. *Proc Natl Acad Sci U S A* 88, 6481-6485.

- Sung, C. H., Davenport, C. M., Nathans, J., 1993. Rhodopsin mutations responsible for autosomal dominant retinitis pigmentosa. Clustering of functional classes along the polypeptide chain. *Journal of Biological Chemistry* 268, 26645-26649.
- Swanson, C. J., Bures, M., Johnson, M. P., Linden, A. M., Monn, J. A., Schoepp, D. D., 2005. Metabotropic glutamate receptors as novel targets for anxiety and stress disorders. *Nat Rev Drug Discov* 4, 131-144.
- Tagawa, Y., Sawai, H., Ueda, Y., Tauchi, M., Nakanishi, S., 1999. Immunohistological studies of metabotropic glutamate receptor subtype 6-deficient mice show no abnormality of retinal cell organization and ganglion cell maturation. *J Neurosci* 19, 2568-2579.
- Takeda, S., Kadowaki, S., Haga, T., Takaesu, H., Mitaku, S., 2002. Identification of G protein-coupled receptor genes from the human genome sequence. *FEBS Lett* 520, 97-101.
- Tam, B. M., Moritz, O. L., 2009. The role of rhodopsin glycosylation in protein folding, trafficking, and light-sensitive retinal degeneration. *J Neurosci* 29, 15145-15154.
- Tanabe, Y., Masu, M., Ishii, T., Shigemoto, R., Nakanishi, S., 1992. A family of metabotropic glutamate receptors. *Neuron* 8, 169-179.
- Tanabe, Y., Nomura, A., Masu, M., Shigemoto, R., Mizuno, N., Nakanishi, S., 1993. Signal transduction, pharmacological properties, and expression patterns of two rat metabotropic glutamate receptors, mGluR3 and mGluR4. *J Neurosci* 13, 1372-1378.
- Tateyama, M., Abe, H., Nakata, H., Saito, O., Kubo, Y., 2004. Ligand-induced rearrangement of the dimeric metabotropic glutamate receptor 1alpha. *Nat Struct Mol Biol* 11, 637-642.
- Teller, D. C., Okada, T., Behnke, C. A., Palczewski, K., Stenkamp, R. E., 2001. Advances in determination of a high-resolution three-dimensional structure of rhodopsin, a model of G-protein-coupled receptors (GPCRs). *Biochemistry* 40, 7761-7772.
- Thomas, J., Ramakrishnan, N., Bailey-Kellogg, C., 2008. Graphical models of residue coupling in protein families. *IEEE/ACM Trans Comput Biol Bioinform* 5, 183-197.
- Tirupula, K. C., Balem, F., Yanamala, N., Klein-Seetharaman, J., 2009. pH-dependent Interaction of Rhodopsin with Cyanidin-3-glucoside. 2. Functional Aspects. *Photochem Photobiol* 85, 463-470.
- Tropp, J. A., 2006. Just relax: convex programming methods for identifying sparse signals in noise. *Information Theory, IEEE Transactions on* 52, 1030-1051.
- Trott, O., Olson, A. J., 2010. AutoDock Vina: improving the speed and accuracy of docking with a new scoring function, efficient optimization, and multithreading. *J Comput Chem* 31, 455-461.

- Tsuchiya, D., Kunishima, N., Kamiya, N., Jingami, H., Morikawa, K., 2002. Structural views of the ligand-binding cores of a metabotropic glutamate receptor complexed with an antagonist and both glutamate and Gd³⁺. *Proc Natl Acad Sci U S A* 99, 2660-2665.
- Tsuji, Y., Shimada, Y., Takeshita, T., Kajimura, N., Nomura, S., Sekiyama, N., Otomo, J., Usukura, J., Nakanishi, S., Jingami, H., 2000. Cryptic dimer interface and domain organization of the extracellular region of metabotropic glutamate receptor subtype 1. *J Biol Chem* 275, 28144-28151.
- Ueda, Y., Iwakabe, H., Masu, M., Suzuki, M., Nakanishi, S., 1997. The mGluR6 5' upstream transgene sequence directs a cell-specific and developmentally regulated expression in retinal rod and ON-type cone bipolar cells. *J Neurosci* 17, 3014-3023.
- Vardi, N., Matesic, D. F., Manning, D. R., Liebman, P. A., Sterling, P., 1993. Identification of a G-protein in depolarizing rod bipolar cells. *Vis Neurosci* 10, 473-478.
- Varney, M. A., Cosford, N. D., Jachec, C., Rao, S. P., Sacca, A., Lin, F. F., Bleicher, L., Santori, E. M., Flor, P. J., Allgeier, H., Gasparini, F., Kuhn, R., Hess, S. D., Velicelebi, G., Johnson, E. C., 1999. SIB-1757 and SIB-1893: selective, noncompetitive antagonists of metabotropic glutamate receptor type 5. *J Pharmacol Exp Ther* 290, 170-181.
- Vassilatis, D. K., Hohmann, J. G., Zeng, H., Li, F., Ranchalis, J. E., Mortrud, M. T., Brown, A., Rodriguez, S. S., Weller, J. R., Wright, A. C., Bergmann, J. E., Gaitanaris, G. A., 2003. The G protein-coupled receptor repertoires of human and mouse. *Proc Natl Acad Sci U S A* 100, 4903-4908.
- Wacker, D., Fenalti, G., Brown, M. A., Katritch, V., Abagyan, R., Cherezov, V., Stevens, R. C., 2010. Conserved binding mode of human beta2 adrenergic receptor inverse agonists and antagonist revealed by X-ray crystallography. *J Am Chem Soc* 132, 11443-11445.
- Wald, G., Brown, P. K., 1953. The molar extinction of rhodopsin. *J Gen Physiol* 37, 189-200.
- Walters, R. J., Kramer, R. H., Nawy, S., 1998. Regulation of cGMP-dependent current in On bipolar cells by calcium/calmodulin-dependent kinase. *Vis Neurosci* 15, 257-261.
- Wang, J. K., McDowell, J. H., Hargrave, P. A., 1980. Site of attachment of 11-cis-retinal in bovine rhodopsin. *Biochemistry* 19, 5111-5117.
- Warne, T., Moukhametzianov, R., Baker, J. G., Nehme, R., Edwards, P. C., Leslie, A. G., Schertler, G. F., Tate, C. G., 2011. The structural basis for agonist and partial agonist action on a beta(1)-adrenergic receptor. *Nature* 469, 241-244.
- Warne, T., Serrano-Vega, M. J., Baker, J. G., Moukhametzianov, R., Edwards, P. C., Henderson, R., Leslie, A. G., Tate, C. G., Schertler, G. F., 2008. Structure of a beta(1)-adrenergic G-protein-coupled receptor. *Nature*.
- Washington, I., Brooks, C., Turro, N. J., Nakanishi, K., 2004. Porphyrins as photosensitizers to enhance night vision. *J Am Chem Soc* 126, 9892-9893.

- Washington, I., Zhou, J., Jockusch, S., Turro, N. J., Nakanashi, K., Sparrow, J. R., 2007. Chlorophyll derivatives as visual pigments for super vision in the red. *Photochemical and Photobiological Sciences* 6, 775-779.
- Weinstein, H., 2005. Hallucinogen actions on 5-HT receptors reveal distinct mechanisms of activation and signaling by G protein-coupled receptors. *AAPS J* 7, E871-884.
- Weng, K., Lu, C., Daggett, L. P., Kuhn, R., Flor, P. J., Johnson, E. C., Robinson, P. R., 1997. Functional coupling of a human retinal metabotropic glutamate receptor (hmGluR6) to bovine rod transducin and rat Go in an in vitro reconstitution system. *J Biol Chem* 272, 33100-33104.
- Wessling-Resnick, M., Johnson, G. L., 1987. Transducin interactions with rhodopsin. Evidence for positive cooperative behavior. *J Biol Chem* 262, 12444-12447.
- Wood, M. R., Hopkins, C. R., Brogan, J. T., Conn, P. J., Lindsley, C. W., 2011. "Molecular Switches" on mGluR Allosteric Ligands That Modulate Modes of Pharmacology. *Biochemistry*.
- Wright, R. A., Arnold, M. B., Wheeler, W. J., Ornstein, P. L., Schoepp, D. D., 2000. Binding of [3H](2S,1'S,2'S)-2-(9-xanthylmethyl)-2-(2'-carboxycyclopropyl) glycine ([3H]LY341495) to cell membranes expressing recombinant human group III metabotropic glutamate receptor subtypes. *Naunyn Schmiedebergs Arch Pharmacol* 362, 546-554.
- Wu, B., Chien, E. Y., Mol, C. D., Fenalti, G., Liu, W., Katritch, V., Abagyan, R., Brooun, A., Wells, P., Bi, F. C., Hamel, D. J., Kuhn, P., Handel, T. M., Cherezov, V., Stevens, R. C., 2010. Structures of the CXCR4 chemokine GPCR with small-molecule and cyclic peptide antagonists. *Science* 330, 1066-1071.
- Yamashita, T., Kai, T., Terakita, A., Shichida, Y., 2004. A novel constitutively active mutation in the second cytoplasmic loop of metabotropic glutamate receptor. *J Neurochem* 91, 484-492.
- Yamashita, T., Terakita, A., Kai, T., Shichida, Y., 2008. Conformational change of the transmembrane helices II and IV of metabotropic glutamate receptor involved in G protein activation. *J Neurochem*.
- Yan, E. C. Y., Epps, J., Lewis, J. W., Szundi, I., Bhagat, A., Sakmar, T. P., Kliger, D. S., 2007. Photointermediates of the Rhodopsin S186A Mutant as a Probe of the Hydrogen-Bond Network in the Chromophore Pocket and the Mechanism of Counterion Switch†. *The Journal of Physical Chemistry C* 111, 8843-8848.
- Yanagawa, M., Yamashita, T., Shichida, Y., 2009. Activation switch in the transmembrane domain of metabotropic glutamate receptor. *Mol Pharmacol* 76, 201-207.

- Yanamala, N., Tirupula, K. C., Balem, F., Klein-Seetharaman, J., 2009. pH-dependent Interaction of Rhodopsin with Cyanidin-3-glucoside. 1. Structural Aspects. *Photochem Photobiol* 85, 454-462.
- Yanamala, N., Tirupula, K. C., Klein-Seetharaman, J., 2008. Preferential binding of allosteric modulators to active and inactive conformational states of metabotropic glutamate receptors. *BMC Bioinformatics* 9 Suppl 1, S16.
- Yanamala, N. V., 2009. *Allosteric Modulation of G Protein Coupled Receptors.*, Molecular Biophysics. University of Pittsburgh, Pittsburgh.
- Yang, K., Farrens, D. L., Hubbell, W. L., Khorana, H. G., 1996. Structure and function in rhodopsin. Single cysteine substitution mutants in the cytoplasmic interhelical E-F loop region show position-specific effects in transducin activation. *Biochemistry* 35, 12464-12469.
- Yeagle, P. L., Choi, G., Albert, A. D., 2001. Studies on the structure of the G-protein-coupled receptor rhodopsin including the putative G-protein binding site in unactivated and activated forms. *Biochemistry* 40, 11932-11937.
- Zeitz, C., van Genderen, M., Neidhardt, J., Luhmann, U. F., Hoeben, F., Forster, U., Wycisk, K., Matyas, G., Hoyng, C. B., Riemsdag, F., Meire, F., Cremers, F. P., Berger, W., 2005. Mutations in GRM6 cause autosomal recessive congenital stationary night blindness with a distinctive scotopic 15-Hz flicker electroretinogram. *Invest Ophthalmol Vis Sci* 46, 4328-4335.